Development of the fixed-vane revolving vane compressor

Tan, Kok Ming

2012

Tan, K. M. (2012). Development of the fixed-vane revolving vane compressor. Doctoral thesis, Nanyang Technological University, Singapore.

https://hdl.handle.net/10356/50477

https://doi.org/10.32657/10356/50477

DEVELOPMENT OF THE FIXED-VANE REVOLVING VANE COMPRESSOR TAN KOK MING 2012

NANYANG TECHNOLOGICAL UNIVERSITY

DEVELOPMENT OF THE FIXED-VANE REVOLVING VANE COMPRESSOR

TAN KOK MING

SCHOOL OF MECHANICAL AND AEROSPACE ENGINEERING

2012

DEVELOPMENT OF THE FIXED-VANE REVOLVING VANE COMPRESSOR

TAN KOK MING

TAN KOK MING

School of Mechanical and Aerospace Engineering

A thesis submitted to the Nanyang Technological University

in partial fulfilment of the requirement for the degree of

Doctor of Philosophy

2012

Acknowledgements

Firstly, I would like to express my deepest gratitude to my thesis supervisor, Associate Professor Ooi Kim Tiow, who has providing me with the opportunity to carry out this research project under his guidance. He has also supported and guided me closely in the realization of this research goal while allowing me the room to manoeuvre and express my own way freely. Working with him has been a wonderful learning experience. He has also significantly influenced, motivated and enlightened me on my research life as well as personal life. Without his countless inspiration and encouragement, it would not be possible for me to complete this thesis and I truly appreciate everything he has done in shaping me to become a more confident person and researcher today.

Secondly, I would like to thank Nanyang Technological University for the research scholarship and School of Mechanical & Aerospace Engineering (MAE) for providing me the research opportunity and facilities. In addition, I am indeed grateful to the School of MAE for being granted the opportunities to participate in a one-week overseas workshop in Japan Tohoku University as well as teaching assignments for undergraduate laboratory projects. This has been a fruitful memorable experience.

I should not forget to mention one important person: Mr. Seow Shih Tet, the director of Weta Engineering Pte Ltd, for showing his ultimate professionalism in the prototyping of the small scale fixed-vane revolving vane compressor. I would like to express my heartfelt gratitude to him for taking time off his busy schedule and delivered the functional fixed-vane revolving vane compressor. Without his strong support, the

practical development of the fixed-vane revolving vane compressor would not be possible to be completed.

Next, I would like to thank several lab technicians in the School of MAE and they are Mr. Eric Yap Pow Khim from Fluid Mechanics Lab, Ms. Tan How Jee, Mr. Elson Ng Moo Kheo and Mr. Kong Seng Ann from Manufacturing Process Lab, Ms. Ong Pek Loon from Metrology Lab, Mr. Ow Yong See Meng from Aerodynamics Lab, and Ms. Chia Hwee Lang from Aerospace Structure Lab, Mr. Steven Cheong Yuen Kong and Mr. Foo Jong Hin from Thermodynamics Lab and Mr. Yuan Kee Hock from Thermal & Fluid Research Lab, for providing their assistance in one way or another during the course of completing the research project. Apart from that, in and out of my daily work, I am blessed to have a friendly and cheerful group of friends, who are my mates for having lunch and playing badminton. I am thankful for their friendship and the listening ears.

Last but not least, I owe my loving thanks to my mother for her unconditional love and concern throughout my life. Special gratitude goes to my three dedicated elder brothers, Kok Wei, Kok Peng and Kok Soon for their strong supports whenever I need them. To my dearest girlfriend, Choy Ling, who has been understanding and considerate to me. Finally, I would like to show my emotional thanks to my father, who had passed away in year 1992, but had left admirable never-say-die spirit in my mind firmly.

Table of Contents

Chapter 7

Design of a Fixed-vane Revolving Vane Compressor Prototype

Chapter 8

Lubrication System of Fixed-vane Revolving Vane Compressor

List of Figures

List of Tables

Nomenclature

A	area [m^2]
A_c	cross sectional area of valve [m^2]
A_f	effective force area on discharge valve [m^2]
A_{flow}	flow area [m^2]
A_g	cross sectional area of the spiral groove [m^2]
c	damping constant [N s m^{-2}]
C_d	discharge coefficient [-]
D	width of the spiral groove [m]
e	offset distance between the cylinder centre and the rotor centre [m]
E	summation of kinetic energy, potential energy and internal energy [J]
E_v	elastic modulus of valve material [Pa]
$f_r(x)$	valve response profile at r^{th} mode [m]
$f(x,t)$	force per unit length acting on the valve [N]
F_f	frictional force [N]
F_{cp}	the working fluid pressure force on the cylinder [N]
F_{cx}	the resultant force acting on the cylinder in x direction [N]
F_{cy}	the resultant force acting on the cylinder in y direction [N]
F_{cpx}	the working fluid pressure force on the cylinder in x direction [N]
F_{cpy}	the working fluid pressure force on the cylinder in y direction [N]
F_{rp}	the working fluid pressure force on the rotor [N]
F_{rpx}	the working fluid pressure force on the rotor in x direction [N]
F_{rpy}	the working fluid pressure force on the rotor in y direction [N]
F_{rx}	the resultant force acting on the rotor in x direction [N]
F_{ry}	the resultant force acting on the rotor in y direction [N]
F_{vn}	the vane contact force [N]
F_{vf}	the frictional force at the vane contact [N]
F_x	the resultant force on the journal in x direction [N]
F_y	the resultant force on the journal in y direction [N]
g	acceleration of gravity [m s^{-2}]
$g_r(t)$	variation of valve response profile amplitude at r^{th} mode [-]
h	specific enthalpy of working fluid [J kg^{-1}] / minimum oil film thickness [m] / flow path height [m]
h_1	specific enthalpy of working fluid at upstream [J kg^{-1}]
h_2	specific enthalpy of working fluid at downstream [J kg^{-1}]

$h_{2,is}$ specific enthalpy of working fluid at downstream at isentropic condition [J kg^{-1}]

h_c specific enthalpy of working fluid in the chamber[J kg^{-1}]

h_i specific enthalpy of working fluid at the inlet [J kg^{-1}]

H depth of the spiral groove [m]

I_r rotational inertia of the rotor [kg m^4]

I_v moment of inertia of valve [m^4]

K flow coefficient [-]

L length of the discharge valve [m]

L_{Br} length of the journal bearing [m]

L_c axial length of the compressor working chamber [m]

L_{vn} length of vane exposed to the working chamber [m]

m mass of valve [kg]

m_c working fluid mass in the working chamber [kg]

m_i working fluid mass at the inlet [kg]

m_o working fluid mass at the outlet [kg]

m_r mass of the rotor [kg]

m_{rs} mass of the rotor shaft [kg]

M bending moment [N m]

N_r modal force [s^{-2}]

p_r natural frequency of the valve at r^{th} mode [rad s^{-1}]

P lubricant pressure profile [Pa] / point pressure along lubrication path [Pa]

P_c working fluid pressure in the working chamber / pressure in the compression working chamber [Pa]

$P_{f,Br}$ journal bearing frictional loss [W]

P_{ILA} lubricant pressure profile under infinitely long approximation [Pa]

P_{ISA} lubricant pressure profile under infinitely short approximation [Pa]

P_s pressure in the suction working chamber [Pa]

$q_{d,r}$ damped response frequency of discharge valve at r^{th} mode [rad s^{-1}]

q_r response frequency of discharge valve at r^{th} mode [rad s^{-1}]

Q specific heat exchange between fluid and surroundings [J kg^{-1}] / oil flow rate [m^3 s^{-1}]

Q_c convective heat transfer in the working chamber [J]

r moment arm of the frictional force [m]

R distance between the centre of the cylinder and the rotor circumference [m] / the radial location of the discharge valve from the centre of the cylinder [m] / flow resistance [Pa s m^{-3}] / the radius [m]

R_{Br} bearing radius [m]

R_c cylinder radius [m]

R_i inner shaft radius [m]

R_o outer shaft radius [m]

R_r	rotor radius [m]
R_{rs}	rotor shaft radius [m]
R_v	vane exposure length [m]
t	time [s]
T_c	working fluid temperature in the working chamber [K]
u_c	specific internal energy of working fluid in the working chamber [J kg^{-1}]
U_a	tangential velocity of the journal [m s^{-1}]
U_b	tangential velocity of the bearing [m s^{-1}]
V	velocity [m s^{-1}] / volume [m^3] / shear force [N]
V_c	working chamber volume [m^3]
V_s	specific volume [m^3 kg^{-1}]
w_a	normal velocity of the journal [m s^{-1}]
w_b	normal velocity of the bearing [m s^{-1}]
W	work [J]
W_{ind}	indicated work [J]
x	location along the valve length [m]
y	valve displacement [m]
z	elevation [m] / axial direction of the bearing [m]
α_r	angular acceleration of the rotor [rad s^{-2}]
β	angle between the bearing axial direction and the groove [rad]
δ_{Br}	bearing radial clearance [m]
δ_{ef}	end face clearance [m]
δ_{rs}	Kronecker delta [-]
ε	eccentricity ratio [-]
η_{is}	isentropic efficiency [-]
η_{vs}	vane side frictional coefficient [-]
θ	coordinate in circumferential direction of lubricant pressure profile [rad]
μ	dynamic viscosity of the lubricant [Pa s]
ξ	damping coefficient [-]
ρ	working fluid density / valve material density / lubricant density [kg m^{-3}]
φ	attitude angle [rad]
φ_c	rotational angle of the cylinder [rad]
φ_r	rotational angle of the rotor [rad]
ω	rotational velocity of the valve [rad s^{-1}]
ω_{av}	average angular velocity of the journal and the bearing [rad s^{-1}]
ω_c	angular velocity of the cylinder [rad s^{-1}]
ω_J	angular velocity of the journal [rad s^{-1}]
ω_r	angular velocity of the rotor [rad s^{-1}]
ΔP	pressure difference [Pa]

Abstract

The dissertation deals with the development of a newly introduced positive displacement rotary compressor, named fixed-vane revolving vane compressor. The compressor design is conceived with the motivation for eliminating the dependency of the vane-side frictional loss on the working fluid pressures. Prediction shows that a reduction of frictional loss of 40% is achieved in one design and this has translated to 3.0% improvement in the coefficient of performance of the refrigeration cycle.

The development begins with the formulation of the mathematical models to understand the operational characteristics and the performance of the compressor. The geometric and the kinematics models were first formulated. The variations of the pressure, temperature and the mass of the working fluid inside the working chamber are then predicted employing the conservation of the energy approach. The internal leakages, the suction and discharge flow model were also considered. The dynamic response of the discharge valve is also investigated analytically by assuming that the valve behaves like a beam under forced vibration. The mathematical models were solved simultaneously using 4^{th} order Runge-Kutta numerical integration by a Fortran program developed in-house. The results show that the sizes of the suction and discharge ports and the thickness of the valve reed are among some important parameters in affecting the performance of the compressor. In the case examined, the suction and discharge loss increases by 113 W and 9.3 W as the corresponding port size decreases from 18.0 mm to 3.0 mm and from 17.0 mm to 5.0 mm. The discharge loss increases by 52 W when the valve reed thickness increases from 0.2 mm to 1.4 mm.

The unique geometrical configuration of the working chamber poses a challenge to appropriately analyse the in-chamber convective heat transfer between the working fluid and the chamber wall. In this research by defining the mean flow velocity to be the arithmetic mean of the tangential velocities of the driving and the driven component with respect to the centre of the driving component, and taking the hydraulic diameter to be the quadruple of the ratio between the vane exposure area and the wetted perimeter of the area, the mathematical model is able to predict the pressure-angle histories within 2.0% accuracy.

The lubrication model for the journal bearing reveals that the surface roughness requirement for the compressor bearing surfaces can be reduced by 0.1 μm and 0.3 μm for an increment of 5.0 mm in bearing length and bearing radius respectively at a penalty of higher additional bearing loss of 26.0 W and 101.4 W. The lubrication system design, which consists of the complete oil flow network together with the details of oil grooves, oil flow channels, feeding and returning oil paths, has been designed and shown to work well in the experiment. The study shows that the oil flow rate increases by 17.4 mm^3/s and 49.4 mm^3/s as the groove width increases from 1.0 mm to 5.0 mm and the groove depth decreases from 0.9 mm to 0.1 mm respectively.

A fixed-vane revolving vane compressor prototype has been designed, fabricated, instrumented and tested. The prototype was tested using air as the working fluid and was running from 2350 rev/min to 3800 rev/min with pressure ratio of up to 2.4. The discrepancy between the predicted and the measured mechanical power is well below 10.0% and the lubricating oil viscosity is found to be closely related to the operating

speed. The measured air flow rate is greater than the prediction when the discharge pressure is less than 1.8 bar and the operating speed is above 2350 rev/min.

After the verification, the mathematical model has been linked with a direct-search, multi-variable, constrained optimization algorithm due to Box [147]. Three cases of optimization studies for the compressor have been carried out to search for the best combinations of design dimensions for under these three objective functions: minimum frictional loss, minimum leakage loss and maximum coefficient of performance. The optimization studies point towards a better understanding of the performance characteristics of the compressor.

The research work shows that fixed-vane revolving vane compressor is a feasible practical proposal and it certainly has the potential to outperform the existing state of the art rotary compressors.

Chapter 1

Introduction

1.1 Background and Motivation

The compressor is a primary component in applications of refrigeration, air conditioning and gas compression used in household and industrial systems. It is used for increasing the pressure of a compressible fluid such as air and refrigerants.

Compressors come in various types and sizes, each of which fulfil a given need and represent the optimum configuration for a given set of requirements. Generally speaking, the compressors can be divided into positive displacement and dynamic types. The positive displacement compressor induces and displaces successive volumes of working fluids while the dynamic compressor produces a static pressure rise by converting kinetic energy into pressure energy. Alternatively, compressors can be grouped into intermittent or continuous categories based on the mode of compression. The intermittent mode of compression is cyclical in nature, whereby a specific quantity of gas is induced by the compressor and discharged before the cycle is repeated. The continuous mode of compression is one in which the gas is moved into compressor, acted upon, moved through the compressor and discharged without the interruption of the flow at any process.

Compressors have been used for centuries and their usage is growing in demand all over the world. Hence, the energy demand for the compressor operation is undoubtedly increasing at a staggering rate and the efficiency of the compressor would have a final say on energy-saving issues. Over the years, the compressor technology has dramatically improved due to the relentless development and design efforts. The researchers and industries are working hard to bring up the compressor performance to the next height by either altering the existing compressor designs or inventing a new compression mechanism.

In 2006, a new compressor mechanism called revolving vane compressor has been proposed. The new compressor mechanism employs a new concept in which a significant reduction in energy loss as compared to the other types of positive displacement compressors can be achieved [1]. Several analyses concerned with the performance aspects of the new compressor mechanism have been conducted [2-4]. The functionality of the new compressor with a volume displacement of 32.5 cc has also been tested under pressure ratio of 8 and the operating speed ranges from 600 rev/min to 1200 rev/min [5]. The establishment of the new compressor is not deemed as completed at this stage and it is motivated to discover the potential of this new compressor mechanism. The dependency of the vane-side contact force on the working fluid pressure in the working chamber of the revolving vane compressor design can be entirely eliminated by fixing the vane onto the driving component. A fully detailed analysis for the fixed-vane revolving vane compressor involves mathematical modelling, simulation studies, prototype design, experimentation and geometrical optimization are to be conducted.

1.2 Objectives and Scope

The objective of this research project is to design and develop the fixed-vane revolving vane compressor. The outline of tasks in order to accomplish the project is given in chronological order as follows:

i. Review existing compressor designs to acknowledge the advantages and the disadvantages of the designs
ii. Review the development in simulation studies of compressor chronologically
iii. Understand the working principles of revolving vane compressor mechanism and analyse the possible design variants
iv. Develop mathematical models which facilitate the theoretical analysis of the fixed-vane revolving vane compressor performance and followed by parametric studies
v. Design and fabricate the fixed-vane revolving vane compressor prototype
vi. Conduct experimental studies on the fixed-vane revolving vane compressor prototype. The theoretical work completed in precedence will be validated at this stage
vii. Obtain three different sets of design dimensions for minimizing the frictional losses, minimizing the leakage loss and maximizing the coefficient of performance respectively by applying available optimization technique after substantial theoretical and experimental investigations have been completed

The endeavours as mentioned above are not only to engage the author in an academic excursion for the fulfilment of doctoral research but also to gain valuable

experience in development of a practical compressor application which eventually brings a true benefit to the society.

1.3 Overview of Thesis

This dissertation presents the detailed establishment of the fixed-vane revolving vane compressor. The dissertation begins by recognizing the motivations of the research project. Chapter 2 illustrates the reasons for the emergence of revolving vane compressor, where a review of existing compressor designs is presented. In addition, a review of mathematical modelling on compressor performance is also included in this chapter. Chapter 3 shows the evolution and the working principles of the revolving vane compressor. The chapter concludes with an evaluation of all possible design variants of revolving vane compressor and one is chosen for further investigation in this dissertation.

Chapters 4 to 6 show the formulation of mathematical models, which are used to investigate the performance characteristics of the fixed-vane revolving vane compressor. The governing equations for each aspect of the compressor namely, volume-time variation, thermodynamics, mass flow and valve response are presented in Chapter 4. The unique in-chamber convective heat transfer model for rotary type revolving vane compressor will be proposed in Chapter 5. The force analysis for mechanical losses and journal bearing design methodology for fixed-vane revolving vane compressor are discussed in Chapter 6.

After detailed theoretical studies have been completed, the design details of the prototype of a fixed-vane revolving vane compressor are presented in Chapter 7. The component design, the method of lubrication and the dynamic balancing issues are

addressed in this chapter. Chapter 8 presents a useful method on designing the lubrication system for the compressor. The experimental work commences in Chapter 9. The setup of experimental test bed and the preparation of the prototype are presented in this chapter. In addition, the findings from the measurements will be compared with theoretical predictions to validate the mathematical models. The chapter concludes with a post experimental analysis.

Chapter 10 presents three optimization studies to minimize frictional losses, leakage losses and maximize the coefficient of performance respectively for fixed-vane revolving vane compressor after the aforementioned mathematical models are validated. The dissertation concludes with Chapter 11 with a summary of the contributions during the course of this research project. The future works are listed to further develop this new compressor mechanism with an ultimate objective of finalizing it into an actual commercial product.

Chapter 2

Literature Review

2.1 Introduction

This chapter consists of three sections. Firstly, a review of existing compressor designs and their characteristics are presented. Secondly, the evolutions in the simulation studies for positive displacement compressors performance evaluation are discussed. The chapter ends with concluding remarks on the compressor research directions.

2.2 Review of Compressor Designs

A number of positive displacement type compressor designs will be shown in this section with the attention to the mechanism design and its limitations.

2.2.1 Reciprocating Compressor

Reciprocating compressor is one the earliest compressors being used. Figure 2.1 shows the schematic view of a reciprocating compressor. The reciprocating compressor comprises of a piston, which is connected to the assembly of a crank and a connecting rod. The crank rotates in a full revolution and drives the piston into a reciprocating motion. The working fluid enters the working chamber through suction port when the volume expands. The working fluid is being compressed by the piston as the volume reduces and discharges out of the working chamber through discharge port according to

the prescribed discharge pressure. In the reciprocating compressor design, suction and discharge valves are required in order to ensure the direction of working fluid flow.

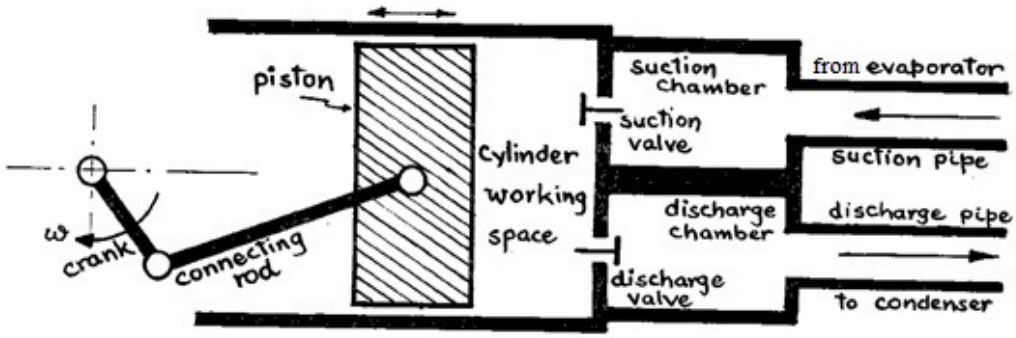

Figure 2.1 Schematic view of a reciprocating compressor [6]

Suefuji and Nakayama [7] presented the experimental evaluation of reciprocating compressor performance. The results had shown that the mechanical losses increase with an increase in the piston stroke. In addition, the increment in the ratio of the connecting rod length to the crank radius reduces the mechanical losses while the other losses such as suction and discharge losses are unchanged. On the other hand, the working chamber volume at the end of the discharge process is known as the clearance volume. The remaining working fluid in this volume will undergo re-expansion, which affect the intake of fresh working fluid. Furthermore, the amount of working fluid intake is also dependent on the suction valve behaviour. As a result, the volumetric efficiency of reciprocating compressor is poor due to these two factors.

The valve system in reciprocating compressor has a decisive influence on the compressor performance as it is involved in the intake and the delivery of the working fluid [8]. The valve system in reciprocating compressor belongs to automatic reed valve type and it is subjected to two types of fatigue damages such as bending fatigue and

impact fatigue. Therefore, it is expected that the life span of the valve will deteriorate and the reliability of the compressor is downgraded.

The vibration and noise generated during the operation is one of the serious issues in reciprocating compressor performance. The inertia force from the reciprocating motion of the piston and the compression pressure force acting on the piston are unequal. Therefore, unbalance force results and contributes to vibration and noise. Saito et al. [9] reported that the reduction in reciprocating compressor noise can be achieved by restricting the compressor shell shape. In the same year, Tojo et al. [10] improved the shell structure to reduce noise production. Futakawa [11] reported that the development in noise and vibration control for reciprocating compressor moves towards to the reduction in compressor shell vibration due to the inherent shortcomings of reciprocating compressor design. Levecque et al. [12] proposed a multi-stage balancing method based on finite element model.

On the other hand, the frictional losses in this compressor design are significant due to frequent rubbing between several parts such as the contact between the cylinder and the piston, the joint between the crank and the connecting rod, the joint between the connecting rod and the piston. In addition, the size disadvantage is obvious when compared to the rotary type compressor as the reciprocating compressor is usually bulky and requires more space due to the crank mechanism. However, Kaiser and Kruse [13] stated that the reciprocating compressor which have piston rings is at an advantage in terms of volumetric efficiency. The piston ring effectively seals the axial leakage through the clearance between the outer circumferential surface of the piston and the inner surface of the stationary cylinder wall.

2.2.2 Sliding Vane Compressor

Figure 2.2 shows the schematic view of a rotary type sliding vane compressor. The rotor has several radial or non-radial slots in which the vanes are allowed to slide. The rotor, which is eccentrically placed to the stationary cylinder, rotates and set the vanes into rotational motion with their tip sliding on the inner cylinder wall. Hence, the space surrounded by the inner cylinder wall, the rotor and any two adjacent vanes forms the working chamber. The suction and the compression process of the working fluid take place simultaneously in the sliding vane compressor design. The pressurized working fluid is being delivered when the working chamber is exposed to the discharge port. It is observed that the tip of the vane must always kept in contact with the inner cylinder wall in order to have compression effect or otherwise. This is achieved by the centrifugal force from the rotation of the rotor, where the centrifugal force pushes the vane tip against the inner cylinder wall.

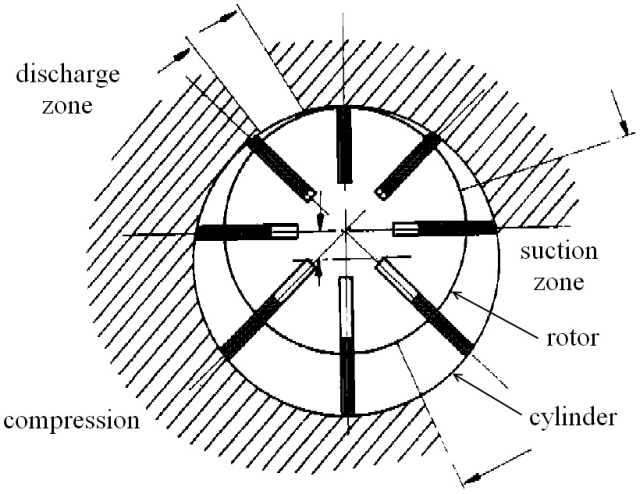

Figure 2.2 Schematic view of a sliding vane compressor [14]

Tojo et al. [15] reported the dynamic behaviour of the sliding vanes theoretically and experimentally. A chattering phenomenon was found under low-speed operation as the vane tip is detached and pushed back to the inner cylinder wall. As a result, the durability of the sliding vane compressor is doubtful since the vanes suffer from impact fatigue. In addition, the short detachment between the vane and the inner cylinder wall induces internal leakage, and thus volumetric efficiency is reduced. Shu et al. [16] suggested an appropriate constant vane slot back pressure can effectively guarantee the contact of vane tip and the inner cylinder wall.

In sliding vane compressor, the suction and the discharge processes are continuous and thus, it is a valve-less machine. This unique characteristic greatly enhances the reliability as the valve fatigue failure can be avoided. As a result, sliding vane compressor has a built-in volume compression ratio and the pressure of the working fluid at the end of the compression process is predetermined by the suction pressure. Tramschek and Ooi [14] reported that the matching between the positions and the geometry of the suction and the discharge ports with the built-in volume ratio is important in order to optimize the compressor performance. In other words, the sliding vane compressor requires a discharge valve for serving a wide range of pressure ratios.

From the viewpoint of vibration, the excitation of sliding vane compressor is mainly due to the vane imbalance. With reference to the work conducted by Yee and Soedel [17], the compressor has no rotating imbalance in the case of four identical vanes at equal spacing. Thus, in terms of the vibration issue, the sliding vane compressor is superior as compared to reciprocating compressor. On the other hand, the dynamic analysis for tilted vane has also been investigated. Tramschek and Mkumbwa [18] analyzed the performance of a six-vane sliding vane compressor having

inclinations in the range of -30˚ and +30˚ . The results have shown that the compressor fitted with forward inclination angle of 5˚ have enhanced specific capacity. However, the increment is relatively small as compared to the compressor with radially aligned vane and this would not justify the increasing manufacturing cost associated with inclined vanes.

Despite the aforementioned advantages of sliding vane compressor, the compressor is not without its disadvantages, particularly the frictional loss. The constant rubbing between the vane tip and the inner cylinder wall generates enormous frictional loss [19, 20] and thus, the mechanical efficiency is low. The vane requires special surface treatment [21] and inherently increases the production cost. As a result, the sliding vane compressor lost its popularity among the positive displacement type compressors due to inherent high frictional loss and wear.

2.2.3 Rolling Piston Compressor

Figure 2.3 shows the schematic sketch of a rolling piston compressor. During the operation, the eccentric which is connected to the driving shaft rotates the roller and causes the volume trapped within the inner wall of the cylinder, the roller and the vane to vary and hence results in a compressor cycle. In the rolling piston compressor design, only discharge valve is required as the compression chamber is isolated from the suction chamber.

As compared to reciprocating compressor, the rolling piston compressor is well known to its compactness, light weight and high volumetric efficiency. The most notable characteristic of the rolling piston compressor is the use of vane-spring assembly. The vane is attached to a spring and the other end of the vane is kept in

contact with the roller during the operation. Ooi et al. [22] discussed the effect of spring stiffness on compressor performance. It was found that the magnitude of spring stiffness is related to the pressure in the compressor shell. The frictional losses of rolling piston compressor in a low-pressure shell will be marginally reduced when a spring of high stiffness is used but incurs higher starting torque.

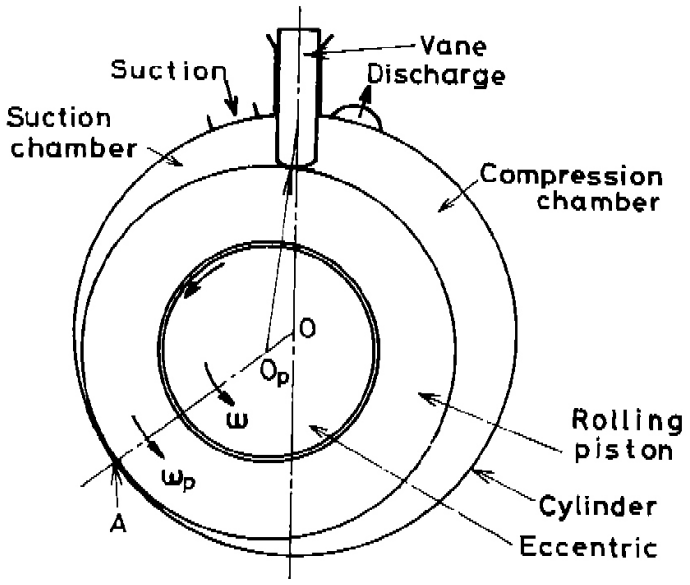

Figure 2.3 Schematic view of a rolling piston compressor [23]

Liu and Kosco [24] discussed the tilt angle of vane in rolling piston compressor. The theoretical results have shown that with a certain positive titled angle, the normal force to the vane tip is the minimum but the frictional loss at the vane tip remains unchanged. Thus, the titled vane only improves the durability and the reliability of the vane and roller, whereas the mechanical efficiency is not. Apart from this, the vane jumping phenomenon is also observed during start-up process and causes loud noise. Bae et al. [25] shown that the vane jumping phenomenon graphically and suggested a light vane should be used to prevent jumping behaviour.

Yanagisawa et al. [26] examined the vibration behaviour of rolling piston compressor. It was found that the vibration is induced by the change in gas compression moment, the motion of the roller with the eccentric and the reciprocating motion of the vane. The analysis has shown that the vibration amplitude during steady state operation can be approximately predicted by the maximum gas compression moment and moment of inertia of the stationary part. The vibration magnitude decreases with increasing moment of inertia but it is hardly affected by the spring stiffness. In addition, during the start-up and shut-off process, the vibration magnitude decreases as spring stiffness increases but the influence of moment of inertia on it is weak.

The rolling piston compressor has high frictional loss at the vane side due to the high relative velocity between the reciprocating vane and the stationary cylinder and the normal force resulted mainly from the pressure difference between both suction and discharge chambers. Therefore, extra surface treatments are necessary to be applied on the roller, vane and the eccentric [27-29] to maintain the reliability of the rolling piston compressor at an additional production cost.

2.2.4 Screw Compressor

The screw compressor (also known as twin screw compressor) is a rotary type positive displacement compressor and it is often applied in medium to large capacity applications such as chillers. As shown in Figure 2.4, the screw compressor has two intermeshing helical rotors, where the lobe (male rotor) meshing into the corresponding flute (female rotor). The working chamber is the space in between the lobe and flute. Similarly to sliding vane compressor, screw compressor operates without valves and has built-in volume ratio.

Fujiwara and Sakurai [30] described the entire working process of screw compressor as four consecutive phases. The first phase is a suction phase, where the pair of lobe and flute starts to un-mesh, a space is created and the gas is drawn through the suction port until the trapped pocket of working fluid is isolated from the suction and the discharge port. During the transfer phase, the pocket of working fluid is being transferred by moving circumferentially due to continuous rotors rotation. Subsequently, the mesh point moves axially towards the discharge port, the volume of trapped working fluid is gradually reduced and the pressure is thus increased. Lastly, at the moment which is pre-determined by the built-in volume ratio, the pocket of compressed working fluid is released through the discharge port. It is observed that the male and the female rotor are concentric to their own axis of rotation during the operation. In the same paper, a preliminary experimental analysis for the screw compressor was carried out. During the operation, the dynamic forces are induced and cause vibrations along the axial and the radial directions. These vibrations are transmitted through the bearings to the compressor casing. However, the magnitude of the vibration is experimentally shown to be relatively low as compared to reciprocating compressor.

Fujiwara et al. [31] shown that the torque requirement and the volumetric efficiency decreases as the intermeshing rotors clearance increases. The leakage through the clearance has severe effect on the volumetric efficiency of the screw compressor. Nevertheless, the great improvement in machining techniques nowadays has dramatically enhanced the performance by engaging tighter clearance. However, the tighter clearance increases the viscous loss of the flow in between the intermeshing rotors, which leads to the reduction in mechanical efficiency.

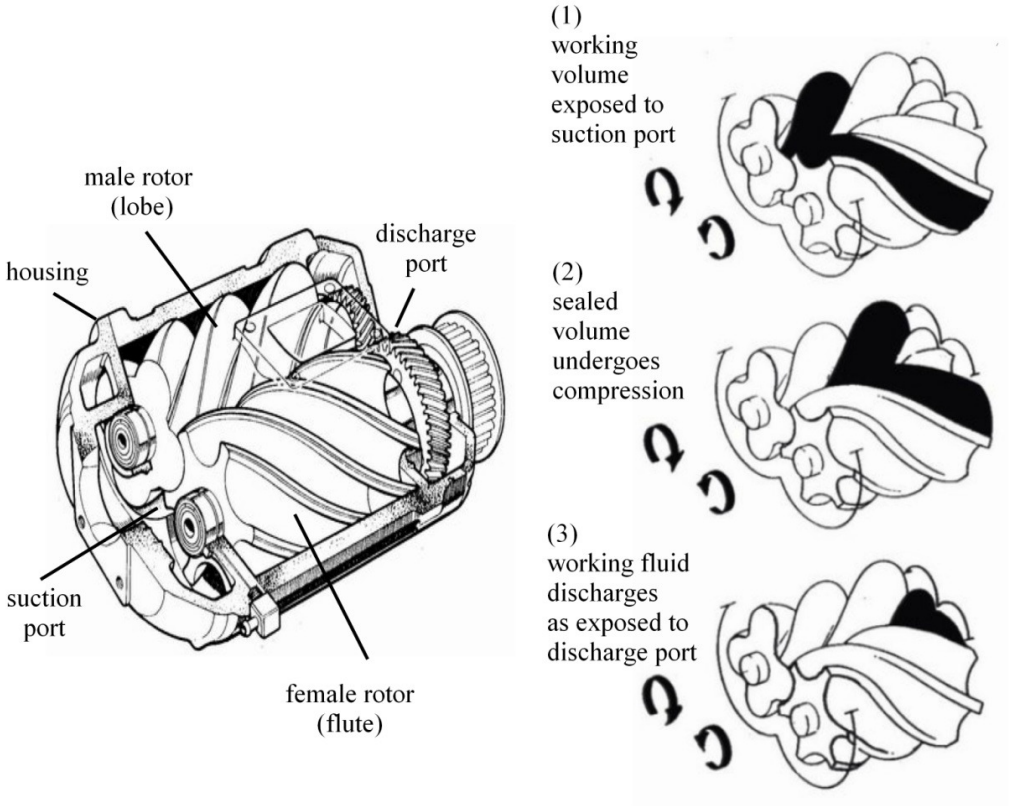

Figure 2.4 Schematic view of a screw compressor [32]

Sangfors [33] formulated an analytical modelling for the screw compressor performance and experimentally proved that a newly developed rotor profile has greatly improved the specific power consumption. In addition, Mujic et al. [34] discovered that the gas pulsation of the screw compressor can be improved by altering the discharge port shape. On the other hand, the application of the dry screw compressor is achievable by impinging the volatile liquid to the hottest position of the compressor component, which is in the vicinity of the end of the discharge process [35]. The vastly improved computational capabilities enhance the design of the screw compressors. The multi-variable optimization study is introduced to establish an efficient screw compressor for a given duty[36, 37].

Shaw [38] did a projection for screw compressor future. The author deemed that the compressor has innate potential in reliability since it involves only two purely rotational rotors and no valves are required. However, the screw compressor is not forgiving of its profile. As a result, the best available manufacturing and inspection technique needs to be employed in order to achieve the inherent good reliability potential [39-42].

2.2.5 Scroll Compressor

The working process of a scroll compressor is shown in Figure 2.5. The main elements of a scroll compressor are the two identical involute spiral scrolls. The scrolls are assembled at a relative angle of 180° such that both scrolls touch each other at several points and form a series of crescent-shaped pockets. During the operation, one of the scroll members is fixed and the other scroll orbits around the centre of the fixed scroll. The inlet port of the scroll compressor is at the periphery of the scrolls. As the orbiting scroll rotates, the working fluid is drawn through the periphery and trapped inside a pocket. The working fluid is then being compressed due to volume reduction while moving towards to the centre of the scroll. The gas is exhausted through the discharge port, which is at the centre of the fixed scroll. As similar to the screw compressor, the working fluid flow is continuous and no valves are required.

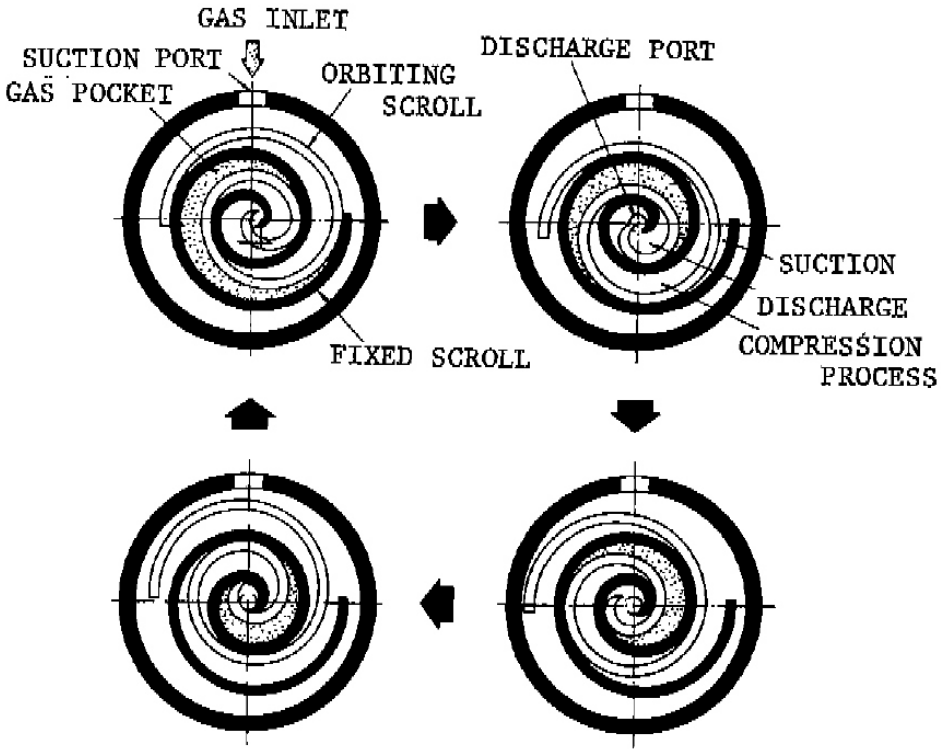

Figure 2.5 Schematic view of a scroll compressor [43]

The concept of scroll compressor was firstly described in 1905 by Creux [44]. The concept was not fully developed for practical application due to the lack of precise production techniques and component wear resulted from large axial working fluid force. In 1984, Tojo et al. [43] had developed a unique controlled thrust force mechanism for scroll compressor and put into commercial production. As compared to conventional reciprocating compressor, the scroll compressor was 10% higher in mechanical efficiency, 40% smaller in size, 15% lighter in weight and noise level is lower. In addition, the fluctuation of the driving torque in the scroll compressor is about one-tenth of that in reciprocating and rolling piston compressor because there are two to three working chamber volumes are under compression simultaneously during the operation. Hence, the operation is significantly smoother. Ishii et al. [45] shown that the scroll compressor is superior in terms of capability of alleviating the vibration problems,

as compared to reciprocating and rolling piston compressors. Nevertheless, the mechanical efficiency of scroll compressor is lowered by 10.8 % and 12.0 % as compared to rotary type compressors. This is because the scroll compressor requires thrust bearing support due to the large thrust force and hence, the mechanical efficiency is suffered due to higher energy consumption.

It is observed from the scroll compressor design that the geometry and the profile of the scrolls are complicated. Etemad and Nieter [46] conducted a parametric study and reported that the scroll wrap thickness is an important role in the scroll compressor performance. The scroll wrap must be rigid enough to sustain the working fluid force and thermal distortion during the operation. In addition, general design process for the scroll profiles is also proposed [47, 48]. On the other hand, a number of studies have reported that the leakage through the axial clearance at the tip of the scroll wrap has more dominant effect than the leakage through the radial clearance at the flank of the scroll wrap [49-51].

The applications of the scroll compressor have becoming more popular as it is frequently adopted for the CO_2 refrigeration system. A number of studies have been performed to improve the volumetric efficiency by considering the effects of the surface roughness of the mating scroll parts [52] and the thermal expansion on the volumetric efficiency have been studied too [53]. In addition, the thrust bearing design due to the large pressure difference at both ends of the compressor has been improved [54, 55]. On the other hand, the scroll compressor is also adopted in the automotive air conditioning system [56-60].

Although the reliability of the scroll compressor can be improved with the aid of greater computing capability [61-63] and the efficiency is higher as compared to reciprocating compressor, it is not yet completely dominant in the compressor markets. It is deduced that the complicated spiral profiles of the scroll and the required precise manufacturing technique, which is closely related to the production cost, are the main blocks as compared to the purely cylindrical components of rolling piston compressor. Furthermore, as same as the screw compressor, the leakages through the tip and the flank of the scroll compressor will be significant if the clearances are not well controlled. Hence, the best performance of the scroll compressor would be limited to those inherent properties.

2.3 Review of Simulation Studies

In general, the theoretical models for evaluating compressor performance can be classified into two categories, i.e., general-purpose model and special-purpose model. The former represents the thermodynamics and valve dynamics models in the compressor while the latter includes the leakage of the working fluid, the heat transfer inside the working chamber and the entire compressor lubrication model. Thus, the integration of both kinds of models will form the most comprehensive compressor model. In this section, the developments in the simulation studies for compressors performance evaluation will be presented.

2.3.1 Thermodynamics Model

Thermodynamics model is important as it describes the process of working fluid in a compressor operation and reveals the variations of pressure, temperature and mass inside the compressor working chamber. In summer 1972, Soedel [64] published a short

course text which describes the fundamental computer simulation for a positive displacement reciprocating type compressor. The working fluid behaviour is modelled as a polytropic process and some experiments were carried out to obtain the empirical coefficients. In the same year, Squarer and Kothmann [65] conducted a simplified analysis for reciprocating compressor computer simulation. The model was done by considering the working fluid as ideal gas behaviour and it is able to predict the primary characteristics of reciprocating compressor performance. Karll [66] also demonstrated the use of equation of state in the First Law of Thermodynamics analysis for a reciprocating compressor. Prakash and Singh [6] applied First Law of Thermodynamics to model the process of working fluid under assumption of ideal gas behaviour. The authors claimed that the simulation model is not adequate to evaluate basic compressor cycle and suggested the real gas properties should be considered in the future simulation model.

In 1976, Rottger and Kruse [67] incorporated the real gas equation of state into the simulation model to compare the both applications. It was found that the real gas behaviour is favourable in the compressor performance evaluation. In addition, Hiller and Glicksman [68] also adopted real gas properties in their total compressor system simulation model. The simulation models were verified by conducting the experiments for three different compressors and the agreement is close. In 1980, Ng et al. [69] carried out the simulation for a reciprocating compressor when the thermodynamic properties of the working fluid properties are represented by real gas equation of state and compared the results with that from the ideal gas behaviour approach. The authors claimed that the usage of real gas behaviour gives a significant improvement in accuracy of various parameters of interest only when the superheat at the compressor

suction inlet is as small as 10 ˚F or pressure ratio is as large as 14. On the other hand, Lee et al. [70] investigated the difference in adopting first law analysis and polytropic model to describe the compression or expansion process using ideal gas relationship. The results show that both approaches provide good match with the provided benchmark working chamber pressure but the prediction on working fluid temperature inside the chamber is better in first law analysis than in polytropic model.

Sun and Ren [71] conducted the computer simulation for working process in a reciprocating compressor using First Law of Thermodynamics and real gas equations. The simulation results agreed well with the practical measurements, particularly the working chamber pressure and the displacements of suction and discharge valve. In addition, Ooi and Wong [72] also presented an analytical studies for rotary type rolling piston compressor. The state of the working fluid in the study is obtained by applying the First Law of Thermodynamics and real gas equations. The study has shown that the model is capable of predicting the compressor performance with a discrepancy of about 10 % when compared with the available experimental data.

The adoption of real gas equation of state reveals the true thermodynamic behaviour of working fluid but incurs a lot more computational time in the early days. However, the tremendous increase of computational power solves the dilemma between adoption of ideal gas and real gas equation of state. A fully comprehensive description of working fluid behaviour is now available in commercial packages and it is easily integrated into main simulation studies. Undoubtedly, the applications of First Law of Thermodynamics and real gas equation of state are now the way to model the process of working fluid in the research of various refrigeration compressors [73, 74], although ideal gas equation is still employed purely for convenience [75].

2.3.2 Valve Dynamics Model

The valve performance is another important model to accurately simulate the process of working fluid in a compressor. In most positive displacement compressors, the valve is applied at the suction or (and) the discharge port to prevent the reverse flow of the working fluid. The valve has infinite combination of geometries and thus the behaviour can be complex. The performance of the valve is one of the major influences on compressor performance [76] because some compressor failure cases are attributed to the valve failure, which is normally due to fatigue fracture [77].

Since 1950, a number of relatively simple numerical mathematical models have been developed to describe the interaction between the compressor valve and the working fluid. Basically, the valve movement is described by a non-linear differential equation. According to the review by MacLaren [78], the first worthwhile mathematical model for the reciprocating compressor and its valves was presented by Costagliola [79] in 1950. The model was claimed as essentially correct although the calculated results were not shown superimposed on the experimental results. Since then, all the valve models were based to some degree on the pioneer analysis by Costagliola [79]. In 1967, MacLaren and Kerr [80] concluded that an analytical model for valve performance is important as it could provide qualitative results much more rapidly and cheaper than an extensive experimental approach. Two years later, Wambsganss and Cohen [81] developed a similar model and made comparisons to the experimental results. The authors concluded that the single degree of freedom approximation is not sufficient to represent valve reed dynamics in a high speed compressor and the effect of valve stiction is large at low values of compressor pressure ratio. Traversari and Lacitignola [82] in 1970 constructed a model based on the work by Costagliola [79]. The authors

concluded that the differences between analytical and experimental results were mainly due to the error in selection of values of empirical coefficients such as discharge and damping coefficients. As a result, all of the aforementioned models are semi-analytical since several empirical coefficients have been included and generally evaluated by experiment.

The analytical study for the valve performance progressed and many researchers actively published on different numerical approaches. Gatecliff and Lady [83] presented a model for forced vibration of a cantilever valve reed with a non-uniform width. The model excludes the damping effect and it was solved by using Rayleigh-Ritz method and Galerkin's method. The calculated results agree well with the experimental results. Woollatt [84] presented a numerical method for calculating the lift and pressure drop for self-actuating compressor valves based on single degree of freedom approach. The method was compared with measured results and the agreement is shown to be good. Gatecliff et al. [85] has outlined a simplified procedure, which is used to design a cantilever valve reed and indicates the valve performance approximately. Piechna [86] conducted a numerical study on dynamic behaviour of a reed valve of constant thickness and rectangular cross-sectional area with the special attention to the configuration of the valve plate. It was found that the valve plate with constant height causes a strong bending and oscillation of the valve reed and thus, oblique shape valve stop is preferred. Ooi et al. [87] presents a simulation model for a typical reed valve in a small refrigeration rolling piston compressor. The mode shape function of the reed valve is taken as a standard polynomial function and the valve deflection resulted from it is in good agreement with that of finite element analysis. The authors concluded that

the valve thickness has a remarkable effect on the compressor performance in terms of discharge loss and indicated power.

Friley and Hamilton [88] became the first to apply finite element method (FEM) to predict the stress experienced by the valve in 1976. The valve is modelled by using triangular element with three nodes and each of which possesses six degrees of freedom (DOF), results in an 18-DOF element. Santos et al. [89] proposed that a 9-DOF element is sufficient for evaluating the natural frequency and mode shape of the valve. The authors agreed that Cowper element, which is an 18-DOF element, is recommended to use for conducting stress analysis on the valve. Fagotti et al. [90] emphasized the flexibility in finite element approach by proposing a valve with a variable width. The results show that the valve displacement evaluated through the mass-spring model is higher than that predicted by the finite element approach, as compared to the experimental results. On the other hand, the computational fluid dynamics (CFD) techniques were also introduced into valve performance studies, with special emphasize on the suitability of applying CFD technique [91] and the fluid structure interaction [92, 93].

The general developments of the valve modelling techniques have been reviewed and all of the above are deemed as exhaustive in computing effort. The complete modelling for the valve performance will not only include the valve displacement behaviour, but also include the analysis of impact and stress, the effective flow and force areas, the failure mechanism, the fluid flow visualization and others.

2.3.3 Heat Transfer Model

During the compressor operation, the heat transfer between the working fluid and the surrounding working chamber is important as it affects the pressure variation inside the working chamber and thus, the bearing load and the coefficient of performance are also affected. Literature shows that heat transfer correlations for in-chamber convective heat transfer for positive displacement machines were mainly developed during early 70s and late 80s. The correlations are mainly for reciprocating engine and only a few are for reciprocating compressors. The importance of the heat transfer model in a comprehensive study of compressor has been proposed and debated during 80s-90s. Brok et al. [94] and Chen [95] indicated that the in-chamber heat transfer does have an influence on the volumetric efficiency and the indicated work of a compressor. In addition, Prasad [96] pointed out that the temperature is a defining parameter in the compressor operation as it affects the dimensional stability and integrity of the components. Hence, the impact of heat transfer should be addressed from the reliability point of view. The basic focus for the heat transfer model in compressor study is to determine the instantaneous convective heat transfer coefficient for the convective heat transfer between the working fluid and the surrounding chamber wall. Adair et al. [97] reviewed, discussed and compared the available correlations for in-chamber convective heat transfer in internal combustion reciprocating engines. The authors derived a new correlation which suitably addressed the effect of in-chamber convective heat transfer in reciprocating compressor and correlates the experimental data within 20%. Annand [98] proposed another correlation for internal combustion reciprocating engine, which is expressed as a function of Reynolds number only. In addition, Liu and Zhou [99] incorporated the heat transfer model into their reciprocating

compressor simulation model. The proposed correlation is similar to Adair's correlation with different empirical constant. On the other hand, the instantaneous convective heat transfer between the working fluid and the surrounding chamber has been studied by numerical techniques too [100-103]. This kind of approach does not require any heat transfer correlation but it is computationally expensive.

The development of in-chamber convective heat transfer correlation ceases after late 80s and the available convective heat transfer correlations contributed by early researchers were frequently applied in the energy analysis of hermetic compressors. In the energy studies of hermetic reciprocating compressors, the influences of different correlations for the convective heat transfer coefficient between the gas and the cylinder walls on compressor performance were evaluated. Todescat et al. [104], Fagotti et al. [105] and Longo et al. [106] indicated that the correlation by Annand works in good agreement with experimental data. In addition, Ooi [107] applied the correlation proposed by Adair et al. in the heat transfer study of a hermetic reciprocating refrigeration compressor. The prediction is in good agreement with the measured results, with discrepancies mostly less than 10%. On the other hand, in the heat transfer analysis of a hermetic rolling piston rotary compressor by Padhy et al. [108, 109], the correlation by Adair et al., which was originally derived for reciprocating compressor, was used. The experimental data agreed very well with the theoretical predictions of the heat transfer model.

On the more recent studies, convective heat transfer between the working fluid and the surrounding chamber was considered in the studies of scroll compressors and screw compressors. Chen et al. [73, 110] incorporated the heat transfer model into the compression process of scroll compressor by approximating the convective heat transfer

coefficient with a correlation for a spiral plate heat exchanger. Jang et al. [111] concluded that by having considered the heat transfer between the scroll plate and the working fluid, the prediction of discharge temperature is in better agreement with the measured values. In addition, Ooi and Zhu [112] concluded that heat transfer should be considered for accuracy of thermodynamic process in scroll compressor simulation. Sun et al. [113] also included the convective heat transfer between the working fluid and the surrounding chamber by adopting the empirical correlation proposed by Jang et al. [111]. Wu et al. [114] addressed the effect of convective heat transfer between the working fluid and the surrounding chamber too in the study of twin screw refrigeration compressor.

2.3.4 Leakage Model

All positive displacement type compressors operate with undesirable mass loss due to internal leakages of working fluid [115, 116]. Internal leakages decrease volumetric efficiency and thus, the cooling capacity and coefficient of performance of the compressor are affected. As a result, the behaviour of the leakage flow through the clearances in a compressor is worthwhile for investigation.

In 1978, Pandeya and Soedel [117] and Chu et al. [118] identified the various leakage paths in a rolling piston compressor. The leakage flow is modelled as a gas flow driven by pressure difference through a convergent-divergent nozzle under the consideration of ideal gas properties, constant flow area and the upstream pressure are approximated as an average of the suction and discharge pressures. Reed and Hamilton [119] questioned the nature of the leakage fluid and proposed two extremes cases for leakage flow investigation in a rolling piston compressor, where the upper bound is

assumed to be entirely compressible gaseous refrigerant filling the clearance and the lower bound is assumed to be an incompressible mixture of lubricating oil and gaseous refrigerant. The flow is also derived based on pressure differential flow through a convergent-divergent nozzle. The leakage flow measurement is found to be in between the upper bound and the lower bound. Rodgers and Nieter [120] claimed that the liquid oil-refrigerant mixture leakage flow model is the most appropriate model to predict realistic leakage flow. Yanagisawa and Shimizu [121, 122] investigated the leakage losses with a rolling piston compressor with the attention to flows through the radial clearance and rolling piston end face clearances. The dynamic change of the clearance and the frictional loss occurring in the narrow leakage flow channel, which have been neglected in the previous investigations are addressed. Since then, the leakage flow analysis includes the viscous effect [123-125].

2.3.5 Oil Lubrication Model

The lubricant is important in compressor operation as it is used to lubricate the sliding surfaces from excessive wear and improves the reliability and mechanical losses of the compressor. Therefore, a suitably designed lubrication system is crucial for a proper operation of a compressor and number of studies related to the lubrication system is therefore proposed. The fundamentals concerning the influence of oil on the various components of refrigeration system, particularly on the compressor has been addressed [126, 127]. The compressor is required to be well maintained at low temperature and the low miscibility between oil and refrigerant is desired to increase the oil viscosity and improve the hydrodynamic lubrication.

The oil feed mechanism of a high-side rotary type rolling piston compressor shaft has been studied [128]. The oil feed characteristics of the main bearing under no-load and dynamic conditions have been examined and it was found that the viscosity and the shaft rotational speed are the main factors to determine the oil flow rate. In addition, the oil feeding characteristics through spiral groove on the main bearing for a horizontal rotary type rolling piston compressor has been described theoretically [129]. It was experimentally found that the oil flow rate increases linearly with the groove depth up to 0.5 mm. The oil flow rate increases with the angle between the spiral grooves with axial direction, from 25˚ to 65˚.

The earlier analysis on the lubrication performance focus on the individual flow path, for example, the flow through journal bearing and the flow through spiral groove. In later days, the lubrication system analysis is extended to the analysis of entire flow paths assembly. The oil supply system in scroll compressor has been analytically studied [130]. The equivalent circuit has been employed to calculate the supply flow rate in order to match the required flow rate for the lubrication and the cooling effect of the bearings. It was found that the oil flow rate increases when the rotational speed increases. Similarly, the oil supply into various elements in a vertical [131, 132] and a horizontal [133] rolling piston compressor under steady state conditions has been studied by employing equivalent electric circuit network. The effect of journal bearing groove shape and the inclination angle of the groove on the oil flow rates have been investigated. In more recent studies, the oil pumping system design in reciprocating compressor with the attention to the oil climbing time from the oil sump to the required bearing surfaces has been studied using computational fluid dynamics [134-136].

2.4 Concluding Remarks

The research and development of compressor is still ongoing in the aspects of theoretical performance assessment and the practical investigation. In general, the review of existing positive displacement compressor designs reveals that the trend of the compressor design is moving towards to some common features, for example:

- The design is preferably to have minimum moving parts in order to keep frictional loss as low as possible
- The design should involve fewer components and simpler geometries. Hence, the compressor can be light in weight, compact in size, and low in production cost
- The design should possess inherent low vibration and noise level in the case where quiet operation is needed.

As a result, it can be foreseen that the rotary type compressors will gain the popularity and widespread usage over the veteran reciprocating compressor design in terms of size, efficiency, noise and vibration. Nowadays, equipped with the great improvement in computational power, the theoretical assessment for existing compressors designs and performance analysis can be improved and thus, the possibilities of a more energy-efficient existing compressor or even a new compressor design is expected.

Chapter 3

Revolving Vane Compressor – The Mechanism Design

3.1 Introduction

The inception details of a new rotary compressor called revolving vane compressor will be presented in this chapter. The compressor mechanism design is conceived with the objective to eliminate the limitations present in the current rolling piston compressor. This chapter starts with the analysis of the rolling piston compressor and the possible solutions for the limitations in the compressor. Subsequently, the novel revolving vane compressor design will be introduced and the possible design variants of it will be revealed. The type of the compressor design, which is going to be examined in the rest of the dissertation, will be concluded at the end of this chapter.

3.2 The Analysis of Rolling Piston Compressor Design

The rolling piston compressor is widely used in air conditioning and refrigeration industries owing to its simplicity in geometrical configuration, low production cost, the ease of manufacturing, low vibration and low noise. In its basic form, the rolling piston compressor has five components namely a cylinder, a roller, a shaft with an eccentric, a vane and a spring, as shown in Figure 3.1.

During the operation, the eccentric which is connected to the drive shaft rotates the roller and causes the volume trapped within the inner wall of the cylinder, the rotor

and the vane to vary and hence results in a complete compressor cycle. However, detailed analysis reveals that the rolling piston compressor is not without disadvantages due to its mechanism configuration from the point of view of frictional losses, especially during higher speeds of operation. With reference to Figure 3.1, the frictional losses associated with rolling piston compressor occur at the following six locations.

i. The roller and the eccentric
ii. The vane and the vane slot
iii. The tip of the vane and the roller
iv. The end faces between the eccentric and the cylinder
v. The end faces between the roller and the cylinder
vi. The shaft journal bearings

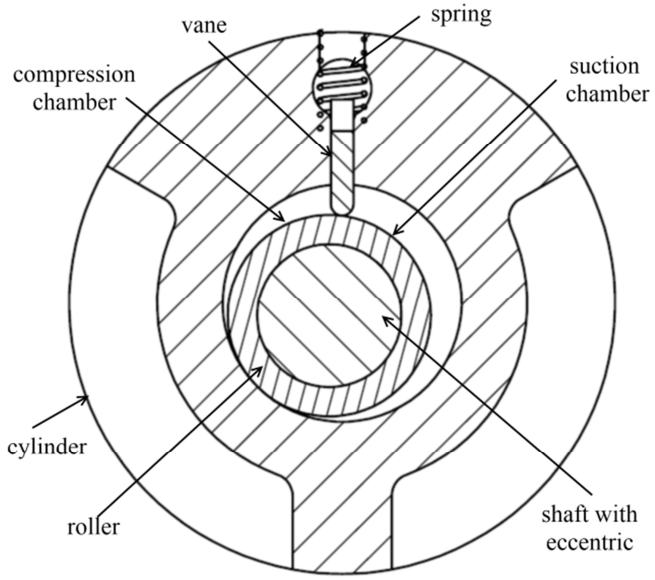

Figure 3.1 Schematics of a rolling piston compressor

The frictional losses in a rolling piston compressor during a typical compressor operation are presented in Table 3.1. It is known that if the frictional losses at various

contact locations in the rolling piston compressor can be eliminated or at least, significantly reduced, a better compressor design can be achieved.

Table 3.1 Frictional analysis of the rolling piston compressor [137]

Frictional Loss	Contribution
Loss due to vane side reactions to the vane slot	0.4 %
Loss due to vane tip and roller contact	0.9 %
Loss due to eccentric and roller contact	45.7 %
Loss due to roller and cylinder end faces	8.8 %
Loss due to eccentric and cylinder end faces	17.3 %
Loss due to journal bearing	26.9 %

3.2.1 Elimination of Roller and Eccentric Friction

The rubbing between the roller and the eccentric in the rolling piston compressor is mainly due to the contact between these two components, as shown in Figure 3.1. The role of the roller in the compressor is to reduce the friction at the vane tip. During the operation, the roller is always in contact with the vane tip on its external surface and the eccentric in its internal surface. If the friction at the vane tip is higher, the roller will rotate relative to the eccentric. However, if the friction between the inner surface of the roller and the eccentric is higher, the roller will rub against the vane tip. The use of the roller is able to lower the friction at the vane tip and at the roller; else the vane tip is constantly rubbing against the roller, which causes significant wear to the vane during a long-term operation.

By leading the lubricant to the contact area will effectively reduce the frictional loss at the interfaces of these components. However, it can be totally eliminated by

merging the roller and the eccentric to become only one component, as shown in Figure 3.2. The combination of the roller and the eccentric is named as rotor. In this case, the roller is no longer present and therefore, the energy loss due to the roller and the eccentric friction, which is as high as 45.7% of the total frictional loss as presented in Table 3.1, is completely eliminated. Furthermore, the number of components in the compressor has been reduced by one and the concentricity issues between the roller and the eccentric is no longer the concern, which is closely related to the manufacturing cost.

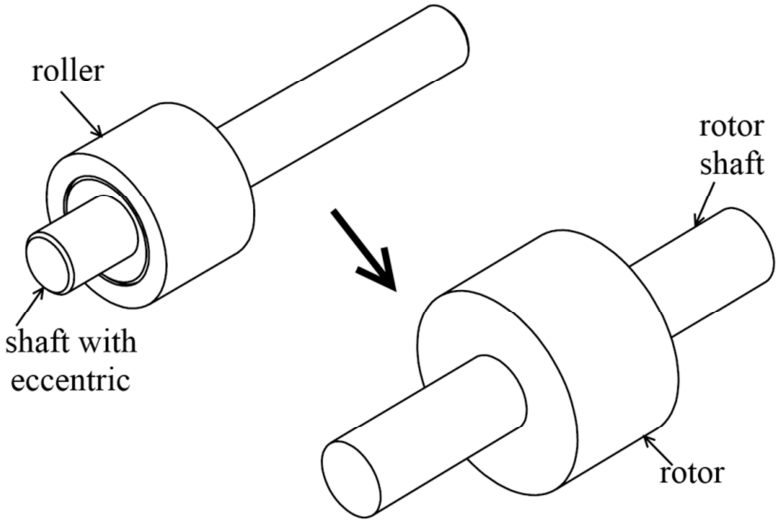

Figure 3.2 Merging the roller and the eccentric as one component – rotor

3.2.2 Removal of the Spring

As referred to Figure 3.1, the reciprocating motion of the vane inside the vane slot of the rolling piston compressor is constrained by the spring. In fact, the spring can be replaced by a vane pin joint and the vane slot can be created in the rotor, as shown in Figure 3.3. Thus, the friction between the vane tip and the roller can be totally eliminated. In addition, the vane tip is not in contact with any other component as a sufficiently deep vane slot in the rotor can be created such that the vane tip will not be

in contact with the base of the vane slot, as shown in the same figure. However, it is noticed that the friction due to the reaction forces between the vane side and the vane slot remains. The number of components has been further reduced by one since the usage of the spring is dropped and thus, the production cost can be lowered and the reliability can be improved.

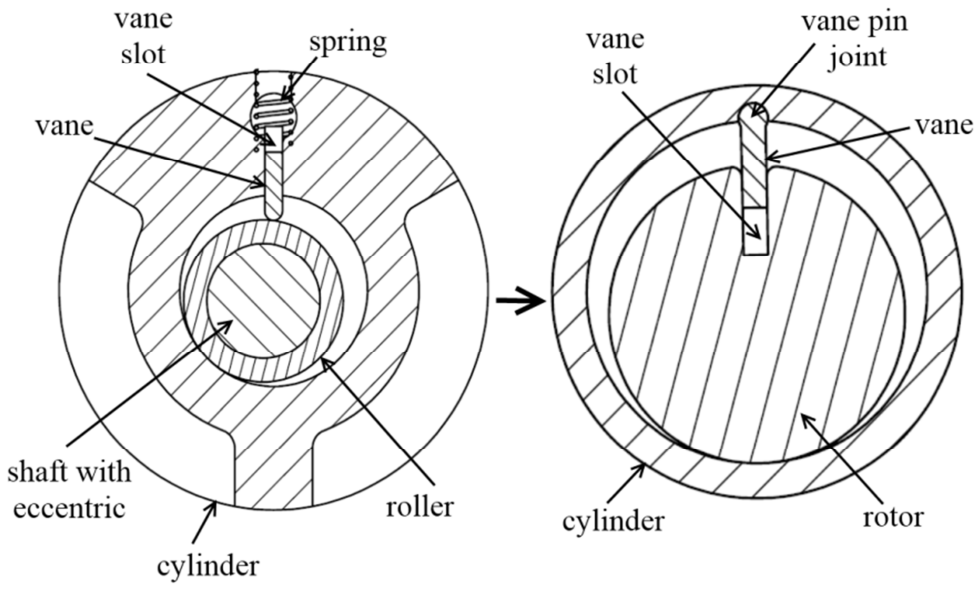

Figure 3.3 Replacement of the spring and the change of vane slot location

3.2.3 Reduction of End Face Friction

During the operation of rolling piston compressor, as the shaft rotates, both end faces of the roller and the eccentric rub against the stationary cylinder and hence results in a significant energy loss due to friction, as presented in Table 3.1. This friction can be significantly reduced by having a rotating cylinder together with the rotor. Since both rotor and cylinder rotate together at the same time, the relative velocity between them is relatively low and hence results in a lower end face friction.

3.3 The Novel Revolving Vane Compressor

The previous analysis for rolling piston compressor mechanism reveals that a better compressor mechanism can be achieved by

i. Merge the roller and the eccentric into one component (known as the rotor) to eliminate the friction between roller and the eccentric and reduce the number of components by one
ii. Remove the spring and replaced by vane pin joint on one end of the vane to further reduce the number of components by one. The other end of the vane stays in the vane slot inside the rotor
iii. Set the cylinder into rotational motion to lower the end face friction between the rotor and the cylinder

Based on the proposals above, a novel compressor design, known as revolving vane compressor is introduced, as shown in Figure 3.4. In its basic form, the revolving vane compressor consists of three main components, namely a rotor, a cylinder and a vane. The centres of the cylinder and the rotor are offset such that there is a line contact at the outer circumference of the rotor and the inner wall of the cylinder and this line separates the working chamber into two. These working chambers are formed by this line, the outer rotor surface, the inner cylinder surface and the vane. During the operation, the rotor rotates the vane which in turn rotates the cylinder. This causes the volume of the working chambers to increase and decrease in size and hence completes the working process of a compressor cycle. In the same figure, it can be observed that the suction and the discharge port are located at the rotor and the cylinder respectively. The valve reed is placed on the top of the discharge port.

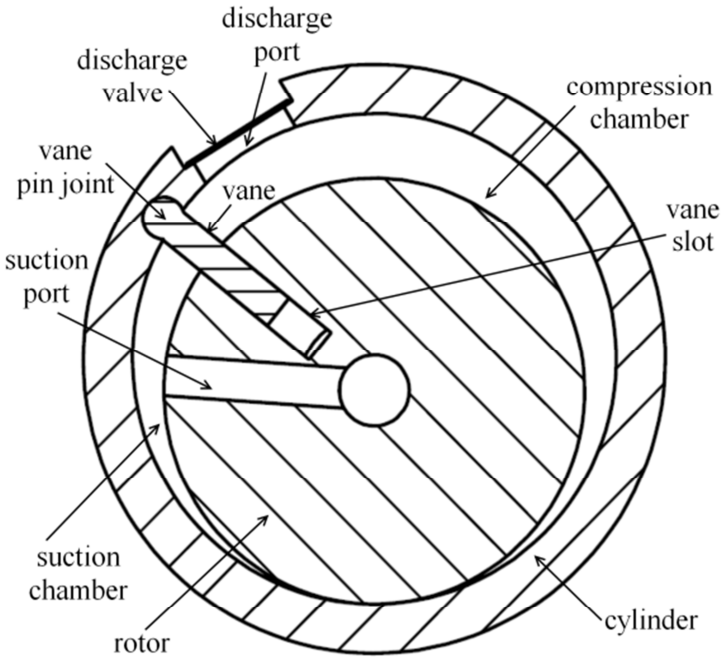

Figure 3.4 Schematics of a revolving vane compressor

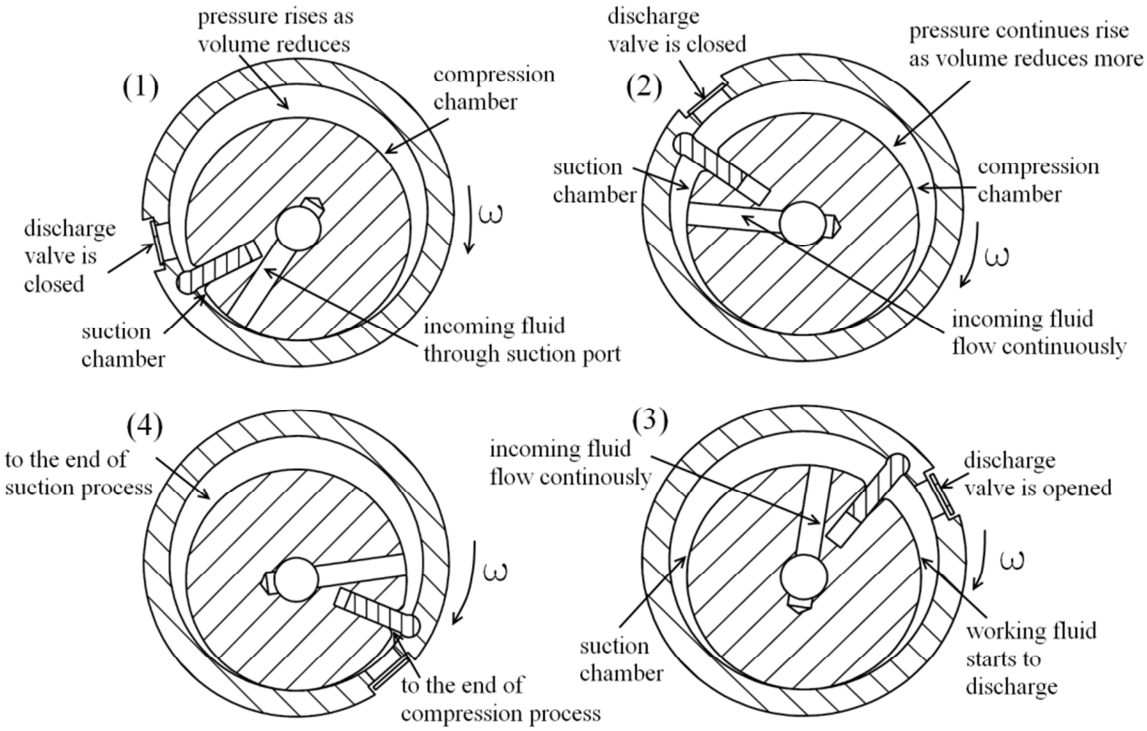

Figure 3.5 Snapshots of revolving vane compressor operation

Figure 3.5 shows the snapshots of the revolving vane compressor operation. The working fluid travels from the centre of the rotor shaft to the suction chamber, which experiences an increase in volume through the suction port. On the other side, the working fluid inside the compression chamber experiences increases in pressure since the chamber volume reduces with automatic valve reed kept closed. The discharge of working fluid starts when the working fluid pressure overcomes the valve stiffness and the prescribed discharge pressure. On the other hand, the rotor and the cylinder are supported by the journal bearings concentrically at their own centre of rotation on both ends, as shown in Figure 3.6. Further observations from the Figures 3.4 and 3.6 reveal that the frictional losses associated with this new compressor design are at the vane top, the vane side, the journal bearings and the end faces.

One of the frictional losses in revolving vane compressor is the friction that occurs at the end faces between the rotor and the cylinder and it is caused by the relative velocity between these two components. In addition, the journal bearing used to support the compressor also generates the friction caused by the hydrodynamic lubrication. Furthermore, the vane of the compressor is mounted in the cylinder with a pin joint on one end, and the vane slot in the rotor at the other end. The vane is therefore free to swivel about its pin joint and at the same time, it slides in and out of the vane slot, which incurs the vane top friction and the vane side friction respectively.

The total number of frictional loss sources has been significantly reduced to 4 as compared to 6 in a rolling piston compressor. However, the number of frictional loss sources is a secondary factor to determine the total frictional loss reduction. The

primary influences on the frictional loss are the total contact area and the relative velocity between the surfaces.

The total contact area between the surfaces is similar in both the rolling piston and the revolving vane compressors. The vane slides in the slot of the stationary cylinder in rolling piston compressor while the vane slides in the same manner in the slot of the rotor in revolving vane compressor. Thus, the vane-side contact areas in both compressors are similar. Furthermore, the vane tip is pressed on the eccentric component of the rolling piston compressor while the vane top swivels about the hinge joint in the rotating cylinder of revolving vane compressor. The vane tip (vane top for revolving vane compressor) contact areas are similar as the vane thickness are the same. In addition, the end face contact areas in both compressors are the same. The eccentric and the piston rub against the stationary cylinder at both ends while the combination of both (called rotor) rubs against the rotating cylinder in revolving vane compressor.

The difference in the total frictional loss between both compressor designs lies in the relative velocity between surfaces. The instantaneous dimensionless relative velocities at the vane side, vane tip and the end faces in both compressors over one operation cycle are disclosed in Figure 3.7. The decrease in the relative velocity between surfaces in the revolving vane compressor improves the performance in terms of the frictional losses as compared to the rolling piston compressor, especially in the frictional loss at the end face and at the vane tip.

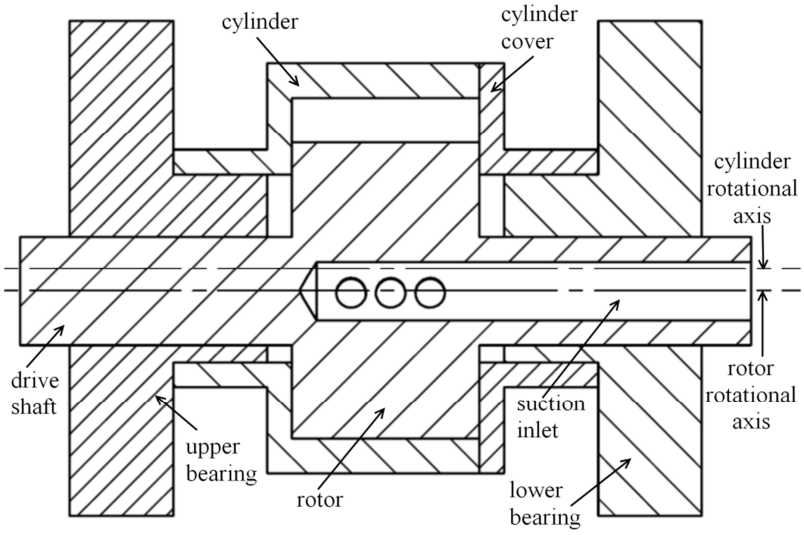

Figure 3.6 Side view of revolving vane compressor

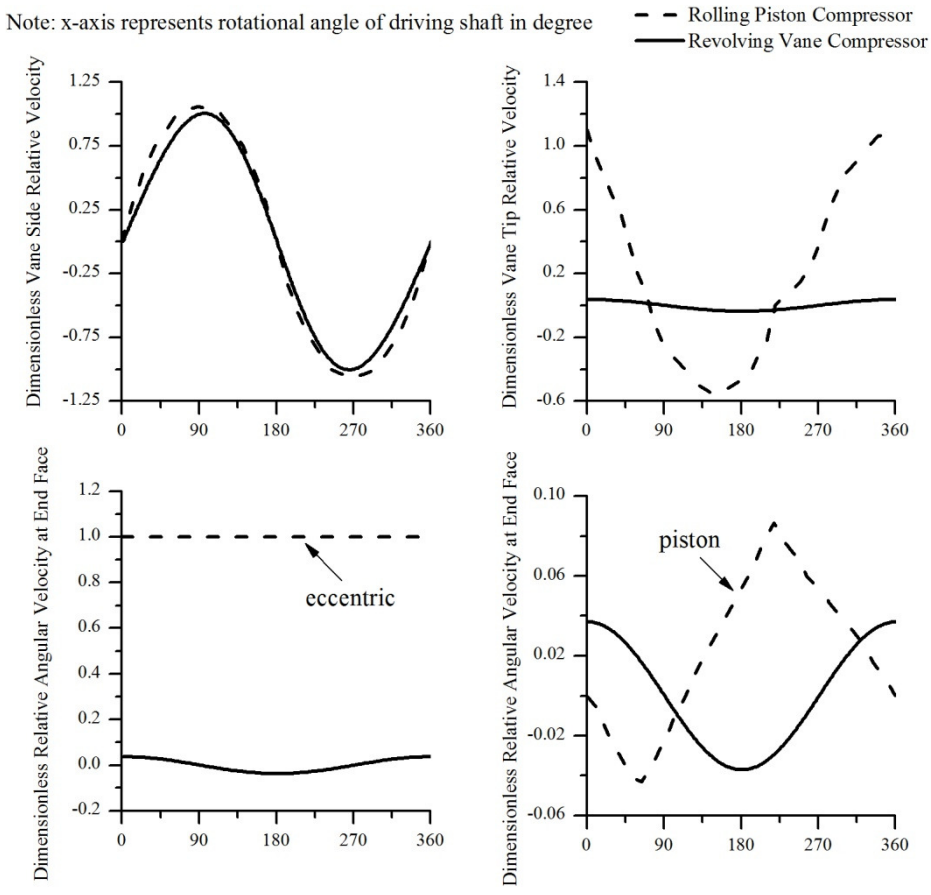

Figure 3.7 Comparisons of dimensionless relative velocities in rolling piston and revolving vane compressors

During the operation, both sides of the vane are subjected to the gas pressure force due to the suction chamber pressure (P_s) and the compression chamber pressure (P_c). The difference in the gas pressure force acting on the sides of the vane causes the vane to be hard pressed against the vane slot and hence resulted in high vane-side contact forces (F_1 and F_2), which in turns results in a significant frictional loss caused by the vane-side friction, as shown in Figure 3.8. It is noted that the vane slot clearance is being enlarged for demonstration purpose. The free body diagram of the vane shown in Figure 3.9 indicates that the magnitudes of the vane-side contact forces are mainly dependent on the gas pressure differential force across the vane (F_{spv} and F_{cpv}) and the tangential force (F_4) to drive the cylinder into rotational motion [138]. The contact forces can be expressed by equations (3.1) and (3.2).

$$F_1 = \frac{(L_1 - L_3)F_4 + (L_2 - L_3)(F_{cpv} - F_{spv}) - L_3F_c}{L_4 + L_3} \tag{3.1}$$

$$F_2 = \frac{(L_1 + L_4)F_4 + (L_2 + L_4)(F_{cpv} - F_{spv}) + L_4F_c}{L_4 + L_3} \tag{3.2}$$

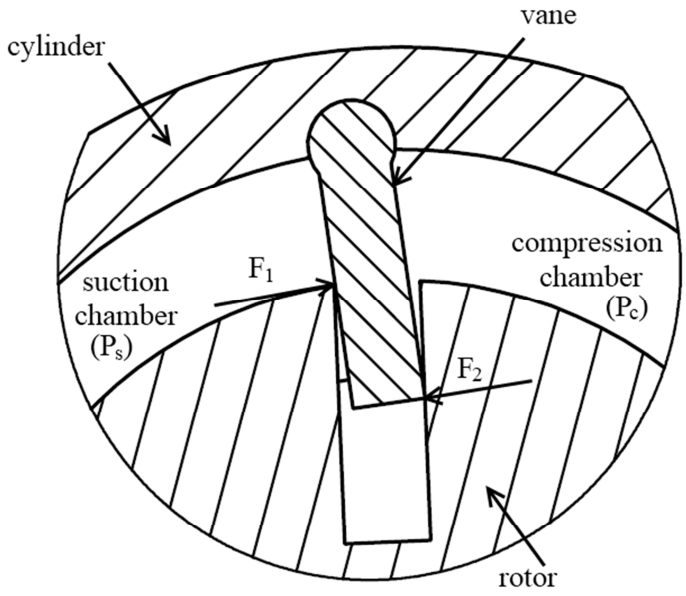

Figure 3.8 An enlarged view of vane and vane slot

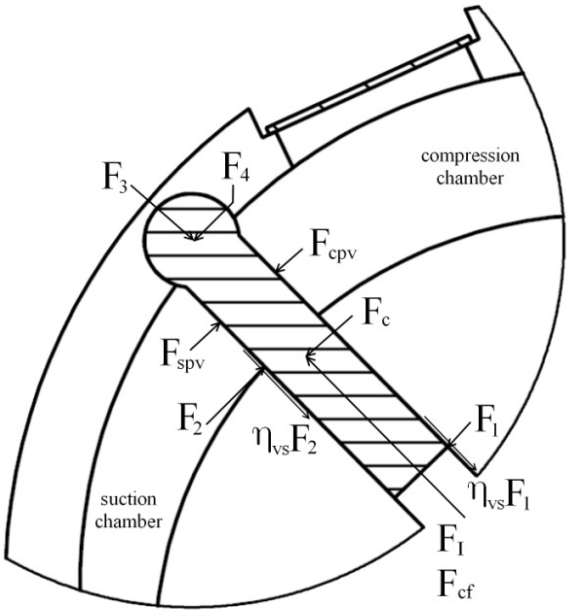

Figure 3.9 The free body diagram of the vane [138]

However, the dependency of the vane-side contact forces on the gas pressure differential force can be eliminated in the improved design concept, as presented in the following section.

3.4 Design Variants of Revolving Vane Compressor

In the design variants of the revolving vane compressor, the vane can be rigidly attached to the driving component, either the cylinder or the rotor, to restraint the ability of the vane movement along the tangential direction with respect to the rotational centre of the driving component such that the effect of the gas pressure differential force on the vane-side contact force can be eliminated.

3.4.1 Fixed Vane Design with Rotor Drives

In the first design variant of revolving vane compressor, the vane is rigidly fixed to the rotor, as shown in Figure 3.10. The vane is now in a pure rotational motion together with the rotor. The contact point between the vane and the driven component (cylinder) becomes one. The contact force (F_v) is independent of the gas pressure differential force and only affected by the rotational inertia of the driven component, as shown by equation (3.3). The rotor assembly (rotor and vane) is coupled to the motor shaft and drives the cylinder into rotational motion about its own centre. It can be seen from the same figure that the wall thickness of the cylinder becomes thicker as it needs to provide the room to accommodate for the entire vane length when the rotational angle of the rotor assembly is at zero degree.

$$F_v = \frac{I_c \alpha_c - \sum\left(\overrightarrow{F_f} \times \vec{r}\right)_c}{R_c \cos\gamma} \tag{3.3}$$

Therefore, a heavier cylinder is expected to be driven and may cause unnecessary high vane-side contact force as a result of a higher rotational inertia although the pressure dependency of vane-side contact force is removed. The thickness of the cylinder wall is not necessarily to be uniformly thick and thus, without sacrificing the structural rigidity, partial amount of the cylinder wall material can be removed and the vane-side contact force can be lowered as compared to the original design, as shown in Figure 3.11.

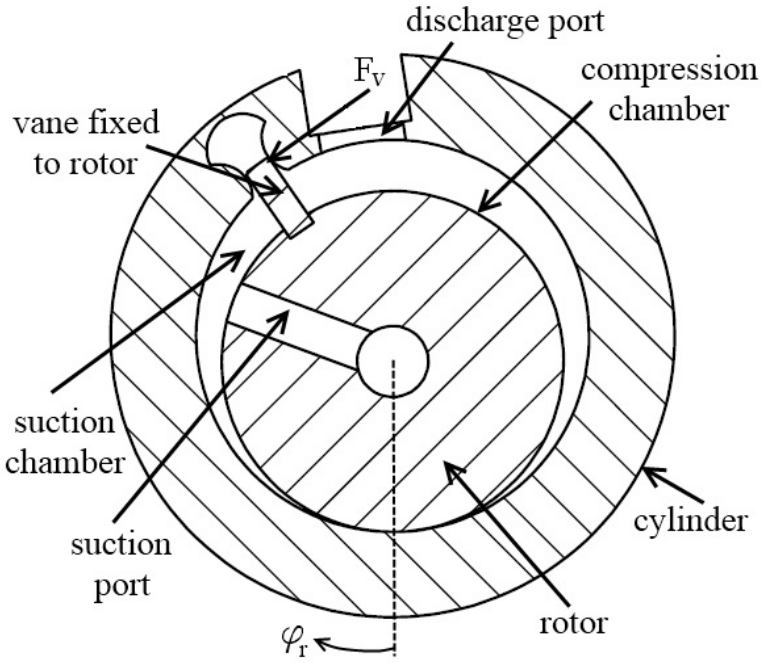

Figure 3.10 Fixed-vane revolving vane compressor with rotor drives

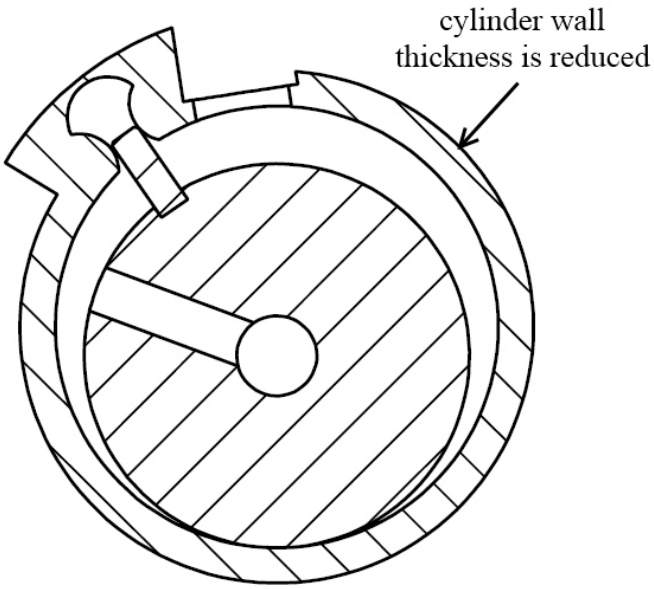

Figure 3.11 Fixed-vane revolving vane compressor with rotor drives and material removal

3.4.2 Fixed Vane Design with Cylinder Drives

Since the vane-side contact force is now dependent only on the rotational inertia of the driven component, the vane can be attached to the cylinder and in this case, the cylinder is used to drive the rotor, as shown in Figure 3.12. As a result, the vane-side contact force in this design variant can be further reduced as the cylinder assembly (cylinder and vane) is used to drive the lighter component, i.e. the rotor. The expression for the vane-side contact force in this design is given by equation (3.4).

$$F_v = \frac{I_r \alpha_r - \sum\left(\overrightarrow{F_f} \times \vec{r}\right)_r}{R_r \cos\gamma} \tag{3.4}$$

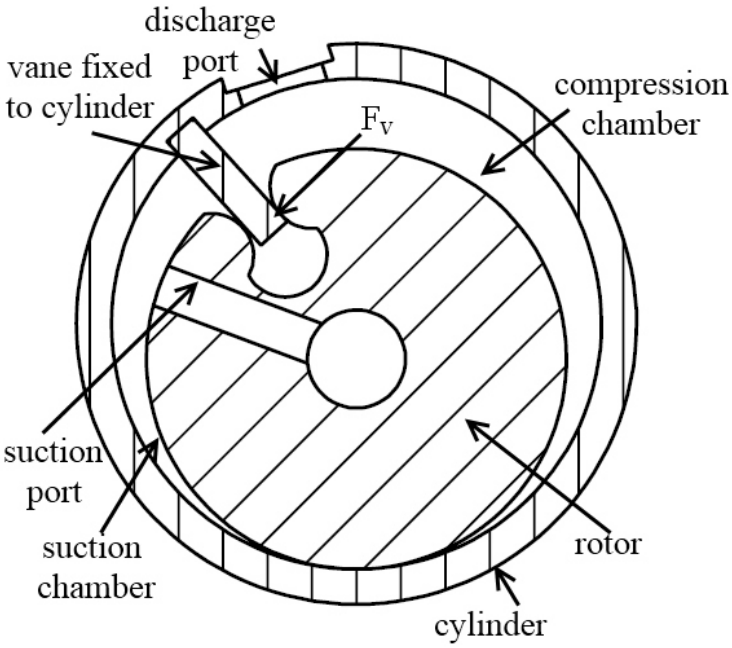

Figure 3.12 Fixed-vane revolving vane compressor with cylinder drives

The comparisons of the vane-side frictional loss due to the vane-side contact force in these three different revolving vane compressor designs are presented in Table 3.2. The prediction shows that a reduction of frictional loss of 40% can be achieved and this has translated to 3.0% of improvement in coefficient of performance.

Table 3.2 Frictional losses analysis of revolving vane compressor designs [138]

	Swivelling vane with rotor drives	Fixed-vane with rotor drives	Fixed-vane with cylinder drives
Vane-side frictional loss (W)	58	40	14
Other frictional losses (W)	43	43	46
Mechanical power (W)	1418	1400	1378

(evaporating/condensing: 7.2˚C/54.4˚C; operating speed: 2875 rev/min; working fluid: R22; displacement volume: 32.5 cc; motor efficiency: 0.8)

3.4.3 Other Design Considerations

With reference to Figures 3.11 and 3.12, the design variants of revolving vane compressor require the profiles of the vane slot to be extraordinarily precise in order to maintain the contact point between the vane and the vane slot at any instant of time during compressor operation. In order to remove this high precision requirement, or in other words, to save the production cost, an additional component known as bush is introduced into the design. The bush is just a simple piece to accommodate the vane and the placements of the bush in both rotor-drives and cylinder-drives designs are shown in Figures 3.13 and 3.14 respectively. The designs are simpler as the complicated profile of the previous vane slot design has been removed.

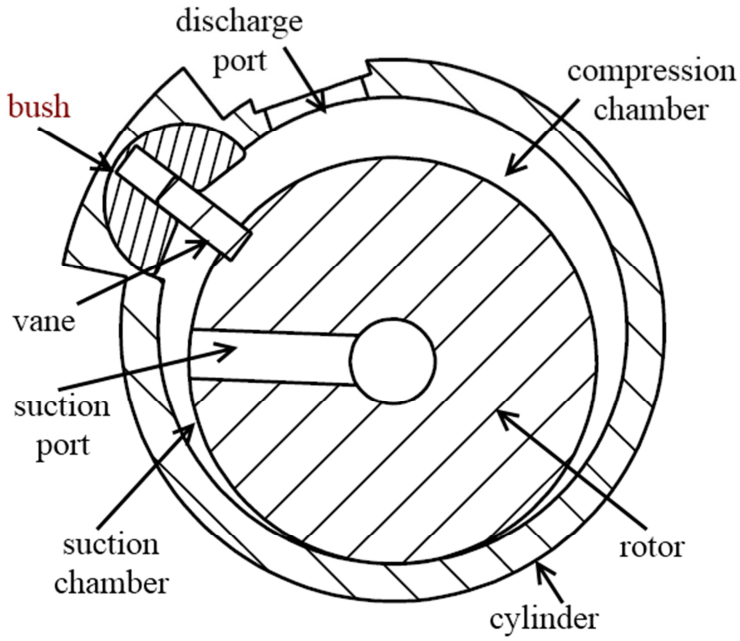

Figure 3.13 Fixed-vane revolving vane compressor with rotor drives and bush

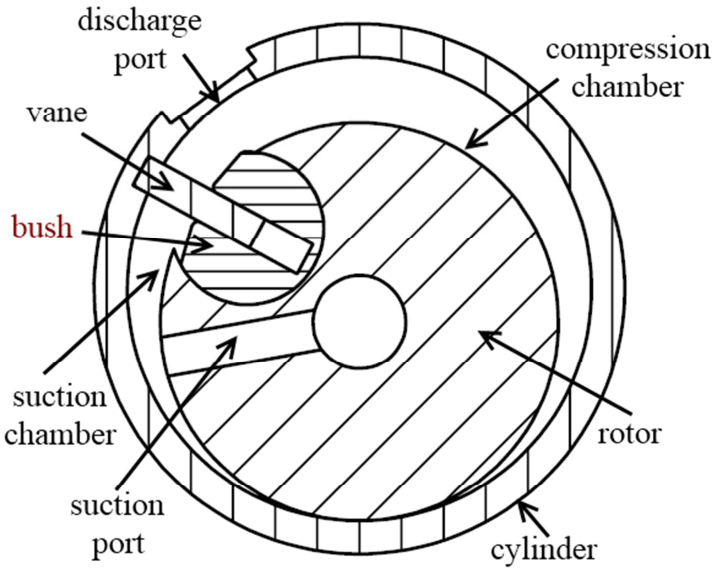

Figure 3.14 Fixed-vane revolving vane compressor with cylinder drives and bush

3.5 Concluding Remarks

The concept of original revolving vane compressor and its design variants have been discussed in details. The story of this new rotary type compressor has just begun and there are more to discover about this new compressor mechanism. In this dissertation, the fixed-vane revolving vane compressor with cylinder drives is selected for further investigation. In the next chapter, the mathematical modelling regarding the compressor will be presented.

Chapter 4

Theoretical Study I:

Geometrics, Thermodynamics and Valve Response

4.1 Introduction

In general, the performance characteristics of a compressor can be transformed into a set of manageable mathematical expressions and solved by appropriate numerical treatment such that the compressor performance can be predicted theoretically with the aid of computing effort. The complete theoretical analysis can be served as the tool for parametric studies and optimization in order to obtain better compressor design.

In this chapter, the variation of the working chamber volume and the kinematics of the main compressor components, namely, the rotor and the vane will be shown in Section 4.2. Subsequently, Sections 4.3 and 4.4 discuss the variation of thermodynamics properties of the working fluid due to the change in physical volume and the mass flow situation through the suction and the discharge port respectively. The detailed analysis for the valve response under the free and the forced vibrations will be shown in Section 4.5. At the end of this chapter, the theoretical predictions for the compressor performance and the effect of various design parameters, i.e. the geometries of the discharge valve, the sizes of suction and discharge port will be discussed.

4.2 Geometrical Model

The geometrical model is used to evaluate the working chamber volume variation with the shaft rotational motion. In addition, the model also includes the kinematics of different moving components and these are the rate of change of vane exposure length, the angular velocity and the angular acceleration of the driven component, which is the rotor in this case.

4.2.1 The Working Chamber Volume

As referred to Figure 4.1, in this case, the cylinder is the driving component which will be connected to the motor shaft (not shown) and the rotor is driven through the vane which is rigidly fixed to the cylinder.

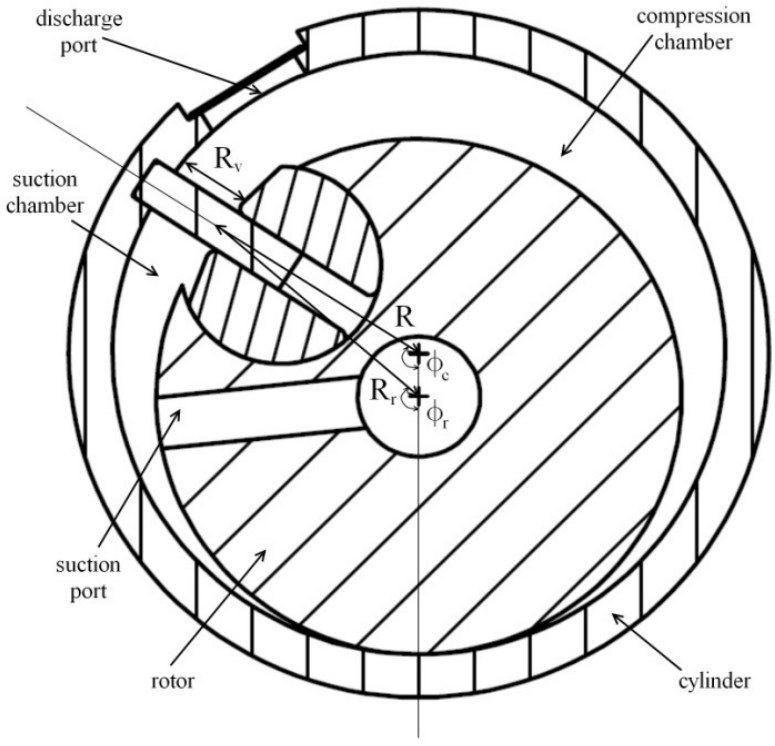

Figure 4.1 A fixed-vane revolving vane compressor with cylinder drives

By utilizing cosine rules, the rotor radius (R_r), the cylinder radius (R_c) and the distance from the centre of the cylinder to the rotor circumference (R) can be related by the following equation.

$$R_r^2 = R^2 + (R_c - R_r)^2 - 2 \times R_v \times (R_c - R_r) \times \cos\phi_c$$

The expression for R after rearrangement is shown by equation (4.1),

$$R = e\cos\phi_c + \sqrt{R_r^2 - (e\sin\phi_c)^2} \tag{4.1}$$

where $e = R_c - R_r$. The length of the vane which is exposed to the working fluid pressure inside the working chamber is defined as vane exposure length and it can be obtained by equation (4.2).

$$R_v = R_c - R \tag{4.2}$$

As a result, the working chamber volume at any angular position (ϕ_c) can be expressed by equation (4.3).

$$V_c = \frac{L_c}{2}\int_0^{\phi_c} (R_c^2 - R^2)\, d\phi_c \tag{4.3}$$

where L_c is the axial length of the compressor working chamber. Based on equation (4.3), the analytical expression for the working chamber volume and its rate of change with respect to the rotational angle can be written as equations (4.4) and (4.5) respectively.

$$V_c = \frac{L_c}{2} \times \left\{ (R_c^2 - R_r^2)\phi_c + \frac{1}{2}e^2 \sin(2\phi_c) + e \sin\phi_c \sqrt{R_r^2 - (e \sin\phi_c)^2} \right.$$
$$\left. + R_r^2 \tan^{-1}\left[\frac{e \sin\phi_c}{\sqrt{R_r^2 - (e \sin\phi_c)^2}} \right] \right\} \quad (4.4)$$

$$\frac{dV_c}{d\phi_c} = \frac{L_c}{2}(R_c^2 - R^2) \quad (4.5)$$

4.2.2 The Kinematics of Compressor Components

The exposure length of the vane to the working fluid inside the compressor working chamber is expressed by equation (4.2). The rate of change in this exposure length can be obtained by differentiating the equation with respect to time which yields equation (4.6).

$$\frac{dR_v}{dt} = \frac{dR_v}{d\phi_c} \times \frac{d\phi_c}{dt} = \frac{eR \sin\phi_c}{R - e\cos\phi_c} \times \omega_c \quad (4.6)$$

On the other hand, the angular position of the rotor with respect to the centre of the cylinder can be found by applying cosine rule, as shown by equation (4.7).

$$\phi_r = \cos^{-1}\left(\frac{R^2 - R_r^2 - e^2}{2eR_r} \right) \quad (4.7)$$

The angular velocity of the rotor varies during the operation as it is at an eccentric position to the centre of the cylinder. The magnitude can be obtained by differentiating equation (4.7) with respect to time, which yields equation (4.8).

$$\omega_r = \frac{d\phi_r}{d\phi_c} \times \frac{d\phi_c}{dt} = \left(\frac{R\frac{dR_v}{d\phi_c}}{eR_r \sin\phi_r} \right) \times \omega_c \quad (4.8)$$

The angular acceleration of the rotor can be found by further differentiating equation (4.8) with respect to time and this is shown by equation (4.9).

$$\alpha_r = \frac{d\omega_r}{d\phi_c} \times \frac{d\phi_c}{dt} = \frac{1}{\sin\phi_r}\left\{\frac{1}{eR_r}\left[R\frac{d^2R_v}{d\phi_c^2} - \left(\frac{dR_v}{d\phi_c}\right)^2\right] - \cos\phi_r\left(\frac{d\phi_r}{d\phi_c}\right)^2\right\} \times \omega_c^2 \quad (4.9)$$

It is noted that during the operation, the torque required to drive the cylinder into rotational motion is varying due to the variations in the fluid pressure forces**,** the contact reaction forces and the frictional forces acting on it. The angular velocity of the cylinder can be a constant only if the instantaneous power supplied by the electric motor to drive the cylinder is sufficient during the entire operation cycle. The angular velocity of the cylinder will vary if there is a response delay in the transfer of power required to drive the cylinder under high torque situation.

In a compressor design, a constant velocity for the cylinder can be achieved only if the instantaneous power requirement can be fulfilled. However, the rotor is not at constant velocity throughout the cycle as it is at an eccentric position relative to the centre of the driving component, i.e. the cylinder. The angular velocity of the rotor will vary throughout the cycle and the magnitude of it is determined by the radii of the rotor and the cylinder as well as the distance between the centres of the rotor and the cylinder, as shown by equation (4.8).

4.3 Thermodynamics Model

Generally, the operation cycle of a compressor can be described by a number of phenomena, each interacting and taking place in the working chamber within a complete rotation of the rotor-cylinder pair. During the operation, the pressure and the temperature of the working fluid inside the chamber vary due to the change in the

physical volume and the interaction of the working fluid flow through the suction and discharge port. These phenomena can be described mathematically in thermodynamics model. Prior to formulate these happenings in compressor analytically, it is assumed that the properties of the working fluid are instantaneously propagated throughout the whole working chamber volume. In other words, the properties are uniform and have no spatial variation. In addition, the flows through the suction and the discharge ports are treated as unidirectional.

By applying First Law of Thermodynamics to the control volume of interest as shown in Figure 4.2, the following equation is obtained.

$$\frac{dQ_c}{dt} - \frac{dW}{dt} = \frac{d}{dt}\int_{CV} E\rho dV + \int_{CS} E\rho\vec{V}\cdot\vec{A} \tag{4.10}$$

E represents the summation of kinetic energy, potential energy and internal energy. Since the kinetic energy and potential energy are insignificant to internal energy, equation (4.10) can be simplified as

$$\frac{dQ_c}{dt} - \frac{dW}{dt} = \frac{d}{dt}\int_{CV} u\rho dV + \int_{CS} u\rho\vec{V}\cdot\vec{A} \tag{4.11}$$

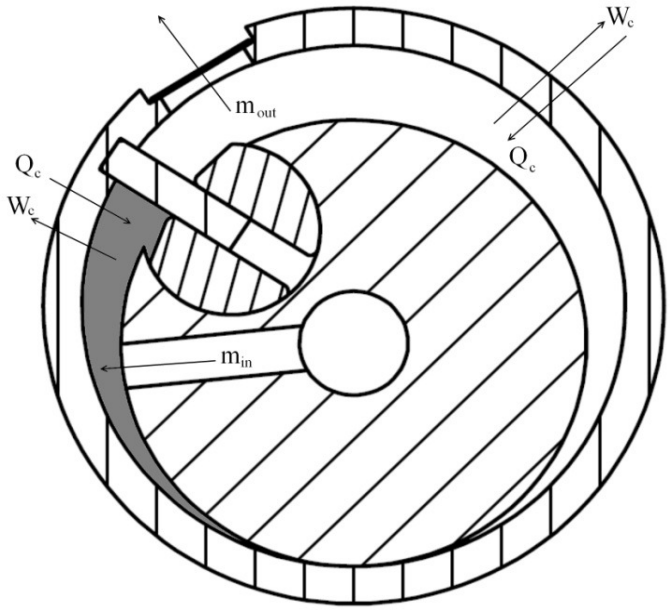

Figure 4.2 Thermodynamics approach to the fixed-vane revolving vane compressor

In conjunction with the flow work concept, equation (4.11) is rewritten as

$$\frac{dQ_c}{dt} - \frac{dW_{other}}{dt} = \frac{d}{dt}\int_{CV} u\rho dV + \int_{CS} h\rho\vec{V}\cdot\vec{A} \tag{4.12}$$

The second term on the left hand side of equation (4.12) represents the work done due to volumetric change and it can be expressed by equation (4.13).

$$\frac{dW_{other}}{dt} = P_c\frac{dV_c}{dt} \tag{4.13}$$

The second term on the right hand side of equation (4.12) represents the energy carried by the working fluid flow. Assuming the compressor is perfectly sealed, the integral sign can be removed from the term since the compressor under investigation has one suction port and one discharge port. Thus, the combination of equations (4.12) and (4.13) gives equation (4.14).

$$\frac{dQ_c}{dt} - P_c\frac{dV_c}{dt} = \frac{d}{dt}(m_c u_c) - h_i\frac{dm_i}{dt} + h_c\frac{dm_o}{dt} \tag{4.14}$$

The rate of change of internal energy in the working fluid can be obtained using chain rule and it is in the form of equation (4.15).

$$\frac{d}{dt}(m_c u_c) = m_c\frac{du_c}{dt} + u_c\frac{dm_c}{dt} \tag{4.15}$$

The definition of specific enthalpy is given by equation (4.16).

$$h_c = u_c + P_c V_s \tag{4.16}$$

Combine with the definition for specific volume (V_s), the expression for the rate of change in specific internal energy is found to be as equation (4.17).

$$\frac{du_c}{dt} = \frac{dh_c}{dt} - \frac{1}{m_c}\left(V_c\frac{dP_c}{dt} + P_c\frac{dV_c}{dt} - \frac{P_c V_c}{m_c}\frac{dm_c}{dt}\right) \tag{4.17}$$

Substitution of equations (4.16) and (4.17) into equation (4.15) gives equation (4.18).

$$\frac{d}{dt}(m_c u_c) = m_c\frac{dh_c}{dt} - V_c\frac{dP_c}{dt} - P_c\frac{dV_c}{dt} + h_c\frac{dm_c}{dt} \tag{4.18}$$

On the other hand, the conservation of mass states that

$$\frac{dm_c}{dt} = \frac{dm_i}{dt} - \frac{dm_o}{dt} \tag{4.19}$$

As a result, the combination of equations (4.14), (4.18) and (4.19) yields equation (4.20).

$$\frac{dQ_c}{dt} = m_c\frac{dh_c}{dt} - V_c\frac{dP_c}{dt} + (h_c - h_i)\frac{dm_i}{dt} \tag{4.20}$$

In general, the real gas law states that pressure is a function of temperature and specific volume. Thus, the total derivatives of pressure can be simply expressed as equation (4.21).

$$\frac{dP_c}{dt} = \left(\frac{\partial P_c}{\partial T_c}\right)_{V_s} \frac{dT_c}{dt} + \left(\frac{\partial P_c}{\partial V_s}\right)_{T_c} \frac{dV_s}{dt} \tag{4.21}$$

The specific enthalpy is the sum of specific internal energy and product of pressure and specific volume. Since specific internal energy depends on temperature, specific enthalpy thus can be seen as a function of temperature and specific volume. Mathematically, the total derivatives of specific enthalpy can be written as equation (4.22).

$$\frac{dh_c}{dt} = \left(\frac{\partial h_c}{\partial T_c}\right)_{V_s} \frac{dT_c}{dt} + \left(\frac{\partial h_c}{\partial V_s}\right)_{T_c} \frac{dV_s}{dt} \tag{4.22}$$

The rate of change of specific volume with respect to time is shown by equation (4.23).

$$\frac{dV_s}{dt} = \frac{1}{m_c}\left(\frac{dV_c}{dt} - \frac{V_c}{m_c}\frac{dm_c}{dt}\right) \tag{4.23}$$

Substituting equation (4.22) into equation (4.20) results

$$\frac{dQ_c}{dt} = m_c\left[\left(\frac{\partial h_c}{\partial T_c}\right)_{V_s} \frac{dT_c}{dt} + \left(\frac{\partial h_c}{\partial V_s}\right)_{T_c} \frac{dV_s}{dt}\right] - V_c\frac{dP_c}{dt} + (h_c - h_i)\frac{dm_i}{dt} \tag{4.24}$$

Since the input rotational velocity (ω_c) is a constant, equations (4.21) and (4.24) can be rewritten as equations (4.25) and (4.26) respectively.

$$\frac{dP_c}{d\phi_c} = \left(\frac{\partial P_c}{\partial T_c}\right)_{V_s} \frac{dT_c}{d\phi_c} + \left(\frac{\partial P_c}{\partial V_s}\right)_{T_c} \frac{dV_s}{d\phi_c} \tag{4.25}$$

$$\frac{dQ_c}{d\phi_c} = m_c \left[\left(\frac{\partial h_c}{\partial T_c} \right)_{V_s} \frac{dT_c}{d\phi_c} + \left(\frac{\partial h_c}{\partial V_s} \right)_{T_c} \frac{dV_s}{d\phi_c} \right] - V_c \frac{dP_c}{d\phi_c} + (h_c - h_i) \frac{dm_i}{d\phi_c} \quad (4.26)$$

Equations (4.25) and (4.26) represent two coupled first order ordinary differential equations for pressure and temperature of the working fluid under the effect of volumetric change and interaction of incoming and outgoing fluid in a fixed-vane revolving vane compressor. The enthalpy terms and the partial derivatives of thermodynamics properties can be obtained from real gas properties. In addition, the mass flow rate through suction or discharge port can be found analytically through the mass flow model, which is presented in the next section.

The heat transfer model appears in the equation (4.26) dictates the effect of the convective heat transfer between the working fluid and the surrounding chamber on the pressure variations of the working fluid. The heat transfer to or from the working fluid along the suction and discharge ports are not considered. Hence, the working fluid temperature at the suction port, which is used together with the suction pressure to dictate the working fluid density and suction mass flow rate, is treated as the sum of the evaporating temperature and the degree of superheat. In addition, the temperature at the discharge port is treated as same as the working fluid temperature at the end of isentropic compression process from suction pressure to discharge pressure. If the heat transfer along the suction and the discharge ports were to be considered, the flow configurations from the suction origin to the entrance of suction chamber and from the exit of compression chamber to the end of discharge port have to be identified. The identifications allow the convective heat transfer model to be described and classified into free or forced convection.

4.4 Mass Flow Model

The mass flow through the suction and the discharge ports can be modelled as flow through an orifice. In Figure 4.3, consider a volume of fluid bounded by two streamlines in steady and compressible conditions, the energy equation can be written as

$$Q + \left(h + \frac{V^2}{2} + gz\right)_1 = \left(h + \frac{V^2}{2} + gz\right)_2$$

Q is the specific heat exchange between working fluid and surroundings. Neglecting the potential energy term and assuming the upstream velocity is negligible, the equation above is reduced to

$$Q + h_1 = h_2 + \frac{V_2^2}{2}$$

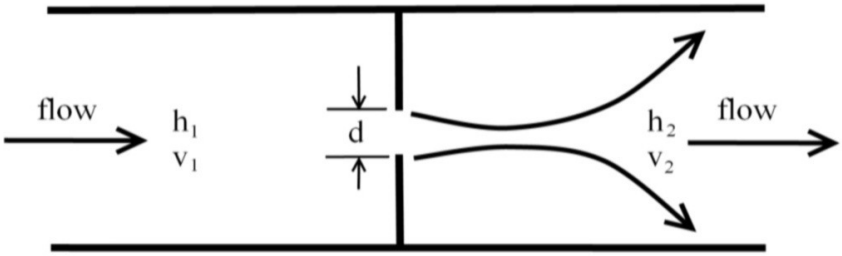

Figure 4.3 Schematic diagram for an orifice flow

In the absence of heat exchange, which means the system is adiabatic, the downstream velocity can be expressed as

$$V_2 = \sqrt{2(h_1 - h_2)} \tag{4.27}$$

Hence, the mass flow rate through the orifice with a cross sectional area (A_{flow}) is given by

$$\frac{dm}{dt} = \rho_1 \times \sqrt{2(h_1 - h_2)} \times A_{flow} \tag{4.28}$$

Introducing flow coefficient (K) to account for flow losses, equation (4.28) is revised to be

$$\frac{dm}{dt} = K \times \rho_1 \times \sqrt{2(h_1 - h_2)} \times A_{flow} \tag{4.29}$$

Physically, the flow must accelerate itself in order to enter or leave the small opening. This can be done by transforming part of enthalpy to increase its kinetic energy and ideally, after passing the opening, the flow will back to its original state. Hence, the flow under this ideal phenomenon is addressed as reversible flow. Generally, the flow under adiabatic and reversible condition is known as isentropic flow. However, due to the fact that friction and dissipative effects always exist within the flow, the isentropic flow cannot be achieved and therefore, an isentropic efficiency is brought in and it is defined as

$$\eta_{is} = \frac{h_1 - h_2}{h_1 - h_{2,is}}$$

Combine the isentropic efficiency and the flow coefficient as discharge coefficient, the resultant expression for mass flow rate is

$$\frac{dm}{dt} = C_d \times \rho_1 \times \sqrt{2(h_1 - h_{2,is})} \times A_{flow} \tag{4.30}$$

where C_d is the discharge coefficient and has the value in between 0.5 and 0.6.

As a result, the expression for the mass flow rate with respect to the input shaft rotational angle can be restated as equation (4.31).

$$\frac{dm}{d\phi_c} = \frac{1}{\omega_c} \times C_d \times \rho_1 \times \sqrt{2(h_1 - h_{2,is})} \times A_{flow} \quad (4.31)$$

The mass flow rate depends on the flow area. For the suction flow, the mass flow rate is dictated by the size of the suction port and for the discharge mass flow rate, the flow area is dictated by the discharge valve dynamic behaviour, which is discussed in the next section.

4.5 Valve Response Model

The valves in a compressor are often automatic reed valves. The purpose of having a valve at the suction and (or) the discharge port is to ensure that the working fluid flow is unidirectional. During the compressor operation, the valve opens only when there is enough force to overcome the stiffness of the valve and the prescribed pressure in the shell of the compressor. At the instant of the valve opening, the working fluid flows through the gap between the valve port and the valve plate. The magnitude of the gap opening dictates the flow rate of the working fluid and therefore, it is important to conduct an analysis on the valve response behaviour under the influence of its own characteristics and the external loading.

In a revolving vane compressor, the discharge valve is placed on the outer circumference of the rotating cylinder. Therefore, the valve is set into rotational motion during the compressor operation, unlike the common positive displacement compressors where the valve is stationary. As a consequence, the valve is subjected not only to the pressure loading from the both sides of the valve but also the centrifugal force loading due to the rotation. On the other hand, the magnitude of the valve motion is limited by a valve plate, which is used to inhibit extra valve oscillations and hence alleviates fatigue

behaviour. In the analysis of the valve, the valve is considered as a beam as the cross sectional dimensions are small as compared to its length.

The free body diagram for an infinitesimal small element of valve is shown in Figure 4.4. The small element of valve is under shear force, bending moment, damping force, centrifugal force and the external loading force. The force balance across the valve thickness direction for this particular case is thus written as equation (4.33).

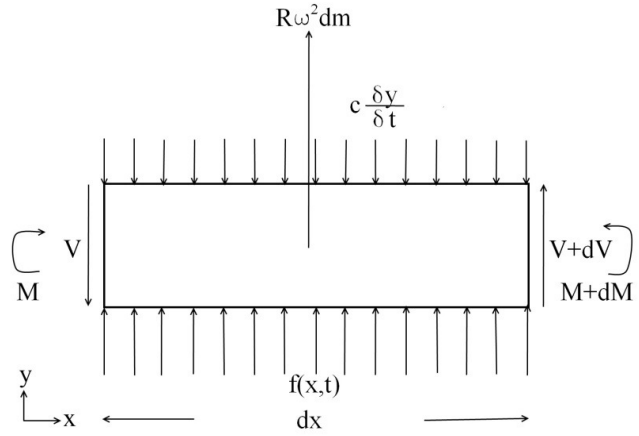

7

Figure 4.4 Free body diagram for an infinitesimal small element of valve

$$-V + (V + dV) + f(x,t)dx - c\frac{\partial y}{\partial t}dx + (R + y)\omega^2 dm = dm\frac{\partial^2 y}{\partial t^2} \qquad (4.33)$$

Apply moment equilibrium about the right edge of the infinitesimal small element gives equation (4.34).

$$Vdx - M + (M + dM) - f(x,t)dx \cdot \frac{dx}{2} + c\frac{\partial y}{\partial t}dx \cdot \frac{dx}{2} - (R + y)\omega^2 dm \cdot \frac{dx}{2} = 0 \qquad (4.34)$$

Using $dV/dx = \partial V/\partial x$ and$dm = \rho A_c dx$, equation (4.33) can be rewritten as equation (4.35).

$$\frac{\partial V}{\partial x} + f(x,t) - c\frac{\partial y}{\partial t} + (R+y)\omega^2 \rho A_c = \rho A_c \frac{\partial^2 y}{\partial t^2} \tag{4.35}$$

Ignore second and higher order terms in dx, equation (4.34) can be simplified into equation (4.36)

$$V = -\frac{\partial M}{\partial x} \tag{4.36}$$

Based on an elementary flexural theory, the relationship between the beam deflection and the bending moment is

$$M = E_v I_v \frac{\partial^2 y}{\partial x^2} \tag{4.37}$$

Combination of equations (4.37) and (4.35) gives

$$E_v I_v \frac{\partial^4 y}{\partial x^4} + \rho A_c \frac{\partial^2 y}{\partial t^2} + c\frac{\partial y}{\partial t} - \rho A_c \omega^2 y = \rho A_c \omega^2 R + f(x,t) \tag{4.38}$$

Equation (4.38) is a linear, non-homogeneous partial differential equation with fourth order in space, second order in time. Both terms on right hand side of equation (4.38) show the effect of centrifugal loading and pressure excitation in determining the valve motion respectively.

In general, the valve is a distributed system rather than a discrete system. Hence, in seeking a solution to vibration problems for distributed systems, free vibration problem is considered first which naturally leads to a differential eigenvalue problem.

Subsequently, the response under the effect of the external excitation, which is usually known as forced vibration, is formulated.

4.5.1 Free Vibration Analysis

With reference to equation (4.38), the centrifugal force due to the rotation contributes to the homogeneous part (left-hand side) and the non-homogeneous part (right-hand side) of the equation. It implies that the rotation of the valve reed not only forms the external excitation but also affects the natural characteristics of the valve reed system. In mechanical vibration, the "free vibration" refers to the homogeneous solution. Therefore, the fourth term on the left-hand side remains in the free vibration analysis since it is part of the homogeneous equation but the first and the second terms on the right-hand side vanish. Therefore, equation (4.38) is reduced to equation (4.39).

$$E_v I_v \frac{\partial^4 y}{\partial x^4} + \rho A_c \frac{\partial^2 y}{\partial t^2} + c\frac{\partial y}{\partial t} - \rho A_c \omega^2 y = 0 \qquad (4.39)$$

As for a distributed system, the circumstance for the valve motion is synchronous. The synchronous motion indicates that every point along the valve executes the same motion in time, passing through equilibrium at the same time and reaching the maximum excursion at the same time. The implication behind is that during the synchronous motion, the valve exhibits a certain unique profile, and the profile does not change with time, only the amplitude of the profile does. In mathematical terminology, the solution to such a case is said to be separable in the spatial variable and time variable. It can be expressed in the form of equation (4.40).

$$y(x,t) = f(x) \cdot g(t) \qquad (4.40)$$

The profile of the valve response is represented by $f(x)$ and $g(t)$ indicates how the amplitude of the profile varies with time. Introduce equation (4.40) into equation (4.39) and divided the whole equation by $\rho A_c f(x)g(t)$ yields

$$\frac{E_v I_v}{\rho A_c}\frac{1}{f}\frac{d^4 f}{dx^4} = \omega^2 - \frac{c}{\rho A_c}\frac{1}{g}\frac{dg}{dt} - \frac{1}{g}\frac{d^2 g}{dt^2} \tag{4.41}$$

It is noted that the partial derivatives have been replaced by the total derivatives since both sides are only dependent on space and time respectively. Using the argument in the method of separation of variables, both sides of the equation must be equal to the same real constant. Hence, denote the constant by p^2 and introduce $a^2 = E_v I_v / \rho A_c$, equation (4.41) can be rewritten as two ordinary differential equations.

$$\frac{d^4 f}{dx^4} - \beta^4 f = 0 \tag{4.42}$$

$$\frac{d^2 g}{dt^2} + \frac{c}{\rho A_c}\frac{dg}{dt} + (p^2 - \omega^2)g = 0 \tag{4.43}$$

where $\beta^4 = p^2/a^2$.

Equation (4.42) is recognized as a well established differential eigenvalue problem for transverse vibrations of a stationary beam too. Therefore, by the exact identity of both, it can be concluded that the rotational motion of the valve does not affect its natural mode of vibration. Other than this, it is a fourth order ordinary differential equation. Therefore, the solution $f(x)$ contains four constants of integration, in addition to the real constant p^2, a total of five unknowns. To evaluate the five unknowns, boundary conditions must be invoked. However, it is impossible to evaluate all five unknowns as there are only four boundary conditions for a valve beam system.

Hence, four boundary conditions can be used to derive a characteristic equation for p^2 and to determine the other three integration constants in terms of the other. The characteristic equation has an infinite number of roots p_r^2 $(r = 1,2,3, \dots)$ known as eigenvalues. Corresponding to each of these roots, there is one function $f_r(x)$ $(r = 1,2,3, \dots)$ known as eigenfunctions.

The square roots of eigenvalues are recognized as the natural frequencies of the system and the eigenfunctions are also known as the natural modes. The natural frequencies can be determined uniquely but not the natural modes. As mentioned earlier, the three integration constants can be expressed in terms of the other constant. Thus, if that constant is determined uniquely through a normalization process and thus determine the natural modes uniquely, then the natural modes are referred to as normal modes.

The rotating discharge valve in the revolving vane compressor is in clamped-free configuration. The boundary conditions are stated as follows.

The deflection and the rotation of the valve at $x = 0$ are zero since it is clamped. Thus,

$$f(x) = 0 \text{ and } df/dx = 0$$

The shear force and the bending moment at $x = L$ is zero since the end of the valve is free. Thus,

$$d^2f/dx^2 = 0 \text{ and } d^3f/dx^3 = 0$$

The general solution to equation (4.42) is

$$f(x) = A \sin \beta x + B \cos \beta x + C \sinh \beta x + D \cosh \beta x \qquad (4.44)$$

in conjunction with the prescribed boundary conditions, the characteristic equation is found to be

$$\cos \beta_r L \cosh \beta_r L = -1 \tag{4.45}$$

Hence, the associated eigenfunction is

$$f_r(x) = A_r \left[(\sin \beta_r x - \sinh \beta_r x) - \frac{\sin \beta_r L + \sinh \beta_r L}{\cos \beta_r L + \cosh \beta_r L} (\cos \beta_r x - \cosh \beta_r x) \right] \tag{4.46}$$

On the other hand, equation (4.43) resembles entirely the equation of motion of a damped single degree of freedom system. Hence, the solution of equation (4.43) can be written as

$$g_r(t) = e^{(-\xi q_r t)} \left[\frac{\xi q_r g_r(0) + \dot{g}_r(0)}{q_{d,r}} \sin q_{d,r} t + g_r(0) \cos q_{d,r} t \right] \tag{4.47}$$

where $g_r(0)$ and $\dot{g}_r(0)$ represent the initial modal displacement and the initial velocity respectively, and $q_r^2 = p_r^2 - \omega^2$.

As seen from equation (4.47), under the free vibration, the valve responds at the damped frequency ($q_{d,r}$), which is defined as $q_r\sqrt{1-\xi^2}$. This implies that in an undamped condition ($\xi = 0$), the response frequency is given by q_r, differs from its natural frequency p_r. Therefore, it can be said that the response frequency of the rotating valve under a free vibration is not equal to its natural frequency, but at a lower frequency which depends on the angular velocity of the rotational motion. In other words, the stiffness of the valve diminishes while undergoes a rotational motion.

As a conclusion, the free vibration response in r^{th} mode for a rotating valve is

$$y_r(x,t) = f_r(x)\left\{e^{(-\xi q_r t)}\left[\frac{\xi q_r g_r(0) + \dot{g}_r(0)}{q_{d,r}}\sin q_{d,r}t + g_r(0)\cos q_{d,r}t\right]\right\} \quad (4.48)$$

The natural frequency for r^{th} mode is

$$p_r = (\beta_r L)^2\sqrt{\frac{E_v I_v}{\rho A_c L^4}} \quad (4.49)$$

4.5.2 Forced Vibration Analysis

The solution of the valve response under the effect of non-homogeneous term presented in equation (4.38) is ready to be presented. The solution is assumed to be in variable separable form and by considering the principles of superposition for linear vibration, the solution has the form of

$$y(x,t) = \sum_{r=1}^{\infty} f_r(x)g_r(t) \quad (4.50)$$

On the other hand, the natural modes are orthogonal and have been normalized to satisfy orthonormality conditions, namely

$$\int_0^{L_v} f_s(x)f_r(x)dx = \delta_{rs} \qquad \text{and} \qquad \int_0^{L_v} f_s(x)\frac{d^4 f_r(x)}{dx^4}dx = \left(\frac{p_r}{a_r}\right)^2\delta_{rs}$$

where δ_{rs} is Kronecker delta.

Substitute equation (4.50) into equation (4.38), divide the whole by ρA_c and multiply by $f_s(x)$, integrating over the entire length of valve and invoke the orthonormality conditions. The following equation is obtained.

$$\frac{d^2 g_r}{dt^2} + \frac{c}{\rho A_c}\frac{dg_r}{dt} + (p_r^2 - \omega^2)g_r = \int_0^{L_v} f_r(x)\left[\omega^2 R + \frac{f(x,t)}{\rho A_c}\right]dx \qquad (4.51)$$

Equation (4.51) can be recognized as an independent modal equation with the right hand side of the equation is known as modal forces. It is mentioned that the natural modes which were presented in equation (4.46) have been normalized according to orthonormality conditions. Therefore, A_r has the following relationship.

$$A_r^2 \int_0^{L_v} \left[(\sin\beta_r x - \sinh\beta_r x) - \frac{\sin\beta_r L + \sinh\beta_r L}{\cos\beta_r L + \cosh\beta_r L}(\cos\beta_r x - \cosh\beta_r x)\right]^2 dx = 1$$

The integral can be solved numerically in order to obtain the particular magnitude of A_r for any mode of vibration. On the other hand, with a closer look on equation (4.51), the nature of $f(x,t)$ is discussed in the following.

During the derivation of force and moment equilibrium based on free body diagram presented in Figure 4.4, $f(x,t)$ represents the force per unit length. The existence of $f(x,t)$ is true for certain length of the valve as the valve exposes to the working fluid pressure through the discharge port only. As such, let x be the starting of the discharge port measured from the clamped end and Δx is the diameter of the discharge port. Therefore,

$$\int_0^{L_v} f_r(x)\frac{f(x,t)}{\rho A_c}dx = \int_x^{x+\Delta x} f_r(x)\frac{f(x,t)}{\rho A_c}dx$$

In addition, equality can be established between $f(x,t)$ and $P_c(t)$ as

$$f(x,t) = \frac{\left[P_c(t) - P_{discharge}\right] \times A_f(y)}{\Delta x}$$

Using $\Delta P(t) = P_c(t) - P_{discharge}$ and substitute the equality to equation (4.51) results

$$\frac{d^2 g_r}{dt^2} + 2\xi q_r \frac{dg_r}{dt} + q_r^2 g_r = \omega^2 R \int_0^{L_v} f_r(x)\, dx + \int_x^{x+\Delta x} f_r(x) \frac{\Delta P(t) \times A_f(y)}{\rho A_c \Delta x} dx$$

Since the diameter of the discharge port is small as compared to the length of the valve,

$$\int_x^{x+\Delta x} f_r(x) \frac{\Delta P(t) \times A_f(y)}{\rho A_c \Delta x} dx = f_r(x + \frac{\Delta x}{2}) \times \Delta x \times \frac{\Delta P(t) \times A_f(y)}{\rho A_c \Delta x}$$

As a result, equation (4.51) becomes

$$\frac{d^2 g_r}{dt^2} + 2\xi q_r \frac{dg_r}{dt} + q_r^2 g_r = \omega^2 R \int_0^{L_v} f_r(x)\, dx + f_r\left(x + \frac{\Delta x}{2}\right) \times \frac{\Delta P(t) \times A_f(y)}{\rho A_c} \quad (4.52)$$

To this end, a second order ordinary differential equation has been formulated to describe the nature of modal coordinate under the effect of centrifugal and pressure differential force on the valve. In order to get a solution for equation (4.52), an analytical expression for $\Delta P(t)$ is required. However, the working fluid pressure inside the working chamber is dependent on the valve displacement. In other words, the forcing excitation due to the working fluid pressure is coupled to the valve response. Hence, a general solution for second order ordinary differential equation is not allowed to apply here. Recall equation (4.52) and let $\phi_1 = dg_r/dt$ and $\phi_2 = g_r$, the equation can be decomposed into two first order ordinary differential equations, which are

$$\frac{d\phi_2}{dt} = \phi_1 \quad (4.53)$$

$$\frac{d\phi_1}{dt} = N_r - 2\xi q_r \phi_1 - q_r^2 \phi_2 \tag{4.54}$$

where N_r is known as modal force and it is shown by equation (4.55).

$$N_r = \omega^2 R \int_0^{L_v} f_r(x)\, dx + f_r\left(x + \frac{\Delta x}{2}\right) \times \frac{\Delta P(t) \times A_f(y)}{\rho A_c} \tag{4.55}$$

In general, solving equations (4.53) and (4.54) in conjunction with thermodynamics model simultaneously, the value of the modal coordinate is obtained. Subsequently, the model coordinate is multiplied by normalized mode shape in order to obtain the value for the displacement of the valve.

4.6 Results and Discussions

The thermodynamics equations, the mass flow equation and the equations to describe the modal coordinate of the valve are all ordinary differential equations. These equations are initial value problem and can be solved using the fourth order Runge-Kutta method together with the analytical expression of the working chamber volume to obtain the thermodynamic properties of the working fluid inside the working chamber throughout one complete operating cycle of the revolving vane compressor. In addition, the kinematics of the compressor components, which are the vane exposure length and rate of change of it, the angular velocity and the angular acceleration of the rotor can be solved independently. The operating conditions and the main dimensions of compressor components used in the calculation are summarized in Table 4.1.

Table 4.1 Operating conditions and design dimensions of fixed-vane revolving vane compressor

Operating Conditions			
Evaporating temperature	7.2 °C	Operating speed	3000 rev/min
Condensing temperature	54.4 °C	Working fluid	R22
Compressor Dimensions			
Radius of cylinder	27.0 mm	Diameter of suction port	14.0 mm
Radius of rotor	23.5 mm	Diameter of discharge port	14.0 mm
Length of compressor	17.1 mm		
Valve Design Dimensions			
Length	20.1 mm	Elastic modulus	200 GPa
Width	15.0 mm	Density	7800 kg m^{-3}
Thickness	0.2 mm	Radial location	28.0 mm

Figures 4.5(a) and (b) show the kinematics of the compressor components over one full rotation. In Figure 4.5(a), the vane exposure length increases initially, reaches maximum when the rotational angle is 180° and decreases after that. The rate of change in the vane exposure length is also shown in the same figure. Figure 4.5(b) shows that the angular velocity of the rotor is greater than the constant cylinder angular velocity during the first and the last quarter of the operation. The angular acceleration of the rotor exhibits the sinusoidal variations.

In general, the fixed-vane revolving vane compressor completes the suction, the compression and the discharge of the working fluid in a span of two full rotations. Figure 4.5(c) shows the variation of the working chamber volume over the entire working process. The working chamber volume increases during the suction process and reaches a maximum, which indicates the end of suction process and the beginning

of the compression process. The working chamber volume starts to decrease after one full rotation. Figures 4.5(d) and (e) show the trends of the pressure and the mass of the working fluid inside the working chamber respectively. Initially, the pressure remains constant and the mass increases steadily during the suction process. Subsequently, the compression process starts at an angle of 360°, the pressure thus increases due to the reduction in the working chamber volume while the mass remains constant since there is no more intake from the suction port and no internal leakage under the consideration of perfectly-sealed compressor. Eventually, the pressure reaches the discharge pressure but the discharge process does not commence immediately at this moment. A continuous increase in the pressure is observed. This is because the working fluid is in the process of overcoming the valve stiffness and the flow resistance in order to initiate the valve opening. Therefore, a hump is observed in the pressure profile. The working fluid starts to flow out form the working chamber when there is an enough force to open the valve, which is shown by the decreasing trend in the chamber mass.

The variation of the valve displacement is presented in Figure 4.5(f). At the instant of the opening of the valve, the force exerted on the valve is extraordinary high due to the high pressure differential force across the valve. Thus, the valve displacement is the greatest at this instant. Subsequently, the valve displacement is observed to decrease since the pressure force exerted on the valve is getting lower due to a decreasing mass. An earlier opening of the discharge valve with an earlier commencement of the discharge process occur for the rotating discharge valve as compared to the stationary valve, where the latter is often applied in all existing compressors such as the reciprocating and the rolling piston compressors. The number

of oscillations in the variations of the valve displacement is reduced and hence, the valve experiences fewer cyclic stresses.

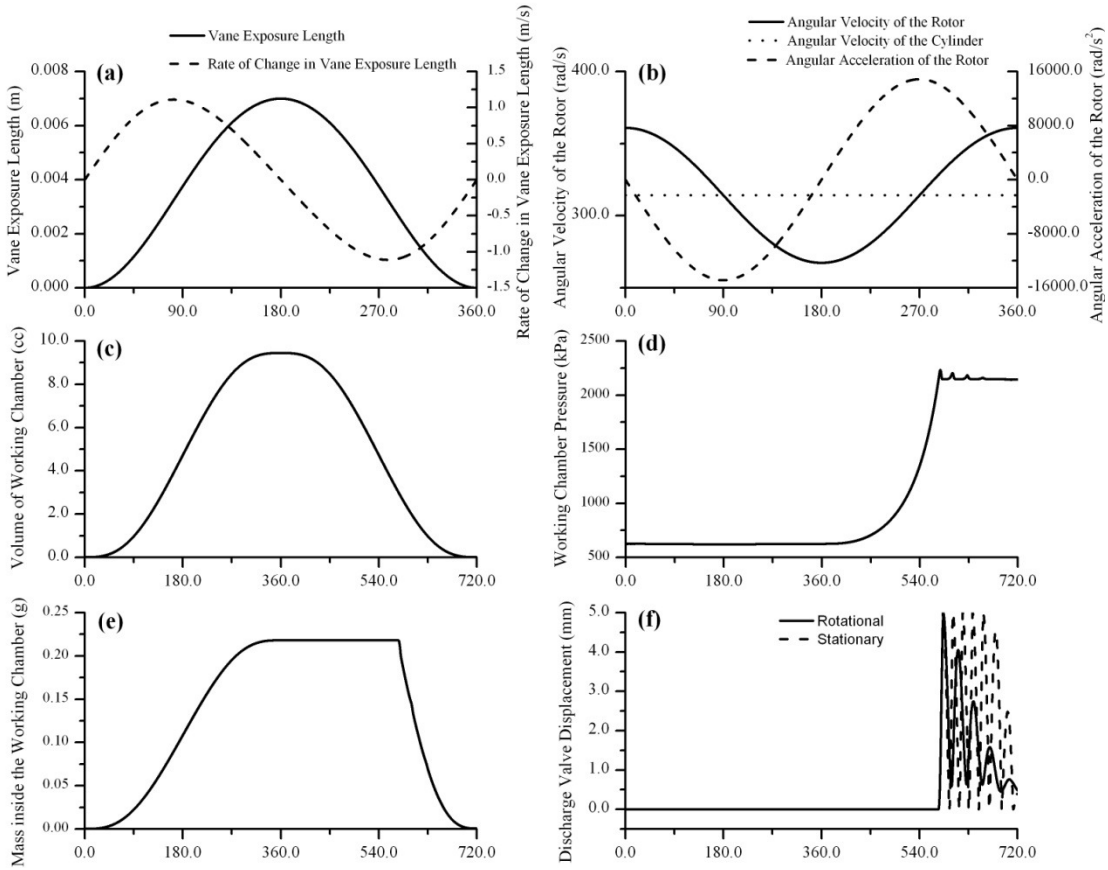

Figure 4.5 Basic simulation results of fixed-vane revolving vane compressor (x-axis represents rotational angle of cylinder)

Figure 4.6 shows the pressure and the volume history of the compressor cycle. It is noted that the area bounded by the whole cycle is known as the indicated work and it can be expressed as

$$W_{ind} = \int_{0}^{4\pi} \left(P_c \frac{dV}{d\phi_c} \right) d\phi_c$$

Generally, the indicated work comprises of the total work done to the working fluid, the suction and the discharge losses. As shown in the same figure, the suction loss is the

area below the nominal suction pressure level whereas the discharge loss is the area above the nominal discharge pressure level. Both losses are related to the design geometries of the valve and the sizes of suction and discharge ports, which will be discussed the following sections.

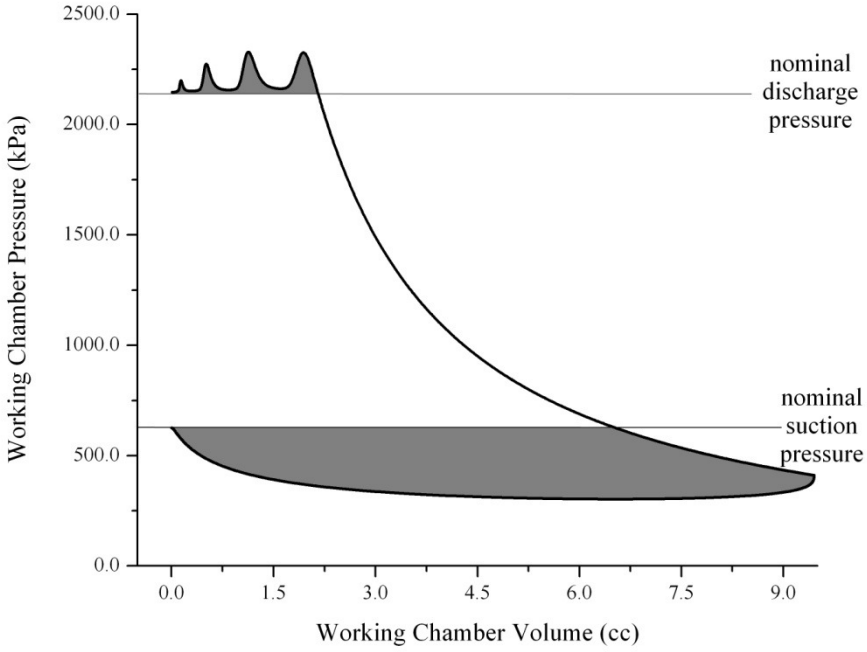

Figure 4.6 Pressure-volume diagram for fixed-vane revolving vane compressor

4.6.1 Effect of Suction Port Size

In the revolving vane compressor design, the suction port is generally without a suction valve. Hence, the suction upstream is always in communication with the suction chamber through the suction port. For a good suction port design, the size of the port must be sufficiently big to allow easy flow of the working fluid during the suction process, which is one of the primary influences on the total mass flow rate of the working fluid through the compressor. If the suction port is undersized, the mass inside

the working chamber is not sufficient and leads to an undesired pressure drop since the volume is increasing during the suction process. Therefore, an extra energy is required to recover the pressure to the suction pressure level before the compression process begins and this amount of energy is known as the suction loss. Furthermore, the insufficient intake mass will also deteriorate the cooling capacity.

As shown in Table 4.2, the suction loss is high in the case of suction port diameter equals to 3.0 mm and it decreases remarkably as the suction port diameter increases. The mass flow rate improves when a sufficiently large suction port diameter is used. In addition, the results show that any suction diameter that is bigger than 14.0 mm is unnecessary since the change in mass flow rate is very small. The variations of the mass and the pressure-volume are shown in Figure 4.7. Figure 4.7(a) shows that the amount of the working fluid in the working chamber at the end of the suction process is very low for the suction port diameter of 3.0 mm as compared to the properly sized suction port of 14.0 mm. In addition, the pressure inside the working chamber during the suction process is far below the nominal suction pressure level and it incurs more suction loss, as shown in Figure 4.7(b). It is also observed that the discharge process starts at a later stage in the case of an undersized suction port as compared to the properly designed suction port. As a result, the diameter of the suction port should be well designed such that sufficient working fluid is induced into the working chamber and thus, incurs a lower suction loss.

The flow coefficient used in the prediction is 0.6 and the coefficient variation is not considered in the simulation model. Flow coefficient is used to relate the flow characteristics through a restricted area. In compressor study, the flows through the

suction and discharge ports are treated as an orifice flow. The exact value of flow coefficient of an orifice involves number of factors, namely, the shape of the orifice, the pressure drop across the orifice, the density change and the Reynolds number. However, according to British Standard (BS1042), an average flow coefficient value of 0.60 to 0.65 can be applied to a wide range of flow conditions and therefore, flow coefficient of 0.60 is assumed and used in the compressor theoretical study. The true value of the flow coefficient however can only be obtained through measurement of the flow under the actual conditions and it is believed that the value should close to the range of 0.60 – 0.65.

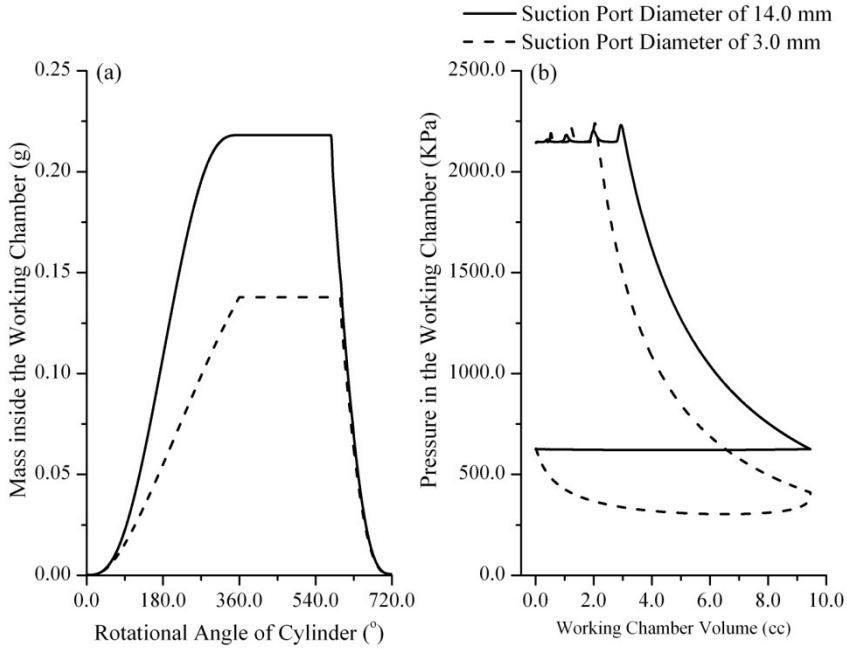

Figure 4.7 Effect of suction port diameter on compressor performance

Table 4.2 Effect of suction port diameter of compressor performance

Suction port diameter (mm)	Suction loss (W)	Mass flow rate (g s^{-1})
3.00	114	6.89
6.00	32.7	10.7
10.0	5.44	10.9
14.0	1.46	10.9
18.0	0.533	10.9

4.6.2 Effect of Discharge Port Size

In general, the diameter of the discharge port is required to be sufficiently large to allow the sufficiently pressurized working fluid to be discharged out of the working chamber without incurring unnecessary over-pressure. The under designed discharge port diameter will not allow sufficient working fluid to be discharged and hence the working fluid will be further compressed and causes the fluid pressure to increase beyond the necessary level, as shown by the oscillations in the pressure in Figure 4.8. It is observed that if the diameter of the discharge port increases, the oscillation in the pressure profile is reduced, which results in lower discharge loss. The results suggest that the discharge port diameter is required to be at least 11.0 mm and larger than 14.0 mm is unnecessary since any larger discharge port does not bring any significant positive effect in terms of discharge loss, as shown in Table 4.3.

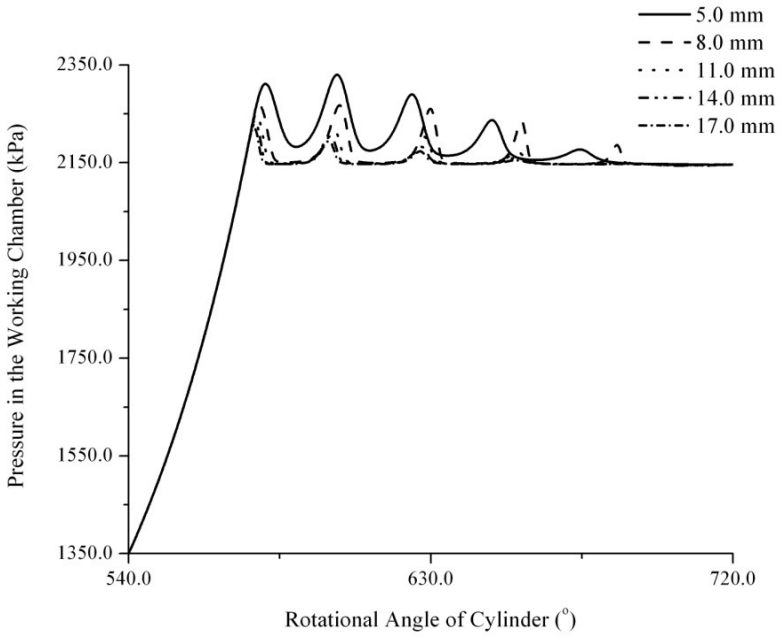

Figure 4.8 Effect of discharge port diameter on pressure profile

Table 4.3 Effect of discharge port diameter on compressor performance

Discharge port diameter (mm)	Discharge loss (W)	Indicated power (W)
5.00	10.8	399
8.00	4.57	393
11.0	2.70	391
14.0	1.90	390
17.0	1.47	390

4.6.3 Effect of Valve Thickness

In general, the natural frequency of the valve increases as the valve thickness increases, thus, the stiffness of the valve increases with thickness. Figure 4.9 shows the variations of the valve displacement and the pressure under the variation of the valve thickness. The magnitude of the valve displacement decreases when the valve thickness increases from 0.2 mm to 1.4 mm due to a higher stiffness. In addition, due to the

stiffness augmentation, the valve finds it difficult to open and therefore, the working fluid is unable to flow out from the working chamber completely causing the discharge loss to increase. As referred to Figure 4.9, the maximum pressure increases as the valve thickness increases and it reaches an extraordinary high value in the case of the valve thickness of 1.4 mm. As shown in Figure 4.9(f), the indicated power rises drastically from 390 W to 442 W as the discharge loss increases from 1.90 W to 53.8 W.

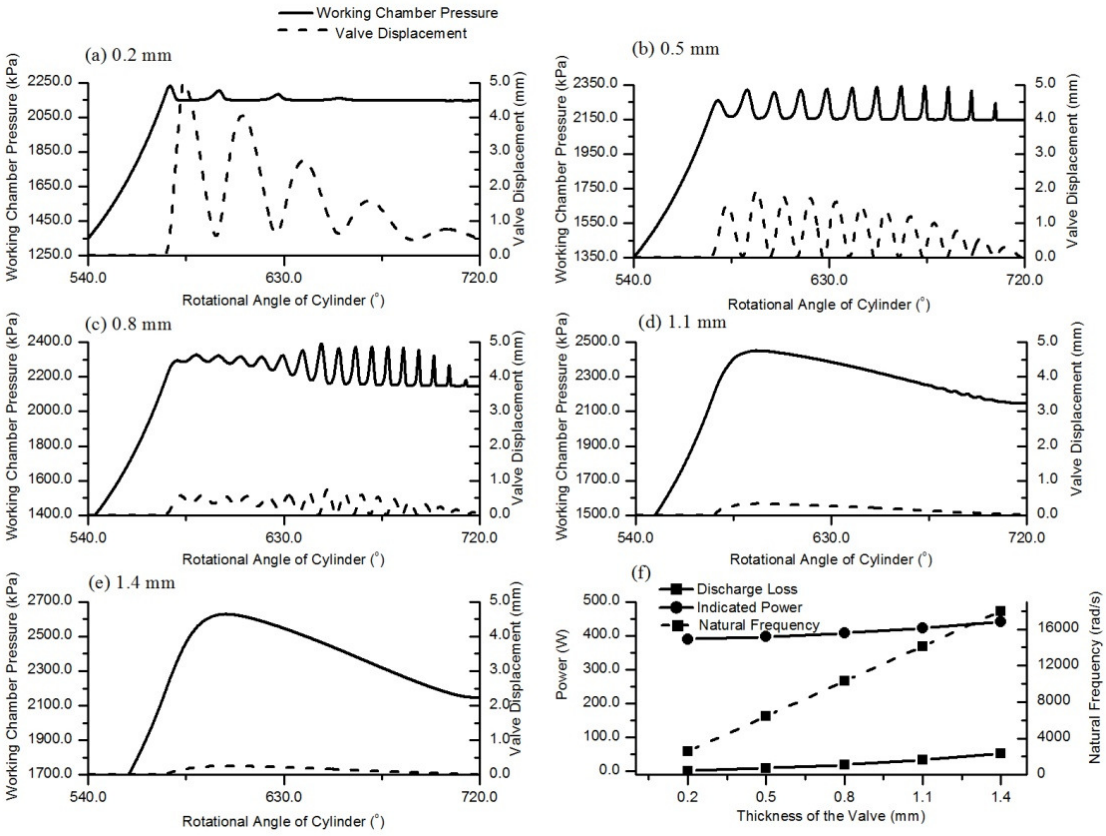

Figure 4.9 Effect of discharge valve thickness

4.6.4 Effect of Valve Width

With reference to equation (4.49), for a valve reed having a rectangular cross-sectional area, the width does not participate in the formulation of the natural frequency. Therefore, the natural frequency remains constant. However, the centrifugal force acting

on the valve increases due to the increment in the weight of the valve. Figure 4.10 shows that more valve oscillations and thus more pressure oscillations are induced due to the increment in the centrifugal force term. The discharge loss increases from 1.90 W to 3.35 W. However, unlike the effect due to the thickness of the valve, the width of the valve is not a dominant factor for the valve performance in terms of the discharge loss and the indicated power. In the practical design, the valve width should be sufficient in order to cover the discharge port completely.

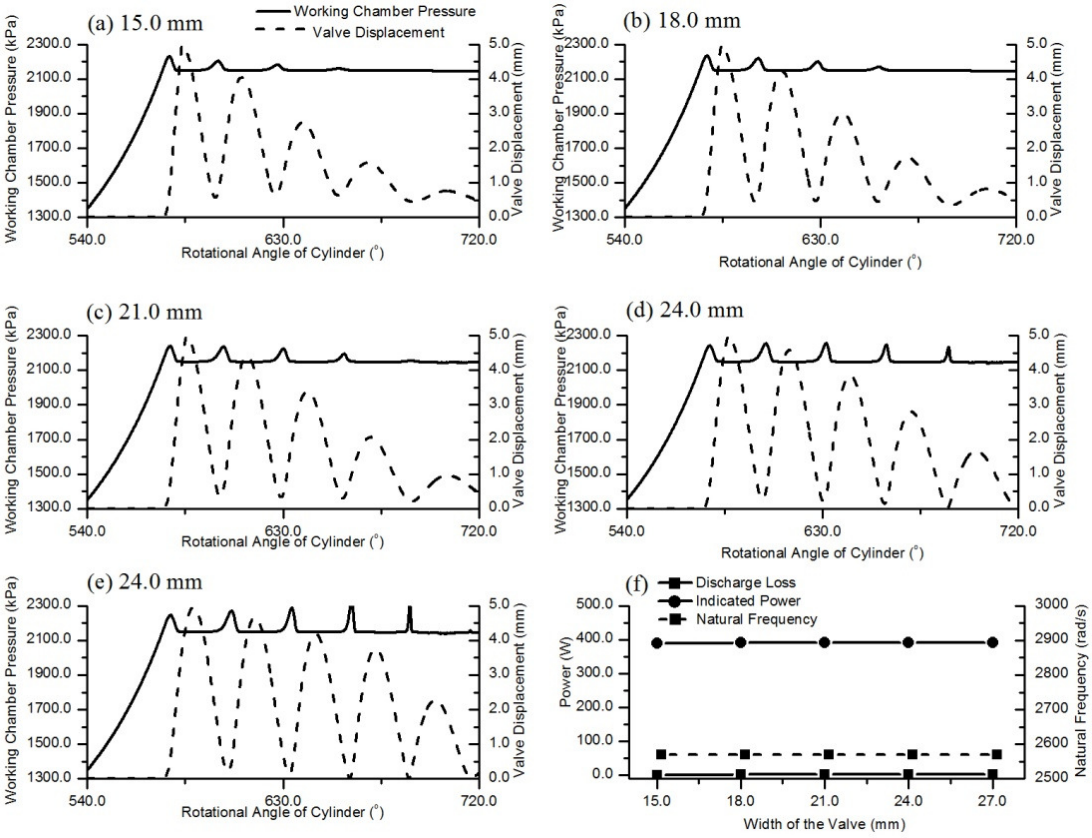

Figure 4.10 Effect of discharge valve width

4.6.5 Effect of Valve Length

Theoretically, the natural frequency of the valve will be reduced if the valve is longer. Thus, the longer valve is softer and easier to open during the discharge process

and incurs lower discharge loss. As shown in Figure 4.11, in the case of the valve length of 16.0 mm, the valve is short and stiff and thus, the working fluid is not able to be discharged out of the working chamber completely since the valve opening is small and it incurs more oscillations and the discharge loss. The number of oscillations in the variations of pressure and the valve displacement reduce as the length of the valve increases. As shown in Figure 4.11(f), the discharge loss decreases from 2.65 W to 1.90 W as the valve length increases from 16.0 mm to 24.0 mm. As a result, the valve length is not a dominant factor too in terms of the discharge loss and the indicated power. However, the frequency of the valve oscillating should be taken into consideration from the point of view of fatigue failure.

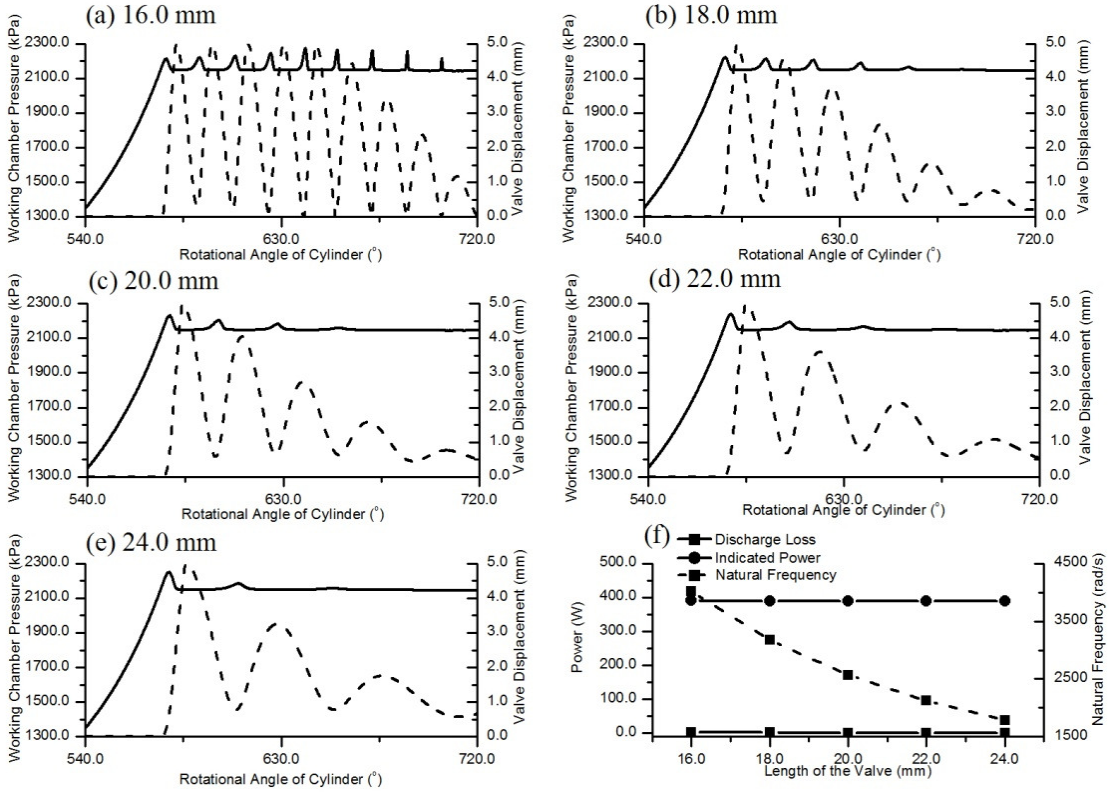

Figure 4.11 Effect of discharge valve length

4.6.6 Effect of damping coefficient

Damping is an inherent property of an oscillatory system. It tends to dissipate the energy of the system and reduce the amplitude of the oscillatory motion but does not affect the natural frequency of the system. Therefore, a lower value of the damping coefficient indicates more oscillations and vice versa. Figure 4.12 shows the variations of the pressure and the valve displacement under different damping coefficients and more oscillatory motions are found for lower damping coefficients. Figure 4.12(f) shows that the discharge loss decreases from 3.5 W to 1.5 W as the damping coefficient increases from 0.0 to 0.8 since a lower damping coefficient results in more frequent pressure oscillations.

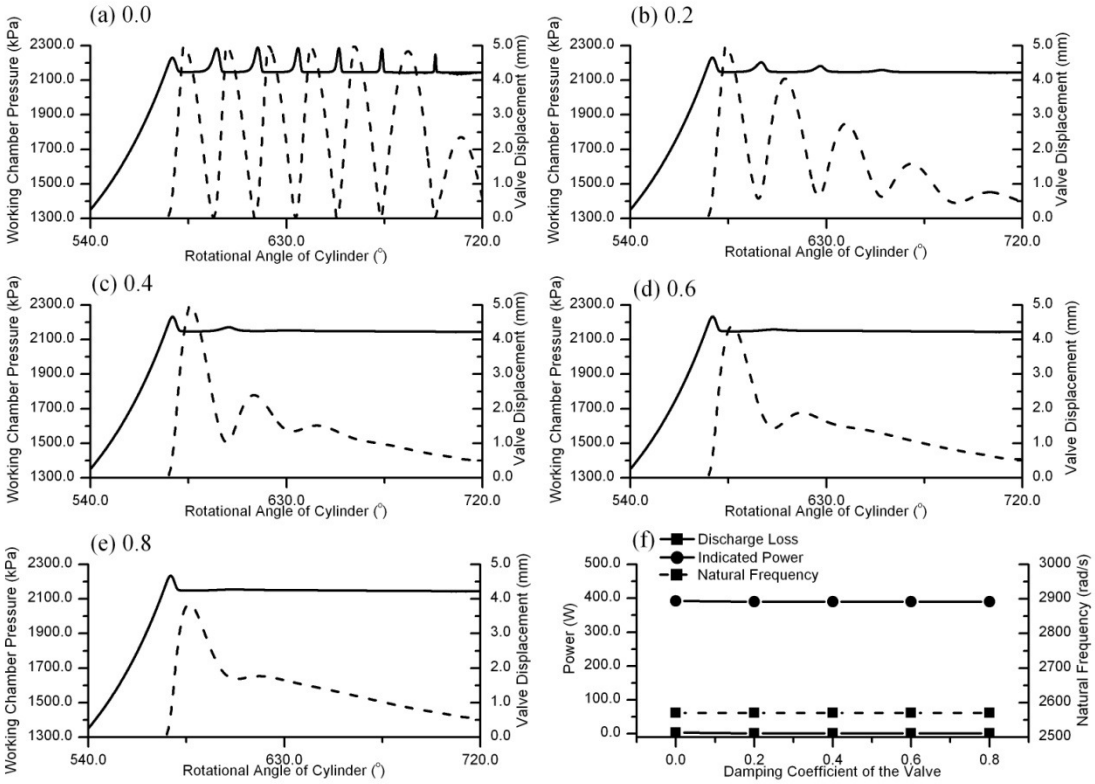

Figure 4.12 Effect of damping coefficient

4.7 Concluding Remarks

The geometrical, thermodynamics, mass flow and valve response models for fixed-vane revolving vane compressor are theoretically formulated and analyzed. The study reveals that the discharge valve in rotational motion enhance the valve opening behaviour and incurs lower discharge loss as compared to the stationary valve found in other types of positive-displacement compressors. In addition, the indicated power of the compressor is found to be characterized by the following:

- An undersized suction port results in a higher suction loss as more energy is required to recover the pressure loss during the suction process. In addition, the subsequent discharge process commences late.

- An undersized discharge port incurs more discharge loss as the working fluid is unable to be discharged out of the working chamber completely and hence, more frequent valve opening is required and thus, incurs higher discharge loss.

- The discharge loss is also affected by the valve design dimensions, such as the valve thickness, the valve width, the valve length and the damping coefficient. In particular, the discharge loss increment is 52.0 W for a thickness increment of 1.2 mm whereas the increments in the discharge loss for the changes in the valve width, the valve length and the damping coefficient, are all below 2.0 W. This indicates that the most dominant dimension in the valve design is the valve thickness from the point of view of compressor indicated power.

Chapter 5

Theoretical Study II:

Heat Transfer in Working Chamber

5.1 Introduction

The main performance characteristics of the fixed-vane revolving vane compressor in the area of thermodynamics and valve response have been examined. In addition, there are other areas worth to be investigated as their effect on the compressor performance are unknowingly great if without properly addressed. The heat transfer between the working fluid and the surrounding working chamber during the operation affects the pressure variation of the working fluid. Thus, the force acting on the compressor components will be affected and the bearing design requirements need to be altered for a reliable compressor operation.

The theoretical model for predicting the effect of in-chamber convective heat transfer between the working fluid and the surrounding chamber will be derived based on the test data of the revolving vane compressor [5]. The unique heat transfer parameters such as the characteristic velocity and hydraulic diameter will be defined.

5.2 Heat Transfer Model

The basic focus for the heat transfer model in compressor study is to determine the instantaneous convective heat transfer coefficient for the convective heat transfer between the surrounding chamber wall and the working fluid in the chamber. Generally, the convective heat transfer coefficient can be expressed as equation below.

$$h = \frac{k_f \frac{\partial T}{\partial \hat{n}}}{(T_\infty - T_{wall})}$$

where k_f is the thermal conductivity of the working fluid, T_∞ is the bulk fluid temperature outside the thermal boundary layer, T_{wall} is the wall temperature and $\partial T/\partial \hat{n}$ represents the temperature gradient which is normal to the surface of the wall. In the case of revolving vane compressor, the temperature gradient can be obtained by solving a set of coupled differential equations, which governs the conservation of mass, momentum and energy for the working fluid inside the working chamber. Hence, the evaluation of this temperature gradient requires an undoubtedly huge expense of computing effort. As a result, a simple convective heat transfer coefficient correlation is the matter of concern in the revolving vane compressor simulation studies. Since there is no convective heat transfer correlations derived specifically for rotary compressors in compressor heat transfer literature, the instantaneous convective heat transfer correlations proposed by several researchers, which were originally derived for reciprocating compressor are examined.

5.2.1 Heat Transfer Correlations

- **Correlation by Adair et al. [97]**

$$\mathrm{Nu} = 0.053 \times \mathrm{Re}^{0.8} \times \mathrm{Pr}^{0.6}$$

The correlation proposed by Adair et al. [97] is a function of Reynolds number and Prandtl number. Prandtl number is a ratio of kinematic viscosity and thermal diffusivity and hence it is a dimensionless number and it is a function of fluid properties. On the other hand, Reynolds number is a ratio between inertia force and viscous force, which is geometrically and flow dependent. In their study, the characteristic velocity of the working fluid inside the chamber of reciprocating compressor is treated as the product of swirl velocity and equivalent hydraulic diameter, which are represented by the two equations below, respectively.

$$\omega_g = \begin{cases} 2\omega(1.04 + \cos 2\theta) & \text{for } \frac{3}{2}\pi < \theta < \frac{1}{2}\pi \\ \omega(1.04 + \cos 2\theta) & \text{for } \frac{1}{2}\pi < \theta < \frac{3}{2}\pi \end{cases}$$

$$D_h = \frac{6V}{A} = \frac{6\left[\pi\left(\frac{D}{2}\right)^2 Z\right]}{\pi DZ + 2\pi\left(\frac{D}{2}\right)^2}$$

where ω is the crankshaft rotational speed, D is the piston bore diameter and Z is the distance between piston and cylinder head.

- **Correlation by Annand [98]**

$$\mathrm{Nu} = 0.7 \times \mathrm{Re}^{0.7}$$

In contrast to the correlation by Adair et al., the correlation proposed by Annand [98] in his simulation model for a four-stroke ignition engine is a function of Reynolds number only. The author treated the characteristic velocity of the working fluid inside

the chamber as the piston speed and the equivalent hydraulic diameter as cylinder bore diameter.

- **Correlation by Liu and Zhou [99]**

$$\mathrm{Nu} = 0.75 \times \mathrm{Re}^{0.8} \times \mathrm{Pr}^{0.6}$$

The form of correlation proposed by Liu and Zhou [99] is similar to Adair et al.'s correlation. The authors indicated that the magnitude of convective heat transfer in the chamber of reciprocating compressor is significant and hence introduce a larger empirical constant. Furthermore, the swirl velocity of the working fluid inside the chamber has been modified to the following expressions too.

$$\omega_g = \begin{cases} 2\omega(1.04 + 0.5\cos 2\theta) & \text{for } \frac{3}{2}\pi < \theta < \frac{1}{2}\pi \\ \omega(1.04 + 0.45\cos 2\theta) & \text{for } \frac{1}{2}\pi < \theta < \frac{3}{2}\pi \end{cases}$$

5.2.2 Heat Transfer Parameters

The frequently used convective heat transfer correlations in compressor heat transfer modelling literature are presented and it is known that the approach on characteristic velocity and the equivalent hydraulic diameter are crucial in the quantitative analysis of in-chamber convective heat transfer for the case of revolving vane compressor.

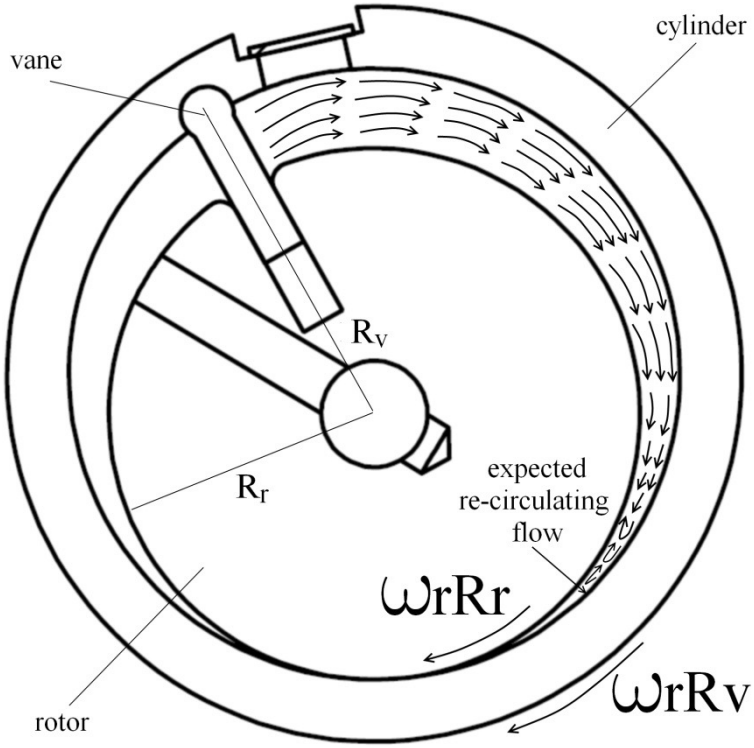

Figure 5.1 Expected flow field in compression chamber of revolving vane compressor

The original revolving vane compressor design is presented in Figure 5.1. During compression process, the vane is not only in rotation but also moves in a reciprocating fashion radially while the rotor and the cylinder rotate. Therefore, it can be visualized that the working fluid is being pushed by the rotating vane and at the same time, it is also dragged by the motion of the rotor and the cylinder to the compression end of volume. Besides that, the working fluid which is at the vicinity of the vane will also follow the reciprocating motion of the vane during the operation. The angular velocity of the cylinder and the reciprocating velocity of the vane are expressed by equations (5.1) and (5.2) respectively.

$$\omega_c = \omega_r \left[\frac{R_v \frac{dR_v}{d\varphi}}{R_c a \sin \varphi_c} \right] \tag{5.1}$$

$$V_v = \omega_r \left[a \sin \varphi - \frac{a^2 \sin(2\varphi)}{2\sqrt{R_c^2 - (a \sin \varphi)^2}} \right] \tag{5.2}$$

where $R_v = \sqrt{R_c^2 - (a \sin \varphi)^2} - a \cos \varphi$.

The comparison of equations (5.1) and (5.2) illustrated in Figure 5.2 shows that the maximum velocity of the reciprocating motion of the vane is one order of magnitude smaller than the rotational velocity of the rotor and the cylinder.

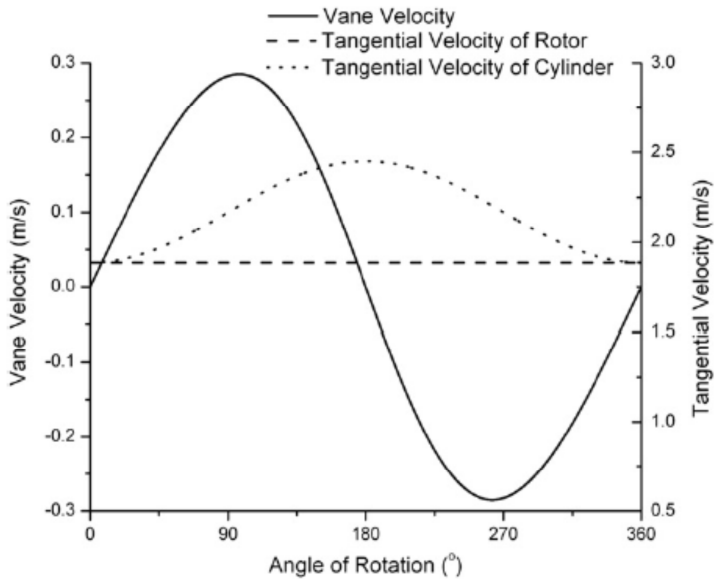

Figure 5.2 The velocity profiles of vane, rotor and cylinder at 600 rev/min

As a result, the magnitude of the flow velocity inside the chamber is mainly bounded by the rotational velocities of the rotor and the cylinder. In other words, the rotational motions of the vane, the rotor and the cylinder constitute the main flow inside the working chamber of revolving vane compressor. Based on the deduction, the velocity profile of the main flow inside the working chamber assuming no-slip condition at the boundary of the inner cylinder and outer rotor surface can be modelled as a trapezoidal profile, with lower side being the tangential velocity of the rotor and the

upper side being the tangential velocity of the cylinder as referred to the centre of the rotor. Thus, the average velocity of the main flow inside the working chamber can be expressed as equation (5.3).

$$\overline{U} = \frac{1}{(R_v - R_r)} \int_{R_r}^{R_v} \omega_r R dR = \frac{\omega_r}{2}(R_v + R_r) \tag{5.3}$$

The average velocity will be used as characteristic velocity in the calculation of Reynolds number. However, it should be noticed that the full details of the flow inside the compression chamber of revolving vane compressor shall include the abrupt flow through the discharge port and the re-circulating flow occurs during the later period of the compression process at the end of compression volume, where high velocity gradient and turbulence intensity were expected. All these flow phenomena are disregarded in the present analysis. Subsequently, since the characteristic velocity is evaluated, the equivalent hydraulic diameter can be determined. By definition, the equivalent hydraulic diameter is the quadruple of the ratio between the cross-sectional area as seen by the flow and the wetted perimeter of that cross-section. Thus, the cross-sectional area as seen by the "main flow" inside the chamber can be regarded as the area of the protruded part of the sliding vane, which is the part of the vane that is exposed to the working fluid. As a result, the equivalent hydraulic diameter can be expressed as equation (5.4).

$$D_h = 4 \times \frac{(R_v - R_r) \times L_c}{2(R_v - R_r + L_c)} \tag{5.4}$$

The definition of the equivalent hydraulic diameter and the characteristic velocity of the flow inside the compression chamber are now fully defined and hence

the heat transfer model can be included into the simulation study, in which the instantaneous convection heat transfer coefficient can be calculated by

$$h = Nu\left(\frac{k_f}{D_h}\right)$$

and the instantaneous in-chamber convective heat transfer can be written as equation (5.5).

$$\frac{dQ_c}{d\theta} = \frac{1}{\omega_r} \times h \times A_{ht} \times (T_{wall} - T_c) \tag{5.5}$$

where A_{ht} is the total heat transfer area and T_{wall} is the instantaneous temperature of the wall of the surrounding chamber in contact with the working fluid. Since the thermal mass of the chamber material is relatively large as compared to the cycle time of the compressor cycle, it is expected that the value of T_{wall} is relatively constant throughout a compressor cycle. In this study, it is assumed to be a constant and it is equal to the arithmetic mean of the suction and discharge gas temperature.

5.2.3 Results and Discussions

The measurements of the pressure-angle histories in the experimental studies of revolving vane compressor were carried out based on the operating conditions and the main design dimensions are presented in Table 5.1.

Table 5.1 Operating conditions and main dimensions of RV prototype [5]

Operating Conditions (Air is the working fluid)			
Volume displacement	34.65 cc/rev	Suction pressure	1.01 bar
Operational speed	600, 800 and 1000 rpm	Discharge pressure	2.00 bar
Main Dimensions			
Rotor radius	30.0 mm	Vane length	18.0 mm
Cylinder radius	34.5 mm	Vane thickness	5.0 mm
Compressor length	38.0 mm	Vane tip radius	3.0 mm
Suction port diameter	10.0 mm	Discharge port diameter	10.0 mm

Figures 5.3 to 5.5 show the comparison between the prediction (without in-chamber convective heat transfer) and the measurement of pressure-angle histories for the compressor shaft speeds of 600, 800 and 1000 rev/min.

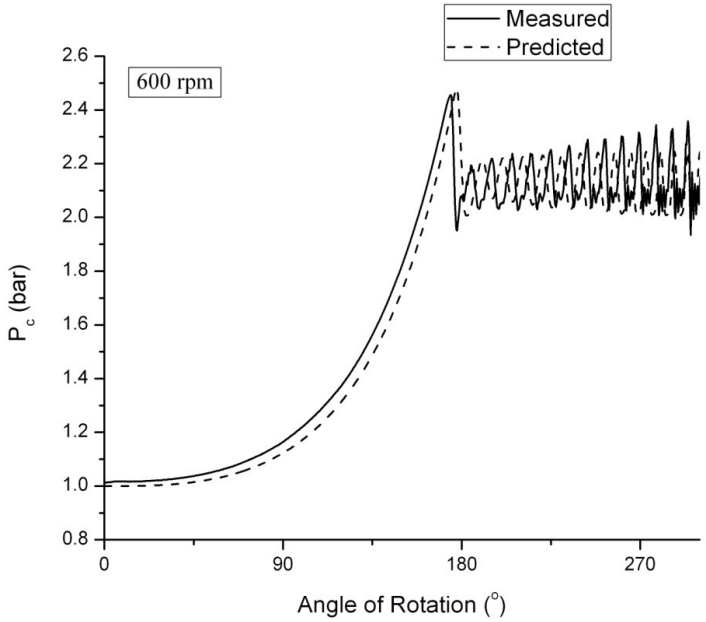

Figure 5.3 Measured and predicted pressure variations in compression chamber of revolving vane compressor (600 rpm, prediction is without heat transfer)

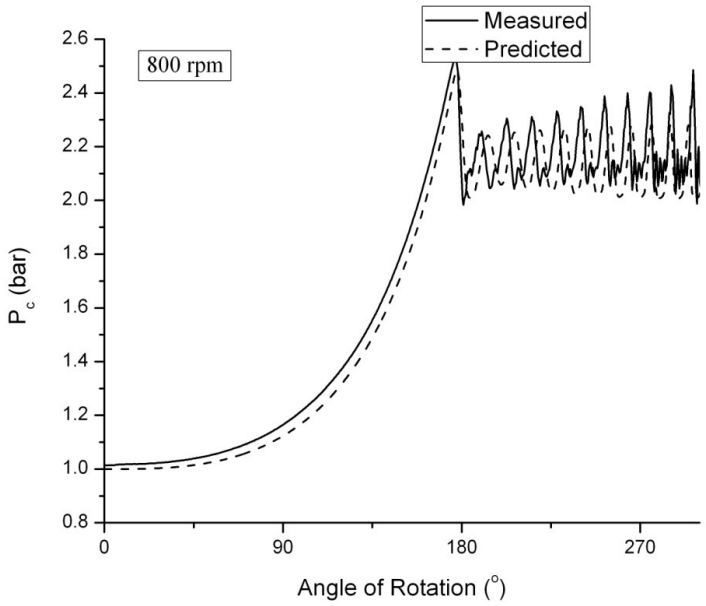

Figure 5.4 Measured and predicted pressure variations in compression chamber of revolving vane compressor (800 rpm, prediction is without heat transfer)

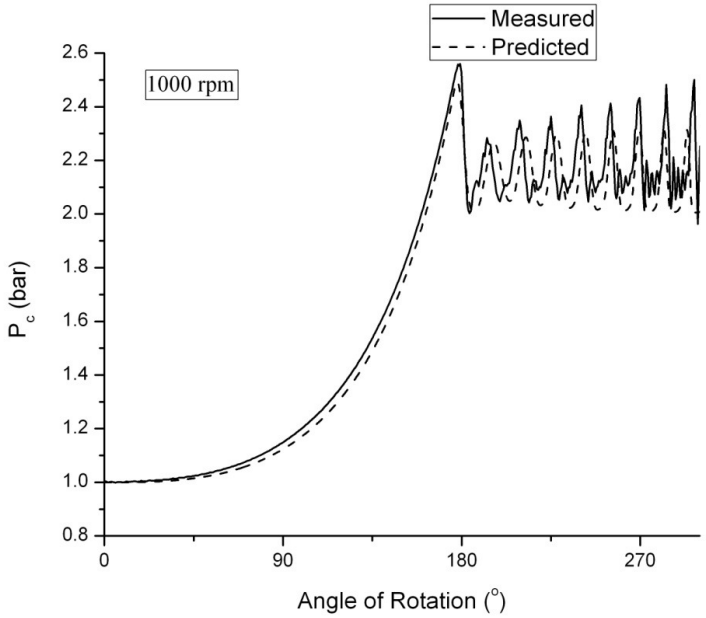

Figure 5.5 Measured and predicted pressure variations in compression chamber of revolving vane compressor (1000 rpm, prediction is without heat transfer)

Generally, it is observed that both predicted and measured pressure-angle histories follow the same trend during compression and discharge process, which is in consistency with the assumption in compressor thermodynamics model using spatially independent approach. However, the theoretical prediction always under predicts the variation of the chamber pressure. It is deduced that the discrepancy is caused by the exclusion of the in-chamber convective heat transfer between the surrounding chamber and the working fluid during the compression process. In addition, this argument is supported by the fact that the discrepancy decreases as the compressor speed increases. This is because at higher operational speeds, the heat transfer effect is lower as there is shorter time for heat transfer to occur since the cycle time gets shorter. To validate the above deductions, the in-chamber convective heat transfer has been included in the compressor simulation model by using the available convective heat transfer correlations as discussed earlier.

Figure 5.6 shows the measured and predicted pressure variations from different convective heat transfer correlations for shaft speed at 600 rev/min. The comparison shows that the correlation presented by Liu and Zhou gives the best prediction. In addition, it is also noted that the correlations by Adair and Annand underestimated the heat transfer effect and Annand's correlation gives the poorest prediction. Figure 5.7 shows the instantaneous and average heat transfer rate and heat flux with different correlations at 600 rev/min. The correlation from Annand is not suitable among the correlations as it predicts the reverse heat transfer direction. The heat transfer effect is obvious when the rotational speed is at 600 rev/min. The thermal interaction duration is longer when the rotational speed is lower. Therefore, correlation from Liu & Zhou gives a better prediction than Adair's at 600 rev/min.

In the case for the higher shaft speed of 800 rev/min, as shown in Figures 5.8 and 5.9, Liu and Zhou's correlation gives the prediction that matches the measured pressure variation well while the predictions from the other two correlations still underestimate the heat transfer effect. For the case when the shaft speed is increased to 1000 rev/min, the result shown in Figure 5.10 reveals that the prediction given by Liu and Zhou correlation matches the measured data well while correlations from Annand and Adair remain underestimating, though the latter moves closer to the measured values. This is because the available duration for the heat to be transferred is shorter and therefore, the heat transfer is expected to be less effective and the lower average heat transfer rate is expected, as shown in Figure 5.11. It can be concluded that Liu and Zhou's correlation gives the best-fit description for in-chamber convective heat transfer for revolving vane compressor over the ranges of speeds evaluated. This correlation is found to give a maximum discrepancy of less than 2.0% and occurs during the initial compression process when the chamber pressure is low.

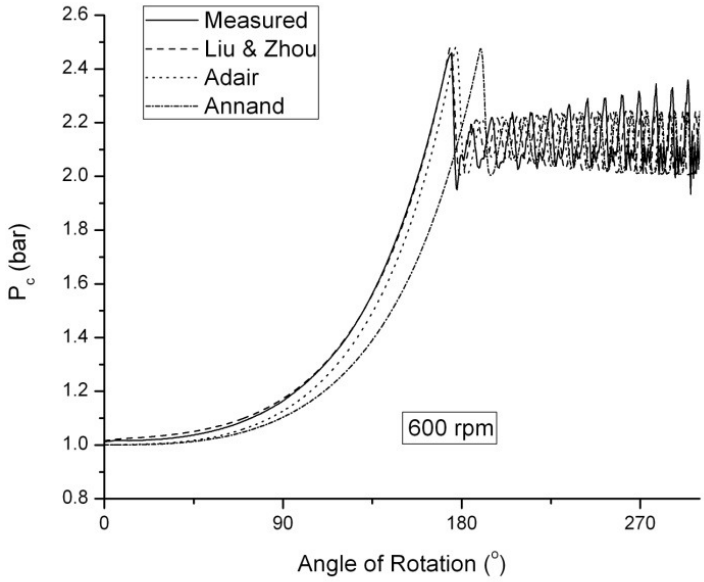

Figure 5.6 Measured and predicted pressure variations in compression chamber of revolving vane compressor (600 rpm, prediction is with heat transfer effect)

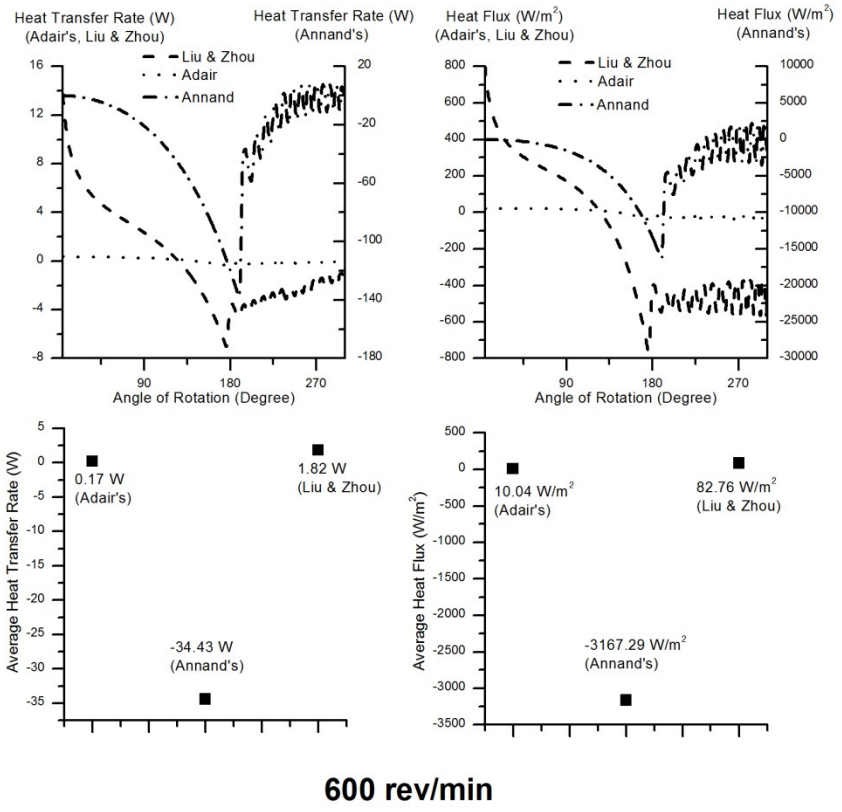

Figure 5.7 The instantaneous and average heat transfer rate and heat flux with different correlations at 600 rev/min

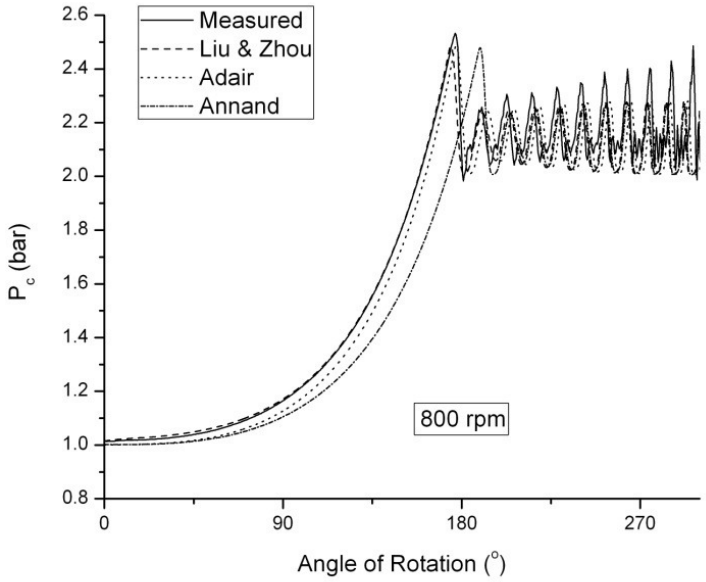

Figure 5.8 Measured and predicted pressure variations in compression chamber of revolving vane compressor (800 rpm, prediction is with heat transfer effect)

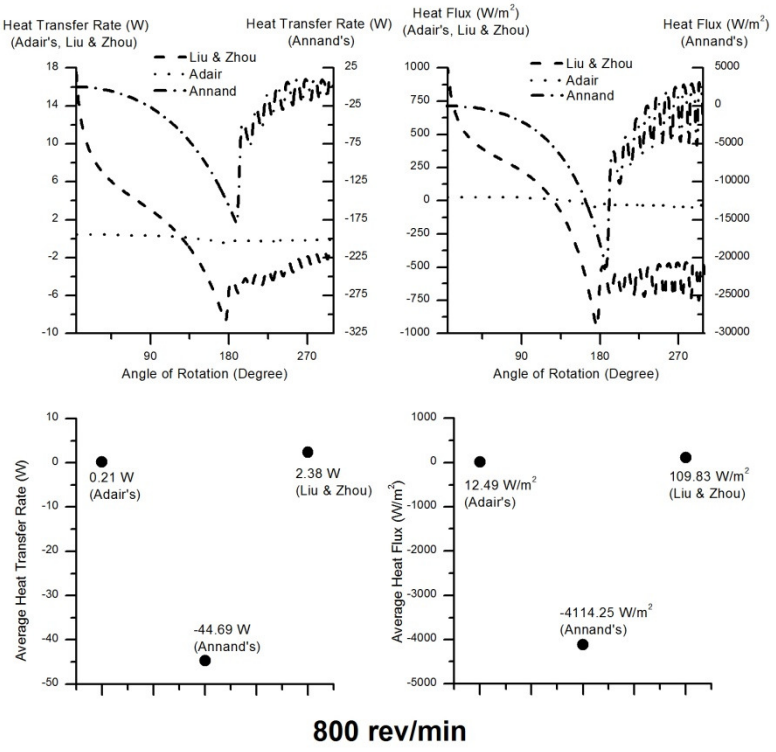

Figure 5.9 The instantaneous and average heat transfer rate and heat flux with different correlations at 800 rev/min

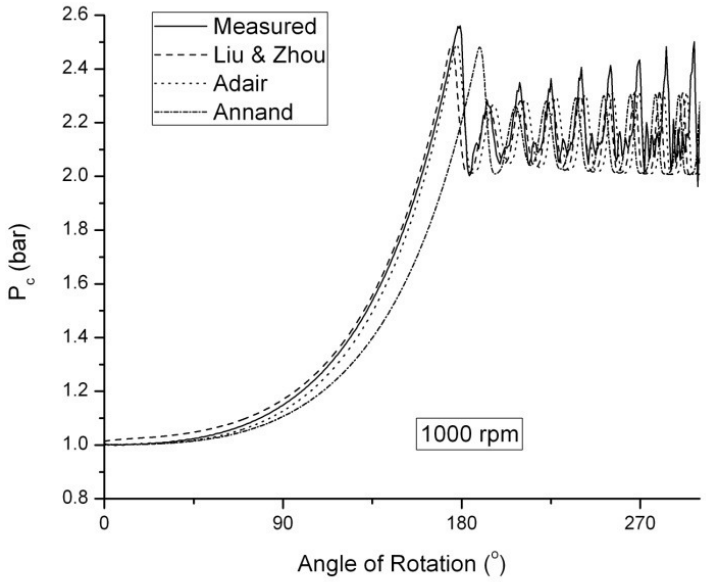

Figure 5.10 Measured and predicted pressure variations in compression chamber of revolving vane compressor (1000 rpm, prediction is with heat transfer effect)

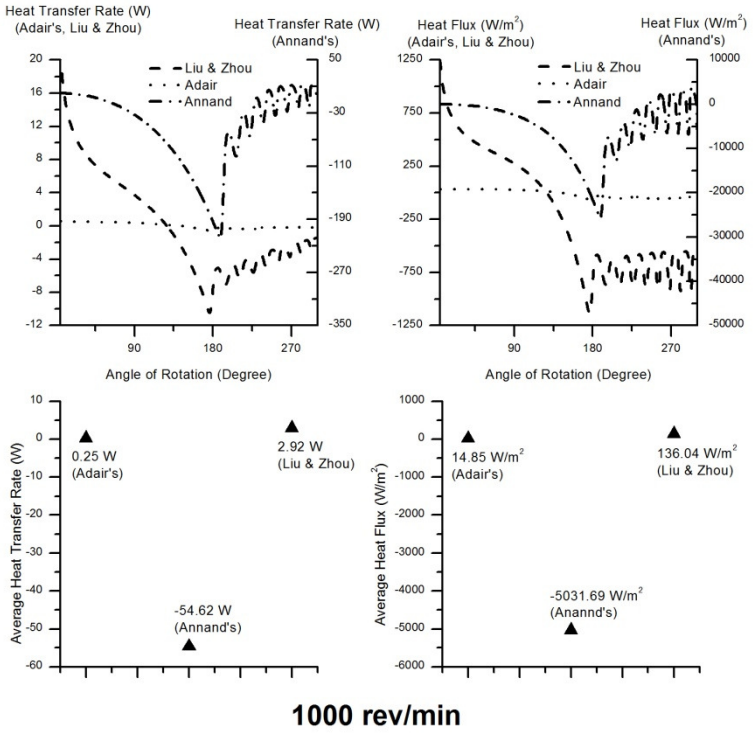

Figure 5.11 The instantaneous and average heat transfer rate and heat flux with different correlations at 1000 rev/min

5.3 Concluding Remarks

The accuracy of the theoretical prediction of the revolving vane compressor has been improved by the inclusion of the instantaneous in-chamber convective heat transfer between the working fluid and the surrounding chamber wall. The heat transfer correlation derived by Liu and Zhou gives the best fit when comparing the predicted chamber pressure to the measured pressure data for shaft speeds of 600, 800 and 1000 rpm. The maximum discrepancy has been reduced from 5.2 % to 1.8 %.

The details account for the convective heat transfer in this unique crescent-shaped compressor working chamber with both rotor and cylinder rotating at their own centres are presented. The flow inside the compression chamber is mainly characterized by the rotational velocities of the rotor and the cylinder. Thus, the characteristic velocity of the flow inside the chamber can be approximated as the arithmetic mean of the rotor and the cylinder tangential velocities. In addition, the equivalent hydraulic diameter is uniquely defined as the quadruple of the ratio between the area of the protruded portion of the vane and the wetted perimeter of that area. The comparison between the measured and the predicted results clearly shows that the inclusion of the in-chamber convective heat transfer model is significant and the compression process is not adiabatic.

Chapter 6

Theoretical Study III:

Force Analysis and Journal Bearing Design

6.1 Introduction

The design of a compressor is incomplete without understanding of the forces acting on every compressor component. The forces acting on the compressor are dynamic in nature and the analysis allows the designer to understand the actual instantaneous load on the compressor. Normally, journal bearings are used to support the dynamically loaded compressor components. The journal bearing is a hollow cylinder which wraps the rotating component (usually known as journal) and filled with the lubricant within the space separating them. The lubricant acts as a medium that supports the journal and prevents the occurrence of the metal to metal contact.

In this chapter, the theoretical details of the forces analysis and the journal bearing design for the revolving vane compressor will be presented. The forces acting on the revolving vane compressor components will be discussed by examining the free body diagrams of the components. Subsequently, the design analysis for the dynamically loaded journal bearing of the compressor will be presented. The influence of the pressure ratio, operating speed, compressor configuration as well as the bearing

design parameters, namely the bearing radius and the bearing length on the journal bearing performance will be discussed.

6.2 Force Analysis

The main forces acting on the rotor, the cylinder and the vane in the fixed-vane revolving vane compressor are shown in Figure 6.1. During the operation, the cylinder is driven by a motor and it rotates the rotor through split bush by using the vane that is rigidly attached to it. Hence, there exists a contact force between the vane and the split bush. The magnitude of the contact force (F_v) can be found by considering the torque equilibrium for the rotor as given in equation (6.1).

$$I_r \times \alpha_r = F_{vn} \times R_r \times \cos(\phi_r - \phi_c) + \sum \left(\overrightarrow{F_f} \times \vec{r}\right)_r \tag{6.1}$$

It can be seen that the magnitude of the contact force is dependent on the rotational inertia of the rotor and the torque caused by the friction. It is noted that the latter is negligible as compared to the former and therefore, the vane contact force can be presented by equation (6.2) approximately.

$$F_{vn} = \frac{I_r \times \alpha_r}{R_r \cos(\phi_r - \phi_c)} \tag{6.2}$$

The contact force (F_{vn}) is used to drive the rotor into rotational motion and the magnitude depends on the rotor inertia. In equation (6.2), I_r represents the rotational inertia of the rotor and it can be expressed by equation (6.3).

$$I_r = \frac{1}{2} m_r R_r^2 + \frac{1}{2} m_{rs} R_{rs}^2 \tag{6.3}$$

It is noted that equation (6.3) is valid under the consideration of a solid rotor piece whereby in fact, the rotor is lighter due to the necessary features, namely suction port and vane slot. In addition, due to the vane contact force, there is a friction force occurs at the vane side and its slot, as shown in Figure 6.1. The frictional force depends on the magnitude of the contact force and the local friction coefficient, which can be expressed by equation (6.4). As a result, it is deduced that the vane side friction increases as the rotor inertia increases.

$$F_{vf} = \eta_{vs} \times F_{vn} \tag{6.4}$$

The vane reciprocates inside the vane slot provided by the split bush in the rotor during operation. The reciprocating motion of the vane resembles the vane motion inside the rolling piston compressor. The vane side friction coefficient in a rolling piston compressor is experimentally found as 0.15 [139]. Hence, this value of friction coefficient is adopted in the theoretical analysis on vane-side frictional loss of revolving vane compressor due to the similarities in motion and lubrication condition.

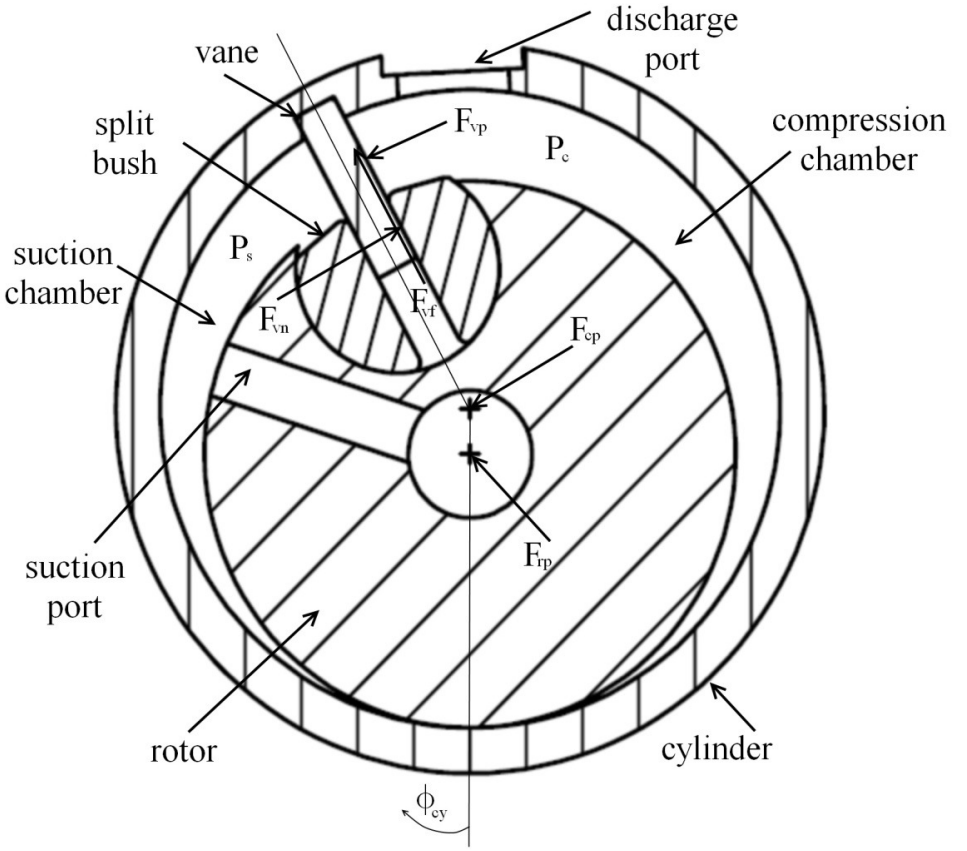

Figure 6.1 Force diagram of fixed-vane revolving vane compressor

In addition to the contact force and the friction force at the vane side, part of the vane body is exposed to the working fluid in the working chamber and hence both sides of the vane are subjected to the working fluid pressure in the suction and the compression chamber respectively. The magnitude of this pressure force on the vane is

$$F_{vp} = (P_c - P_s) \times L_{vn} \times L_c \tag{6.5}$$

Besides, the outer surface of the rotor and the inner surface of the cylinder are exposed to the working fluid pressure in the suction and the compression chambers, which are denoted by F_{rp} and F_{cp} respectively. As a result, the resultant force acting on the rotor and the cylinder in the horizontal and the vertical planes can be obtained by summing all the forces in the respective directions, which are shown in equations (6.6a) to (6.6d).

$$F_{rx} = F_{rpx} - F_{vn}\cos\phi_c - F_{vf}\sin\phi_c \quad (6.6a)$$

$$F_{ry} = F_{rpy} + F_{vn}\sin\phi_c - F_{vf}\cos\phi_c \quad (6.6b)$$

$$F_{cx} = F_{cpx} + F_{vp}\cos\phi_c + F_{vn}\cos\phi_c + F_{vf}\sin\phi_c \quad (6.6c)$$

$$F_{cy} = F_{cpy} - F_{vp}\sin\phi_c - F_{vn}\sin\phi_c + F_{vf}\cos\phi_c \quad (6.6d)$$

The variations of the resultant force acting on the rotor and the cylinder considering the internal leakage losses [121] are shown in Figure 6.2. The resultant force acting on the rotor and the cylinder are determined by the inertia force and the force due to the working fluid pressure. The internal leakage occurs at the clearances between compressor components due to the pressure difference across the high-pressure compression chamber and the low-pressure suction chambers. As a result, under the consideration of internal leakage, the pressure profile in the working chamber over one complete cycle fluctuates more than the perfectly-sealed compressor and hence, the resultant force acting on the rotor and the cylinder will be affected.

The variations of the working fluid pressure in the chamber, the resultant force acting on the rotor and the cylinder with and without leakage consideration are shown in Figure 6.2. The pressure profiles in both cases are similar except during the end of discharge process. However, the variations of the resultant force on the rotor and the cylinder exhibit the similar profile in both cases. The distinct pressure profile difference at the end of the discharge process between both cases has no remarkable effect on the resultant force because the actual area acted by the working fluid pressure towards the end of discharge process is small.

Both forces exhibit identical variations and magnitude throughout the whole compressor cycle. The existence of the first peak is due to the maximum of the product between the vane exposed area and the pressure difference across the vane. The subsequent peaks are due to the pressure fluctuations as a result of discharge valve reed vibration during the discharge process. It can be seen that the force experienced by the rotor and the cylinder are dynamic with respect to the rotation of the compressor and these require journal bearing supports.

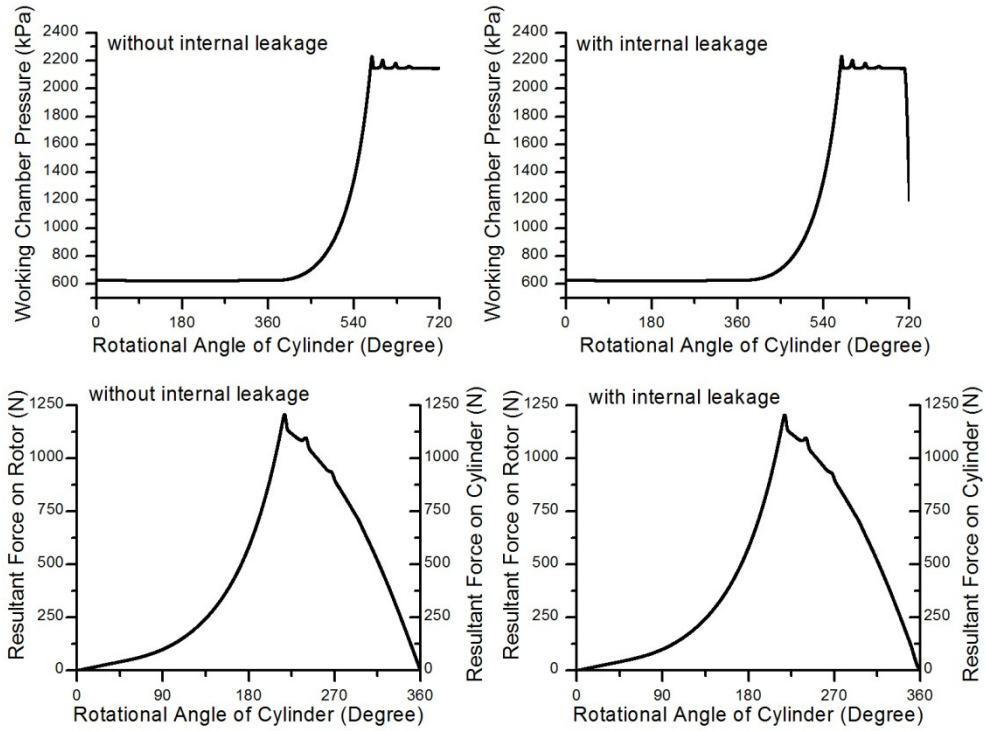

Figure 6.2 The profiles of working fluid pressure and resultant force on the rotor and the cylinder with and without leakages considerations

6.3 Design Method for Journal Bearing

The magnitude of the forces acting on the compressor components can be as high as or greater than 1 kN. These forces can be supported by journal bearings. As

shown in Figure 6.3, the lubricant which fills the space between the journal and the bearing acts as a medium that supports the rotating journal and prevents the occurrence of the metal to metal contact. In the same figure, it can be observed that as the shaft rotates, an oil wedge will be created and the fluid pressure will be developed within the lubricant to support the loaded journal and relocates the journal within the bearing clearance such that the centre of the journal is at a distance away from the centre of the stationary bearing. A proper design of a lubrication oil distribution system for a proper functioning of the journal bearing is important to ensure the oil is sufficiently delivered to the lubricated region at the required flow rates. The details on oil distribution will be presented in Chapter 8.

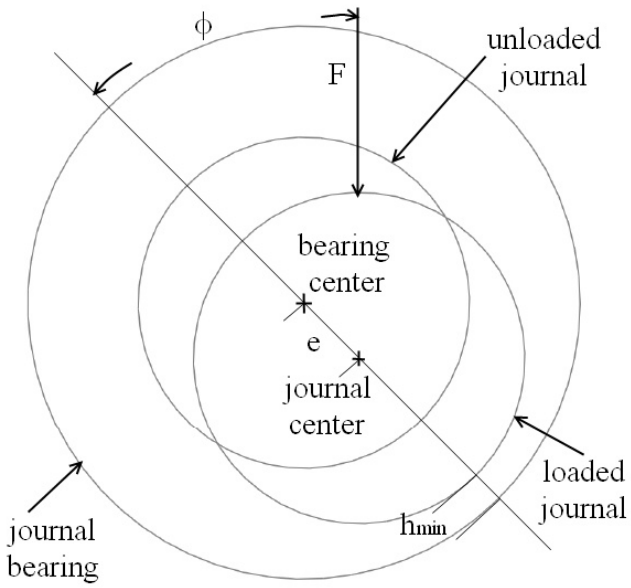

Figure 6.3 Schematics of a journal bearing

With reference to Figure 6.3, it can be seen that if the load (F) varies, the journal centre changes accordingly and causes the fluctuations in the angular position of the starting and the ending of lubricant pressure profile. This results in a varying minimum oil film thickness and varying magnitude of the lubricant pressure supporting the load.

As a result, the interacting surfaces of the journal and the bearing are subjected to fluctuating stress which makes the fatigue strength as an important concern in the selection of the bearing material. In addition, the smallest minimum oil film thickness throughout the entire compressor cycle dictates the specifications of the surface roughness for the surface of the journal and the bearing. Therefore, the variations of the minimum oil film thickness and the maximum film pressure are important parameters required for a reliable journal bearing operation.

To determine the pressure distribution in a journal bearing with an arbitrary film shape, Reynolds equation can be used [140]. From the consideration for conservation of momentum and mass with the assumptions for laminar, Newtonian, inertia-less and thin film flow, the Reynolds equation can be obtained as shown in equation (6.7).

$$\frac{\partial}{\partial x}\left(\frac{\rho h^3}{12\mu}\frac{\partial P}{\partial x}\right)+\frac{\partial}{\partial y}\left(\frac{\rho h^3}{12\mu}\frac{\partial P}{\partial y}\right) = \frac{1}{2}\frac{\partial}{\partial x}[\rho(U_a+U_b)h]-\rho U_b\frac{\partial h}{\partial x}+\rho(w_b-w_a)+h\frac{\partial \rho}{\partial t} \quad (6.7)$$

Both terms on the left hand side of equation (6.7) represent the flow due to pressure gradients, which is known as Poiseuille flow. For the terms on the right hand side, the first term represents the flow due to shear, which is known as Couette flow; the second term indicates the flow due to geometric squeeze; the third term shows the flow due to normal squeeze and the last term indicates the time-variant expansion. The Couette flow term can be expanded into equation (6.8).

$$\frac{1}{2}\frac{\partial}{\partial x}[\rho(U_a+U_b)h]=\frac{1}{2}\left[\rho h\frac{\partial(U_a+U_b)}{\partial x}+\rho(U_a+U_b)\frac{\partial h}{\partial x}+h(U_a+U_b)\frac{\partial \rho}{\partial x}\right] \quad (6.8)$$

The first component of Couette flow takes into account of the physical stretch of the bearing material. In practice, the bearings are made of rigid materials, hence this term is nil. The second term shows the physical wedge and it is the most important term for the pressure generation in the journal bearing. Basically, to generate a positive load-carrying capacity, the surface should have a converging gap, hence $\partial h/\partial x$ is negative. The last term on the right hand side of the equation shows the density wedge, which is capable of generating positive load carrying capacity but the influence is subtle as compared to physical wedge.

For most practical applications, the density wedge, the physical stretch and local expansion terms are neglected. Hence, a simplified Reynolds lubrication equation is formed and it is given as equation (6.9).

$$\frac{\partial}{\partial x}\left(\frac{\rho h^3}{12\mu}\frac{\partial P}{\partial x}\right)+\frac{\partial}{\partial y}\left(\frac{\rho h^3}{12\mu}\frac{\partial P}{\partial y}\right)=\frac{1}{2}\rho(U_a-U_b)\frac{\partial h}{\partial x}+\rho(w_b-w_a) \qquad (6.9)$$

For a closed-form solution, special circumstances are required. One of the special circumstances is known as infinitely short bearing approximation. The approximation states that the length of journal bearing is very much smaller than its diameter and thus the first term on the left-hand side of equation (6.9) is negligible as compared to the second term. Physically, it means the flow due to rotational motion is negligible as compared to the flow to the side of the journal bearing, or in other words, the flow is easier to flow to the side of the bearing. Based on this infinitely short approximation, the pressure distribution can be found and it is given in equation (6.10).

$$P_{ISA}=-6\mu\left(\frac{L_{Br}}{\delta_{Br}}\right)^2\times\left[\frac{1}{4}-\left(\frac{y}{L_{Br}}\right)^2\right]\times\left[\frac{\dot{\varepsilon}\cos\theta+\varepsilon\left(\dot{\phi}-\omega_{av}\right)\sin\theta}{(1+\varepsilon\cos\theta)^3}\right] \qquad (6.10)$$

where ε represents eccentricity ratio, which is defined as the ratio between the centre distance of the rotating journal and the stationary bearing to the bearing clearance and $\dot{\varepsilon}$ represents the rate of change in the eccentricity ratio. On the other hand, the journal bearing configuration can be assumed as infinitely long too. In this case, the term associated with the flow to the side of bearing is negligible as compared to the flow in the direction of rotation and the pressure distribution is given by equation (6.11).

$$P_{ILA} = -6\mu\left(\frac{R_{Br}}{\delta_{Br}}\right)^2 \times \left[\dot{\varepsilon}\cos\theta + \varepsilon\left(\dot{\phi} - \omega_{av}\right)\sin\theta \times \left(\frac{2}{2+\varepsilon^2}\right)\right] \tag{6.11}$$

However, the journal bearing in practical design is neither infinitely long nor infinitely short. The journal bearing has a finite length in reality. Reason and Narang [141] proposed a pressure distribution for a finite-length journal bearing. The expression combines the solutions of infinitely short and infinitely long approximations harmonically and it is given by equation (6.12).

$$P = \frac{1}{(1+\varepsilon\cos\theta)^3} \times \left\{-6\mu\left(\frac{L_{Br}}{\delta_{Br}}\right)^2\left[\frac{1}{4} - \left(\frac{y}{L_{Br}}\right)^2\right]\right\} \times \left[\frac{\dot{\varepsilon}\cos\theta + \varepsilon\left(\dot{\phi} - \omega_{av}\right)\sin\theta}{1 + \frac{0.25 - (y/L_{Br})^2}{B_1}}\right] \tag{6.12}$$

where $B_1 = (1+\varepsilon\cos\theta)(2+\varepsilon\cos\theta)/(L_{Br}/R_{Br})^2$.

As a result, the load-carrying capacity of the fluid film can be found by integrating the pressure variation in the fluid film region over the surface area and it is in balance with the load acting on the rotating shaft. Resolve the forces into the

directions of line of centres and the direction perpendicular to it, the force balance equations can be written as equations (6.13a) and (6.13b).

$$F\cos\phi = -\int_{\theta_1}^{\theta_2}\int_{-L/2}^{L/2} P\cos\theta\, R\, d\theta\, dz \tag{6.13a}$$

$$F\sin\phi = +\int_{\theta_1}^{\theta_2}\int_{-L/2}^{L/2} P\sin\theta\, R\, d\theta\, dz \tag{6.13b}$$

It is clear that both sides of equation (6.13) are function of eccentricity ratio (ε) and attitude angle (ϕ), which are defined as the ratio of the distance between rotating shaft centre and the journal bearing centre to the radial clearance and the angle between the line of action and the line of centres respectively, as shown in Figure 6.3. In dynamically loaded journal bearings, the load on the rotating shaft is known in advance and therefore, the solutions for the eccentricity ratio and the attitude angle can be obtained. Hirani et al. [142] proposed a rapid and convergent computational method by using a two-dimensional Newton-Raphson root finding method in a time marching forward routine. An initial guess on eccentricity ratio and attitude angle are required and the solution will be unfolded when the routine converges. As a result, the variations of the minimum oil film thickness and the maximum film pressure will be known. The corresponding friction power loss caused by the hydrodynamically lubricated journal bearing can be calculated by the following equation [143].

$$P_{f,Br} = R_{Br} \times \omega_J \times \left[\frac{\mu\omega_J R_{Br}^2 L_{Br}\pi}{\delta_{Br}\sqrt{1-\varepsilon^2}}\left(\frac{2+\varepsilon}{1+\varepsilon}\right) + \frac{\delta_{Br}\varepsilon}{2R_{Br}}\sqrt{F_x^2 + F_y^2}\sin\phi\right] \tag{6.14}$$

ε represents the eccentricity ratio, which is defined as the ratio between the centre distance of rotating journal and stationary bearing to the bearing clearance. ε̇ represents rate of change in eccentricity ratio.

In the same paper, Hirani et al. [142] have verified the proposed computational approach by comparing it with the results from other more comprehensive computational approaches such as finite element method, as shown in Table 6.1. The results generated from the proposed scheme match very well with that from the finite element method and it is better than infinitely short approximation. The scheme over predicts the value of minimum oil film thickness as compared to the finite element method but the discrepancy is below 10%.

Table 6.1 Comparison of various analytical methods for journal bearing design [142]

Methods	Maximum oil film pressure (MPa)	Minimum oil film thickness (μm)
Infinitely short approximation	104	2.42
Finite element method	91.5	1.69
Proposed scheme	94.4	1.83

6.4 Journal Bearing Design

For the unique geometrical arrangement of revolving vane compressor, there are two designs to place the journal bearings and these are shown in Figures 6.4 (Type I) and 6.5 (Type II) respectively. For the Type I arrangement shown in Figure 6.4, the rotor and the cylinder are each supported by one journal bearing in a cantilever manner. The load on the rotor (F_{ro}) is transferred to the journal bearing on the right-hand side and the load on the cylinder (F_{cy}) is transferred to the journal bearing on the left-hand

side. The Type II arrangement is shown in Figure 6.5, in which the cylinder is supported at both ends by the journal bearings on both sides, which means the load on the cylinder is shared equally by the two bearings while the rotor remains in cantilever arrangement. The arrangement of the journal bearing dictates the information on how the resultant force on the rotor and the cylinder is transferred to the journal bearing and the magnitude of journal bearing load.

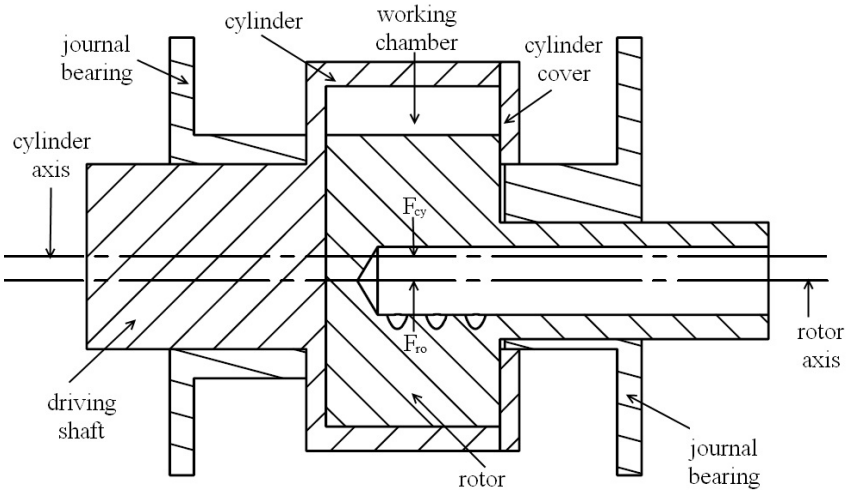

Figure 6.4 Journal bearing arrangement in fixed-vane revolving vane compressor (Type I)

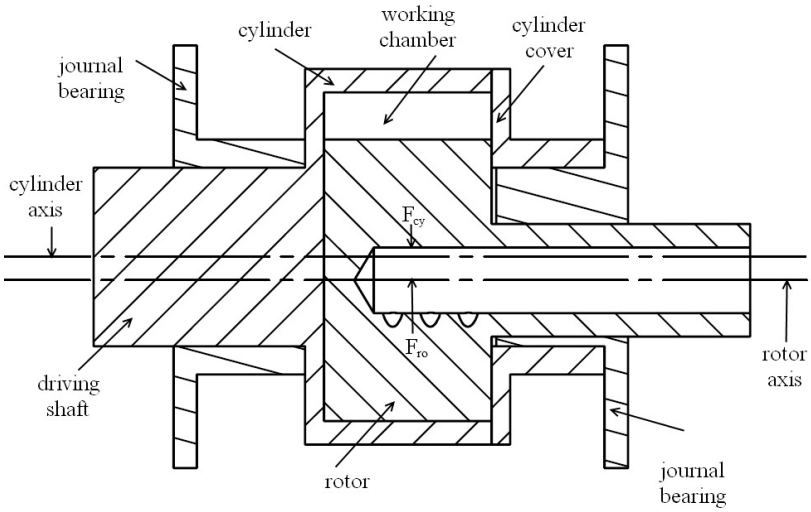

Figure 6.5 Journal bearing arrangement in fixed-vane revolving vane compressor (Type II)

The variations of the minimum oil film thickness (h_{min}) and the maximum oil film pressure (P_{max}) for Type I and Type II are illustrated in Figures 6.6 and 6.7 respectively. The smallest value of h_{min} is particularly important as it dictates the proper function or otherwise of the journal bearing. The adequacy of smallest h_{min} should be checked with the surface roughness requirement based on a specified surface finish, which is closely related to the type of manufacturing process. It is suggested that the smallest h_{min} should be greater than or at least equal to ten times the combined surface roughness values for surfaces [144]. For example, the smallest value of h_{min} for the journal bearing which support the rotor in both arrangements is 4.3 μm, therefore the surface finishing requirement for the rotor and its counterpart journal bearing should be at least 0.2 μm or lower, in which the grinding process would be required. In addition, as referred to Figures 6.6 and 6.7, it is noted that the smallest h_{min} for the journal bearing which supports the cylinder in Type I and Type II arrangement is 4.0 μm and 6.6 μm respectively. It is because the load acting on the journal bearing in cantilever arrangement is magnified as compared to that in the simply-supported arrangement. Thus, a higher journal bearing load requires a higher pressure developed in the oil film by having a lower value of the oil film thickness. On the other hand, it can be observed that the profiles of the maximum oil film pressure are fluctuating and in the same trend as the force variations as presented in Figure 6.2. As a result, based on the maximum oil film pressure information, the decision on the bearing material can be made and a material with compatible yield strength should be recommended.

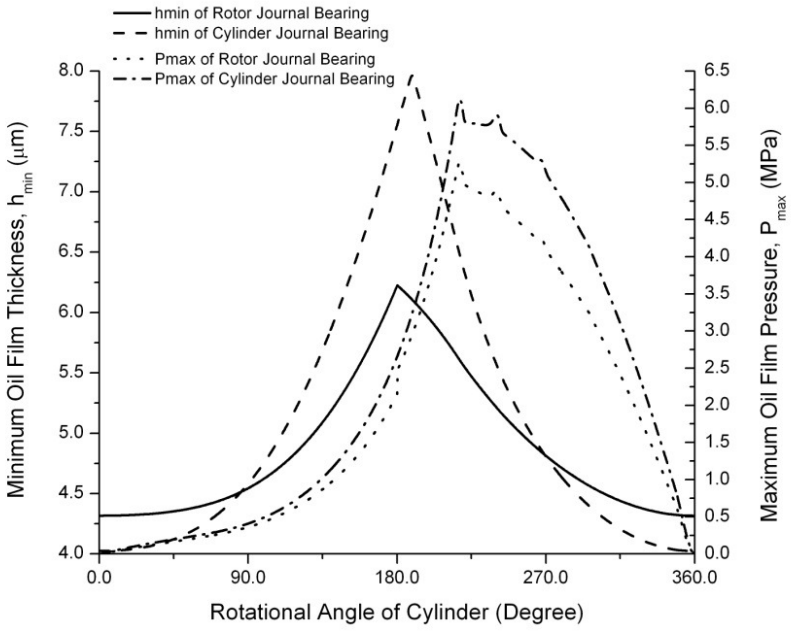

Figure 6.6 Variations of h_{min} and P_{max} for type I arrangement

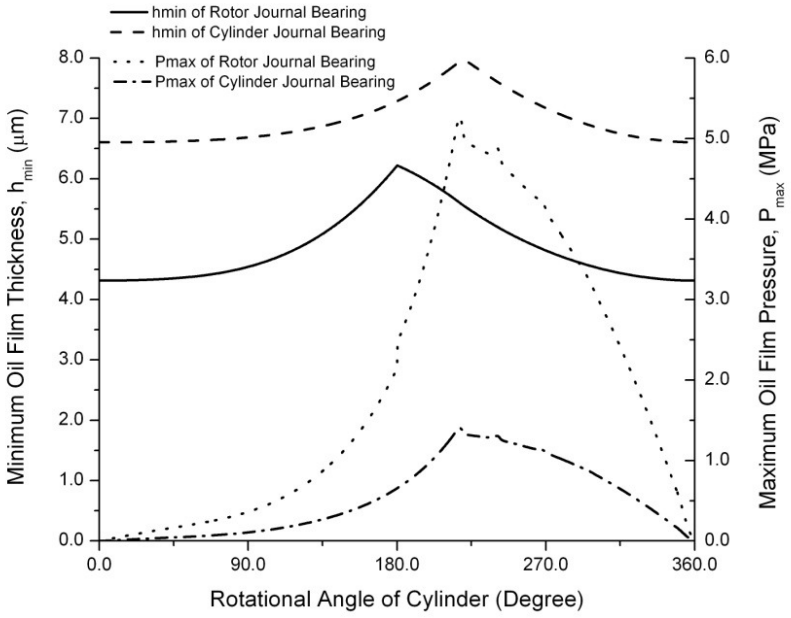

Figure 6.7 Variations of h_{min} and P_{max} for type II arrangement

6.5 Results and Discussions

Journal bearing is crucial to the proper functioning of the compressor, in particular the reliability. By having a different set of journal bearing design parameters,

the smallest h_{min} varies and thus, the allowable surface finish for the shafts of the rotor and the cylinder also varies. In addition, the amount of journal bearing frictional loss is also affected by having different design parameters of the journal bearing. In general, for an efficient journal bearing design, the smallest h_{min} must be generous due to the limitation of the available manufacturing techniques and at the same time the journal bearing frictional loss must be kept as minimum as possible. On the other hand, if the compressor geometrical configuration can be made in such a way that the journal bearing load can be reduced, it would be of great advantages as the surface finish requirements will be significantly reduced. The effect of various design parameters of the journal bearing, compressor configuration and operating conditions will be studied for Type II arrangement.

6.5.1 Effect of Journal Bearing Length

The effect of journal bearing length on the smallest h_{min} is illustrated in Figure 6.8. In general, as the journal bearing length increases, the lubricated surface area of the bearing increases. Thus, there is an increment in the smallest h_{min} since there is more support from the larger lubricated surface area to shoulder the rotating journal. However, it is observed that there is an increase in the journal bearing friction as a result of increasing lubricated surface area. The results also shows that by having an increment of 5.0 mm in journal bearing length, the smallest h_{min} for the journal bearings which support the rotor and the cylinder increases by 0.2 μm and 0.6 μm respectively while the respective journal bearing frictional loss increases by 4.1 W and 21.9 W.

6.5.2 Effect of Journal Bearing Radius

The journal bearing performance is also affected by its radius. Figure 6.9 shows that as the radius of the journal bearing increases by 5.0 mm, the smallest h_{min} increases from 4.2 μm to 4.8 μm for the rotor journal bearing and from 6.5 μm to 6.9 μm for the cylinder journal bearing. The result also shows that the frictional losses for the rotor and the cylinder journal bearing increased by 30.4 W and 71.0 W respectively. Similar to the effect of changing the length of journal bearing, the increment in smallest h_{min} and journal bearing frictional loss are due to the increment in the lubricated surface area.

6.5.3 Effect of Rotor to Cylinder Radius Ratio

Figures 6.10 and 6.11 show the effect of the rotor-to-cylinder radius ratio on the resultant force acting on the rotor and the cylinder and the required values of smallest h_{min} respectively. In general, by having a low rotor-to-cylinder radius ratio, the total swept area between the rotor and the cylinder will be increased. Thus, the axial length of the compressor will be reduced if the total swept volume is kept constant. In other words, the compressor can be in a long and thin or in a short and fat configuration for a prescribed volume flow rate. One of the important results due to different rotor-to-cylinder radius ratios is that if the rotor-to-cylinder radius ratio is smaller, the resultant force is smaller too due to the significant decrement in the compressor axial length. The result shows that the peak resultant force decreases from 1207 N to 695 N when the rotor-to-cylinder radius ratio is decreased from 0.87 to 0.79. Therefore, the load carrying requirement for the journal bearings can be reduced by having a low rotor-to-cylinder radius ratio. As shown in Figure 6.11, the smallest h_{min} is increased due to a lower journal bearing load and hence, the requirements for the surface finish for both

the rotating journal and its bearing are reduced significantly and it is desirable in the compressor design.

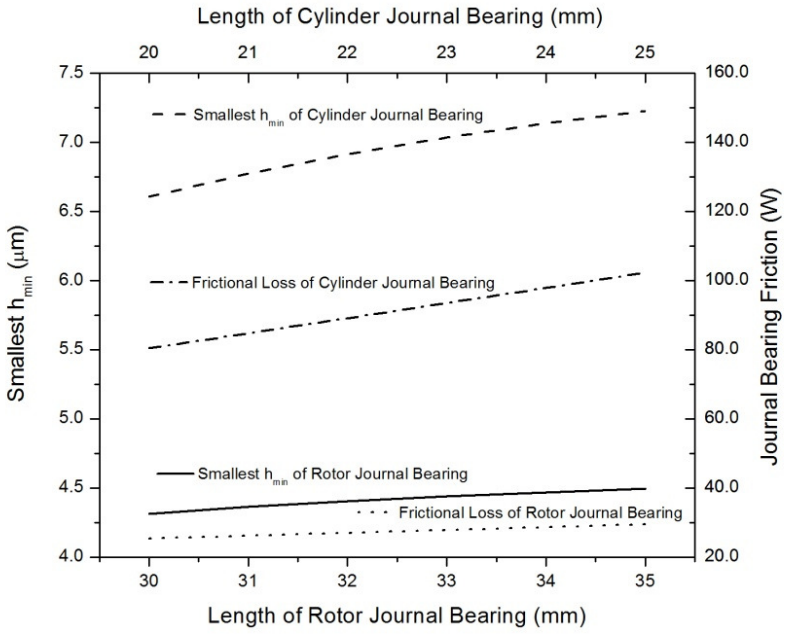

Figure 6.8 Variations of h_{min} and bearing friction due to change in bearing length

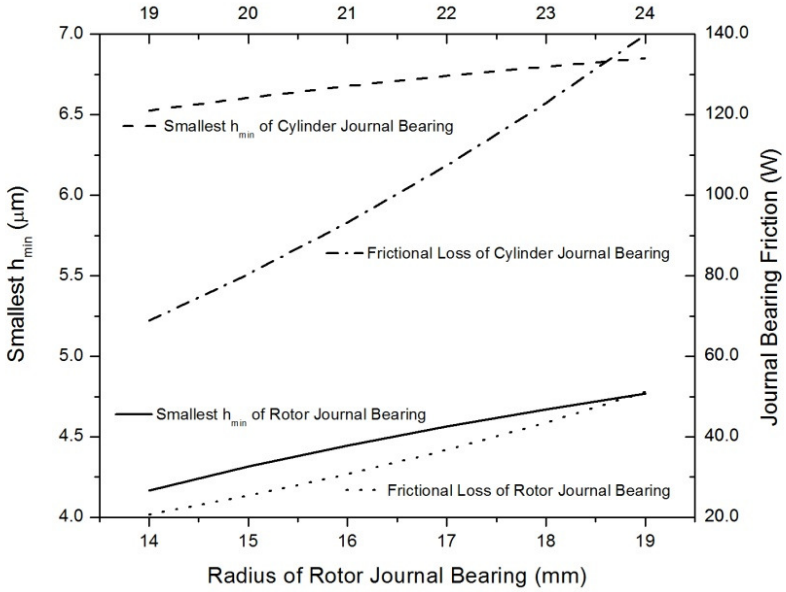

Figure 6.9 Variations of h_{min} and bearing friction due to change in bearing radius

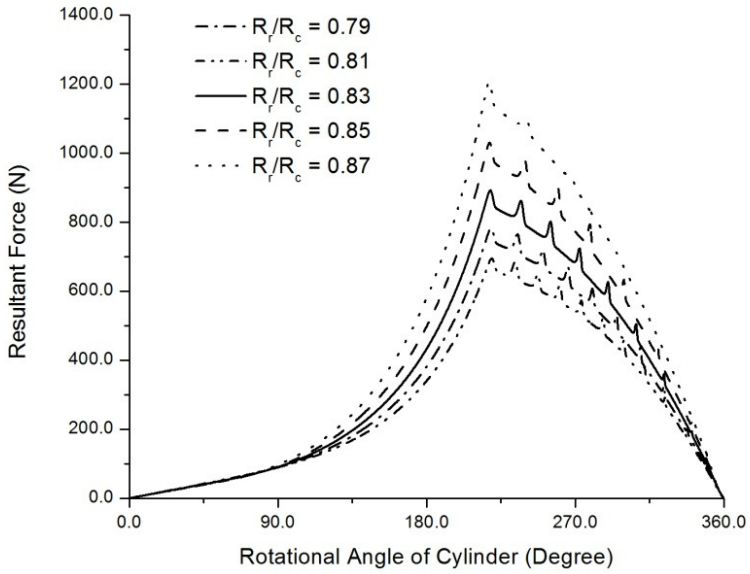

Figure 6.10 Variations of journal bearing load with rotor-to-cylinder radius ratio

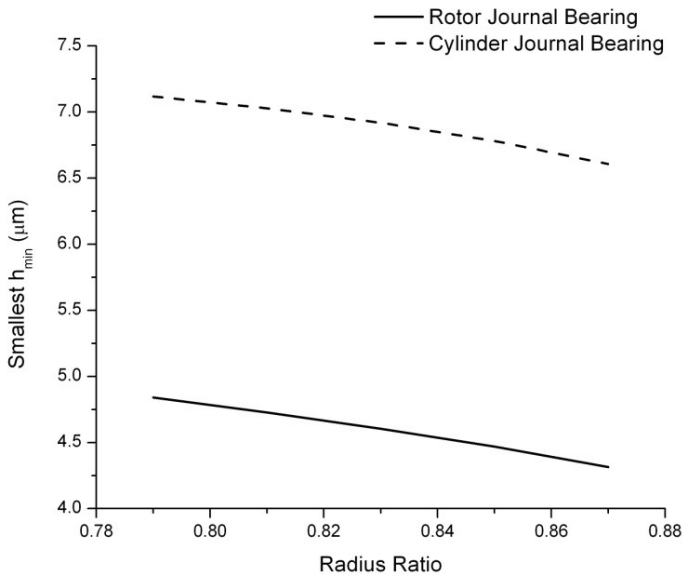

Figure 6.11 Variations of smallest h_{min} with rotor-to-cylinder radius ratio

6.5.4 Effect of Pressure Ratio

The effect of pressure ratio on the journal bearing performance has also been analyzed. Since the pressure ratio depends on the evaporating temperature and the condensing temperature, the range of pressure ratio in this analysis is chosen according

to the commonly used commercial air conditioning compressor testing conditions. Figure 6.12 shows the effect of the pressure ratio on the smallest h_{min}. The trend shows that for a constant evaporating condition, the smallest h_{min} decreases as the condensing temperature increases. This is because when the temperature difference increases, the pressure difference also increases. Therefore, the resultant force acting on the rotor and the cylinder will be larger and the required h_{min} will be smaller so as to generate a more positive oil film pressure force to support the heavier loaded shaft. For example, at evaporating temperature of 7.2 °C, the smallest h_{min} decreases from 5.4 μm to 4.1 μm for the rotor journal bearing when the condensing temperature increases from 37.8 °C to 60.0 °C.

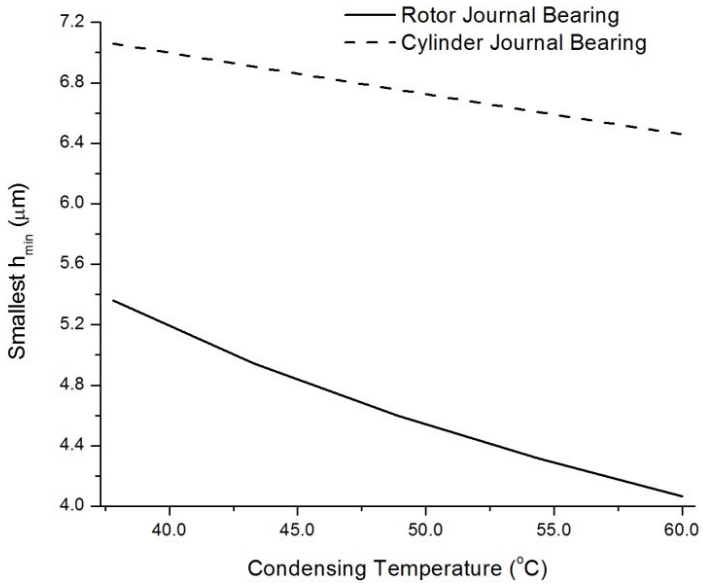

Figure 6.12 Variation of smallest h_{min} with operating conditions

6.5.5 Effect of Operating Speed

The effect of the compressor operating speed is also investigated. As referred to Figure 6.13, the smallest h_{min} increases as the operating speed increases from 20 Hz to 60 Hz under the same operating temperatures. As the compressor operating speed is

increased, the effect of dragging the oil flow into the convergent region which causes the required positive pressure is enhanced and thus, the smallest h_{min} is increased in order to support the same journal bearing load.

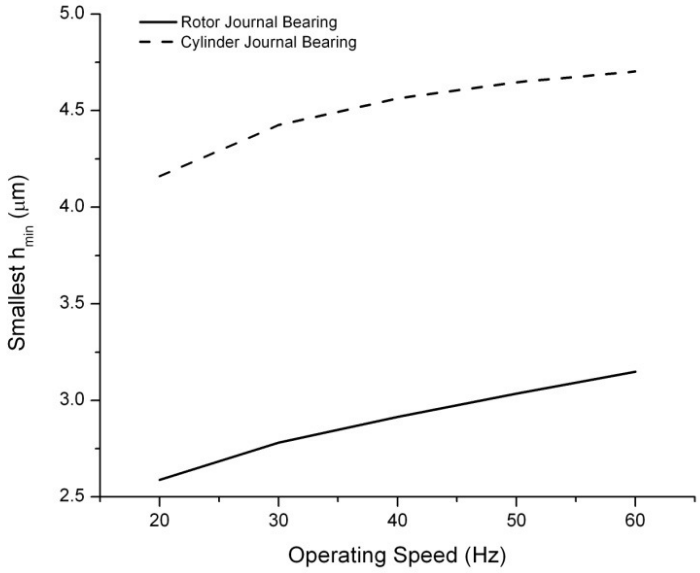

Figure 6.13 Variation of smallest h_{min} with operating speed

6.6 Concluding Remarks

The details on the journal bearing design for the revolving vane compressor have been presented. The possible arrangements for the journal bearing have been shown. The loading on the journal bearings of the revolving vane compressor is mainly due to the inertia force of the driven component and the pressure force acting on the rotor and the cylinder. The loading is varying throughout the whole compressor cycle and the maximum force corresponds to the highest value of the product between the projected areas of the rotor or the cylinder as well as the working fluid pressure. The peak bearing force varies for few hundreds of Newton to a couple of kilo-Newton with the lower one coming from the lower rotor-to-cylinder radius ratio.

The high values of the journal bearing load corresponds to the low value of h_{min}. The value of h_{min} is important as it dictates the surface roughness requirements on the rotating journal and its bearings. In addition, a good compromise between the frictional loss and the required surface finish must be achieved. The theoretical results predicted that the difference between the smallest h_{min} for cylinder journal bearing in simply supported form and cantilever form is 2.6 µm. This indicates that by having the parts simply supported, the requirement on the surface finishing will be lowered. In addition, the results also show that

- Increase the length of the journal bearing, the smallest h_{min} increases. For the journal bearing used to support the rotor and the cylinder, the smallest h_{min} increases from 4.3 µm to 4.5 µm and from 6.6 µm to 7.2 µm respectively, for an increment of 5 mm in the journal bearing length.

- Similarly, by having the increment in the journal bearing radius of 5 mm, the increments in the smallest h_{min} for the journal bearing used to support the rotor and the cylinder are 0.6 µm and 0.4 µm respectively.
- The energy loss due to the journal bearing friction increases when the length or the radius of the journal bearing increases. It is found out that the increment in the journal bearing friction due to the change in journal bearing radius is more significant than the change in journal bearing length. The total increments in the journal bearing frictional loss are 26.0 W and 101.4 W for a 5 mm increment in journal bearing length and journal bearing radius respectively.
- The smallest h_{min} decreases as the difference between the evaporating temperature and the condensing temperature increases. At constant evaporating

temperature of 7.2 °C, the smallest h_{min} decreases from 5.4 μm to 4.1 μm for the rotor journal bearing when the condensing temperature increases from 37.8 °C to 60.0 °C.

- The compressor operating speed determines the rate of dragging the oil into the convergent region, which in turn generates the positive pressure to support the loaded journal. As the compressor operating speed decreases, the smallest h_{min} becomes lower in order to generate a higher oil film pressure to support the loaded rotating journal. It is shown that as the compressor speed decreases from 60 Hz to 20 Hz, the smallest h_{min} drops from 3.2 μm to 2.8 μm for the rotor journal bearing.

Under the limitation of current available manufacturing techniques, the variation of minimum oil film thickness should be carefully assessed so that the reliability of the revolving vane compressor can be enhanced.

Chapter 7

Design of a Fixed-vane Revolving Vane Compressor Prototype

7.1 Introduction

The functionality of the fixed-vane revolving vane compressor which uses the cylinder as the driving component to drive the rotor through the vane will be investigated experimentally. The prototype is designed with a small capacity of 1.7 cc/rev in order to investigate the distinct performance characteristics of a small fixed-vane revolving vane compressor. In this chapter, the detailed design of the compressor prototype used in the experimental investigation will be unveiled. The component design, the method of lubrication and the dynamic balancing issues will be addressed.

7.2 Prototype Design

In the fixed-vane revolving vane compressor prototype, there are nine components and these are the cylinder and its cover, the rotor, the vane, the split bush, the discharge valve reed, the valve plate and the journal bearings. The compressor prototype can be grouped into three assemblies, namely cylinder assembly, rotor assembly and the journal bearing assembly. The rotor and the cylinder assemblies rotate about their respective centres during the operation and are supported by the journal

bearing assembly. In this section, the design features of these assemblies will be revealed.

7.2.1 Cylinder Assembly

The cylinder shown in Figure 7.1 is chosen as the driving component and thus the cylinder shaft is connected to an electric motor during the operation. The shaft of the electric motor shaft is directly coupled to the cylinder shaft by two set screws. In addition, the vane is held fixed to the cylinder by securing two screws to the top and one at the back of the vane.

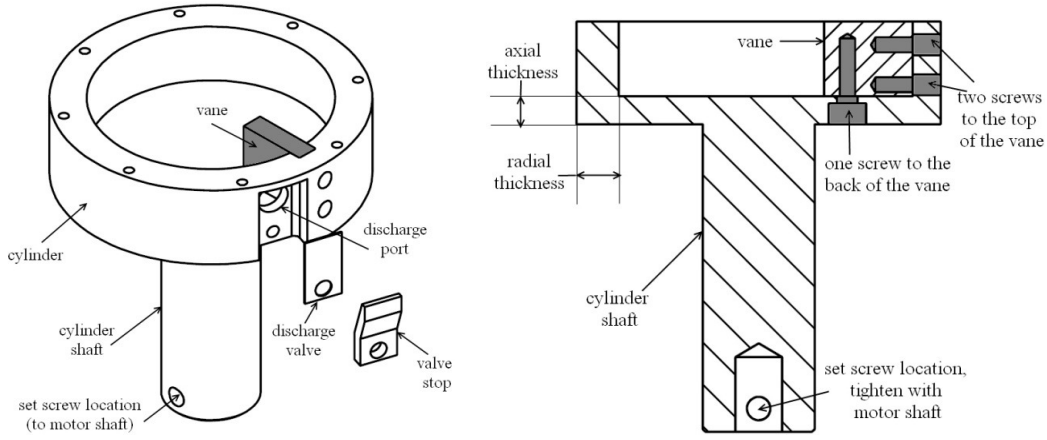

Figure 7.1 Assembly of cylinder, vane, discharge valve and valve plate

The other design feature on the cylinder is the discharge port. The discharge port is located at the outer circumference of the cylinder. The discharge port is covered by a rectangular discharge valve reed, which has one end fixed by a screw on to the cylinder wall and the other remains free. The amplitude of the discharge valve reed motion is restricted by a valve plate. The cylinder is covered by a cover, as shown in Figure 7.2. A groove is cut on the cover to accommodate the O-ring, which is used to seal the possible working fluid leakage through the clearance between the cylinder and its cover. The cylinder and its cover are held together by eight screws.

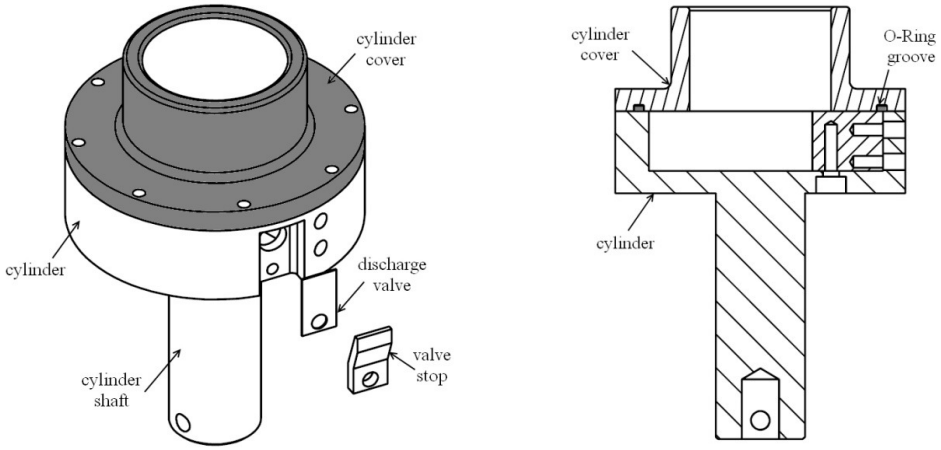

Figure 7.2 Cylinder and its cover

7.2.2 Rotor Assembly

The rotor shown in Figure 7.3 is the driven component in this prototype. During the operation, the rotor is driven by the vane through a split bush. A vane slot is created in order to permit the swivelling motion of the vane.

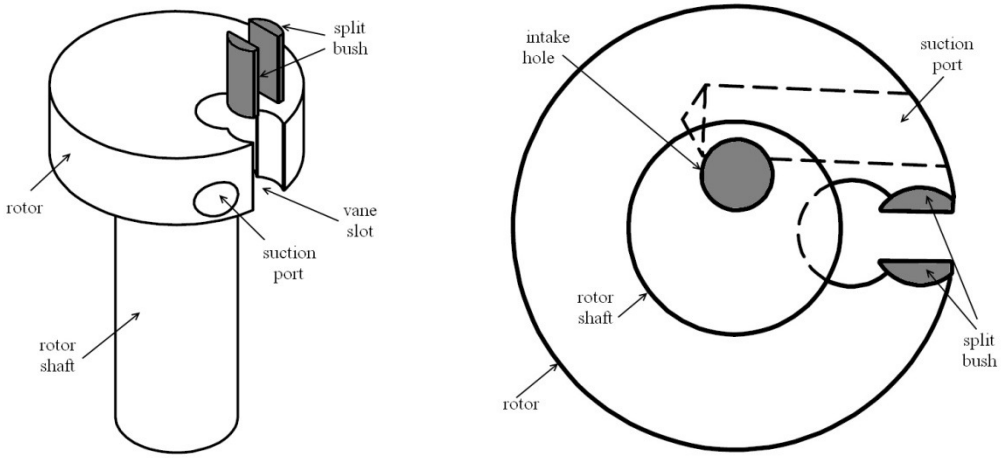

Figure 7.3 The rotor and the split bush

The other design feature on the rotor is the suction port. The suction port is drilled from the rotor circumference vertically at a distance away from the vane slot to

the centre of the rotor shaft. The working fluid goes into the working chamber through this port from the intake hole, which is located at the end of the rotor shaft.

7.2.3 Journal Bearings Assembly

The cylinder and the rotor assemblies constitute the major fixed-vane revolving vane compressor mechanism. The compressor assembly requires support during the operation as the components are subjected to loadings. In this prototype design, the cylinder is supported in a simply supported manner by two journal bearings one on each side and the rotor is supported by a single journal bearing in a cantilevered manner, as shown in Figure 7.4. The lower casing serves as the lower cylinder journal bearing while the upper casing serves as the upper cylinder journal bearing and the rotor journal bearing.

The diameter and the length of the bearings are decided based on the bearing loads and the surface roughness requirement, in which the details have been discussed in Chapter 6. Based on the highest testing pressure ratio (5:1), the distribution of the required minimum oil film thickness over one compressor cycle can be predicted. Figures 7.5 and 7.6 show the distribution of the required minimum oil film thickness for the rotor and the cylinder journal bearings respectively. The surface roughness requirement is required to be at least 10 times smaller than the lowest minimum oil film thickness and since there are two surfaces are involved, the finalized surface roughness requirement will be at least 20 times smaller than the lowest minimum oil film thickness. For example, the lowest minimum oil film thickness required for the rotor journal bearing is 5.76 μm and therefore, the surface roughness for the surfaces of rotor shaft and its bearing will be 0.3 μm. As a result, the dimensions of the journal bearings are

finalized based on the compromise between the surface roughness requirement and the machining capability of the local manufacturing vendor.

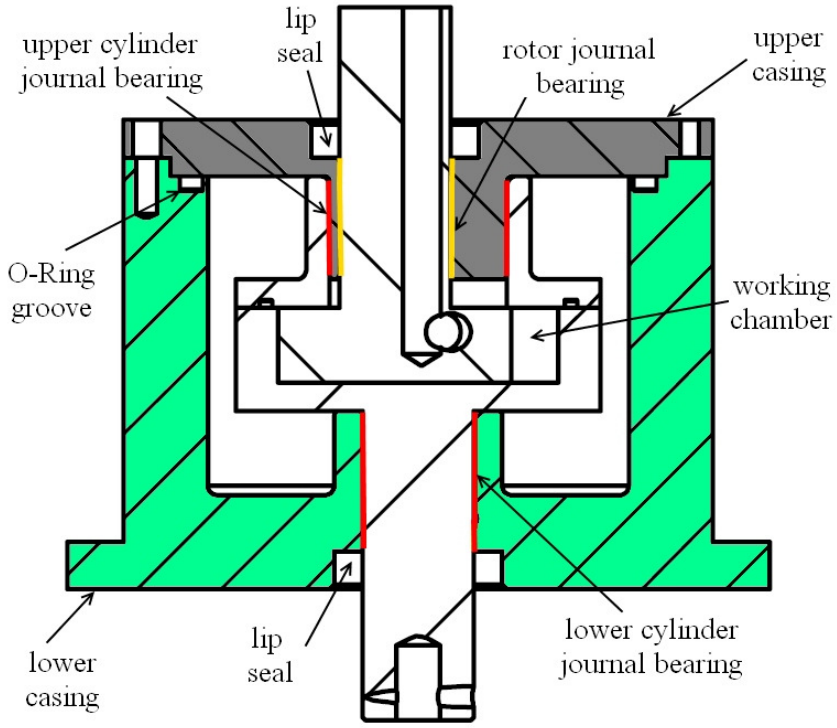

Figure 7.4 Journal bearing arrangement of the revolving vane compressor prototype

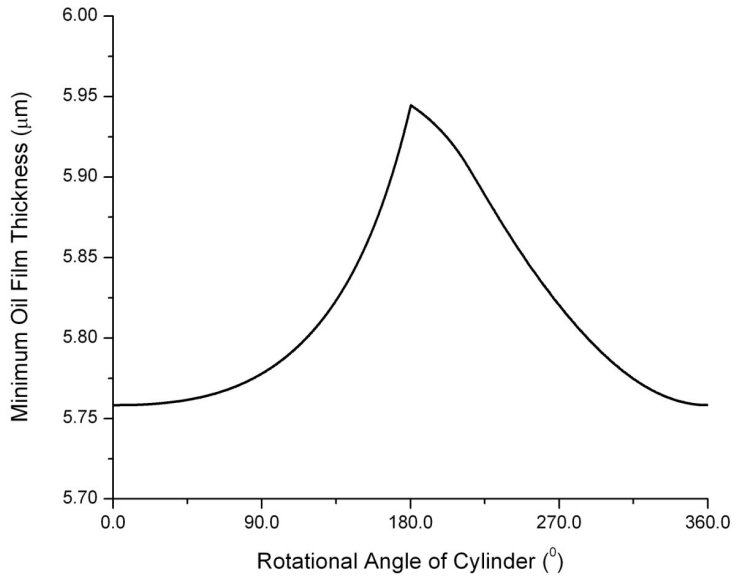

Figure 7.5 Distribution of minimum oil film thickness of rotor journal bearing

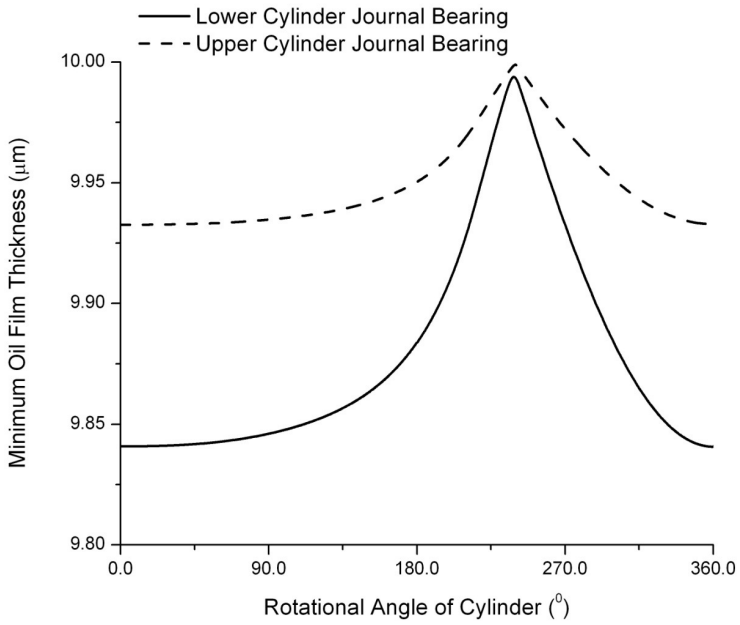

Figure 7.6 Distribution of minimum oil film thickness of cylinder journal bearings

The lower and the upper casings will be secured together by screws. The rotor shaft and the cylinder shaft protrude out from the casings and thus, lip seals are required to prevent possible leakage of the working fluid through the mating clearance of both casings.

7.2.4 Other Design Features

The other main design features can be found on the lower casing, as shown in Figure 7.7. The discharge of the working fluid from the compressor will exit via the pipe connector to the atmosphere. In addition, the transparent sight glass will be placed in front of the compressor shell in order to monitor the experimental situation such as oil level during the compressor operation. The location of the sight glass also serves as oil refill port.

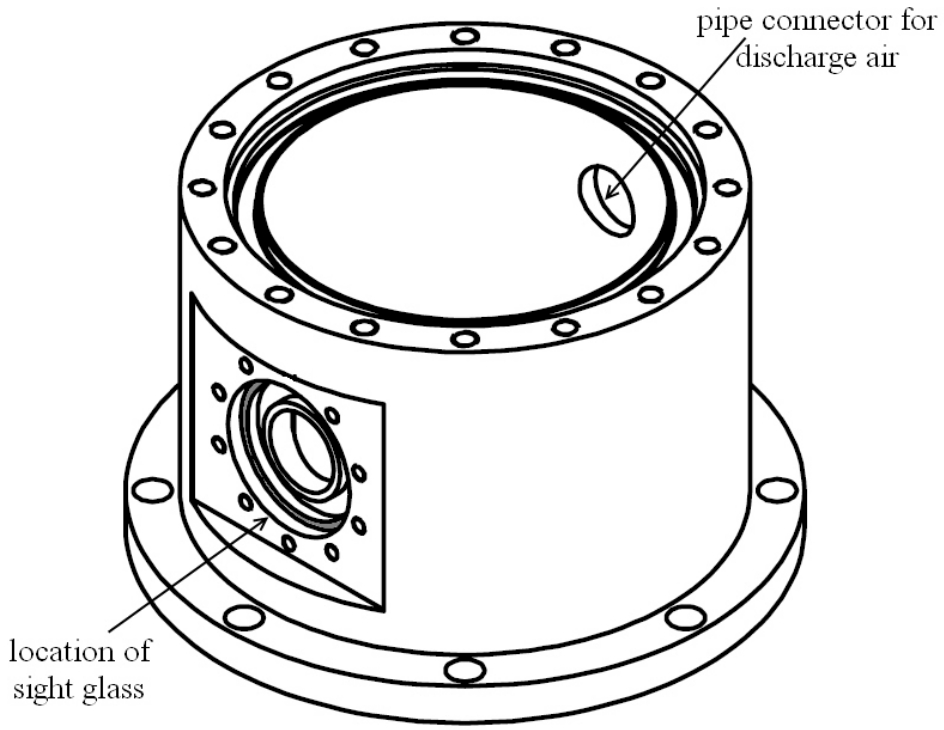

Figure 7.7 Other design features on lower casing

7.3 Method of Lubrication

Lubrication is important during the compressor operation as it protects the components from excessive wear and it also seals the leakage of the working fluid from the high-pressure chamber to the low-pressure chamber. Therefore, an efficient lubrication system is required for the compressor in order to avoid premature compressor failure. In this section, the unique lubrication system design for the revolving vane compressor will be presented and discussed.

In general, lubricant is required for the components which are in contact with other components and often, the lubricant in the compressor is stored at the lowest part of the compressor shell, which is normally known as the oil sump. The oil will be driven from the oil sump to the required location mainly through the pressure difference

and sometime, the oil flow will be assisted by the positive dragging effect from the spiral groove, which is dependent on the oil flow rate requirement.

Figure 7.8 shows the entire oil flow path for lubrication system for the prototype. The oil flow paths are designed based on the oil flow network analysis, in which the details are presented in Chapter 8. The oil is always settled at the lowest part of the compressor shell (point 2) and is subjected to a high discharge pressure in the discharge chamber. The oil will be pushed to the side of the cylinder shaft (point 3) and enters the centre of the cylinder shaft (point 4) through the lower radial hole. The oil continues to flow up to the junction (point 5) where the oil separates into two paths, one to lubricate the lower cylinder journal bearing (point 6) and the other to the lower end face between the rotor and the cylinder (point 7). It is noted that a spiral groove is cut on the cylinder shaft to drag more oil to lubricate the lower cylinder journal bearing. At the lower end face, the oil can flow to the suction and compression chambers due to the pressure difference. The oil also travels up through the slanted hole in the rotor (point 8) and exit through the radial hole on the rotor shaft (point 9) to lubricate the cantilevered-type rotor journal bearing (point 10). It is noted that the spiral groove is also cut on the rotor shaft to enhance the oil flow.

The oil thus reaches the upper end face between the rotor and the cylinder cover (point 11). Similarly, the oil can travel to the suction and compression chambers depending on the pressure difference. Furthermore, the oil can also be dragged up by the inner spiral groove on the cylinder cover to lubricate the upper cylinder journal bearing and circulate back to the oil sump (point 12).

The overall lubrication system design for the revolving vane compressor is presented. The further details on the dimensioning of each oil delivery path will be discussed in the next chapter, where the theoretical analysis on this unique lubrication system of revolving vane compressor is revealed.

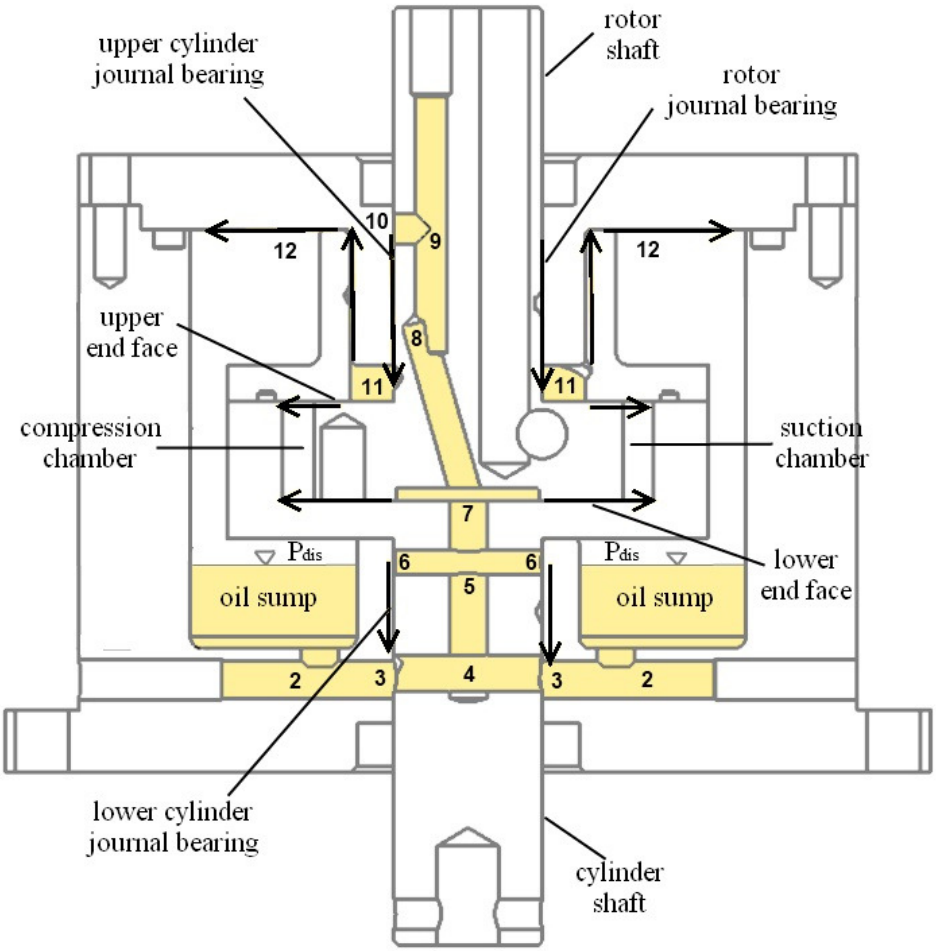

Figure 7.8 Method of lubrication in fixed-vane revolving vane compressor prototype

7.4 Dynamic Balancing

During the compressor operation, the cylinder and the rotor assemblies rotate about their respective own centre. Having all the necessary design features made on the components as shown in the previous sections, the resultant mass centre of each assembly undoubtedly deviates from the rotational axis. Therefore, the unbalance forces

incurred and resulted in an undesirable vibration and noise as well as additional frictional loss, especially at high operating speeds. Therefore, the dynamic balancing is required to ensure the coincidence of the assembly mass centre and its rotational axis. The dynamic balancing procedure is to be carried out after having all the design features, dimensions and after the type of materials used have been confirmed. The balancing can be done by either adding a counterweight to, or removing the materials from the component of interest.

The cylinder, the cover, the vane, the discharge valve reed and its valve plate, which constitute the cylinder assembly, rotate about the same centre during the operation. The cover is perfectly balanced since the features on it are all symmetrical to its rotational axis. Therefore, it can be excluded in the dynamic balancing procedure of the cylinder assembly. As observed from Figure 7.1, the vane, the discharge port, the discharge valve reed and valve plate are all located in the same region of the cylinder and these will move the resultant mass centre away from the rotational axis. The dynamic balancing for the cylinder assembly is done by removing the material in two steps, one to balance the x-direction and other is to balance the z-direction. The resultant design for the balanced cylinder assembly is shown in Figure 7.9.

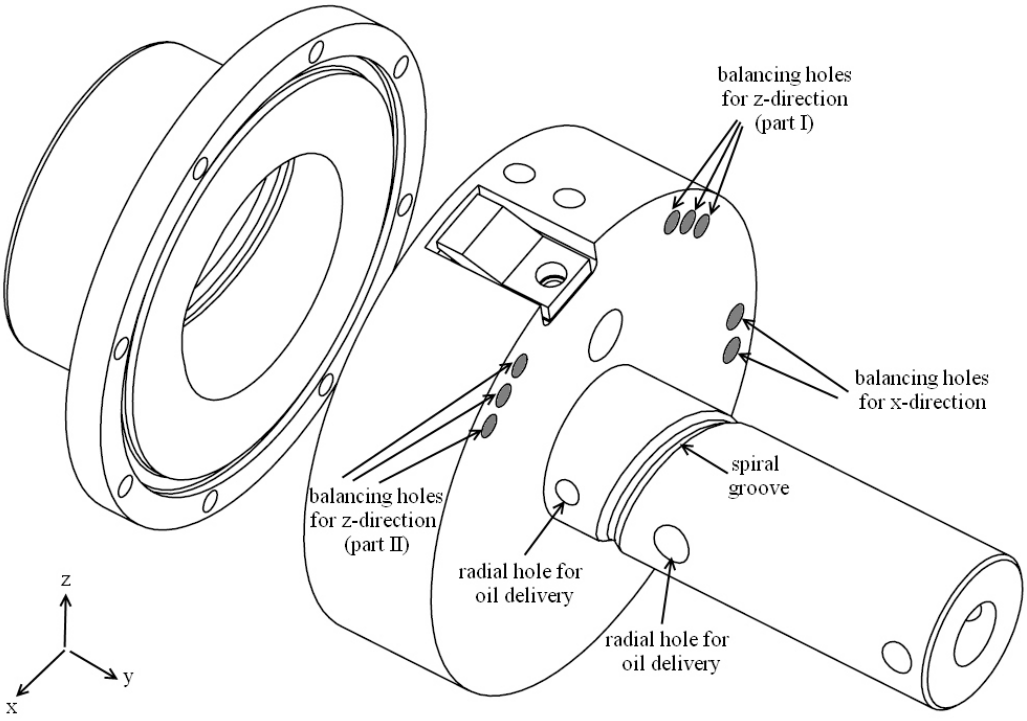

Figure 7.9 Balanced cylinder assembly

Having a suction port, a vane slot, a slanted oil delivery hole created on the rotor and combines with the split bush, the mass centre of the rotor assembly is definitely deviates from its rotational axis. The dynamic balancing for the rotor assembly is carried out by removing material, as shown in Figure 7.10.

The dynamic balancing is a repetitive trial and error process and the mass centres of the assemblies are checked through the CAD modelling software at the end of every trial. The dimensions of the balancing features are finalized by ensuring the mass centres are within four decimal places accuracy to the location of the rotational axis.

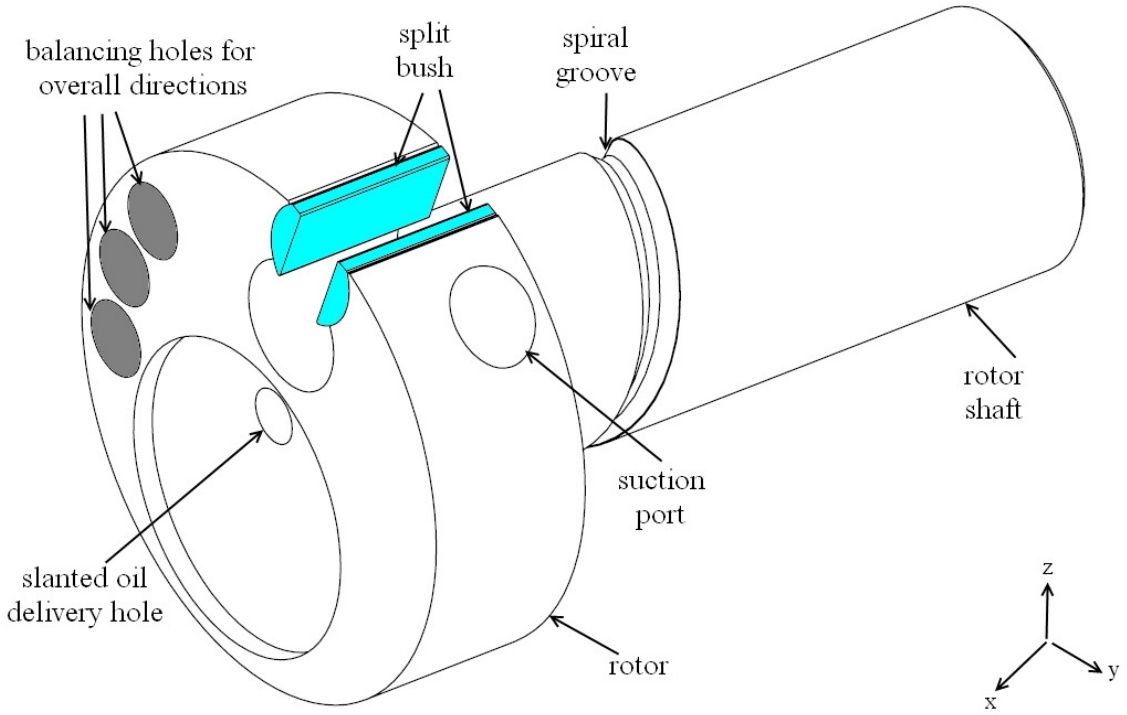

Figure 7.10 Balanced rotor assembly

7.5 Concluding Remarks

The complete design of the revolving vane compressor prototype is shown in Figure 7.11. The prototype consists of 9 major components, i.e. a cylinder, a rotor, a vane, a split bush, a discharge valve reed, a valve plate, a cover, a lower and an upper casing. The capacity is 1.7 cc/rev and the working fluid will be the air. The prototype is going to be tested in an open cycle under various pressure ratios.

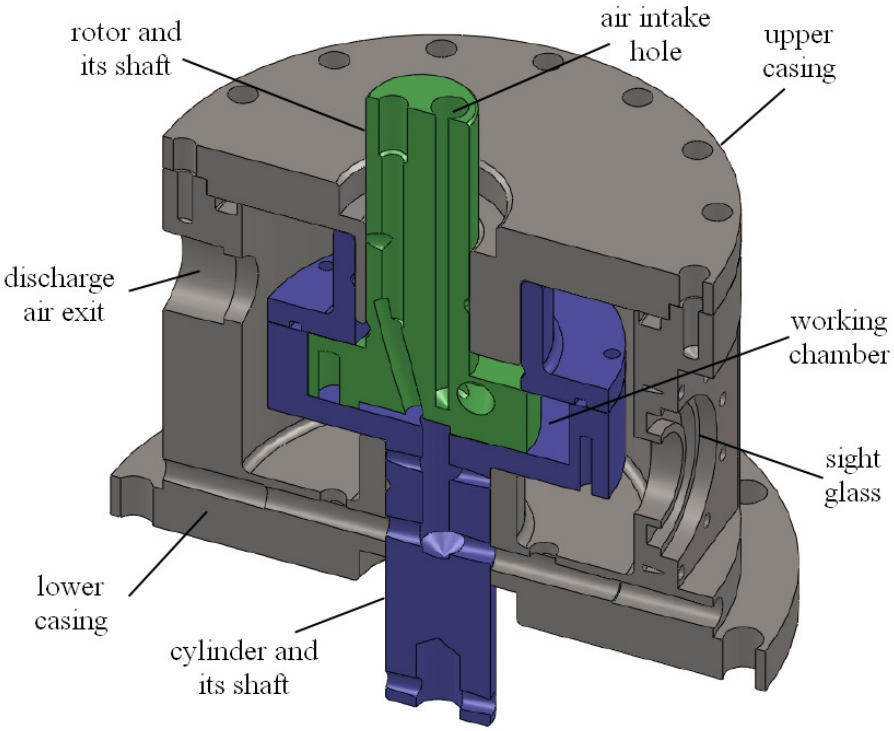

Figure 7.11 Complete design of fixed-vane revolving vane compressor prototype

Chapter 8

Lubrication System of Fixed-vane Revolving Vane Compressor

8.1 Introduction

The role of the lubricant is important in the compressor operation as it is used to lubricate the sliding surfaces from excessive wear and improves the reliability and decreases the mechanical losses of the compressor. In addition, the lubricant also acts as a sealing agent to prevent the gas leakage from the high-pressure compression chamber to the low-pressure chamber. Furthermore, the lubricant is used for cooling of sliding parts which are heated by friction to avoid unnecessary temperature rise in the compressor components and save them from unnecessary thermal stress and deformation. The secondary task of the lubricant is to protect the compressor parts from corrosion and dampening the noise level. As a result, an efficient lubrication system is required in all parts of the compressor where rubbing occurs. Therefore, a suitably designed lubrication system is crucial for a proper operation of a compressor. A complete design of a lubrication system for a compressor should cater for the hydrodynamic lubrication for rotating shafts, oil lubrication at the rubbing parts and the methods to deliver the required oil flow rate to ensure all the rubbing parts have a sufficient lubricant supply.

In this chapter, the design for the lubrication system for the fixed-vane revolving vane compressor will be presented. The location in the compressor which requires lubrication will be identified and the oil flow characteristic for each different type of flow path will be discussed. The individual oil flow paths in the lubrication system will be assembled and form a lubrication system network which can analogue as a form of an electric circuit network, whereby the pressure difference, the volume flow rate and the flow resistance of the oil flow network correspond to the voltage difference, electric current and electric resistance respectively. The set of linear simultaneous equations, which can be solved for the oil flow rates resulted from the oil flow network will be solved by using Gauss Elimination method. The effects of the operating conditions and design parameters on the resulting oil flow rate, namely the shell pressure, the depth and the width of groove, the diameter and the length of hole will be examined.

8.2 Lubrication System and Flow Models

The lubrication system for the fixed-vane revolving vane compressor prototype, which has been presented in the Chapter 7 is shown in Figure 8.1. The lubrication system consists of different flow elements, which include the flows through the following paths: (i) the straight hole, (ii) the radial hole on the rotating shaft, (iii) the journal bearing clearance, (iv) the spiral groove, (v) the axial clearance at the end faces between the rotor and the cylinder.

With reference to Figure 8.1, the oil sump is at the bottom of the revolving vane compressor (Point 2) and the discharge pressure is constantly acting on the oil sump surface (Point 1) since the compressor is in a high-pressure shell. The high discharge pressure at point 1 & 2 pushes the lubricant to the side of the cylinder shaft (Point 3)

through the horizontal holes at point 2. The lubricant at this point has to overcome the pressure generated by the centrifugal force of the rotating cylinder shaft in order to reach the centre of the cylinder shaft (Point 4). The lubricant continuously climbs up along the straight vertical hole and reaches a junction (Point 5).

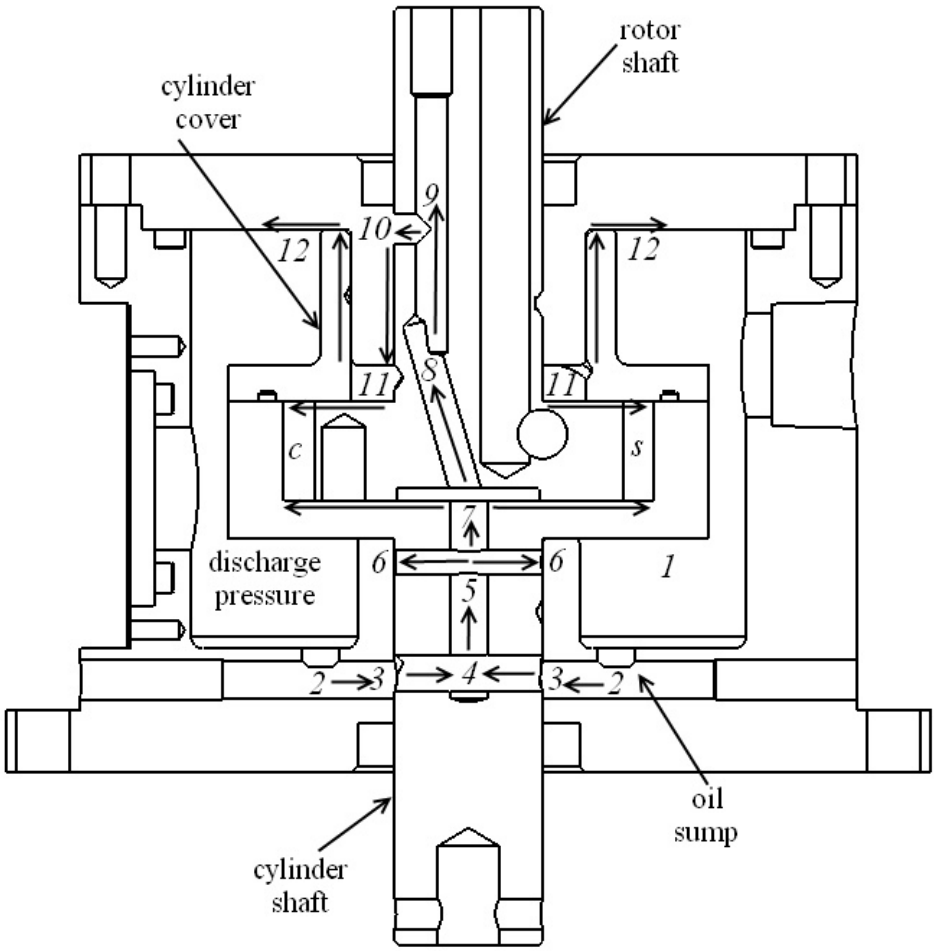

Figure 8.1 Schematics of lubrication system in fixed-vane revolving vane compressor prototype

At this junction, a partial amount of the lubricant will be expelled through radial hole at point 6. This amount of lubricant subsequently flows back to the bottom of oil sump (Point 3) through the lower bearing clearance, and the flow is enhanced by the assistance of the spiral groove, which is cut on the cylinder shaft. The remaining amount of the lubricant will then travel up to the lower end face (Point 7). The lubricant

at this point either flows to the suction chamber (Point S) or to the compression chamber (Point C) through the axial clearance at the end faces or flows to the end of the inclined straight hole (Point 8) with the need of overcoming the height difference.

From the end of the inclined straight hole, the lubricant climbs up to a junction at 9 through a vertical straight hole and part of it is discharged out at the exit of radial hole at 10 on the rotor shaft. Subsequently, the lubricant reaches the upper end face at 11 through the upper bearing clearance and the spiral groove on the rotor shaft. The lubricant at the upper end face at 11 can flow to the suction chamber (Point S) or compression chamber (Point C). In addition, a spiral groove is created on the inner surface of the cylinder cover in order to drag the lubricant out from the upper end face to the end of the cylinder cover at 12. From 12, the lubricant exits radially through the axial clearance between the end faces of cylinder cover and upper bearing and flows back to the oil sump at 2.

One of the most important things in the lubrication system design is to ensure that there is sufficient lubricant circulating within all the oil flow paths. The lubricant should not be trapped and become stagnant at a certain location as this will cause the temperature of the lubricant to rise continually as a result of the heat from the friction. Under such a situation, the viscosity of the lubricant will decrease with temperature and it will eventually lead to an insufficient lubricant viscosity to provide effective lubrication. The design of the lubrication system in revolving vane compressor is proposed and it is observed that the network constitutes of different kinds of flow path and each of these will have their own characteristics defined by the flow resistance.

8.2.1 Flow through Straight Hole

The oil flow in either the vertical or the horizontal holes can be modelled as the flow in a pipe. The difference is that for the flow inside the vertical straight hole, the flow must overcome the gravitational pull, unlike the flow in the horizontal straight hole, it is not affected by the gravity. The flow in the straight holes can be modelled as Hagen–Poiseuille flow, which is driven by pressure difference and the flow is laminar, incompressible and viscous. Based on the force analysis on the differential fluid element, the relationship between the pressure difference across the two ends of the pipe and the volume flow rate in the pipe can be written as equation (8.1).

$$\frac{\Delta P}{Q} = \frac{8\mu L}{\pi R^4} \tag{8.1}$$

In fact, equation (8.1) represents the flow resistance inside a straight hole. It is clear that as the length of the hole becomes longer or the radius of the hole becomes smaller, the flow resistance increases and reduces the flow.

8.2.2 Flow through Radial Hole

The oil flow inside the radial hole in the shaft is expelled from the centre of the shaft to the outer section due to centrifugal force generated by the rotating shaft. The flow resistance in this case is similar to that of the flow in the straight hole, except that there is an additional pressure effect being generated due to the centrifugal force by the rotational motion of the shaft. This extra pressure is an advantage as it assists the oil flow through the radial hole along the rotating shaft from the inner to the outer circumferential surface. Based on the force analysis on the differential element of the fluid, the extra pressure gained can be expressed by equation (8.2)

$$\Delta P = \frac{\rho\omega^2}{2}(R_o^2 - R_i^2) \tag{8.2}$$

As seen from the equation (8.2), the pressure gain increases if there is an increment in the rotational speed of the shaft.

8.2.3 Flow through Bearing Clearance

The oil flow through the bearing clearance is driven by the pressure difference. Based on the Reynolds equation, the volume flow rate along the axial direction of the bearing can be written as the equation below.

$$q_z = \int_0^{\pi} -\frac{h^3}{12\mu}\frac{\partial P}{\partial z} R\, d\theta$$

where h is the oil film thickness which varies from the entrance of the fluid film region ($\theta = 0^{\circ}$) to the end of the fluid film region ($\theta = \pi$) and it can be expressed in the form of

$$h = \delta_{Br}(1 + \varepsilon\ \cos\theta)$$

As a result, the flow resistance for the axial flow across the bearing can be expressed by equation (8.3)

$$\frac{\Delta P}{Q} = \frac{12\mu L}{\delta_{Br}^3 \pi R(1 + 1.5\varepsilon^2)} \tag{8.3}$$

The flow resistance is dependent on the geometry of the bearing, namely the bearing length L, the bearing radius R, the bearing clearance δ_{Br}, the eccentricity ratio ε and the viscosity of the lubricant μ. It can be deduced from equation (8.3) that if the viscosity of the lubricant increases, it is harder for the fluid to flow, in other words, the flow resistance increases due to more viscous lubricant. Similarly, if the bearing length is

longer, the corresponding flow resistance will be greater. Furthermore, the bearing in larger radius and larger clearance will assist the flow through the bearing clearance. The last affecting variable is the eccentricity ratio. It is seen that if the eccentricity ratio gets smaller, the flow resistance increases. This is because for a smaller eccentricity ratio, the distance between the centres of the journal and its sleeve is closer. Thus, the effect of squeezing the flow through the bearing clearance axially is reduced.

8.2.4 Flow through Spiral Groove

The spiral groove is usually cut on the rotating shaft to act as a viscous pump to drag the lubricant effectively to the required lubricating surfaces. The flow inside the spiral groove is due to the positive viscous pumping effect and the effect of positive pressure gradient across the spiral groove length, which is a combination of Couette flow and Hagen- Poiseuille flow. It is noted that the flow rate across the spiral groove under these effects can be represented by equation (8.4).

$$Q = -\frac{H^3 D}{12\mu}\frac{dP}{dz}\cos\beta + \frac{1}{2}A_g R\omega \sin\beta \qquad (8.4)$$

The first term on the right hand side of equation (8.4) represents the flow rate generated by the pressure gradient across the both ends of the groove. The second term represents the flow rate created by the viscous pumping by the spiral groove. It is noted that if the viscous pumping direction is in the same direction of increasing pressure (positive dP/dz), the total flow rate through spiral groove will be decreased.

8.2.5 Flow through Axial Clearance (End Faces)

The oil flow through axial clearance between the end faces of rotor and the cylinder can be modelled as the flow between two fixed parallel, circular disks

separated by a small gap. The fluid flows radially outward owing to the pressure difference between the inner and outer radius respectively. Based on the Navier-Stokes equation under the assumption of laminar, steady and incompressible, the relationship between the pressure difference and the volume flow rate can be derived and it is shown in equation (8.5).

$$\frac{\Delta P}{Q} = \frac{6\mu \ln(r_2/r_1)}{\pi \delta_{ef}^3} \tag{8.5}$$

From equation (8.5), the flow resistance for the radial flow through axial clearance increases when the axial clearance is reduced and the viscosity of the lubricant is increased.

8.3 Oil Flow Network

The characteristics of individual flow paths have been discussed and each of these flow paths can be represented by the combination of flow resistance and the source of pressure or flow rate, if any. All of the flow paths can be linked up to form lubrication system network, as shown in Figure 8.2. The unknown parameters in the network will be the flow rates through each of the flow path and these are Q_1 to Q_{16}. The unknowns can be solved by firstly setting up the simultaneous equations by considering Kirchhoff's current law and Kirchhoff's voltage law. The Kirchhoff's current law states that at any junction, the sum of current inflows is equal to the sum of current outflows. Therefore, a total of seven equations, presented by equations (8.6) to (8.12), can be obtained by applying the Kirchhoff's current law to junction number 3, 5, 6, 7, 10, 11 and 12.

$$Q_1 + Q_2 + Q_3 + Q_{sg6} = Q_4 \tag{8.6}$$

$$Q_6 = Q_2 + Q_3 + Q_{sg6} \tag{8.7}$$

$$Q_4 = Q_5 + Q_6 \tag{8.8}$$

$$Q_5 = Q_7 + Q_8 + Q_9 \tag{8.9}$$

$$Q_7 = Q_{sg10} + Q_{11} + Q_{10} \tag{8.10}$$

$$Q_{sg10} + Q_{11} + Q_{10} = Q_{sg11} + Q_{12} + Q_{13} + Q_{14} + Q_{15} \tag{8.11}$$

$$Q_{sg11} + Q_{14} + Q_{15} = Q_{16} \tag{8.12}$$

In addition, Kirchhoff's voltage law is used to obtain other sets of equations. In general, Kirchhoff's voltage law states that the sum of the voltage within any closed loop is zero. For the circuit shown in the Figure 8.2, there are several closed loops in which the Kirchhoff's voltage law can be applied. For the radial flow through axial clearance at the upper (11 to c & s) and lower (7 to c & s) end faces between the rotor and the cylinder, equations (8.13) and (8.14) can be set up.

$$R_9Q_9 - R_8Q_8 = P_c - P_s \tag{8.13}$$

$$R_{13}Q_{13} - R_{12}Q_{12} = P_c - P_s \tag{8.14}$$

Another three equations can be set up by applying the Kirchhoff's voltage law to the loop which contains spiral groove, namely the cylinder shaft (6 to 3), the rotor shaft (10 to 11) and the cylinder cover (11 to 12), which are represented by equations (8.15) to (8.17) respectively.

$$-R_2Q_2 + R_3Q_3 = \rho g(h_{sg6} - h_6) \tag{8.15}$$

$$-R_{10}Q_{10} + R_{11}Q_{11} = \rho g(h_{sg10} - h_{10}) \tag{8.16}$$

$$-R_{14}Q_{14} + R_{15}Q_{15} = \rho g(h_{11} - h_{sg11}) \tag{8.17}$$

By going through the network from the oil sump surface (Point 1) to the compression chamber through the lower end face (through 2-3-4-5-7) and the upper end face (through 2-3-4-5-7-8-9-10) respectively, equations (8.18) and (8.19) can be set up.

$$\frac{R_1}{2}Q_1 + \frac{R_4}{2}Q_4 + R_{45}Q_4 + R_5Q_5 + R_8Q_8 = P_1 - P_c - P_{rp3} + \rho g(h_1 - h_4 - h_5) \quad (8.18)$$

$$\frac{R_1}{2}Q_1 + \left(\frac{R_4}{2} + R_{45}\right)Q_4 + R_5Q_5 + (R_{78} + R_{89} + R_7)Q_7 + R_{10}Q_{10} + R_{12}Q_{12} = P_1 - P_c - P_{rp3} + P_{rp7} + P_{rp9} + \rho g(h_1 - h_4 - h_5 - h_7 - h_8 + h_{10}) \quad (8.19)$$

The last two equations can be written by taking the closed loop from Point 1 and back to Point 1 (through 2-3-4-5-7-8-9-10-12) and from Point 3 and back to Point 3 (through 4-5-6), as shown by equations (8.20) and (8.21) respectively.

$$\frac{R_1}{2}Q_1 + \left(\frac{R_4}{2} + R_{45}\right)Q_4 + R_5Q_5 + (R_{78} + R_{89} + R_7)Q_7 + R_{10}Q_{10} + R_{14}Q_{14} + R_{16}Q_{16} = -P_{rp3} + P_{rp7} + P_{rp9} + P_{rp12} + \rho g(h_1 - h_4 - h_5 - h_7 - h_8 + h_{10} - h_{11}) \quad (8.20)$$

$$R_2Q_2 + \frac{R_4}{2}Q_4 + R_{45}Q_4 + R_6Q_6 = -P_{rp3} + P_{rp5} + \rho g(h_6 - h_4) \quad (8.21)$$

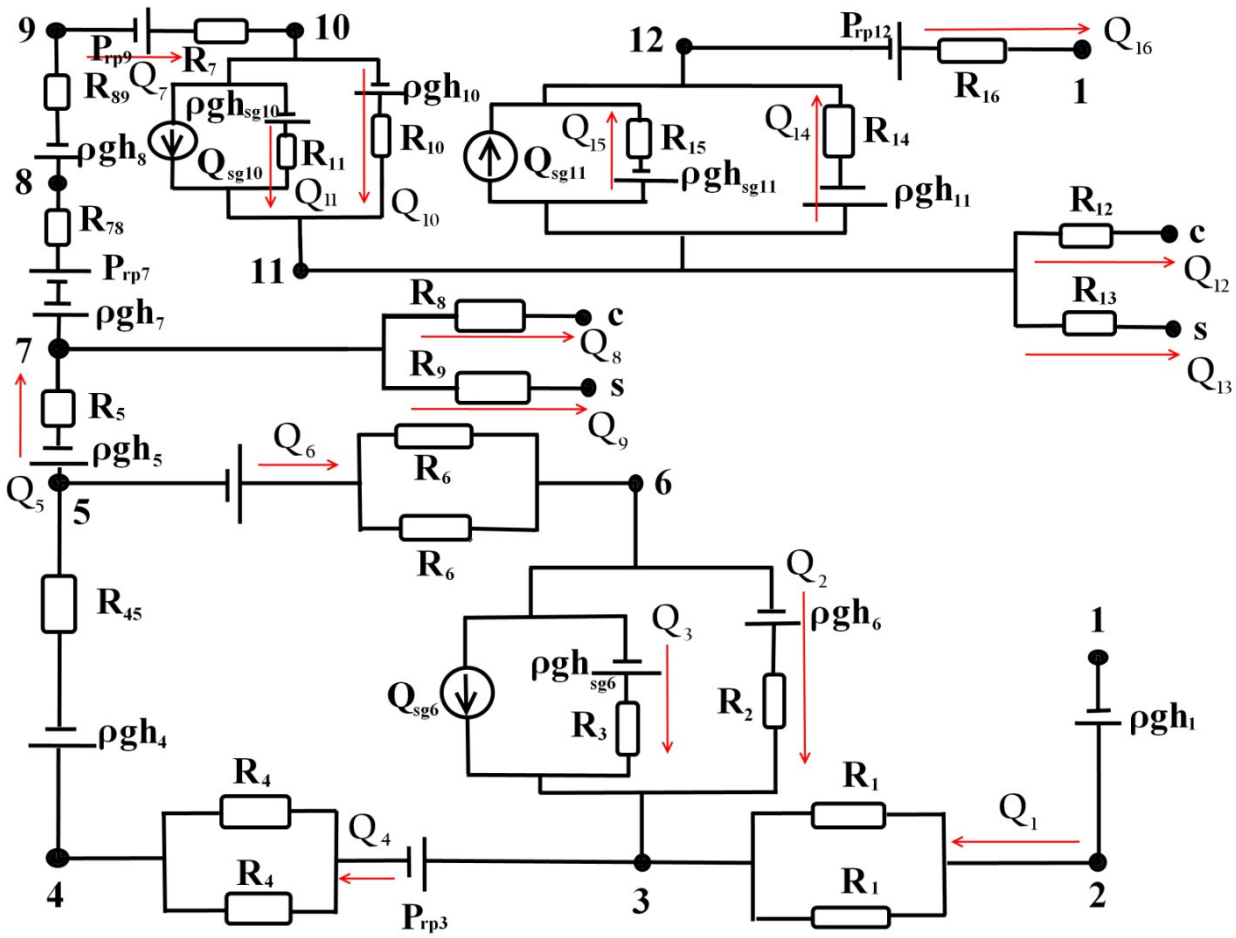

Figure 8.2 Lubrication system circuit network

A total of 16 equations, equations (8.6) to (8.21) have been derived using Kirchhoff's circuit law. These equations have been solved using Gauss elimination method. The parameters used includes: the type of lubricant used, which is Shell Corena P100 and it belongs to a mineral oil type with the viscosity value of 8.3 mPa-s taken at 100 ˚C; the suction and the discharge pressure are 1.0 and 4.0 bar respectively, and the operational speed is 2000 rev/min. The designed dimensions of the oil flow network are shown in Table 8.1.

Table 8.1 The designed dimensions of oil flow network

Description		Dimension (mm)
Journal bearing	Radial clearance	0.00750
End faces	Axial clearance between cylinder and rotor	0.00625
	Axial clearance at cylinder cover	0.025
Spiral Groove	Width	1.00
	Depth	0.30
Horizontal hole	Radius	1.50
	Length	16.5
Cylinder shaft	Radius of lower radial hole	1.50
	Radius of upper radial hole	1.00
	Radius of vertical hole 45	2.50
	Length of vertical hole 45	9.00
	Radius of vertical hole 57	2.50
	Length of vertical hole 57	5.00
	Cylinder shaft radius	6.00
Rotor Shaft	Rotor shaft radius	6.00
	Radius of slanted hole 78	1.25
	Length of slanted hole 78	15.0
	Radius of vertical hole 89	1.25
	Length of vertical hole 89	7.60
	Radius of radial hole	1.25

The flow resistance of each flow path throughout the whole cycle under such operational conditions and designed dimensions is shown from Figures 8.3 to 8.9. As shown in Figures 8.3 and 8.4, the flow resistances of various straight holes and radial holes are in the order of 10^7. Figure 8.5 shows that the resistance to Poiseuille flow through spiral groove is in the order of 10^{10} since the opening of groove area is small as compared to the vertically or radially drilled hole. The flow resistance for the radial

flow through the axial clearance of 25 μm at the cylinder cover is in the order of 10^{11}, as referred to Figure 8.6. These three types of flow resistance are solely dependent on the design geometries and remain constant over entire compressor cycle despite of operational conditions.

The flow resistances for the radial flow through the lower and the upper axial clearances are shown in Figures 8.7 and 8.8 respectively. The flow resistances are in the order of 10^{14}, which is the highest flow resistance in the entire oil network. The magnitude of the flow resistances depend on the span of the working chamber. The flow resistance to the compression chamber increases as the end of compression volume approaches and the flow resistance to suction chamber decreases as the suction volume increases. The last type of the flow resistance belongs to the flow through bearing clearance and it is in the order of 10^{14}. The magnitude of the flow resistance varies over the entire compressor cycle and it follows the profiles of the journal eccentricity ratio since the loading on the compressor is dynamic.

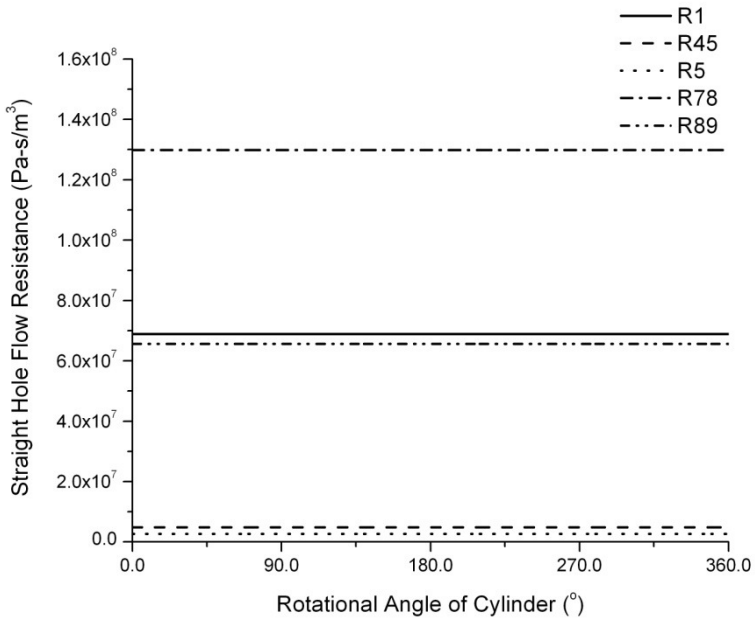

Figure 8.3 Flow resistances of various straight holes

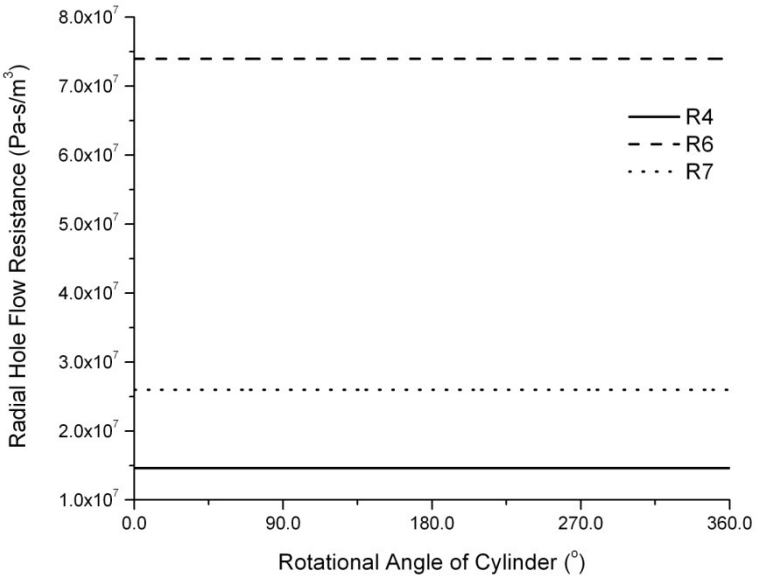

Figure 8.4 Flow resistances of various radial holes

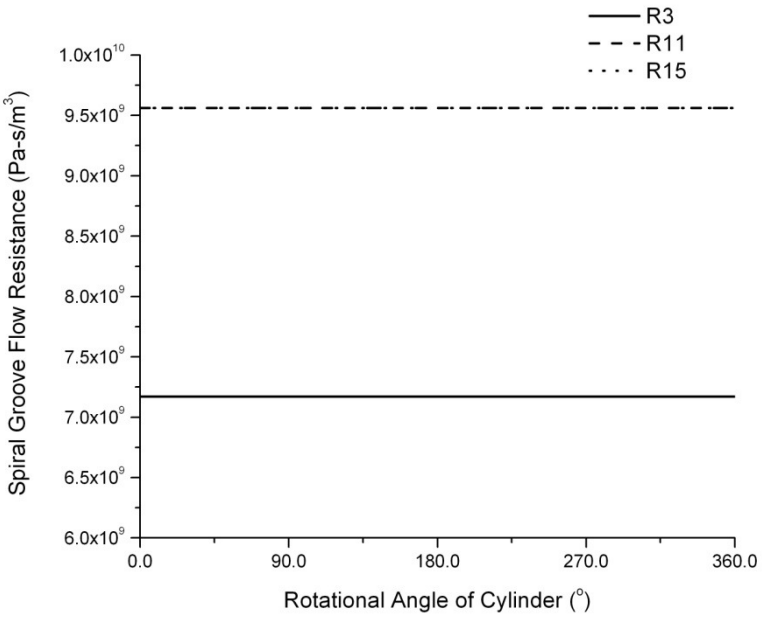

Figure 8.5 Flow resistances of various spiral grooves

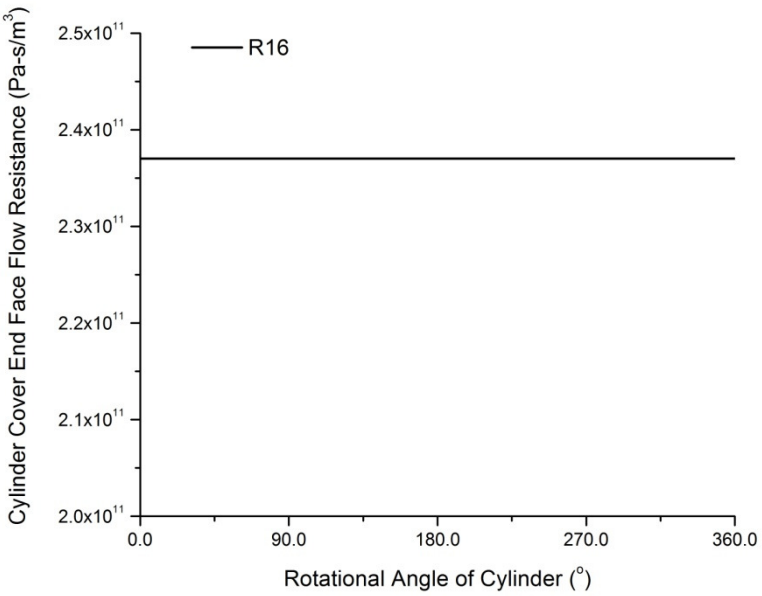

Figure 8.6 Flow resistance at cylinder cover end face

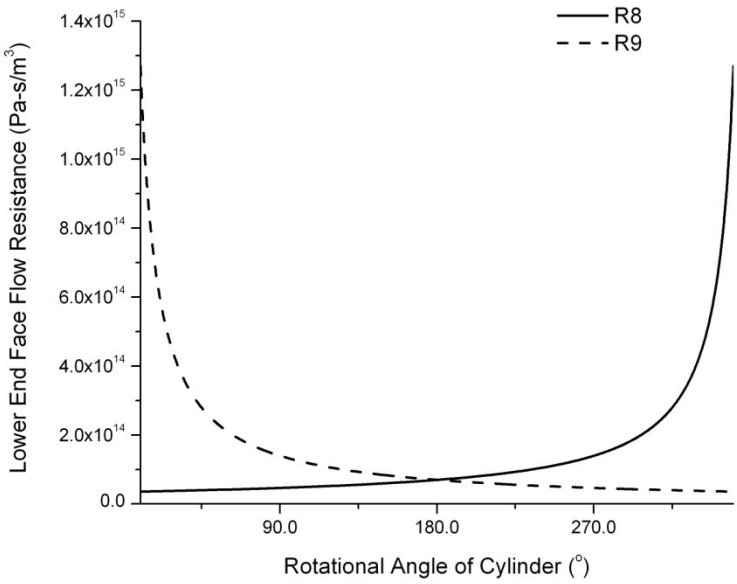

Figure 8.7 Flow resistances at lower end face

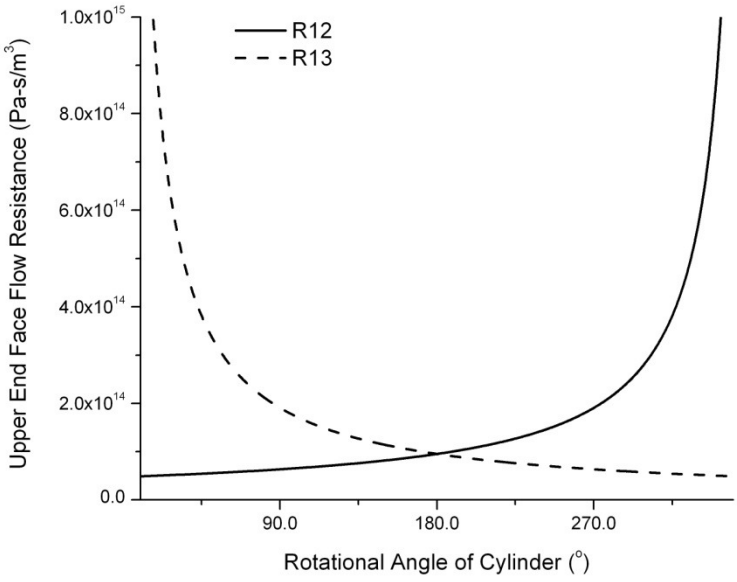

Figure 8.8 Flow resistances at upper end face

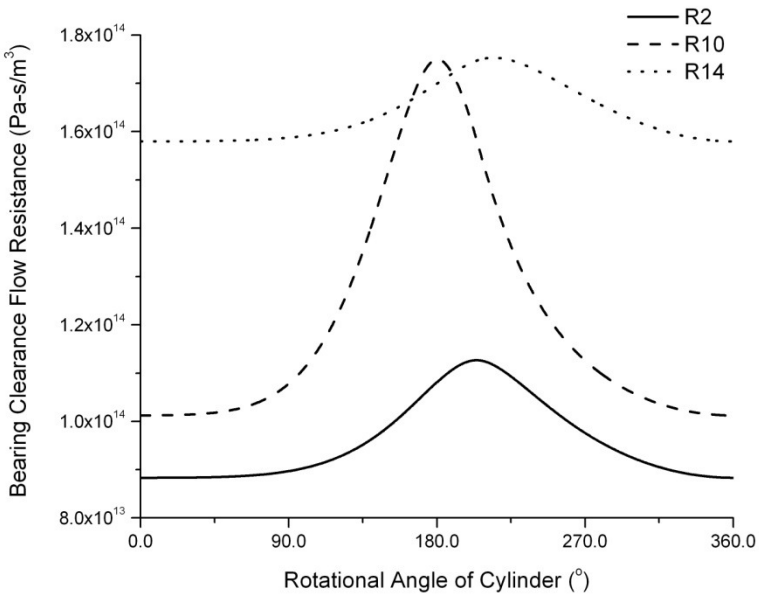

Figure 8.9 Flow resistances at various bearing clearances

As a result, the oil flow rates are dictated by the flow resistance and the results are shown in Table 8.2. From the tabulated results, it can be seen that the oil flow rate through the bearing clearance (Q_2, Q_{10} and Q_{14}) is negligible due to the high flow resistance. In addition, it is observed that the oil flow rate through the axial clearance at the lower and the upper end faces (Q_8, Q_9, Q_{12} and Q_{13}) are limited as compared to the rest of the flow paths since the corresponding flow resistance is high. Furthermore, the negative signs are observed for the Poiseuille flow through the spiral groove on the cylinder shaft (Q_3) and the cylinder cover (Q_{15}). It is because the spiral groove is working against the reverse pressure gradient, which means the spiral groove pumps the oil from low pressure side to high pressure side. Thus, the reverse pressure gradient will push portion of oil along the opposite of the desired direction through the small opening area of spiral groove.

Table 8.2 The oil flow rates in fixed-vane revolving vane compressor

Description	Symbol	Flow Rate (cc s^{-1})
Through horizontal delivery hole at the bottom of oil sump	Q_1	0.07240
Through lower cylinder bearing clearance	Q_2	0.00000
The Poiseuille flow through spiral groove on cylinder shaft	Q_3	-0.00146
The Couette flow through spiral groove on cylinder shaft	Q_{sg6}	0.16324
Through the lower radial hole on the cylinder shaft	Q_4	0.23419
From the centre hole of cylinder shaft to lower end face	Q_5	0.07241
Through the upper radial hole on the cylinder shaft	Q_6	0.16178
Through the radial hole on the rotor shaft	Q_7	0.06519
From lower end face axial clearance to compression chamber	Q_8	0.00293
From lower end face axial clearance to suction chamber	Q_9	0.00429
Through rotor bearing clearance	Q_{10}	-0.00003
The Poiseuille flow through spiral groove on rotor shaft	Q_{11}	-0.09802
The Couette flow through spiral groove on rotor shaft	Q_{sg10}	0.16324
From upper end face axial clearance to compression chamber	Q_{12}	0.00220
From upper end face axial clearance to suction chamber	Q_{13}	0.00319
From upper cylinder bearing clearance to shell	Q_{14}	-0.00005
The Poiseuille flow through spiral groove on cylinder cover	Q_{15}	-0.19862
The Couette flow through spiral groove on cylinder cover	Q_{sg11}	0.25847
Through cylinder cover end face axial clearance to shell	Q_{16}	0.05980

In general, the required oil flow rate to the journal bearing surface is known and thus, the calculated results from the oil flow network is important as it can be used to check whether the designed dimensions fulfils the oil flow rate requirement. Figures 8.10 to 8.12 show the required oil flow rate and the corresponding supply oil flow rate for lower cylinder bearing, rotor bearing and the upper cylinder bearing respectively.

The figures show that the supply oil flow rates under this oil flow network are sufficient to match the bearing oil flow rates requirement.

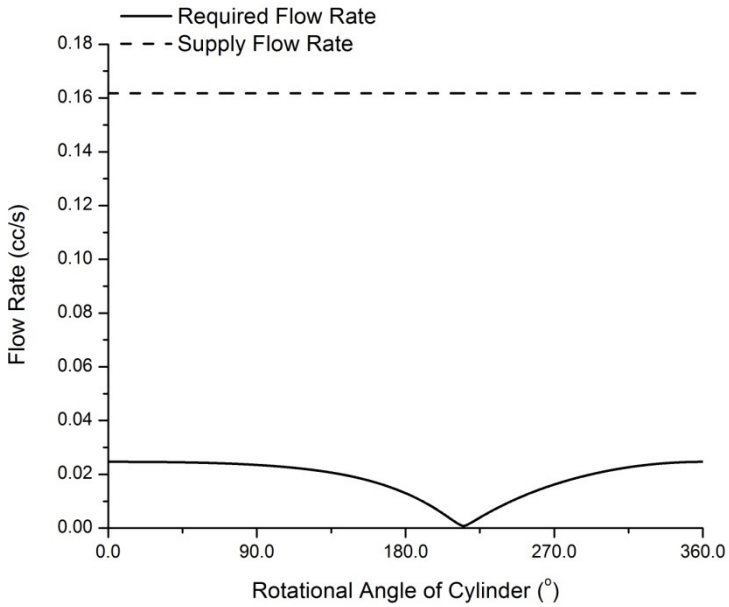

Figure 8.10 Oil flow rates to lower cylinder bearing

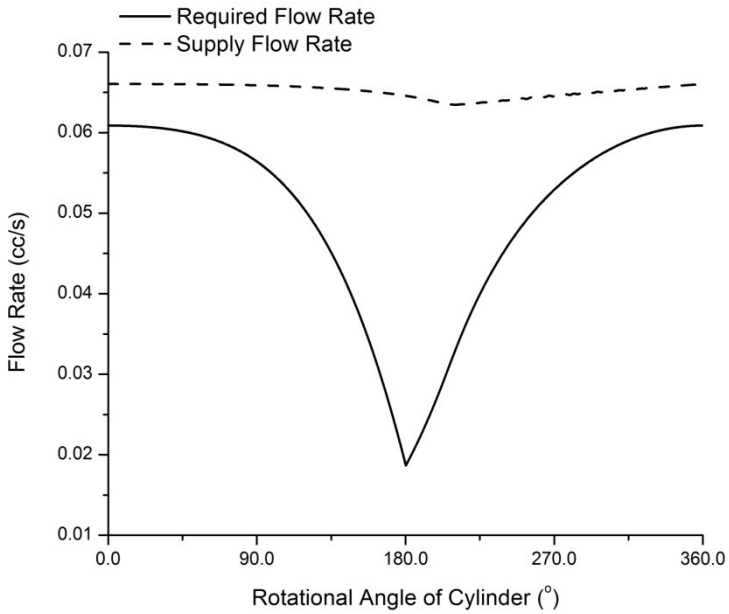

Figure 8.11 Oil flow rates to rotor bearing

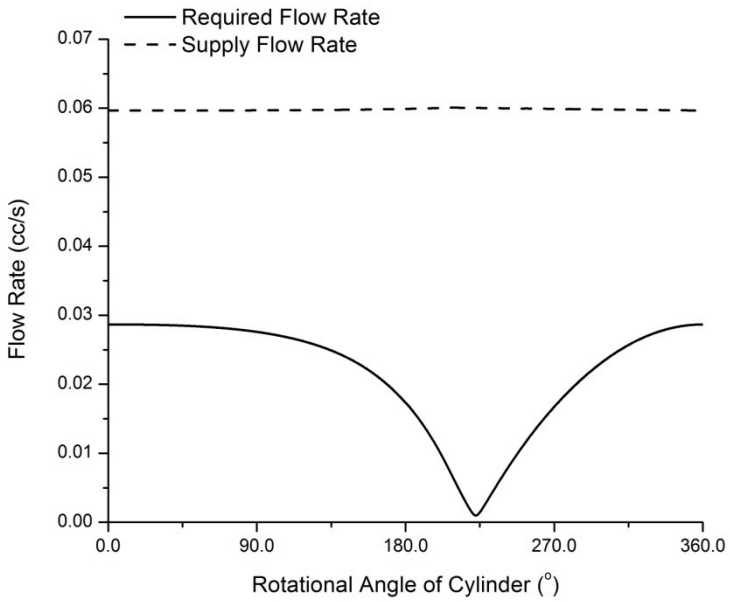

Figure 8.12 Oil flow rates to upper cylinder bearing

8.4 Results and Discussion

The calculated results from the oil flow network indicate that the proper dimensioning of each flow path configuration is important to have a functional lubrication system. In addition, the pressure inside the compressor shell is also a crucial factor to determine the lubrication system performance. In this section, the effects of the diameter and the length of hole, the shell pressure, the width and depth of the groove on the oil flow rate will be examined.

8.4.1 Effect of Hole Diameter and Length

The size of the diameter of the hole for oil flow dictates how easy or otherwise for the flow to flow through. By having a larger diameter of the hole, the flow can easily flow through due to a lower flow resistance. Figure 8.13 shows that as the diameter of the vertically drilled hole on the cylinder shaft (Point 4 to Point 5) increases

from 5.0 mm to 9.0 mm, the corresponding oil flow rate increases from 0.23419 cc/s to 0.23422 cc/s. Similarly for the hole length, the flow resistance associated with a shorter hole will be lower and thus, the oil flow rate will increase. Figure 8.14 shows that the flow rate increases from 0.23419 cc/s to 0.23420 cc/s when the hole length decreases from 9.0 mm to 5.0 mm. However, the results show that the increment of the flow rate is not very significant to the change in hole diameter or length.

8.4.2 Effect of Shell Pressure

For the compressor where the discharge pressure fills the housing, this pressure can be used as the primary source of energy to assist the oil flow. The lubricated region may be starved from the lubricant if the shell pressure is not high enough. Figure 8.15 shows that if the shell pressure (gauge) increases from 1.0 bar to 5.0 bar, the primary flow rate (Q_1) increases from 0.0325 cc/s to 0.0494 cc/s. In practice, when the discharge pressure is not high enough, a more positive pumping effect can be achieved using appropriately designed spiral grooves.

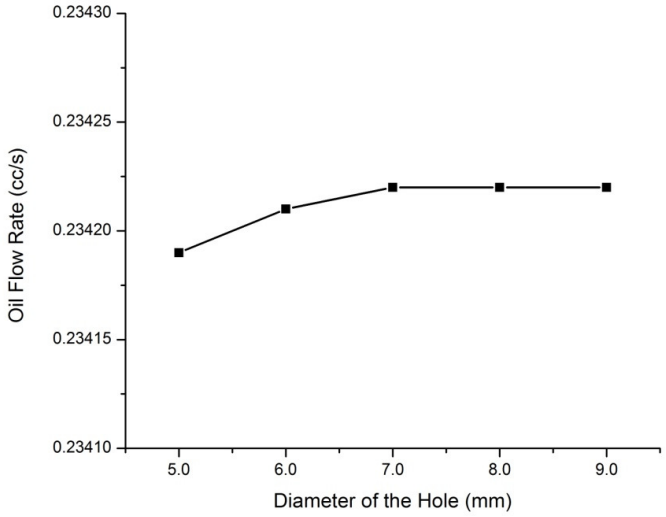

Figure 8.13 The effect of hole diameter

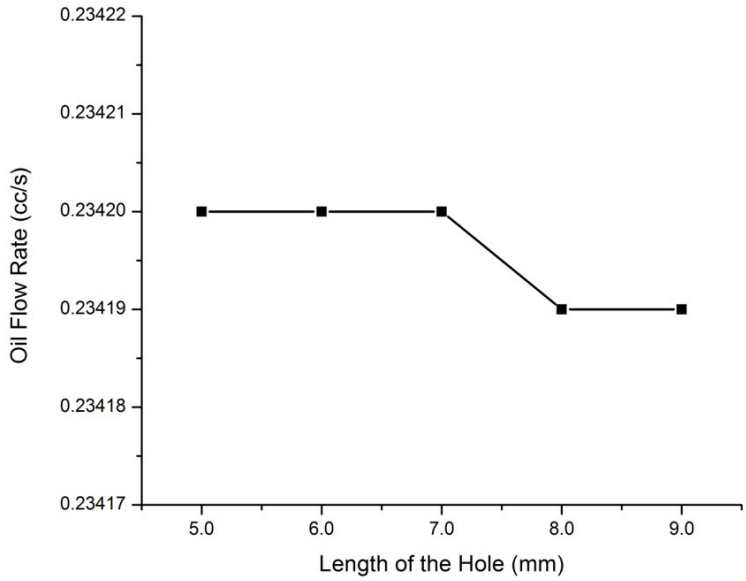

Figure 8.14 The effect of hole length

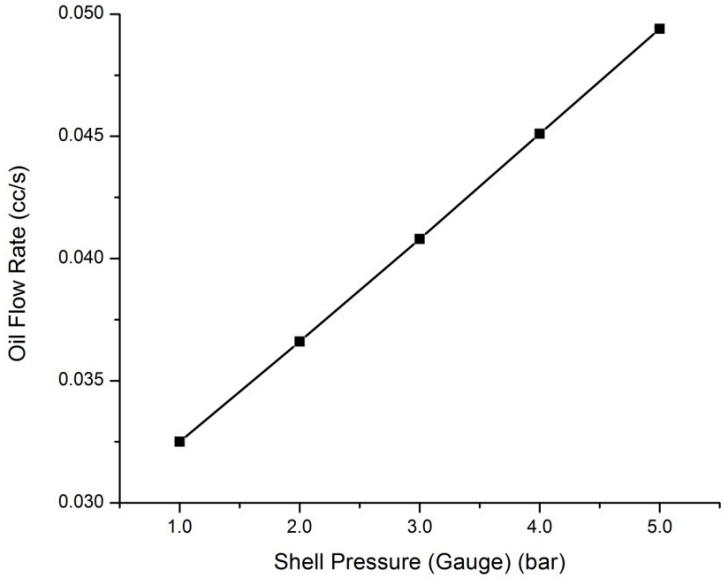

Figure 8.15 The effect of shell pressure

8.4.3 Effect of Groove Width and Depth

The idea of having a spiral groove on the shaft is to enhance the oil delivery to the desired location, especially when pumping under the opposition of the pressure gradient. An effective spiral groove drags the lubricant along its surface by shearing

action which is described by Couette flow. In general, a spiral groove consists of a width and a depth and the combination of these two dimensions will dictate the effectiveness of the shearing action. Figure 8.16 shows the effect of the width of the oil groove on the corresponding flow rate at cylinder cover. It is noted that if the width of the groove is increased from 1.0 mm to 5.0 mm under a constant depth of 0.3 mm, the flow rate dragged by the spiral groove due to shearing action is increased. However, the flow across the spiral groove due to the reverse pressure gradient (known as Poiseuille flow) increases too when the cross-sectional area of the groove is larger, which lowers the flow resistance and induces a higher flow rate as opposed to the desired direction of positive viscous pumping from the spiral groove. As a result, the overall increment in the oil flow rate is 0.01734 cc/s when the groove width increases from 1.0 mm to 5.0 mm under constant groove depth of 0.3 mm, as shown by Figure 8.16. However, the increasing rate is declined as the groove width increases since the reverse pressure gradient pushes more oil to the opposite of the desired direction of positive spiral groove pumping through larger opening area.

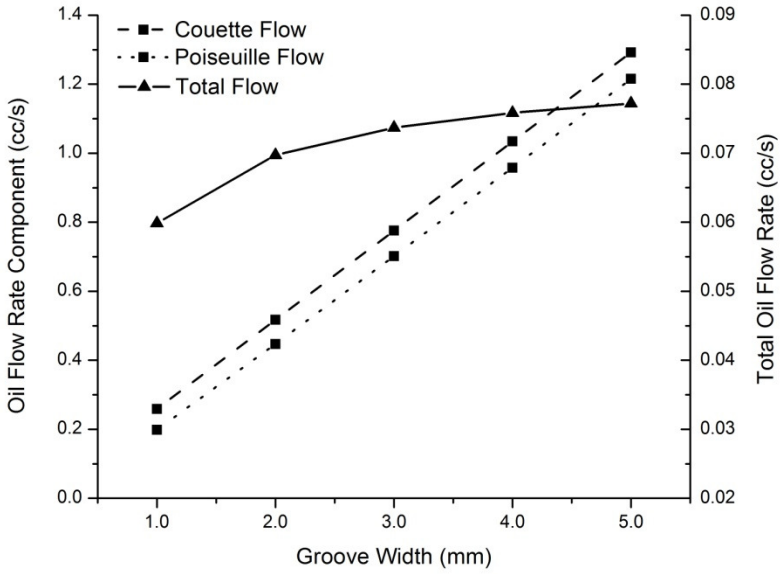

Figure 8.16 The effect of groove width

The effect of the groove width indicates that when pumping against the reversed pressure gradient, the advantages of having a spiral groove will diminish if the cross-sectional area of the spiral groove becomes larger. Figure 8.17 shows that the total delivery of the oil flowing through the spiral groove is increased by having a shallower groove under a constant groove width of 1.0 mm. It can be observed that by reducing the groove depth from 0.9 mm to 0.1 mm, the total oil flow rate is increased 5 times due to the reduction in reversed Poiseuille flow as the flow resistance associated with it is inversely proportional to the cubic of groove depth. From the same figure, it is observed that the increasing rate in the total oil flow rate through spiral groove is declining when the groove depth is smaller than 0.3 mm since the shearing area is too limited for the shearing action to take place.

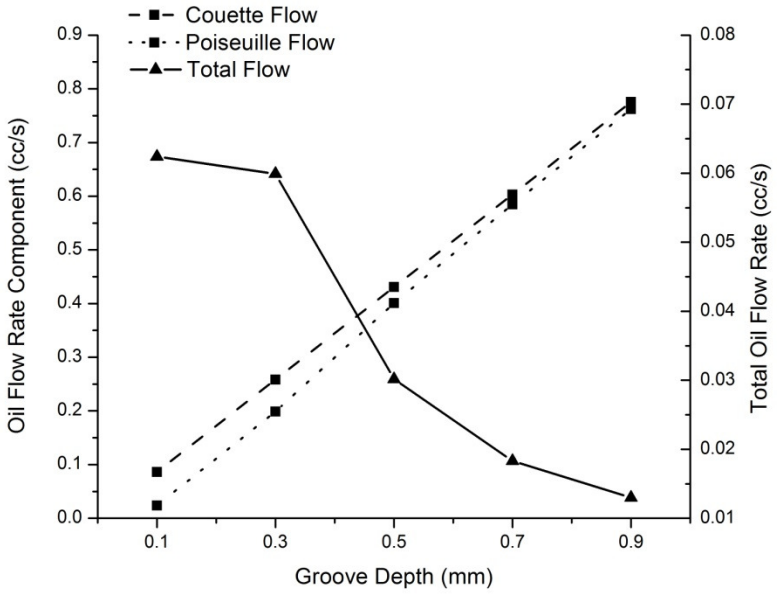

Figure 8.17 The effect of groove depth

8.4.4 Effect of Operating Speed

Nowadays, the compressor runs for a range of speed in an inverter air-conditioning system. The operating speed of the compressor does affect the oil flow rate, especially on the spiral groove. It is known that the spiral groove drags the fluid along its surface and if the shaft spins faster, the corresponding flow rate will be greater. Figure 8.18 shows that the total flow rate through spiral groove at the cylinder cover increases from 0.03 cc/s to 0.09 cc/s as the operating speed increases from 1000 rev/min to 3000 rev/min.

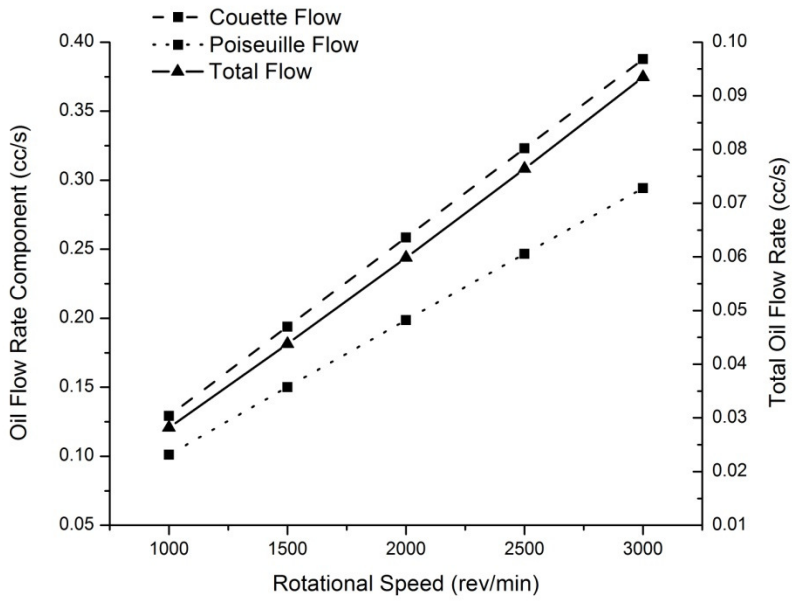

Figure 8.18 The effect of operating speed

8.5 Concluding Remarks

A unique lubrication system for the revolving vane compressor has been proposed and shown in Figure 8.1 and the design dimensions are presented in Table 8.1. The lubrication system consists of the flows through straight holes, radial holes, axial clearance between end faces, bearing radial clearance and spiral groove. The individual flow paths are assembled into a lubrication system network and the flow rates for each flow path are solved by firstly setting up Kirchhoff's circuit law and followed by Gaussian elimination method. The results show that the flow resistances across each flow path dictate the corresponding oil flow rate. The lower-resistance paths for example the radial holes and the vertically drilled hole on the rotating shaft attract more oil flow rates than the flow through end faces axial clearance and bearing radial clearance, which are dimensioned to be in the order of μm. In addition, for the spiral grooves works under the reverse pressure gradient, the dimensions of the depth and the

width of the groove are required to be well-designed in order to satisfy the prerequisite for successful journal bearing lubrication. In addition, the results also show

- By increasing the length of the hole, the flow resistance will be increased. For the hole connecting the first radial hole to the second radial hole on the cylinder shaft, the oil flow rate decreases 0.01 mm^3/s for an increment of 4 mm in the hole length. In addition, by having a larger diameter of the hole, the flow resistance will be decreased. The increments in the oil flow rate in the same hole is 0.03 mm^3/s for an increment of 4 mm in the hole diameter.
- The pressure inside the compressor shell is the primary source of energy to assist the oil flow. The oil flow rate along the horizontal hole at the oil sump increases 16.9 mm^3/s as the shell pressure raises from 1.0 bar (Gauge) to 5.0 bar (Gauge).
- For the spiral groove works under the reverse pressure gradient, the dimensions of the width and the depth for the spiral groove are extremely important. For the spiral groove cut on the cylinder cover, it is shown that the oil flow rate can be increased for 17.4 mm^3/s when the groove width increases from 1.0 mm to 5.0 mm under a constant groove depth of 0.3 mm. However, the positive effect from wider groove ceases as width increases because the wider groove opening area attracts more oil flow rate opposite to the desired flow direction due to the reverse pressure gradient.
- Similarly, the negative effect of reverse pressure gradient on the spiral groove oil flow delivery can be alleviated by employing shallower groove. The results show that by reducing the groove depth from 0.9 mm to 0.1 mm under constant width of 1.0 mm, the flow resistance for the flow due to reverse pressure gradient increases significantly and thus the oil flow rate through the spiral

groove at the cylinder cover increases 49.4 mm^3/s. However, the positive effect from shallower groove is dampened as depth decreases since the shearing action across the groove area is reduced.

- The compressor speed determines the rate of dragging the oil through the spiral groove surface, which in turns provides more oil flow rate to the lubricated region. As the compressor speed increases from 1000 rev/min to 3000 rev/min, the increment in the effective oil flow rate through the spiral groove at the cylinder cover is 65.3 mm^3/s.

The lubrication system analysis is important to ensure sufficient amount of oil is delivered to the rubbing surfaces. The layout and the dimensions of the oil flow paths have to be carefully examined to satisfy the lubrication requirement. A short analysis presented in Appendix A shows how an improper oil flow path layout affects the resultant distribution of the oil flow rate.

Chapter 9

Experimental Study & Validation of Mathematical Models

9.1 Introduction

The fixed-vane revolving vane compressor mechanism uses the combination of a fixed vane and split bush as with a capacity of 1.7cc will be investigated experimentally. This chapter starts by showing the experimental test bed and the preparation of the compressor prototype prior to experimental studies. The experimental procedures will be introduced and the measured data will be compared with the prediction using the aforementioned theoretical models. The measurements agreed well with the prediction in the case of mechanical power with a maximum discrepancy of 10 %. The measured volume flow rate of the air is more than the prediction for the discharge pressure at 1.5 bar, 2.1 bar and 2.4 bar with the motor rotational speed above 2400 rev/min, 3000 rev/min and 3300 rev/min respectively.

9.2 Set Up of Experimental Test Bed

The compressor prototype is intended to be tested under various discharge pressures and operating speeds. The schematic for the experimental test bed is shown in Figure 9.1. The measured parameters are the voltage (V), the current (I) supplied to the

electric motor, the discharge pressure (P), the temperature (T) of the air in the receiver tank, the driving shaft speed (ω) and the volume flow rate of the air (Q).

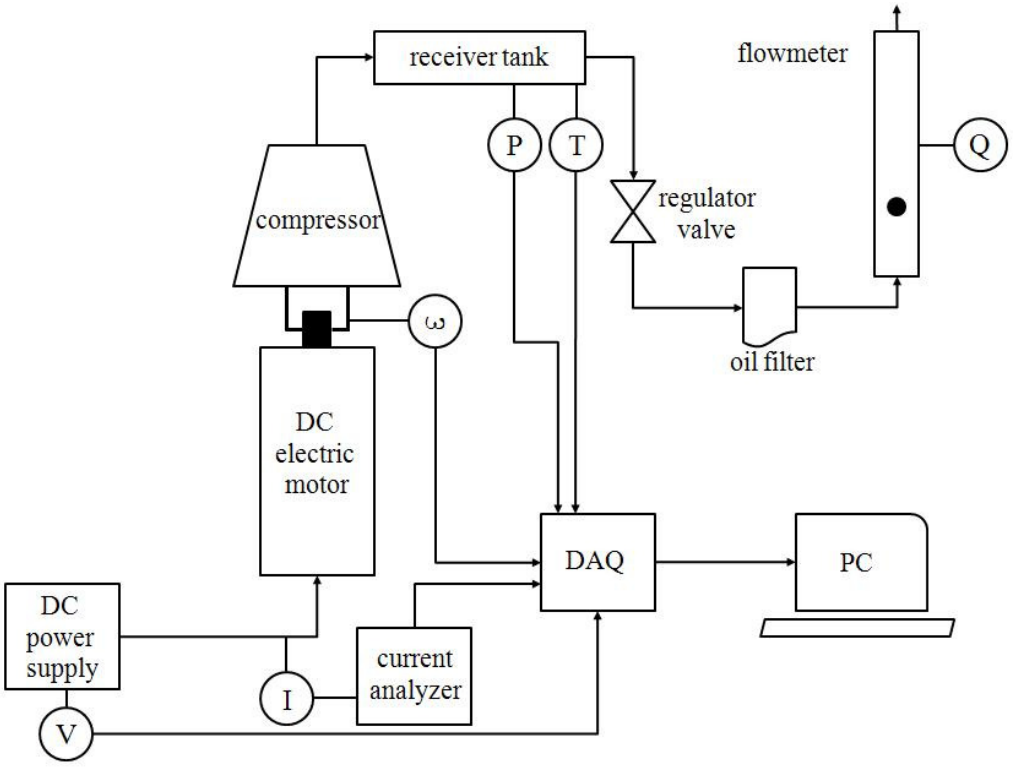

Figure 9.1 Schematic view of the compressor test bed

The compressor is driven by a small direct-current electric motor which is shown in Figure 9.2. The motor sits on a motor cap. The motor shaft which is protruded out from the motor cap is directly coupled to the compressor shaft by using two set screws. The magnetic pick up shown in Figure 9.3 is used to capture the rotational frequency of the compressor shaft by placing it to the vicinity of the set screws. A current signal will be generated when both set screws pass the magnetic pick up. Therefore, the frequency of the current signal pick up is the frequency of the compressor shaft.

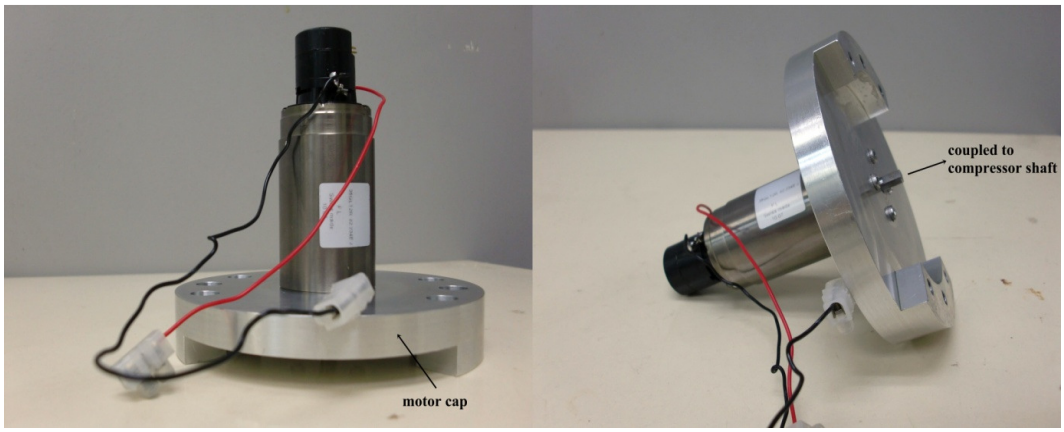

Figure 9.2 The electric motor assembly

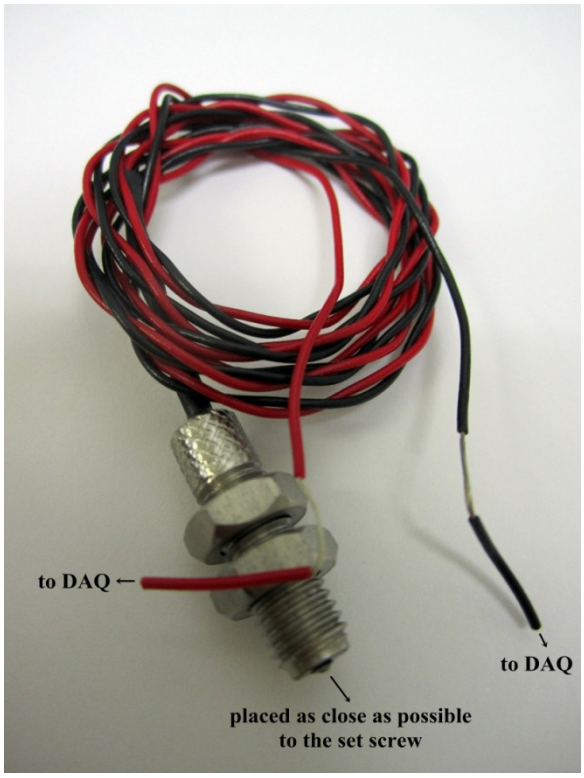

Figure 9.3 Magnetic pick up

The power to the electric motor is supplied by a DC power supply, as shown in Figure 9.4. The DC power supply has the voltage limit of 30.0 V and the current limit of 3.0 A.

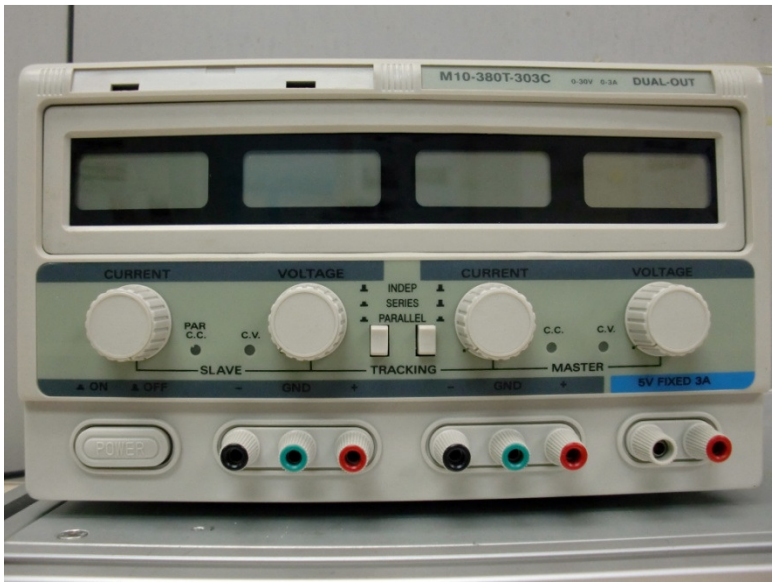

Figure 9.4 The DC power supply

The voltage and the current supplied to the electric motor are recorded through the voltage probe and current probe, as shown in Figure 9.5. The current probe is used together with an analyzer. The outputs from both probes are linked to the data acquisition system (DAQ).

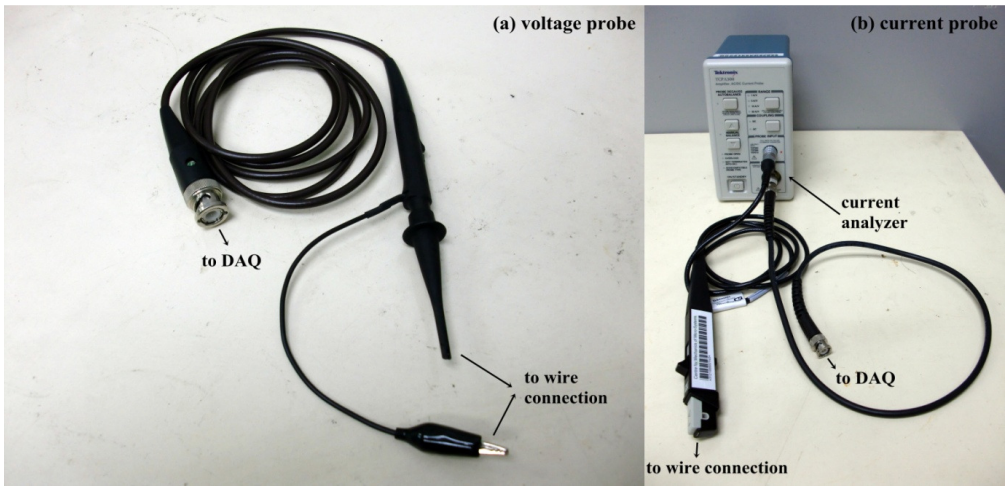

Figure 9.5 Voltage probe, current probe and current analyzer

In addition, the pressure and the temperature of the air in the receiver tank are recorded by a pressure transducer and a thermocouple respectively, which are shown in Figure 9.6.

Figure 9.6 Assembly of pressure transducer, thermocouple and receiver tank

A regulator valve is placed at the downstream of the receiver tank assembly to maintain the desired pressure in the receiver tank. The discharge air is filtered through an oil filter before it goes into the flowmeter. The latter is used to record the volume flow rate of the air. The output signals of all the measurement devices are sent to the data acquisition system. The overall view of the experimental test bed is shown in Figure 9.7.

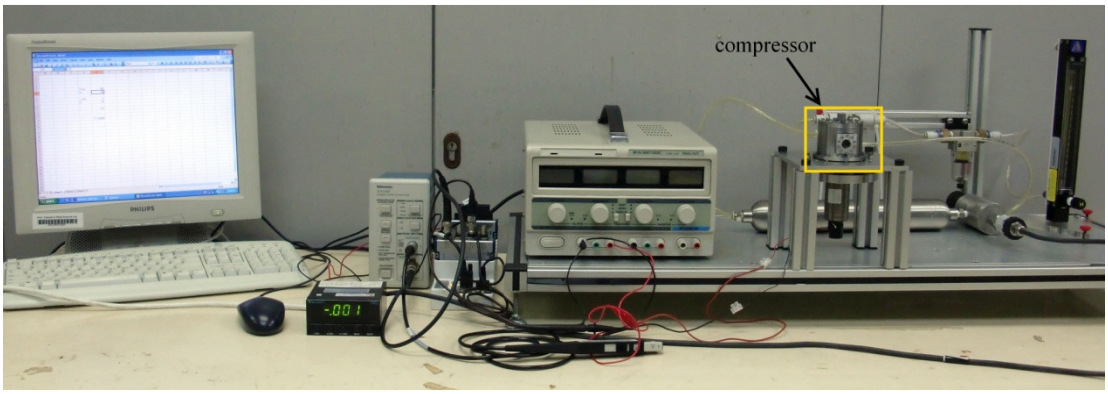

Figure 9.7 Overall view of compressor test bed

9.3 Preparation of Compressor Prototype

Before putting the compressor prototype into any real testing, the compressor components need to be carefully examined for their dimensions and surface finish. The deviation from the required geometrical dimensions may happen due to the inconsistency in fabrication processes and this will lead to compressor assembly failure, let alone putting the compressor into testing. In addition, the poor surface finish on the compressor bearing parts may deteriorate the journal bearing performance and leads to compressor failure. In this section, the two main procedures are carried out prior to the testing. These are discussed in Sections 9.3.1 and 9.3.2.

9.3.1 Inspection of Geometrical Properties

The geometrical dimensions of every compressor components are important as they determine the success or otherwise of the entire compressor assembly. For example, the diameter of the cylinder shaft should be smaller than its bearing in microns and the space in between these two components dictates the bearing clearance. Furthermore, the measured dimensions of the main compressor components form the inputs to the theoretical model for model validation purposes during the research and development phase for a new compressor.

Once the components are received from workshop, different types of micrometers and vernier calipers shown in Figure 9.8 were used to check the dimensions of the compressor components. The dimension checking was taken the room conditions and was finalized after taking multiple measurements for each dimension in order to minimize human error. During the measurement, the tools must be clean as any oil film or particle stick to the tools will cause the measurement deviates from its actual dimensions, in which the deviation can result in obscured predictions for the journal bearing performance. The major dimensions of the compressor components are listed in Table 9.1.

Figure 9.8 Micrometers and vernier calliper

Table 9.1 Measured dimensions of fixed-vane revolving vane compressor prototype

rotor diameter	24.980 mm	cylinder diameter	29.899 mm
rotor shaft diameter	11.993 mm	Cylinder shaft diameter	11.997 mm
rotor bearing diameter	12.025 mm	lower cylinder bearing diameter	12.023 mm
rotor bearing diametrical clearance	32.000 μm	Lower cylinder bearing diametrical clearance	26.000 μm
Axial length of working chamber	8.018 mm	upper cylinder bearing diameter	18.988 mm
Vane length	7.984 mm	Inner diameter of cylinder cover	19.009 mm
Vane thickness	2.789 mm	Lower cylinder bearing diametrical clearance	21.000 μm
Valve length	9.442 mm	Valve thickness	0.175 mm

The surface roughness of the compressor bearings was checked during the preparation stage too. The value of the surface roughness is not required for the theoretical model validation purpose but to avoid compressor bearing failure, the surface roughness must be at least 10 to 100 times lesser than the required minimum oil film thickness, as discussed in the Chapter 6. The surface roughness of the rotating components, i.e. the rotor shaft and the cylinder shaft, were checked and shown in Figure 9.9. The root mean square surface roughness value (R_q) for the rotor shaft and the cylinder shaft are 0.3 μm and 0.4 μm respectively. In addition, the sharp peaks observed in the surface roughness profile need to be carefully handled as any sharp peaks may chip off during the compressor operation and thus accumulate, which may eventually leads to bearing seizure due to the existence of the foreign material. The sharp peaks were smoothened by using an ultra-fine grinding paper meticulously.

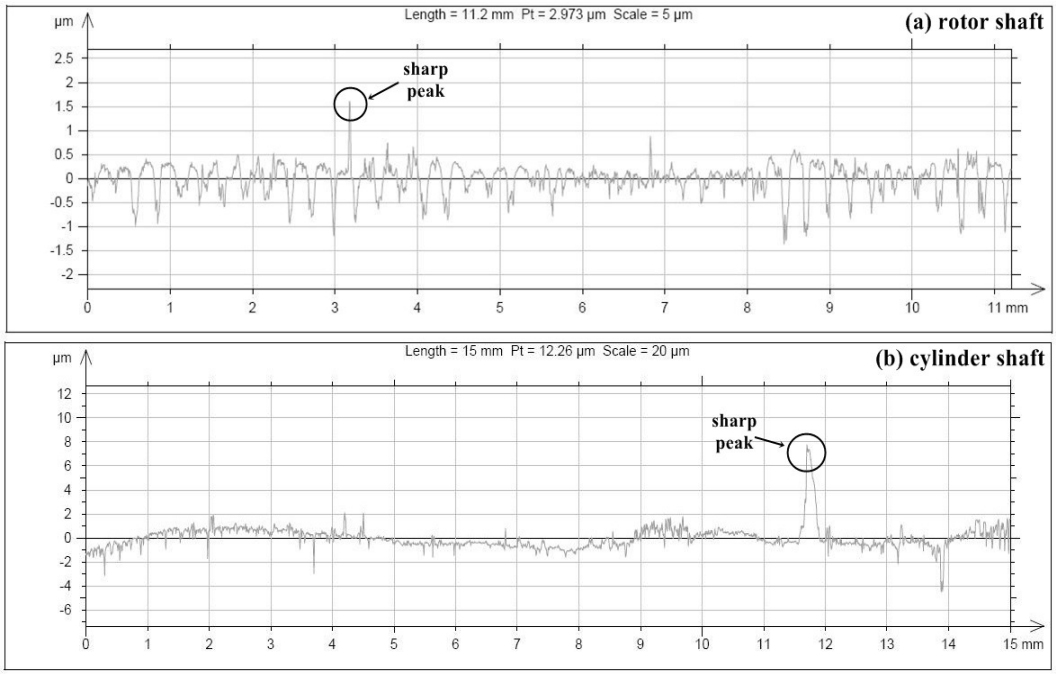

Figure 9.9 Surface roughness profiles for rotor shaft and cylinder shaft

The dimensions of all the compressor components after the surface treatment were checked again by using the coordinate measuring machine.

9.3.2 Inspection of Dynamic Balancing

The mass properties of the rotating assemblies are important because for any rotating assemblies which are not properly dynamically balanced, additional centrifugal forces will be incurred and acts as an extra loading to the journal bearing, which in turns affects the bearing performance characteristics, or to the worst, leads to the entire compressor failure.

During the prototype design phase, the rotating assemblies are dynamically balanced through the use of CAD model. However, due to miscellaneous discrepancies lie in the material density, the depth of the holes and the length of the screw, the final mass properties of the actual components might differ from its CAD model. Therefore,

the actual mass properties for all the rotating assemblies should be carefully examined before putting into any testing.

The rotating assemblies of the compressor prototype are the cylinder assembly and rotor assembly. The balancing properties for the cylinder and the rotor assemblies have been briefly inspected and are illustrated in Figures 9.10 and 9.11 respectively. In the case of a dynamically balanced assembly, the object will be able to stay at rest in any orientation. It can be observed from the figures that the cylinder assembly and the rotor assembly are approximately balanced as the assemblies stay at rest at four different positions.

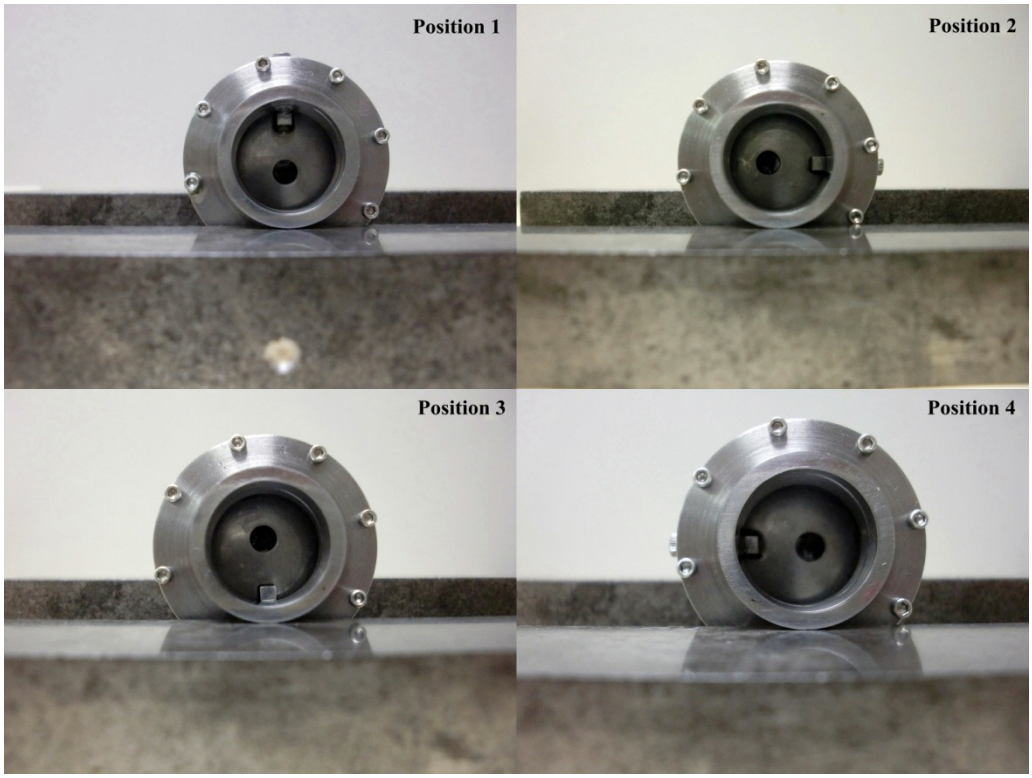

Figure 9.10 Balance check for cylinder assembly

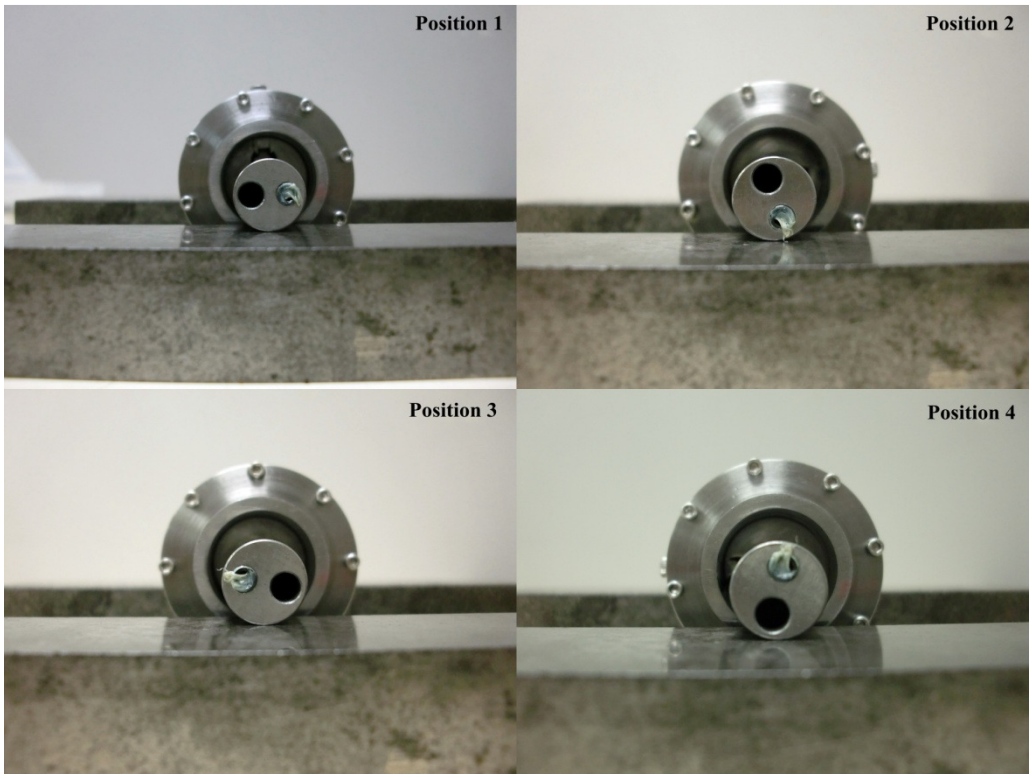

Figure 9.11 Balance check for rotor assembly

9.4 Experimental Study

In this section, the procedures associated with the compressor testing and the comparisons between the measured and the predicted results will be discussed. The compressor was tested to the limit of the DC power supply and the electric motor is kept under the limit of the maximum current supply. The operating speed and the discharge pressure attained were 3800 rev/min and 2.4 bar respectively. The compressor was then disassembled for further investigation on its parts.

9.4.1 Experimental Procedures

The measured parameters in compressor testing are the voltage and the current supplied to the DC electric motor, the average driving shaft rotational speed, the discharge pressure, the air temperature prior to exit to atmosphere and the volume flow

rate of the air. All the measured parameters were taken at steady state. The testing was conducted to the maximum limit of the DC power supply, which is 30.0 V in this case. The discharge pressure ranges from 1.5 bar to 2.4 bar with an interval of 0.3 bar. It is noted that as the discharge pressure goes higher, the leakage flow becomes severe and the resultant volume flow rate of the air is lesser. Hence, higher rotational shaft speed, i.e. higher voltage supply, is required for the test at higher discharge pressure. The voltage settings for various discharge pressures are listed in Table 9.2 and the experimental procedure is described in the chronological order as follows:

i. With no pressure difference involved, the voltage supply is adjusted from 0 V to 12.0 V to start the compressor gradually from rest to approximately 1000 rev/min. This is to warm up the compressor and the data acquisition system before taking the measurement.

ii. The pressure inside the receiver tank is then increased to the prescribed discharge pressure of 1.5 bar by controlling the flow regulator valve. The opening of the regulator valve is controlled to limit the air flow delivered to the flowmeter so that the pressure in the receiver tank can be built up. At the same time, the voltage supply is increased according to the voltage settings shown in Table 9.2

iii. The conditions are maintained for 10 minutes to stabilize the discharge pressure. The various readings are then recorded through data acquisition system.

iv. The voltage supply is then increased according to Table 9.2 so that the compressor speed is increased while maintaining the same discharge pressure by adjusting the flow regulator valve. The steps (iii) and (iv) are

repeated until the maximum voltage of DC power supply system of 30.0 V is reached.

v. The discharge pressure is increased by 0.3 bar and the voltage supply is reset according to Table 9.2. Repeat step (iii) to (v) until a discharge pressure of 2.4 bar is achieved.

vi. Upon the completion of data collection, the pressure difference is unloaded by adjusting the flow regulator valve to the fully open and at the same time, reduces the compressor shaft speed by lowering the voltage supply until completely stops.

It is noted that during the experiment, the external compressor casing is maintained at a moderate temperature of 40 °C by using a standing fan to avoid the compressor suffers from over-heating, which may deteriorate the viscosity of the lubricant. During the entire course of experiment, the casing temperature is carefully observed as fresh lubricant may be required to replenish. The collection of experimental data is deemed as completed and the analysis is then carried out.

It is noted that during the experiment, the system was deemed as at steady state and the measurements were recorded at a time when the compressor body temperature and the air flow rate in the flow meter are stable. The stability of the compressor operation is important as it dictates no abnormality exists in the system. The abnormalities such as the heavy leakage and the severe wear of the compressor components will cause the compressor body temperature increases tremendously and it is required to stop the compressor immediately before the compressor seized.

Table 9.2 Voltage settings in various discharge pressures

Discharge pressure (bar)	Initial voltage (V)	Voltage interval (V)
1.5	22.0	2.0
1.8	22.0	2.0
2.1	26.0	1.0
2.4	27.0	1.0

9.4.2 Additional Considerations to Theoretical Models

Since lip seals are used to prevent the leakage of compressed air, additional considerations uniquely to the fixed-vane revolving vane compressor prototype have been included into the theoretical models presented earlier.

The lip seals are employed to prevent possible compressed air leakage through the clearance between the protruded shaft and the casing. The lip seal is made of PTFE materials and has good lubricity. However, the additional friction occurs at the shaft-seal interface is substantial as compared to the other frictions in the prototype. The friction caused by the lip seal is taken into consideration and calculated based on the method suggested by Muller and Nau [145]. The lip seal friction is given by the equation (9.1).

$$P_{f,ls} = 2\pi\bar{\varphi}R_s^2\omega_s \tag{9.1}$$

which duly accounts for the effect of pressure on the friction. R_s represents the shaft radius and ω_s represents the shaft rotational speed. The tangential friction per unit of circumference ($\bar{\varphi}$) can be read from Figure 9.12. The lip seal employed in the compressor prototype belongs to a conventional PTFE lip seal.

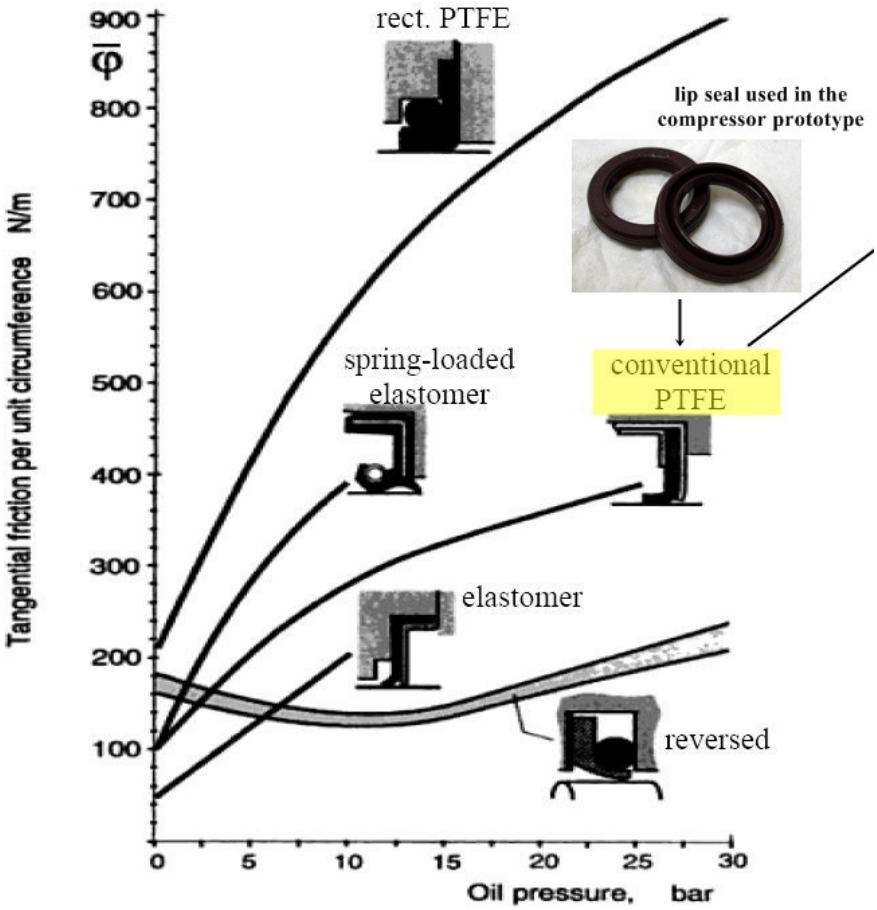

Figure 9.12 Friction at various lip seals as a function of pressure [145]

9.4.3 Comparison of Predicted and Measured Results

The measured voltage and the measured current of the electric motor can be used to calculate the mechanical power input to the compressor using the specific equation provided by the motor catalogue, as shown by equation (9.2).

$$P_{mech} = V \times I - I^2R - kI_0\omega \tag{9.2}$$

where R is winding resistance of 2.25 ohms, k is torque constant of 0.061 Nm/A, I_0 is no-load current of 0.07 A. The variables in the equation (9.2) are the supply voltage (V), the supply current (I) and the operating shaft speed (ω).

The mechanical power at five different motor speeds under four different discharge pressures are shown in Figure 9.13. The mechanical power to the compressor increases as the motor speed increases.

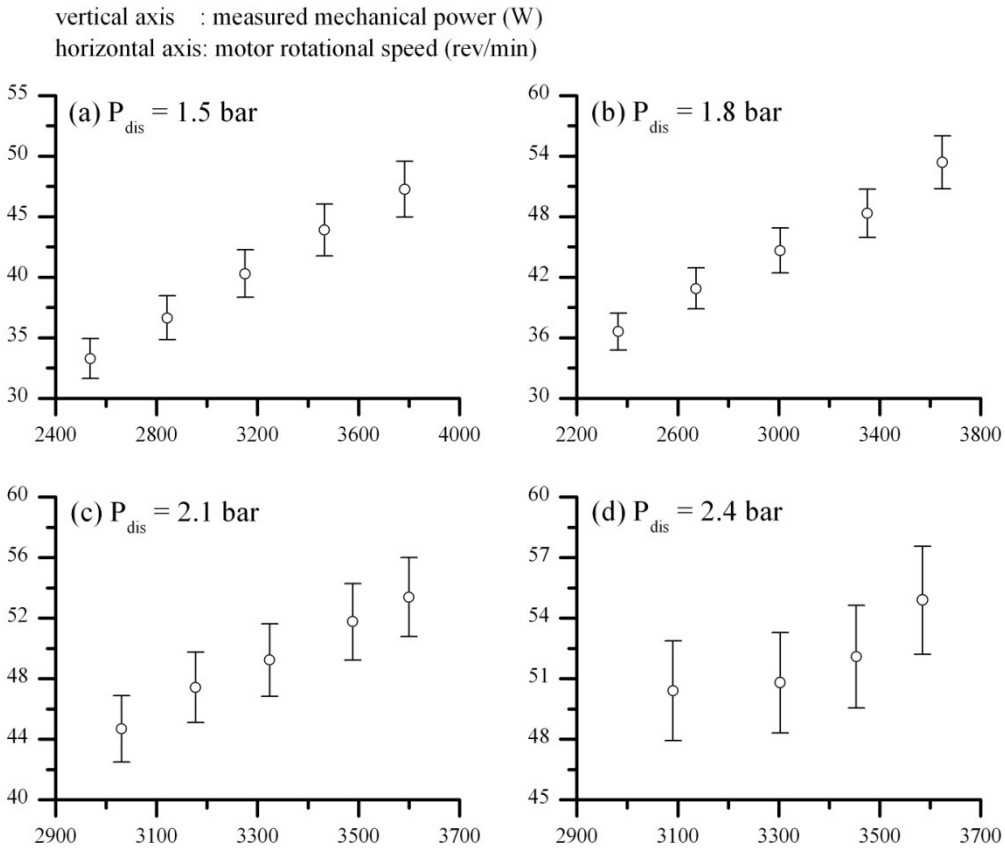

Figure 9.13 The measured shaft rotational speed and mechanical power

The mechanical power supplied to the compressor prototype includes the indicated power and the various frictional losses such as the vane side frictional loss (P_{vs}), the end face frictional loss ($P_{ef,lower}$ and $P_{ef,upper}$), the journal bearing loss ($P_{f,Br}$) and the lip seal frictional loss.

$$P_{vs} = \eta_{vs} \times \frac{I_r \times \alpha_r}{R_r \cos(\phi_r - \phi_c)} \times V_v \tag{9.3}$$

$$P_{ef,lower} = \frac{\mu}{\delta_{ef}} \pi \left[\omega_c^2 e^2 R_r^2 + \frac{1}{2} (\omega_c - \omega_r)^2 R_r^4 \right] \tag{9.4}$$

$$P_{ef,upper} = \frac{\mu}{\delta_{ef}}\pi\left[e^2(\omega_c^2 R_r^2 - \omega_r^2 R_{cc}^2) + \frac{1}{2}(\omega_c - \omega_r)^2(R_r^4 - R_{cc}^4)\right] \quad (9.5)$$

$$P_{f,Br} = R_{Br} \times \omega_J \times \left[\frac{\mu\omega_J R_{Br}^2 L_{Br}\pi}{\delta_{Br}\sqrt{1-\varepsilon^2}}\left(\frac{2+\varepsilon}{1+\varepsilon}\right) + \frac{\delta_{Br}\varepsilon}{2R_{Br}}\sqrt{F_x^2 + F_y^2}\sin\phi\right] \quad (9.6)$$

The vane side frictional loss (P_{vs}) is written in equation (9.3). It is dependent on the rotational inertia of the driven component (I_r) and its angular acceleration (α). The vane side friction coefficient adopted is 0.15, as referred to the paper by Yanagisawa et al. [139]. The end face frictional loss is due to the relative velocity between the rotor and the cylinder at the lower and the upper end faces, expressed by equations (9.4) and (9.5), respectively [146]. The journal bearing frictional loss depends on the viscosity of the lubricant, the operating speed, the bearing dimensions, the force on the bearings and their performance characteristics. It is noted that the frictional loss in the compressor prototype is mainly due to the viscosity of the lubricant (μ), which is strongly dependent on the lubricant temperature. Figure 9.14 shows the relationship between the temperature and the dynamic viscosity of the lubricant used. The viscosity exponentially decreases as the temperature increases.

The estimation of the viscosity of the lubricant for evaluating the frictional loss of the bearing and the end face loss is firstly completed by assuming the isentropic discharge temperature from the compressor according to the suction conditions regardless of the operating shaft speed. The estimated temperature using this assumption and the corresponding lubricant viscosity are shown in Table 9.3. The comparison between the predicted and the experimental mechanical power are shown in Figure 9.15. Most of the predictions do not fall in the agreement with the experimental data.

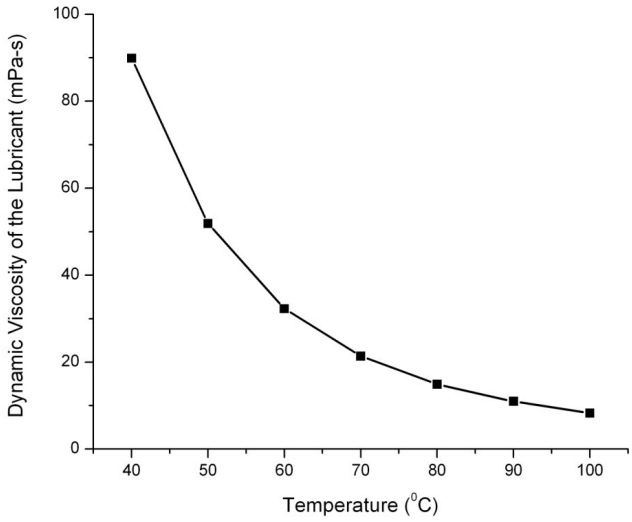

Figure 9.14 Viscosity-Temperature Chart for Shell Corena P100 Lubricant

Table 9.3 The isentropic discharge temperature and the corresponding viscosity

Discharge Pressure (bar)	Isentropic Discharge Temperature (^{o}C)	Dynamics Viscosity (10^{-3} Pa-s)
1.5	62.9	32.4
1.8	79.5	16.9
2.1	95.4	9.1
2.4	108.0	5.6

The predicted mechanical powers are lower than the measured values for discharge pressure at 1.8 bar, 2.1 bar and 2.4 bar while the reverse is true for discharge pressure at 1.5 bar. In the case of 1.5 bar discharge pressure, the estimated temperature is under-predicted so that the lubricant viscosity is higher and thus, generates a higher frictional loss and higher mechanical power as compared to the measured mechanical power. For the remaining cases, the estimated temperature is over-predicted and leads to a lower viscosity of the lubricant and thus, the predicted values are always lesser than the experimental values.

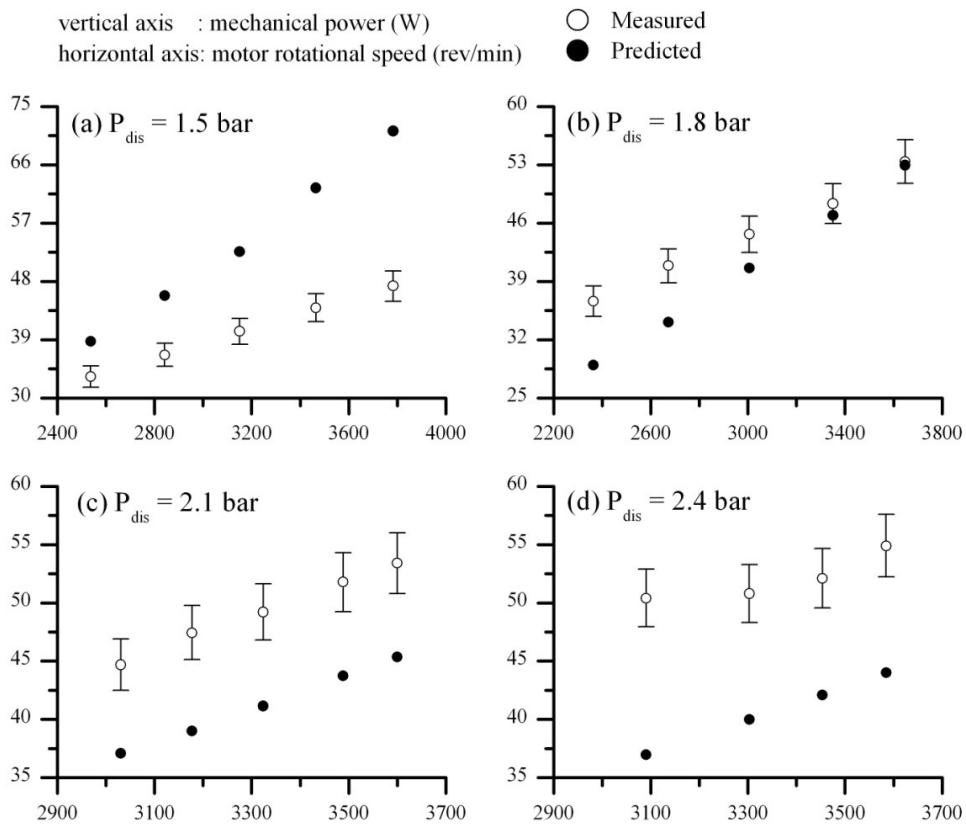

Figure 9.15 Comparisons between experimental and predicted mechanical power (isentropic temperature approach)

Careful examination reveals that the isentropic temperature approach to estimate the lubricant viscosity is not appropriate. The discharge pressure is not a dominant factor in the prediction of the lubricant viscosity. In fact, the viscosities of the lubricant at the bearings and at the end faces are closely related to the localized temperature. The frequent rubbing between the components generates the heat and affects the local lubricant viscosity. The rubbing frequency is affected by the rotational speed of the components in the consideration. The operating speeds conducted in the compressor testing are from 2350 rev/min to 3800 rev/min. It is suggested that the viscosity value should be adjusted according to the operating speed but not the discharge pressure. The operating speed from 2350 rev/min to 3800 rev/min are divided into five groups, each has the range around 300 rev/min. The corrected version is shown in Figure 9.16. The

agreement becomes closer after the correction with a maximum discrepancy of 10%. The localized bearing temperature is not able to be measured in this compressor prototype as the integration of the thermocouple to the bearing may jeopardize the bearing performance and leads to compressor failure during testing. However, the estimated temperature falls reasonably in the region of 70 ˚C to 80 ˚C as the external casing of the prototype was kept around 40 ˚C, as mentioned in the experimental procedures. The values of the viscosity assumed in the calculations associated with Figure 9.16 are presented in Table 9.4.

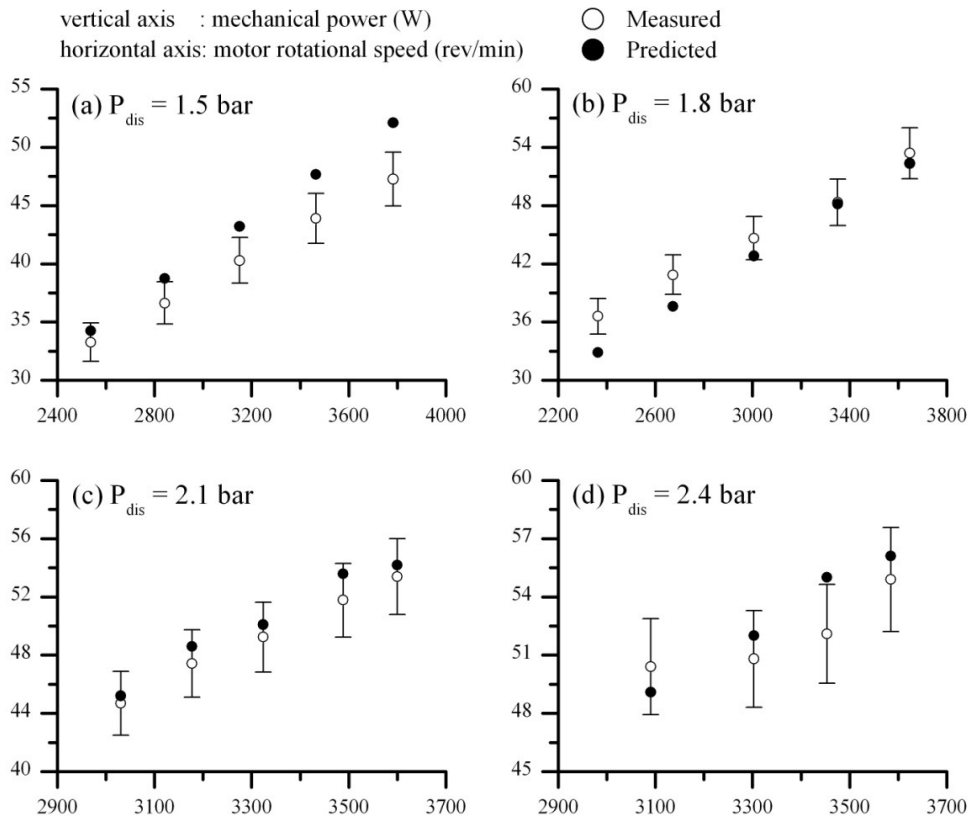

Figure 9.16 Comparisons between experimental and predicted mechanical power (rotational speed approach)

Table 9.4 The values of the viscosity associated with Figure. 9.16

Operating Speed Range (rev/min)	Estimated Bearing Temperature (°C)	Dynamic Viscosity ($x10^{-3}$ Pa-s)
2350 – 2650	70.0	24.5
2650 – 2950	72.5	22.3
2950 – 3250	75.0	20.2
3250 – 3550	77.5	18.3
3550 – 3850	80.0	16.6

The discrepancy between the measured and the predicted result can be further improved by using a high lubricant temperature and hence a lower dynamic viscosity, which is shown in Appendix B. In fact, the energy balance to the lubricant is a more realistic prediction of the lubricant temperature in the bearings. The analysis shall start by having a theoretical analysis on the overall temperature distribution of the compressor using lumped thermal conductance approach in order to predict the temperatures at the entry and the exit points of the bearing. The energy balance is then applied to the lubricant, where the temperature rise between the inlet and the outlet of the bearing equals to the frictional heat generated due to viscous friction. Hence, the lubricant viscosity can be predicted.

The measured mass flow rate of the air is presented in Figure 9.17. It is observed that the measured mass flow rate increases as the rotational speed increases, which conform to the prediction shown in Appendix C. The mass flow rate is the least at the lowest speed for each discharge pressure and at the same motor rotational speed, the measured mass flow rate is lower at higher discharge pressures.

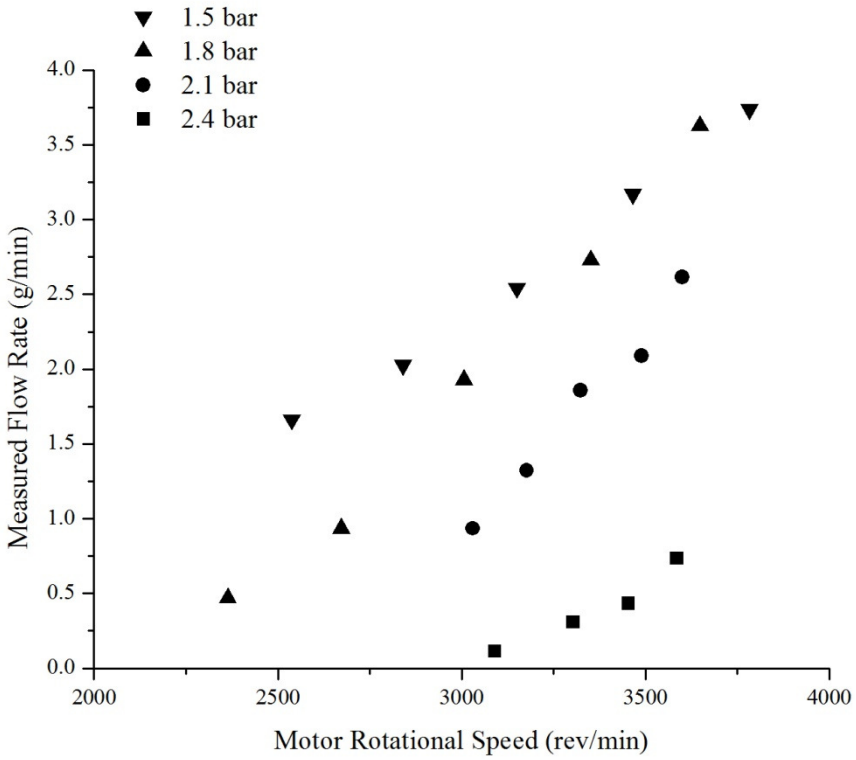

Figure 9.17 The measured mass flow rate

The comparison of measured and predicted mass flow rate of the air is presented in Figure 9.18. The predicted mass flow rate accounts for the leakages from the high-pressure chamber to the low-pressure chamber through the radial clearance and the vane end clearance [100]. The solid line in the figure represents the predicted discharge flow rate after the consideration of the leakage flow through the radial clearance at the virtual line contact of the rotor and the cylinder. The dash line represents the predicted discharge flow rate after considering the combination of the leakages through the radial clearance and the vane-end clearance. In the case of 1.5 bar discharge pressure, the measured flow rate is more than the prediction for speed ranges from 2538 rev/min to 3783 rev/min. A similar situation is observed in the case of 1.8 bar from 2364 rev/min to 3648 rev/min and 2.1 bar from 3324 rev/min to 3600 rev/min. In general, the

lubricant in compressor is not only served as a lubricating agent for the bearings but also the sealing agent to the possible gas leakage flow. The measured flow rate indicates that the lubricant inside the compressor prototype successfully blocks a portion of the possible air leakage flow from the high-pressure chamber to the low-pressure chamber. In addition, it also indicates implicitly that the design for the lubrication oil flow paths is successful. It should be noted that the measured flow rate is lower at the given rotational speed when the discharge pressure is higher. This phenomenon is expected as the leakage flow is pressure driven. However, in the case of 1.8 bar and 2.1 bar discharge pressures, the measured flow rate is less than the predicted flow having considered the leakage through the radial clearance at lower shaft operating speeds, which are below 2673 rev/min and 3177 rev/min respectively. At the discharge pressure of 2.4 bar, the leakage in reality is severe and the measured flow rate is less than the prediction.

The leakage flow itself is a complicated phenomenon as it may be in the form of single phase gas flow, single phase oil flow with dissolved gas or two phase oil-gas mixture flow. The leakage mechanism in reality may be affected by the changes in pressure ratios, the clearance dimensions, the operating speeds and the properties of the lubricant. As a result, the leakage mechanism is not necessarily governed by a single phase flow model at all operating conditions. In addition, the clearance must be tight for a small-size compressor in order to minimize the leakage flow, or alternatively, increase the operating speed.

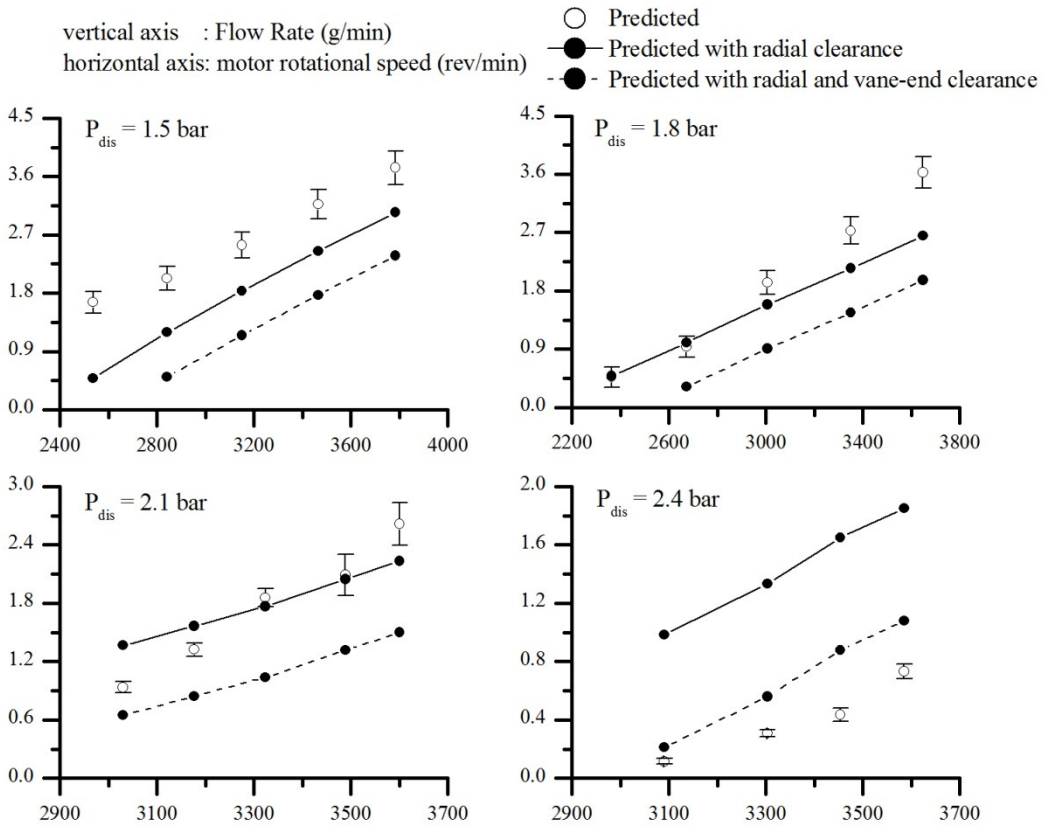

Figure 9.18 Comparisons between measured and predicted discharge mass flow rate

9.4.4 Post-Experiment Analysis

The prototype was carefully disassembled and the components in the compressor prototype appear to be fine after running for a number of days for the testing.

It is observed from Figure 9.19 that substantial oil is found on the upper bearing and the cylinder cover. The oil was accumulated at these regions, which shows lubrication oil paths design presented earlier is successful. The rotor shaft and the cylinder shaft rub against its bearing with lubricating oil in between under a successful design of the lubrication network. There are no obvious scratches or wear marks on the surfaces of the rotor shaft and the cylinder shaft, hence the wear is negligible. However, the interference fit between the lip seal and shafts does leave obvious marks on the shaft

surface, as shown in Figure 9.20. Furthermore, another mark can be easily observed is on the valve. The valve suffers the frequent opening during the compressor operation. The valve is clamped at one end and the amplitude of the motion is impeded by a valve plate. The valve after running it under the discharge pressure of 2.4 bar and operating speed of 3800 rev/min is shown in Figure 9.21.

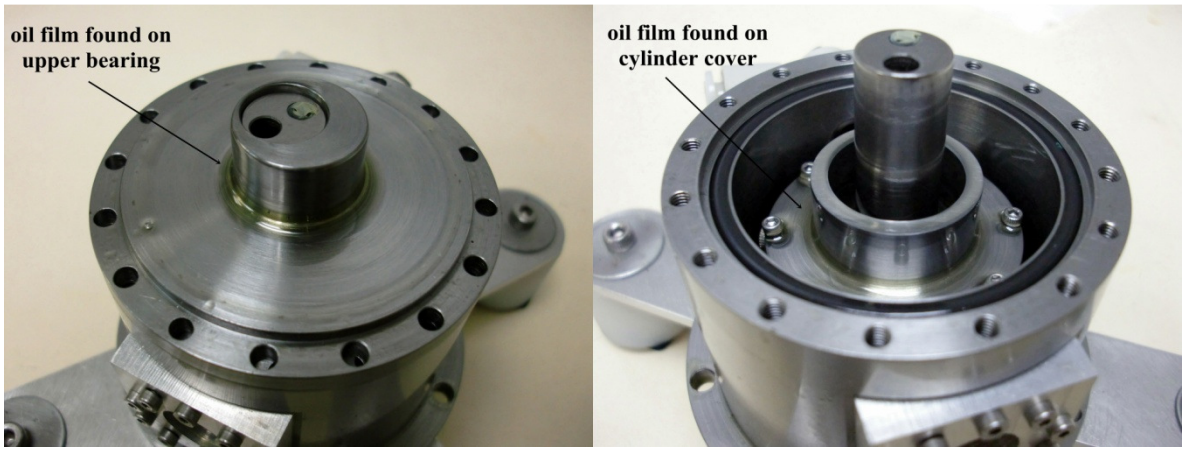

Figure 9.19 Accumulation of oil at expected regions

Figure 9.20 Cylinder shaft and rotor shaft after the compressor test

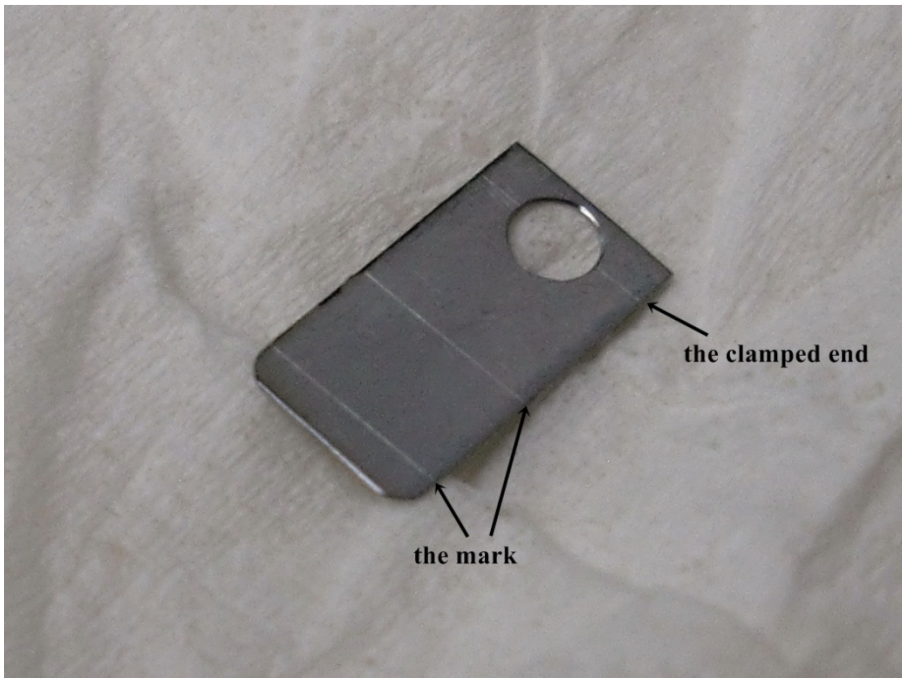

Figure 9.21 The discharge valve after compressor testing

9.5 Concluding Remarks

During the course of compressor testing, there is a lot valuable practical experience gained about the small fixed-vane revolving vane compressor. In fact, prior to the compressor prototyping, the dimensioning is important especially the tolerance accumulation issue. The accumulated tolerance value must be carefully checked before sending for compressor prototyping as it may affect the compressor assembly process. In addition, the checking of the dimensions and the part inspection are equally important after receiving the compressor components. The checking on the important dimensions of the small compressor components is challenging even with the assistance of the coordinate measurement machine as the probe in use is comparable to some dimensions. Therefore, high-end measurement technique for example non-contact metrology may be required for precise measurement for a small compressor.

On the other hand, the measured mechanical power and the prediction agree with each other with a maximum discrepancy of 10 %, which implies the validity of the theoretical models presented earlier. The accuracy of the prediction is made successful by relating the lubricating oil viscosity to the shaft rotational speed. The rubbing effect between the components is more dominant over the pressure effect in evaluating the lubricating oil viscosity.

The pressure ratio achievable in a compressor operation is greatly dependent on the clearances between any two adjacent mating components inside the compressor. The leakage occurs due to the pressure difference between the high-pressure compression chamber to the low-pressure suction chamber and the flows through the clearance in connecting both the chambers. Hence, prior to the discharge process, an amount of working fluid will leak to the suction chamber and mix with the low-pressure working fluid. In the current first fixed-vane revolving vane compressor prototype, the clearance is loose and thus affects the achievable pressure ratio, which is 2.4 in this case.

In the context of revolving vane compressor, the first leakage path is at the line contact between the outer surface of the rotor and the inner surface of the cylinder. The second leakage path is at both end faces of the vane. Therefore, tight control on the geometrical dimension and tolerance for the compressor components, i.e., the outer rotor radius, the inner cylinder radius, the axial lengths of the cylinder, the rotor and the vane is required to minimize the leakage. The dimension check needs to be strict and if possible, ranking and matching of the critical components from the compressor parts pool have to be carried out in order to control the clearance value.

Chapter 10

Geometrical Optimization of the Fixed-vane Revolving Vane Compressor

10.1 Introduction

The theoretical analysis and the practical development of the fixed-vane revolving vane compressor have been illustrated and validated in the previous chapters. The fixed-vane compressor design can be further improved to enhance various aspects of the compressor performance such as to minimize the frictional losses, to minimize the leakages losses and to maximize the coefficient of performance by exploring the possible geometry combinations using optimization technique. A constrained multi-variable direct search optimization technique by Box [147] has been linked with the mathematical models to search for a set of combination of design dimensions that satisfies the required objective under preset design constraints and operating conditions.

10.2 Compressor Optimization

With the aid of the vastly improved computer capability, the compressor designs can be analyzed thoroughly before putting into prototyping stage. The readily available computerized optimization procedures can be used to carry out an optimization study for a compressor design. This is done by combining the mathematical models with the optimization algorithm, in which the combination will generate a set of design

dimensions that produces the desired objective under prescribed operating conditions and design constraints. The method employed in the geometrical optimization for the fixed-vane revolving vane compressor is a multi-variable direct search constrained optimization technique, which is developed by Box [147]. The details of which is included in Appendix C.

In general, an optimization study is to find an optimal solution for an objective under several constraints. The objective is a function of a number of independent variables, which are also normally known as free variables. The optimization procedures will search for a combination of free variables which satisfy the constraints and give the optimum objective value.

The compressor performance has several important aspects, each of which has equal importance. In the worldwide energy-saving issues, the total frictional loss associated with a compressor design is ultimately important and it is worth to investigate which compressor configuration would give the best performance in terms of minimizing the frictional losses. In addition, the leakages losses associated with the compressor determine the effective cooling capacity for the entire refrigeration cycle. Lastly, the coefficient of performance of a refrigeration cycle (usually known as COP) is the indicator for the compressor capability in the competitive compressor market. Hence, the fixed-vane revolving vane compressor will then be explored further to investigate which compressor configuration would satisfy the three objectives respectively, such as minimizing frictional losses, minimizing leakage losses and maximizing coefficient of performance.

10.2.1 Minimizing Frictional Losses

The frictional losses of fixed-vane revolving vane compressor consist of the frictional losses at journal bearing, the vane side and the end faces. The sum of the frictional losses is desirably to be as low as possible in order to reduce the power input. Furthermore, the lower the frictional loss, the heat generated due to rubbing will be lower and thus, the lubricant viscosity will be maintained at a level which is viscous enough to service the journal bearing. The objective in this optimization study is to minimize the total frictional losses for the fixed-vane revolving vane compressor.

The analysis presented for the frictional losses in the fixed-vane revolving vane compressor reveals that the frictional losses are dependent on the geometrical configuration of the compressor and the geometries of the bearings. The geometrical configuration of the compressor is determined by the radius ratio between the cylinder and the rotor at a given size of the cylinder. Furthermore, the analysis in Chapter 6 shows that the increment in the bearing frictional losses due to the change in bearing length is not significant as compared to the change in bearing radius. Thus, the number of free variables in this optimization study is four and these are the radius ratio, the cylinder radius, the radius of the cylinder and the rotor journal bearing.

The free variables have to be examined for their upper and lower limit before the optimization study is carried out. Theoretically, the radius ratio between the cylinder and the rotor can be any value between zero and one. However, a closer look on the compressor design does impose a minimum value for the radius ratio. The maximum exposure length of the vane to the working chamber can be written as equation (10.1).

$$L_{v,max} = 2 \times (R_c - R_r) \tag{10.1}$$

The maximum vane exposure length has to be accommodated in the rotor when the driving rotational angle is at zero degree. Therefore, it is suggested that the maximum vane exposure length should be less than the rotor radius from the point of view of rotor rigidity and design feasibility. As a result, it is found that the radius ratio should be at least greater than two-thirds and thus the lower limit of the radius ratio is formed.

On the other hand, the size of the cylinder can be random as long as the volume displacement is fulfilled. However, the compressor design is always under space constraint and thus, the limit on the cylinder size must be imposed. In this case, the upper limit of the cylinder radius is chosen to be 45.0 mm as the size is comparable to the available compressor in the market, as shown in Appendix D. Similarly, the upper limit for the radius ratio and the lower limit for the cylinder radius are determined such that the length of the compressor working chamber is comparable to the one shown in the appendix.

The combinations of the free variables are subjected to the unique geometrical constraints of the fixed-vane revolving vane compressor. As referred to Figure 10.1, there are two geometrical constraints involved. The contact between the cylinder cover and the rotor (δy) is ultimately important as it seals the possible leakage of the working fluid from the working chamber through the bearing. In addition, it can be observed that the cylinder bearing thickness (δt) is thin. Both values can be expressed in terms of the free variables, as shown by equations (10.2) and (10.3).

$$\delta y = (2a - 1)R_c - R_{cb} \tag{10.2}$$

$$\delta t = R_{cb} - R_{rb} - R_c(1 - a) \tag{10.3}$$

where a represents the radius ratio, R_{cb} and R_{rb} refers to the cylinder and the rotor bearing radius respectively. Both geometrical constraints shall be monitored throughout the optimization study. In addition, the convergence criterion for the optimization search is defined as equation (10.4)

$$|F_{max} - F_{min}| < \varepsilon\,[1 + |F_{min}|] \tag{10.4}$$

where F_{max} and F_{min} are the maximum and the minimum of the objective function during the search respectively. The small number (ε) is given as 0.01 in the optimization studies. The explicit constraints, the geometrical constraints and the operating conditions are summarized in Table 10.1.

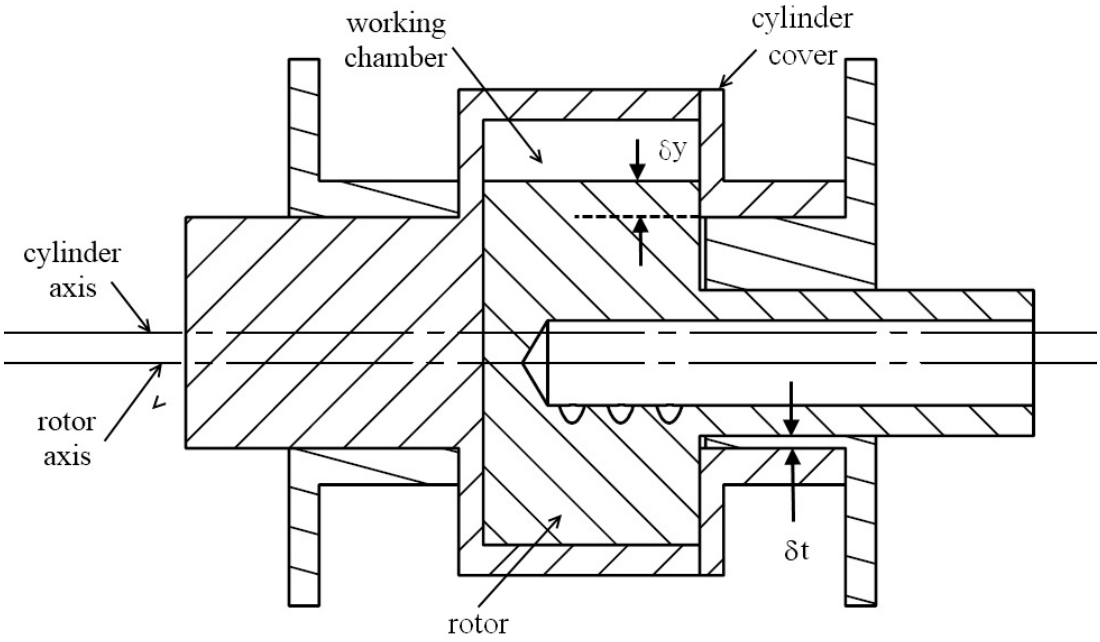

Figure 10.1 The side view of fixed-vane revolving vane compressor

Table 10.1 Explicit constraints, geometrical constraints and operating conditions

Explicit Constraints			
Free variables	Lower limit	Upper limit	Units
Cylinder radius (R_c)	35.0	45.0	mm
Rotor-to-cylinder radius ratio (R_r/R_c)	0.70	0.90	-
Cylinder bearing radius (R_{cb})	20.0	24.0	mm
Rotor bearing radius (R_{rb})	14.0	19.0	mm
Geometrical Constraints			
Contact between cover and rotor (δy)	$[(2a-1)R_c - R_{cb}] > 3.0$ mm		
Cylinder bearing thickness (δt)	$[R_{cb} - R_{rb} - R_c(1-a)] > 2.0$ mm		
Operating Conditions			
Evaporating temperature	7.2 ˚C	Working fluid	R22
Condensing temperature	54.4 ˚C	Displacement volume	9.5 cc

The results of the optimization study are shown in Figure 10.2 and Table 10.2. Figure 10.2 shows the variations of the four free variables, the compressor chamber length and the objective function during the optimization search.

In the fixed-vane revolving vane compressor, the cylinder is used to drive the rotor through the vane. As mentioned earlier, the contact force between the rotor and the vane is dependent on the rotational inertia and the angular acceleration of the rotor. Therefore, the vane-side frictional loss can be reduced if the contact force is lower. The optimized cylinder radius and the radius ratio which are shown in Figure 10.2 (a) and (b) reveals that the rotor size should be as small as possible to reduce its rotational inertia. Furthermore, the optimized radius ratio of 0.93 is to keep the angular acceleration of the rotor low. This is because as the radius ratio goes higher, the variation of the rotational speed for the rotor is lower since the centres of the rotor and the cylinder are closer.

Figure 10.2 (c) shows the variation of the compressor chamber length during the optimization search. As the radius ratio goes higher, the compressor chamber length is longer in order to maintain the desired displacement volume. In addition, the optimization searches for the smallest possible bearing radius to reduce its friction, as shown in Figure 10.2 (d) and (e). The initial and final values for each of the frictional losses are tabulated in Table 10.2. As a result, for a given swept volume and operating conditions, the fixed-vane revolving vane compressor with a long-thin configuration performs better in terms of low frictional losses. In this case, the total frictional loss reduces by 36.5%. The most significant reduction in the frictional losses comes from the reduction in both the cylinder bearing and the end face friction. The variations of the isentropic efficiency and the coefficient of performance in this case study are shown in Figure 10.3.

Table 10.2 Optimization results for minimizing frictional loss

Parameter	Initial value	Optimized value
Cylinder radius	40.0 mm	35.2 mm
Radius ratio	0.85	0.93
Compressor chamber length	6.8 mm	17.3 mm
Rotor bearing radius	15.0 mm	14.3 mm
Cylinder bearing radius	23.5 mm	20.2 mm
Vane side frictional loss	9.6 W	3.7 W
End face frictional loss	11.7 W	2.0 W
Cylinder bearing loss	105.4 W	64.8 W
Rotor bearing loss	40.3 W	35.0 W
Total frictional loss	167 W	106 W
Percent of improvement		**36.5 %**

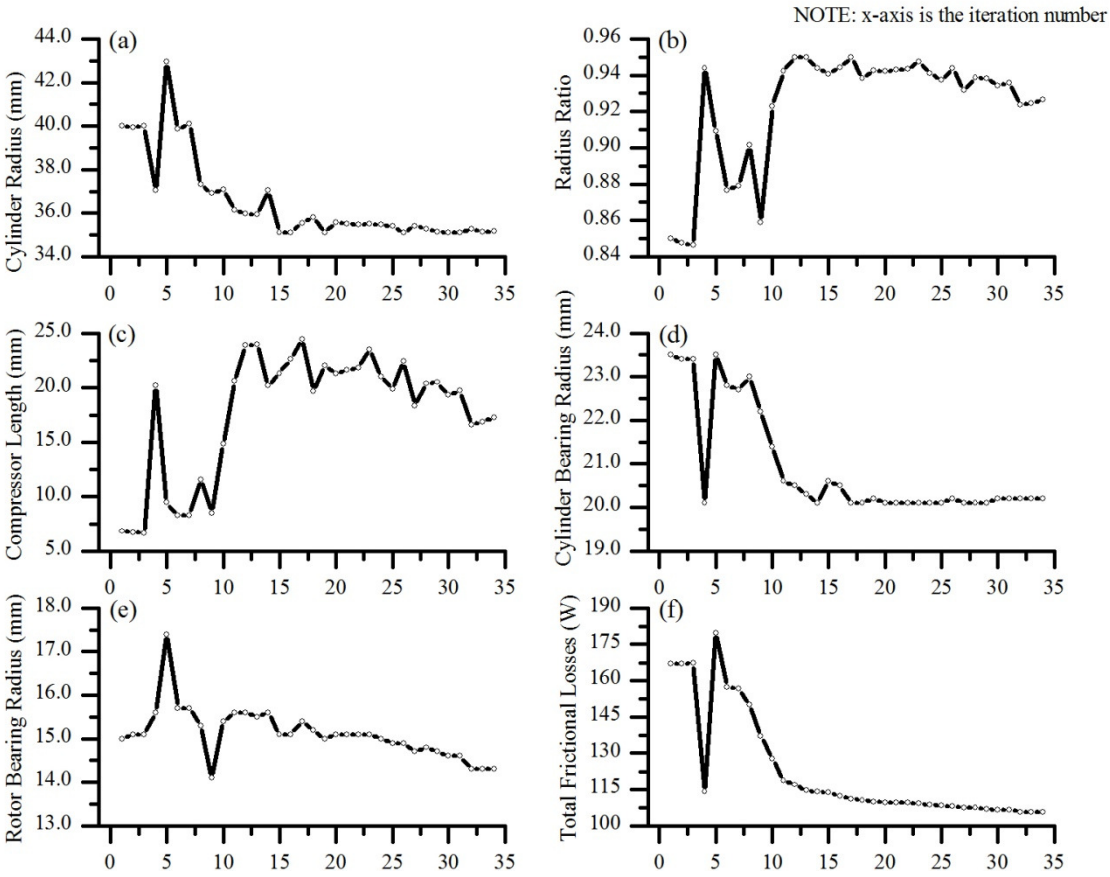

Figure 10.2 Variations of design dimensions and objective function for total frictional loss minimization

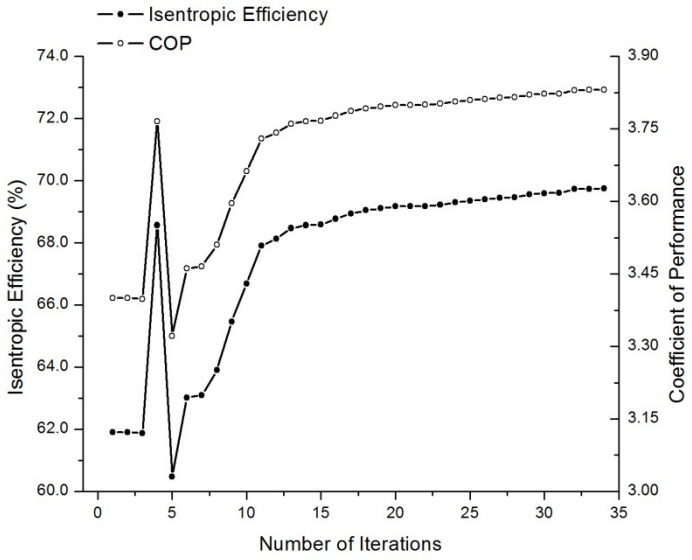

Figure 10.3 Variation of Isentropic Efficiency and COP (minimizing total frictional loss)

10.2.2 Minimizing Leakage Losses

Internal leakages in compressor performance are important as it affects the resultant mass flow rate of the refrigerant in the refrigeration or air-conditioning cycle, which in turn affects the cooling capacity. The leakage in the compressor occurs due to the pressure difference across any leakage paths, which could be caused by the level of precision in manufacturing processes or the need to reduce friction of the contact areas which move relative to each other. In the context of the fixed-vane revolving vane compressor, the leakages may prevail at the radial clearance, which is located at the virtual line contact between the rotor and the cylinder. Furthermore, the leakage may also occur across both ends of the vane. Therefore, it is worth to investigate which compressor geometry configuration would generate the least leakage losses. In this case, the objective function is the total leakage loss and there are two free variables to be considered, which are the cylinder radius and the rotor-to-cylinder radius ratio. The geometrical constraint set is identical to the set in the minimization of the total frictional loss. It is noted that the clearance value at the virtual line contact and at the vane-end faces is assumed to be a generally achievable dimension of 10 μm under most of the manufacturing tolerances.

Figure 10.4 and Table 10.3 show the results of optimization search for minimizing the leakage losses. Figures 10.4 (a) to (d) shows the variations of the cylinder radius, the radius ratio, the rotor radius and the compressor chamber length during the optimization search. During the search, it is observed that the size of the rotor and the cylinder increases in order to have a shorter compressor chamber. The shorter the compressor chamber, the leakage area through the radial clearance at the virtual line

contact can be reduced. However, the vane length exposed to the working chamber increases due to larger size of rotor and cylinder, thus the leakage loss through the vane end clearance increases. Therefore, the optimization search will seek the balance between both leakage sources. The initial and the optimized value for the design dimensions and the total leakage loss are presented in Table 10.3. The total leakage loss is reduced by 4.4 % as compared to the initial design. As a result, the optimization study reveals that the combination of short and fat compressor configuration and a high rotor-to-cylinder radius ratio performs better in terms of minimizing the total leakage loss. The corresponding variations in isentropic efficiency and coefficient of performance are shown in Figure 10.5.

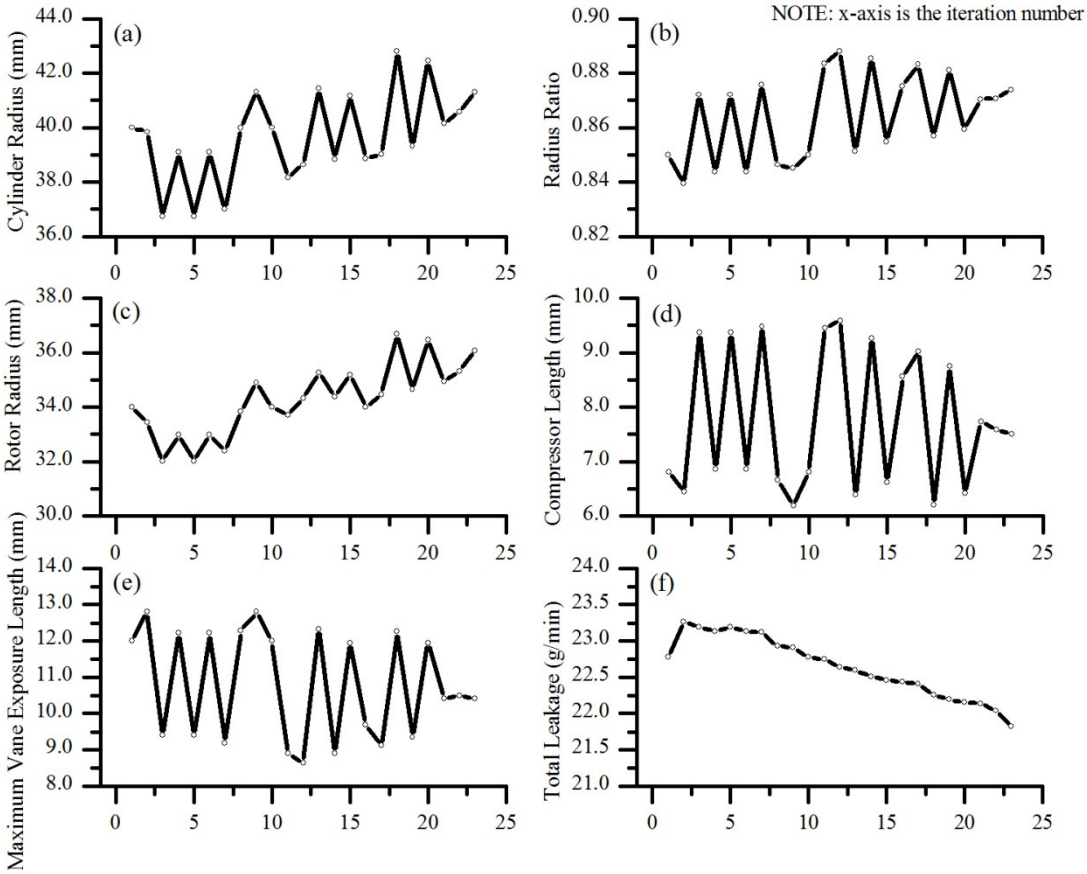

Figure 10.4 Variations of design dimensions and objective function for total leakage loss minimization

Table 10.3 Optimization results for minimizing leakage loss

Parameter	Initial value	Optimized value
Cylinder radius	40.0 mm	41.3 mm
Radius ratio	0.85	0.87
Rotor radius	34.0 mm	36.1 mm
Compressor chamber length	6.8 mm	7.5 mm
Total leakage loss	22.8 g/min	21.8 g/min
Percent of improvement		**4.4 %**

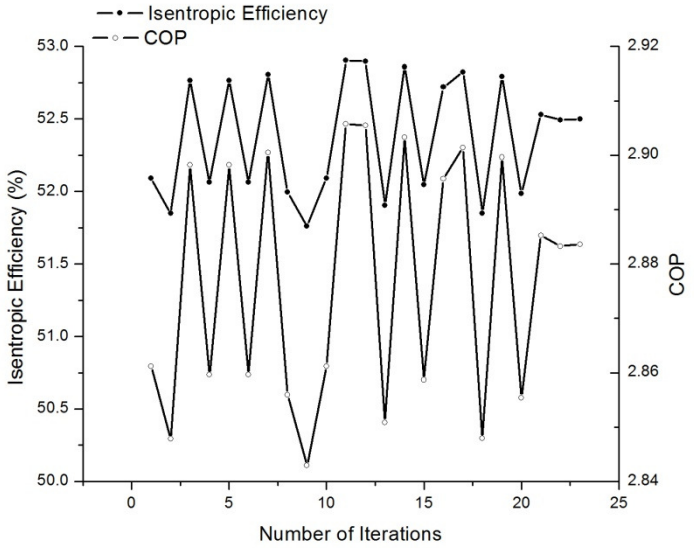

Figure 10.5 Variations of isentropic efficiency and COP (minimizing total leakage loss)

10.2.3 Maximizing Coefficient of Performance (COP)

Coefficient of performance is defined as the ratio between the cooling capacity of the refrigeration cycle and the motor input power. The motor input power can be calculated by the division of the mechanical power required by the compressor and the motor efficiency, as shown by equation (10.4). The mechanical power for a compressor operation is the sum of the indicated power and the frictional losses.

$$\mathrm{COP} = \frac{\dot{m}\Delta h}{P_{motor}} = \frac{\dot{m}\Delta h}{(P_{mech}/\eta_{motor})} \tag{10.5}$$

The coefficient of performance is normally found in the compressor data sheet and it is a performance indicator for the compressor under a standard operational conditions. A higher COP indicates the cooling capacity produced by the compressor is more and the total frictional loss and flow loss generated are less. Therefore, for a high COP compressor, the compressor should maintain low leakage loss, low frictional and low flow losses. In this study, the optimization routine will search for the best combination of design dimensions that maximizes the cooling capacity and at the same time, minimizes the losses, which include the suction loss, discharge loss and the frictional losses. In addition to the four free variables (rotor radius, the rotor-to-cylinder radius ratio, the cylinder bearing radius and the rotor bearing radius) presented in the optimization of the total frictional loss, the diameters of the suction and discharge ports are also included as free variables as the port sizes affect the flow losses. The number of free variables is six and the geometrical constraint set remains the same. The upper limit and the lower limit for the diameters of the suction and discharge ports are 20.0 mm and 10.0 mm respectively, according to the parametric studies conducted in Chapter 4.

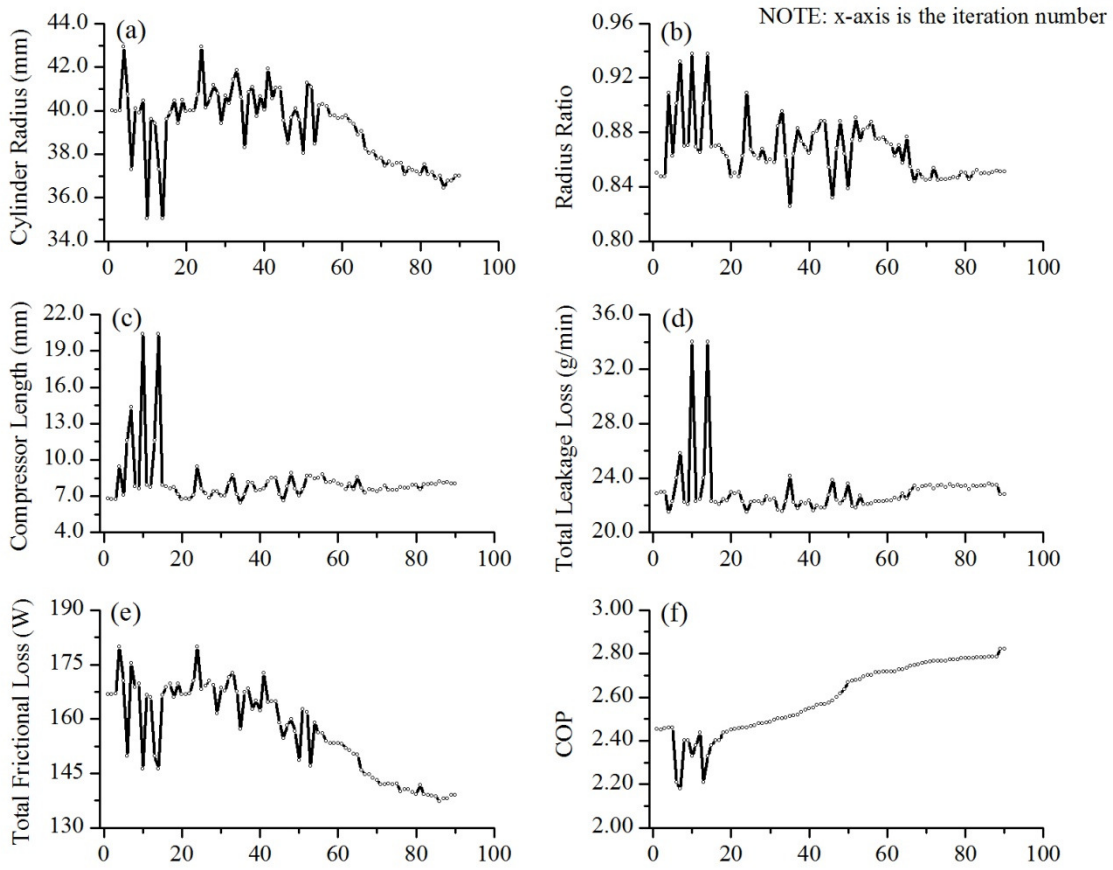

Figure 10.6 Variations of design dimensions and objective function for COP maximization

Figure 10.6 and Table 10.4 show the result of the optimization search for the maximum COP. Figures 10.6 (a) to (c) show that the optimization procedure search for shorter compressor chamber length in order to reduce the leakage through the radial clearance at the virtual line contact. In addition, the combination of the smaller cylinder and the moderate radius ratio generates a smaller rotor. Thus, the vane exposure length decreases and the leakage through the vane end clearance is reduced. The frictional losses have been reduced by 28 W where the most significant reduction comes from the bearing losses as the bearing radius decreases. The coefficient of performance has been improved by 15.1 % from 2.45 to 2.82 and the corresponding variation in isentropic efficiency is shown in Figure 10.7.

Table 10.4 Initial and Optimized Dimensions for Maximizing COP

Parameter	Initial value	Optimized value
Cylinder radius	40.0 mm	37.0 mm
Radius ratio	0.85	0.85
Cylinder bearing radius	23.5 mm	22.2 mm
Rotor bearing radius	15.0 mm	14.2 mm
Diameter of suction port	14.0 mm	10.5 mm
Diameter of discharge port	14.0 mm	13.1 mm
Total leakage loss	22.9 g/min	22.8 g/min
Total frictional loss	167 W	139 W
Cooling capacity	1602 W	1748 W
Coefficient of Performance	2.45	2.82
Percentage of improvement	**15.1 %**	

Note: motor efficiency of 0.85 is assumed

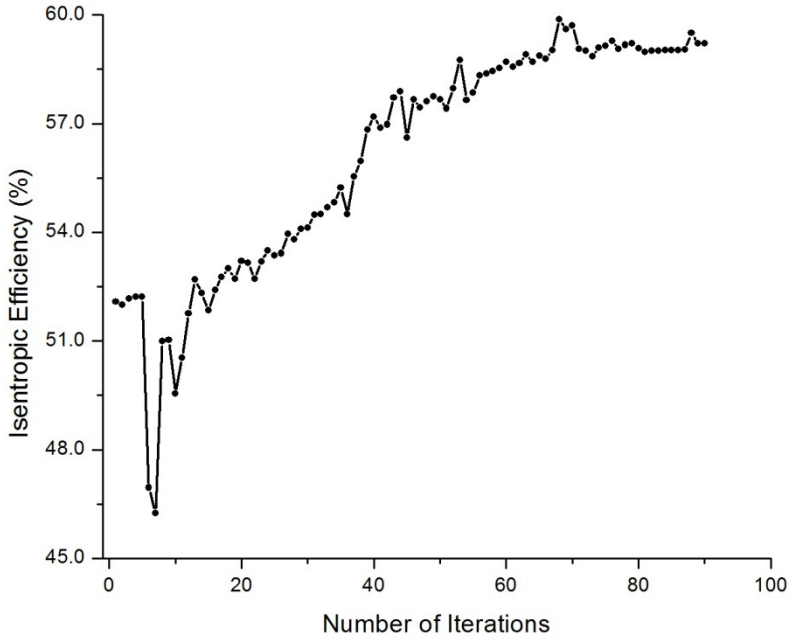

Figure 10.7 Variation of isentropic efficiency (maximizing COP)

10.3 Concluding Remarks

In this chapter, a geometrical optimization study has been carried out to optimize several performance aspects of the fixed-vane revolving vane compressor operation such as the frictional losses, the leakage losses and the coefficient of performance. Results of the optimization suggest that

- In order to have a compressor with low frictional losses, the rotor size should be small and the radius ratio should be high, which results in a long and thin compressor configuration. The study shows that the cylinder radius reduces from 40.0 mm to 35.2 mm and the radius ratio increases from 0.85 to 0.93, which results in a longer compressor chamber length of 17.3 mm. The frictional loss has been significantly reduced by 36.5 %.
- The configuration of the compressor is required to be in a short and fat configuration with a high radius ratio. The short compressor chamber reduces the internal leakage through the radial clearance at the virtual line contact and the compressor with high radius ratio reduces the internal leakage across both ends of the vane through end face clearance. In the case examined, the leakage losses have been reduced by 4.4 %.
- The coefficient of performance of a refrigeration cycle can be improved by 15.1% proper selection of design dimensions according to the optimization study. The study shows that the reductions in bearing friction and leakage losses are the dominant factors to enhance the coefficient of performance of the refrigeration cycle.

Chapter 11

Conclusions and Future Work

11.1 Introduction

In this research project, comprehensive studies have been carried out on the fixed-vane revolving vane compressor. These studies include compressor design, mathematical modelling, experimental studies and design optimization. All these studies point towards a better understanding of the working principles and the performance of the compressor. Simulation studies using R22 as the working fluid have been carried out. A prototype compressor has been designed, fabricated, instrumented and tested. Measurements of compressor performance using air as the working fluid have also been completed. The contributions of the author of this research project are summarized categorically as follows.

(1) Compressor Design

The mechanisms and their limitations of various types of positive displacement compressor have been reviewed. Particular attentions have been paid to focus on the mechanical losses of these mechanisms. The introduction of revolving vane compressor, in particular the fixed-vane revolving vane compressor in this research project has the main objective of further improving the overall performance of the positive displacement compressors.

i. Introduction of the fixed vane

In the latest version of the revolving vane compressor, the author rigidly fixed the vane on to the cylinder of the compressor. In the earlier version of this compressor, one end of the vane moves in a reciprocating fashion inside the vane slot of the rotor and the other end swivels at the pin joint (refer to Figure 3.4). Because of this earlier design, the magnitude of the contact force between the vane and the vane slot depends on the pressure differential caused by the fluid pressure acting on both sides of the vane and, the rotational inertia of the driven component, in this case the cylinder.

The dependency of the vane-side contact force on the pressure differential across the vane can be removed by rigidly fixing the vane onto the driving component of the compressor, in this case the cylinder. Therefore, the vane is constrained and can only rotate with the cylinder in a pure rotational motion. The magnitude of the vane-side contact force is thus independent of the pressure differential across the vane. This contact force is now only dependent on the rotational inertia and the angular acceleration of the driven component, in this case the rotor.

Prediction shows that a reduction of frictional loss of 40% can be achieved for the compressor capacity of 32.5 cc, which operates under evaporating temperature of 7.2˚C and condensing temperature of 54.4˚C, using R22 as the working fluid. This has translated to 3.0% improvement in coefficient of performance.

ii. Design of compressor prototype

A compressor prototype with volume displacement of 1.7 cc has been designed to examine its functionality. The prototype consists of nine major components, namely the cylinder and its cover, the rotor, the vane, the discharge valve reed and the valve plate, the split bush, the lower and the upper casings (refer to Figure 7.11).

iii. Lubrication system design

A continuous and smooth operation of a compressor depends greatly on a proper lubrication of all the rubbing parts. Therefore, an appropriately designed lubrication system is important. A lubrication system typically consists of an oil sump, feeding paths as well as returning paths (refer to Figure 8.1). During the operation, sufficient amount of lubricant must be delivered to all the rubbing surfaces to reduce the friction and the temperature of the rubbing surfaces.

iv. Unique compressor balancing approach

A complete balancing (both static and dynamic) of the compressor can be achieved through statically balance the compressor during the design stage. This is because both the rotor and the cylinder rotate at their own axes during the compressor operation. The static balance of the compressor rotating components is achieved by removing materials (such as through drilling) from the rotor and the cylinder to ensure the mass centres of the rotating assemblies coincide with their respective rotational centres.

(2) Compressor Simulation

During the course of this research project, mathematical models have been derived and formulated for the first time for the fixed-vane revolving vane compressor. These models provide a very useful tool which bring towards a better understanding of

the compressor performance and operational characteristics. These are geometric model describing the compressor geometry, thermodynamics model for the working fluid, kinematics and dynamics models of the compressing mechanism, suction and discharge flow models, valve reed dynamics model, heat transfer between the working fluid and the working chamber wall, lubrication analysis of the journal bearings supporting the rotor and the cylinder, and the analysis on the lubricant flow system for all the rubbing surfaces. These models are summarized as follows.

i. Geometric model

This model considers the geometry of the fixed-vane revolving vane compressor, in particular the working chamber. The model derives the instantaneous working chamber volume and its rate of change.

ii. Thermodynamics model

The thermodynamics model accounts for the variation of the properties of the working fluid in the working chamber by applying the First Law of Thermodynamics to the working chamber. The model assumes the fluid properties are spatially independent. The model computes the time variation of the working fluid properties such as pressure, temperature and mass inside the working chamber.

iii. Kinematics and dynamics model

The kinematics model describes the variations of the rotational kinematics of the driven component, i.e. the rotor. In addition, the vane exposed length is also formulated. It is found that the magnitude of the rotational velocity and the rotational acceleration for the rotor are all inversely proportional to the distance between the centres of the cylinder and the rotor. Through this model,

the contact forces, the rubbing forces and the working fluid pressures force acting on the compressor components have also been analyzed.

iv. Suction and discharge flow model

The suction and the discharge flow models account for the effects of the size of the suction and the discharge ports on the intake and the delivery of the working fluid. Improper sizing of the port incurs undesirable flow losses. For a compressor with an arbitrarily capacity of 9.5 cc, working under evaporating temperature of 7.2 °C and condensing temperature of 54.4 °C, running at 50 Hz with R22 as the working fluid, the suction loss increases from 0.5 W to 114 W as the suction port diameter decreases from 18.0 mm to 3.0 mm. Similarly, the discharge loss increases from 1.5 W to 10.8 W as the discharge port diameter decreases from 17.0 mm to 5.0 mm.

v. Valve reed dynamics model

The model accounts for the dynamics of the valve reed during the discharge process. The result shows that the discharge loss for the revolving vane compressor where the valve reed rotates together with the cylinder decreases from 3.4 W to 1.9 W, a 44 % improvement as compared to the non-rotating valve. In addition, the study also shows that the thickness of valve has the most significant effect on the discharge loss as the loss increases by 52 W when the valve reed thickness increases from 0.2 mm to 1.4 mm.

vi. Heat transfer model

The inclusion of the in-chamber convective heat transfer improves the prediction accuracy such that the discrepancy between the predicted and the measured pressure-angle histories drops below 2 %, as shown in Chapter 5. The

distinctive heat transfer parameters for this unique compressor geometry such as the characteristic velocity found to be the arithmetic mean of the tangential velocities of the driving and the driven component with respect to the centre of the driving component, and the hydraulic diameter is found to be the quadruple of the ratio between the vane exposure area to the working chamber and the wetted perimeter of the area.

vii. Lubrication model for the journal bearing

The prediction from the model gives the minimum oil film thickness and hence it defines the surface roughness requirement on the lubricated surfaces such as the surfaces of the rotating shaft and its counterpart, the bearings. The surface roughness requirement is more demanding when the resultant force increases under the fixed bearing dimensions. The requirement can be relaxed by having a larger bearing area, either by increasing the bearing length or the bearing radius. By having the same increment of 5 mm each in the bearing length and the bearing radius, one at a time, the surface roughness requirement can be reduced by 0.1 μm and 0.3 μm respectively. However, by having a larger bearing area to reduce the surface roughness requirement will incur more bearing frictional loss. Therefore, compromise must be made between the manufacturability and the mechanical efficiency of the compressor.

viii. Lubricating oil flow system

Oil flow paths to various contact and rubbing surfaces have been designed. The flow paths have been analysed using Kirchhoff's current and voltage law to arrive at the oil flow rate of these paths. The study suggests that the oil flow rate increases by 17.4 mm^3/s as the groove width increases from 1.0

mm to 5.0 mm under a constant groove depth of 0.3 mm. Similarly, as the groove depth decreases from 0.9 mm to 0.1 mm under a constant width of 1.0 mm, the oil flow rate increases by 49.4 mm^3/s.

(3) Compressor Experimental Study

The functionality of the fixed-vane revolving vane compressor has been verified through a smooth running of the prototype. The compressor operates successfully using air as the working fluid. The compressor operates from 2350 rev/min to 3800 rev/min and attained the pressure ratio of 2.4. The experimental findings are summarized as follows.

i. Comparison between measured and predicted mechanical power

The maximum discrepancy between the predicted and the measured mechanical power is 10 %. It was discovered that the discrepancy lies in the approximation of the local lubricant viscosity at the bearing sites. The lubricant viscosity is related to the localized bearing temperature, which in turn is affected by the rubbing frequency between the rotating shaft and its bearing, i.e. the rotational speed. It was noted that when the rotational speed varies from 2350 rev/min to 3800 rev/min, the lubricant temperature appears to vary from 70 °C to 80 °C.

ii. Variations of measured flow rate

The observations implicitly indicate that the internal leakages of the working fluid in the compressor varies inversely proportional to the operating speed, which reconfirms the prediction shown in the Appendix B. The measured results show that the flow rate is substantially greater than the prediction when

the discharge pressure is less than 1.8 bar and the operating speed is more than 2350 rev/min. Implicitly, the measurement shows that the lubrication system works well in delivering the lubricant to the desired locations and the lubricant also acts as a sealing agent to inhibit the internal leakage flows. However, the internal leakages in a small-sized compressor are particularly sensitive to the clearances at the contact and the rubbing surfaces, which are largely dependent on the level of precision of the manufacturing process. The measured results also indicate indirectly that at higher operating speeds, the internal leakages reduce as would be predicted, refer to Appendix B.

(4) Compressor Optimization Study

The mathematical models have been validated and they are subsequently used for geometrical optimization study to search for combinations of geometrical dimensions for a specified objective function at a given operational condition. Three cases of optimization studies were carried out and these are: a) minimizing the frictional losses, b) minimizing the leakage losses and c) maximizing the coefficient of performance. The optimization studies were carried out based on a compressor with an arbitrarily capacity of 9.5 cc, working under an evaporating temperature of 7.2 °C and a condensing temperature of 54.4 °C, running at 50 Hz with R22 as the working fluid. The results of these cases are summarized as follows.

i. Minimizing frictional losses

The four free variables are the cylinder radius, the ratio between rotor radius and cylinder radius, the cylinder bearing radius and the rotor bearing radius. The study reveals that a compressor with a radius ratio of 0.93 and

having cylinder radius of 35.2 mm generates the lowest frictional loss. The radius ratio changes from 0.85 to 0.93 and the cylinder radius decreases from 40.0 mm to 35.2 mm so that the angular acceleration and the rotational inertia of the rotor can be lowered. The total frictional loss reduces by 36.5 % and the most significant reduction comes from both the cylinder bearing and the end face.

ii. Minimizing the leakage losses

The free variables in this case are cylinder radius and the radius ratio. The study shows that the cylinder radius changes from 40.0 mm to 41.3 mm and the radius ratio increases from 0.85 to 0.87. The compressor length can be shortened with a larger diameter and this helps to reduce the leakage through the radial clearance at the virtual line contact. Furthermore, the compressor is maintained at a high rotor-to-cylinder radius ratio in order to keep the exposed length of the vane as short as possible to reduce the leakage across the clearance at the vane end.

iii. Maximizing coefficient of performance (COP)

The free variables in this case are the cylinder radius, the ratio between rotor radius and cylinder radius, the cylinder bearing radius, the rotor bearing radius and the diameters of the suction and the discharge port. The COP is improved by 15.1 % from 2.45 to 2.82. The study shows that the compressor length should be shorter and the distance between the centres of the cylinder and the rotor should be closer in order to reduce the internal leakage. On the other hand, the reduction in the frictional losses is mainly due to the smaller bearing radius.

11.2 Future Work

In this project, the fixed-vane revolving vane compressor has been introduced and studied. For future studies, the followings are proposed.

(1) Theoretical Development

i. Noise and vibration analysis

The noise and vibration characteristics of the revolving vane compressor are another great area to be analysed. The compressor induces vibration by the periodic changes of the working fluid compression moment and angular acceleration of the driven component as well as the fluctuation of the motor torque. Another significant source of noise will be fluid shearing noise and pulsating gas flow during the discharge process. The study will reveal the relationship between the vibration characteristics and the compressor design dimensions and hence improves the compressor reliability.

ii. Multi-objective optimization

The single-objective optimization conveys the idea on the compressor configuration for satisfying individual design objective such as frictional losses, leakage losses and coefficient of performance. However, several issues which are equally important will be encountered during the design and development of the compressor. For example, the compressor is required to be energy efficient while uses the least material. In this case, the different but equally important objectives can be collected and approached in an analytical way to reach the final optimized compressor design. The optimization tool will be great to assist the compressor designers to work under several design objectives.

iii. Heat transfer analysis

The conjugate heat transfer analysis can be conducted to describe the processes which involve variations of temperature within the surrounding solid chamber and the working fluid inside the chamber, due to thermal interactions between the solid and the working fluid. In addition, the work may extend to an overall temperature distribution in the compressor using the lumped thermal conductance approach. Furthermore, the temperature measurements on the compressor components under operation have to be carried out to verify the predictions. As a result, the understandings on the heat transfer analysis in revolving vane compressor will be greatly enhanced and the results can be used for improving the compressor reliability and reducing the component material failure.

(2) Practical Development

i. Oil-free and orientation-free compressor

The need for the oil sump to supply the lubricant to the rubbing surfaces of the compressor dictates that the compressor has to be positioned at the orientation such that the oil sump must be located at the bottom of the compressor. Failure to do so will result in the compressor to be starved of lubricant which may further results in seizure. It is suggested that if the compressor can be made to be oil free then the compressor will be able to operate at any orientation, i.e. it will be orientation free. An orientation free compressor has the advantage of serving the need where there is a possibility that the compressor may be positioned where the oil sump is not at the bottom of

the compressor, for example the compressor is used in the cooling system for a high speed notebook computer.

Such an orientation free compressor is not easy to come by. It may achieved through innovative design ideas or using hard surface coating materials to prevent and reduce wear, or both.

ii. Refrigeration Compressor

The fixed-vane revolving vane compressing mechanism has been proven. The continuous development of the compressor should establish for refrigeration use. The compressor will be designed, fabricated, instrumented and tested. The test results will be compared to the performances of the existing compressors in the market to reveal the true value of the revolving vane compressor.

To this end, the dissertation has reached its last line. The study carried out has revealed the great potential of the fixed-vane revolving vane compressor and it is believe that there are more exciting potential to be unveiled in the future.

References

1. Teh Y.L and Ooi K.T, Design and Friction Analysis of the Revolving Vane Compressor, 2006, Proc. Purdue Compressor Technology Conference, C046

2. Teh, Y.L. and Ooi K. T., 2009, Theoretical study of a novel refrigeration compressor-Part I: Design of the revolving vane (RV) compressor and its frictional losses, International Journal of Refrigeration 32 (5), 1092-1102

3. Teh, Y.L. et al., 2009, Theoretical study of a novel refrigeration compressor-Part II: Performance of a rotating discharge valve in the revolving vane (RV) compressor, International Journal of Refrigeration 32 (5), 1103-1111

4. Teh, Y. L. and Ooi K. T., 2009, Theoretical study of a novel refrigeration compressor-Part III: Leakage loss of the revolving vane (RV) compressor and a comparison with that of the rolling piston type, International Journal of Refrigeration 32 (5), 945-952

5. Teh Y.L and Ooi K.T, Experimental Study of the Revolving Vane (RV) Compressor, 2009, Applied Thermal Engineering 29 (14-15), 3235-3245

6. Prakash, R. and R. Singh, Mathematical modeling and simulation of refrigerating compressors, in Purdue Compressor Technology Conference. 1974, Ray W. Herrick Laboratories, School of Mechanical Engineering, Purdue University. p. 274-285.

7. Suefuji, K. and S. Nakayama, Practical Method for Analysis and Estimation of Reciprocating Hermetic Compressor Performance, in Purdue Compressor Technology Conference. 1980, Ray W. Herrick Laboratories, School of Mechanical Engineering, Purdue University. p. 15-23.

8. Villadsen, V., Reciprocating compressors for refrigeration and heat pump application. International Journal of Refrigeration, 1985. 8(5): p. 262-266.

9. Saito, F., et al., Noise Reduction of Hermetic Compressor by Improvement on Its Shell Shape, in Purdue Compressor Technology Conference. 1980, Ray W. Herrick Laboratories, School of Mechanical Engineering, Purdue University. p. 228-234.

10. Tojo, K., et al., Noise Reduction of Refrigerator Compressors, in Purdue Compressor Technology Conference. 1980, Ray W. Herrick Laboratories, School of Mechanical Engineering, Purdue University. p. 235-242.

11. Futakawa, A., Improvements in Compressors with Special Emphasis on Interesting Developments in Japan, in Purdue Compressor Technology Conference. 1984, Ray W. Herrick Laboratories, School of Mechanical Engineering, Purdue University. p. 339-351.

12. Levecque, N., et al., Vibration reduction of a single cylinder reciprocating compressor based on multi-stage balancing. Mechanism and Machine Theory, 2010. 46(1): p. 1-9.

13. Kaiser, H. and H. Kruse, An Investigation on Reciprocating and Rotary Refrigeration Compressors. Proceedings of Purdue Compressor Technology Conference, 1984: p. 611-617.

14. Tramschek, A.B. and K.T. Ooi, Effects of Port Geometry Dimensions and Position on the Performance of a Rotary Compressor, in Purdue Compressor Technology Conference. 1992, Ray W. Herrick Laboratories, School of Mechanical Engineering, Purdue University. p. 1177-1187.

15. Tojo, K., T. Kan, and A. Arai, Dynamic behavior of sliding vane in small rotary compressors, in Purdue Compressor Technology Conference. 1978, Ray W. Herrick Laboratories, School of Mechanical Engineering, Purdue University. p. 29-35.

16. Shu, P.C., et al., Influence of Vane Slot Back Pressure on the Characteristic of Vane Motion in Rotory Vane Compressor, in Purdue Compressor Technology Conference. 1998, Ray W. Herrick Laboratories, School of Mechanical Engineering, Purdue University. p. 415-421.

17. Yee, V. and W. Soedel, Comments on Blade Excited Rigid Body Vibrations of Rotary Vane Compressors, in Purdue Compressor Technology Conference. 1980, Ray W. Herrick Laboratories, School of Mechanical Engineering, Purdue University. p. 243-248.

18. Tramschek, A.B. and M.H. Mkumbwa, Mathematical Modeling of Radial and Non-radial Rotary Sliding Vane Compressors, in Purdue Compressor Technology Conference. 1996, Ray W. Herrick Laboratories, School of Mechanical Engineering, Purdue University. p. 477-484.

19. Kruse, H., Experimental Investigations on Rotary Vane Compressors, in Purdue Compressor Technology Conference. 1982, Ray W. Herrick Laboratories, School of Mechanical Engineering, Purdue University. p. 394-400.

20. Kaiser, H. and H. Kruse, An Investigation on Reciprocating and Rotary Refrigeration Compressors, in Purdue Compressor Technology Conference.

1984, Ray W. Herrick Laboratories, School of Mechanical Engineering, Purdue University. p. 568-575.

21. Lee, Y.Z. and S.D. Oh, Friction and wear of the rotary compressor vane-roller surfaces for several sliding conditions. Wear, 2003. 255(7-12): p. 1168-1173.

22. Ooi, K.T., T.N. Wong, and E.C. Kwek, Effects of Vane Spring Stiffness on Compressor Performance, in Purdue Compressor Technology Conference. 1994, Ray W. Herrick Laboratories, School of Mechanical Engineering, Purdue University. p. 549-553.

23. Yanagisawa, T., et al., Motion Analysis of Rolling Piston in Rotary Compressor, in Purdue Compressor Technology Conference. 1982, Ray W. Herrick Laboratories, School of Mechanical Engineering, Purdue University. p. 185-192.

24. Liu, Y. and Kosco J., Vane Dynamics Analysis of a Tilted Vane Rotary Compressor, in Purdue Compressor Technology Conference. 1998, Ray W. Herrick Laboratories, School of Mechanical Engineering, Purdue University. p. 403-408.

25. Bae, J.Y., et al., Vane Jumping in Rotary Compressor, in Purdue Compressor Technology Conference. 1998, Ray W. Herrick Laboratories, School of Mechanical Engineering, Purdue University. p. 673-678.

26. Yanagisawa, T., et al., Vibration of a rolling piston type rotary compressor. International Journal of Refrigeration, 1984. 7(4): p. 237-244.

27. Tanaka, S., K. Kyogoku, and T. Nakahara, Mixed Lubrication Analysis of Vane Tip in Rotary Compressor, in Purdue Compressor Technology Conference. 1996, Ray W. Herrick Laboratories, School of Mechanical Engineering, Purdue University. p. 287-294.

28. Sung, H.C., Tribological characteristics of various surface coatings for rotary compressor vane. Wear, 1998. 221(2): p. 77-85.

29. Takebayashi, M., et al., A Study on Wear Characteristics of a Rolling Piston Type Rotary Compressor, in Purdue Compressor Technology Conference. 2000, Ray W. Herrick Laboratories, School of Mechanical Engineering, Purdue University. p. 145-152.

30. Fujiwara, A. and N. Sakurai, Experimental analysis of screw compressor noise and vibration, in Purdue Compressor Technology Conference. 1986, Ray W. Herrick Laboratories, School of Mechanical Engineering, Purdue University. p. 566–582.

31. Fujiwara, M., et al., Computer modeling for performance analysis of rotary screw compressor, in Purdue Compressor Technology Conference. 1984, Ray W. Herrick Laboratories, School of Mechanical Engineering, Purdue University. p. 536-543.

32. Ooi, K., Design optimization of a rolling piston compressor for refrigerators. Applied Thermal Engineering, 2005. 25(5-6): p. 813-829.

33. Sangfors, B., Analytical Modeling of Helical Screw Machine for Analysis and Performance Prediction, in Purdue Compressor Technology Conference. 1982, Ray W. Herrick Laboratories, School of Mechanical Engineering, Purdue University. p. 135-139.

34. Elvedin, M., et al., The Influence of the Discharge Port Shape on Screw Compressor Performance and Gas Pulsations. 2008, Ray W. Herrick Laboratories, School of Mechanical Engineering, Purdue University. p. C1170.

35. Stosic, N., I.K. Smith, and A. Kovacevic, Extending the Operating Range of Dry Screw Compressors by Cooling Their Rotors. 2004, Ray W. Herrick Laboratories, School of Mechanical Engineering, Purdue University. p. C025.

36. Stosic, N., I.K. Smith, and A. Kovacevic, Optimization of Screw Compressor Design. 2002, Ray W. Herrick Laboratories, School of Mechanical Engineering, Purdue University. p. C21-3.

37. Wang, Z. and W. Zhang, New Design and Rotor Retrofit to Improve Capacity and Performance of Refrigeration Screw Compressor. 2006, Ray W. Herrick Laboratories, School of Mechanical Engineering, Purdue University. p. C106.

38. Shaw, D., Twin Screws of the Future for Air Conditioning and Refrigeration, in Purdue Compressor Technology Conference. 1990, Ray W. Herrick Laboratories, School of Mechanical Engineering, Purdue University. p. 1-7.

39. Sauls, J., Comparison of Screw Rotor Profiles from a Manufacturing Perspective. 2002, Ray W. Herrick Laboratories, School of Mechanical Engineering, Purdue University. p. C19-1.

40. Holmes, C.S., Inspection of Screw Rotors for the Prediction on Compressor Performance, Reliability and Noise. 2004, Ray W. Herrick Laboratories, School of Mechanical Engineering, Purdue University. p. C070.

41. Zhou, S., et al., The Key Technology of Single Screw Manufacturing by 5-Axis CNC Machining Center. 2006, Ray W. Herrick Laboratories, School of Mechanical Engineering, Purdue University. p. C160.

42. Stosic, N., et al., Profiling of Screw Compressor Rotors by Use of Direct Digital Simulation. 2008, Ray W. Herrick Laboratories, School of Mechanical Engineering, Purdue University. p. C1154.

43. Tojo, K., et al., A Scroll Compressor for Air Conditioning, in Purdue Compressor Technology Conference. 1984, Ray W. Herrick Laboratories, School of Mechanical Engineering, Purdue University. p. 496-503.

44. CREUX, L., Rotary Engine. 1905.

45. Ishii, N., et al., A study on dynamic behavior of a scroll compressor, in Purdue Compressor Technology Conference. 1986, Ray W. Herrick Laboratories, School of Mechanical Engineering, Purdue University. p. 901-916.

46. Etemad, S. and J. Nieter, Computational parametric study of scroll compressor efficiency, design, and manufacturing issues, in Purdue Compressor Technology Conference. 1988, Ray W. Herrick Laboratories, School of Mechanical Engineering, Purdue University. p. 56-64.

47. Lee, Y.R. and W.F. Wu, On the profile design of a scroll compressor. International Journal of Refrigeration, 1995. 18(5): p. 308-317.

48. Li, L., The effect of scroll wraps on the performance of scroll compressors. International Journal of Refrigeration, 1997. 20(5): p. 326-331.

49. Etemad, S. and J. Nieter, Design optimization of the scroll compressor. International Journal of Refrigeration, 1989. 12(3): p. 146-150.

50. Li, L. and Y. Yu, The Theoretical Analysis and Experimental Research for a Refrigerating Scroll Compressor, in Purdue Compressor Technology Conference. 1990, Ray W. Herrick Laboratories, School of Mechanical Engineering, Purdue University. p. 156-163.

51. Ishii, N., et al., Refrigerant leakage flow evaluation for scroll compressors, in Purdue Compressor Technology Conference. 1996, Ray W. Herrick Laboratories, School of Mechanical Engineering, Purdue University. p. 633–638.

52. Ishii, N., et al., Effects of Surface Roughness upon Gas Leakage Flow through Small Clearances in CO2 Scroll Compressors. 2008, Ray W. Herrick Laboratories, School of Mechanical Engineering, Purdue University. p. C1429.

53. Yoshida, H., et al., Clearance Control of Scroll Compressor for CO2 Refrigerant, in Proceedings of Purdue Compressor Technology Conference. 2008, Ray W. Herrick Laboratories, School of Mechanical Engineering, Purdue University. p. C1251.

54. Yano, K., H. Nakao, and M. Shimoji, Development of Large Capacity CO2 Scroll Compressor, in Proceedings of Purdue Compressor Technology Conference. 2008, Ray W. Herrick Laboratories, School of Mechanical Engineering, Purdue University. p. C1189.

55. Nakao, H., et al., Study of Mechanical Loss Reduction on Thrust Bearings for Scroll Compressors Using CO2 Refrigerant, in Purdue Compressor Technology Conference. 2008, Ray W. Herrick Laboratories, School of Mechanical Engineering, Purdue University. p. C1136.

56. Yi, F. and Y. Qian, Developing a Compact Automotive Scroll Compressor, in Proceedings of Purdue Compressor Technology Conference. 2008, Ray W. Herrick Laboratories, School of Mechanical Engineering, Purdue University. p. C1106.

57. Koo, I.-H., B.-Y. Nam, and G.-H. Lee, Design of Back Pressure Control Valve for Automotive Scroll Compressor, in Proceedings of Purdue Compressor Technology Conference. 2008, Ray W. Herrick Laboratories, School of Mechanical Engineering, Purdue University. p. C1234.

58. Yi, F., E.A. Groll, and J.E. Braun, Modeling and Testing of an Automobile AC Scroll Compressor, Part II : Model Validation, in Proceedings of Purdue Compressor Technology Conference. 2004, Ray W. Herrick Laboratories, School of Mechanical Engineering, Purdue University. p. C083.

59. Yi, F., E.A. Groll, and J.E. Braun, Modeling and Testing of an Automobile AC Scroll Compressor, Part I : Model Development, in Proceedings of Purdue Compressor Technology Conference. 2004, Ray W. Herrick Laboratories, School of Mechanical Engineering, Purdue University. p. C082.

60. Perevozchikov, M.M. and H.M. Pham, Scroll Compressor for Mobile HVAC/R Application, in Proceedings of Purdue Compressor Technology Conference. 2004, Ray W. Herrick Laboratories, School of Mechanical Engineering, Purdue University. p. C095.

61. Dugast, P., Global Acoustical Finite-Element Simulation of Scroll Compressor Noise from Internal Sources, in Proceedings of Purdue Compressor Technology Conference. 2008, Ray W. Herrick Laboratories, School of Mechanical Engineering, Purdue University. p. C1262.

62. Yoo, B.-K., B.-C. Lee, and M.K. Kiem, Structure Design of a Scroll Compressor Using CAE Analysis, in Proceedings of Purdue Compressor Technology Conference. 2006, Ray W. Herrick Laboratories, School of Mechanical Engineering, Purdue University. p. C051.

63. Sauls, J., Optimization of Scroll Compressor Performance with Manufacturing Capability and Reliability Constraints, in Proceedings of Purdue Compressor Technology Conference. 2004, Ray W. Herrick Laboratories, School of Mechanical Engineering, Purdue University. p. C022.

64. Soedel, W., Introduction to computer simulation of positive displacement type compressors. 1972: Purdue University.

65. Squarer, D. and R.E. Kothmann, Digital computer simulation of a reciprocating compressor - a simplified analysis, in Purdue Compressor Technology Conference. 1972, Ray W. Herrick Laboratories, School of Mechanical Engineering, Purdue University. p. 502-505.

66. Karll, B., Computer simulation of the cylinder process in a compressor based on the first law of thermodynamics, in Purdue Compressor Technology Conference. 1972, Ray W. Herrick Laboratories, School of Mechanical Engineering, Purdue University. p. 18-21.

67. Rottger, W. and H. Kruse, Analysis of the working cycle of single-stage refrigeration compressors using digital computers, in Purdue Compressor Technology Conference. 1976, Ray W. Herrick Laboratories, School of Mechanical Engineering, Purdue University. p. 18-25.

68. Hiller, C.C. and L. Glicksman, Detailed modeling and computer simulation of reciprocating refrigeration compressors, in Purdue Compressor Technology Conference. 1976, Ray W. Herrick Laboratories, School of Mechanical Engineering, Purdue University. p. 12-17.

69. Ng, E., A. TRAMSHEK, and J. MacLaren, Computer Simulation of a Reciprocating Compressor Using a Real Gas Equation of State, in Purdue Compressor Technology Conference. 1980, Ray W. Herrick Laboratories, School of Mechanical Engineering, Purdue University. p. 33-42.

70. Lee, S., R. Singh, and M. Moran, First law analysis of a compressor using a computer simulation model, in Purdue Compressor Technology Conference. 1984, Ray W. Herrick Laboratories, School of Mechanical Engineering, Purdue University. p. 577-586.

71. Sun, S.Y. and T.R. Ren, New method of thermodynamic computation for a reciprocating compressor: computer simulation of working process. International Journal of Mechanical Sciences, 1995. 37(4): p. 343-353.

72. Ooi, K. and T. Wong, A computer simulation of a rotary compressor for household refrigerators. Applied Thermal Engineering, 1997. 17(1): p. 65-78.

73. Chen, Y., et al., Mathematical modeling of scroll compressors--part I: compression process modeling. International Journal of Refrigeration, 2002. 25(6): p. 731-750.

74. Seshaiah, N., et al., Mathematical modeling of the working cycle of oil injected rotary twin screw compressor. Applied Thermal Engineering, 2007. 27(1): p. 145-155.

75. Srinivas, M. and C. Padmanabhan, Computationally efficient model for refrigeration compressor gas dynamics. International Journal of Refrigeration, 2002. 25(8): p. 1083-1092.

76. Bredesen, A., Influence of valve dynamics on compressor performance. International Journal of Refrigeration, 1979. 2(1): p. 17-21.

77. Glaeser, W., Failure mechanisms of reed valves in refrigeration compressors. Wear, 1999. 225: p. 918-924.

78. MacLaren, J., A review of simple mathematical models of valves in reciprocating compressors, in Purdue Compressor Technology Conference. 1972, Ray W. Herrick Laboratories, School of Mechanical Engineering, Purdue University. p. 180-187.

79. Costagliola, M., The theory of spring loaded valves for reciprocating compressors. J. Appl. Mech, 1950: p. 415-420.

80. MacLaren, J. and S. Kerr, Analysis of valve behaviour in reciprocating compressors. Proc. Int. Cong. Refig., Madrid, paper, 1967: p. 33-39.

81. Wambsganss, M. and R. Cohen, Dynamics of a Reciprocating Compressor with Automatic Reed Values, I. Theory and Simulation. Proceedings of the XIIth Int. Cong. of Refrign, 1969. 2: p. 779-790.

82. Traversari, A. and P. Lacitignola, Use and calculation of ring type valves for reciprocating compressors. Ouanderni Pignone House Journal, 1970. 16.

83. W. Gatecliff, G. and E. R. Lady, Forced Vibration of a Cantilever Valve of Uniform Thickness and Non-uniform Width, in Purdue Compressor Technology Conference. 1972, Ray W. Herrick Laboratories, School of Mechanical Engineering, Purdue University. p. 316-319.

84. Wollatt, D., A Simple Numerical Solution for Compressor Valves with One Degree of Freedom, in Purdue Compressor Technology Conference. 1974, Ray W. Herrick Laboratories, School of Mechanical Engineering, Purdue University. p. 159-165.

85. W. Gatecliff, G. C. Griner, and H. Richardson, A Compressor Valve Model for Use in Daily Design Work, in Purdue Compressor Technology Conference. 1980, Ray W. Herrick Laboratories, School of Mechanical Engineering, Purdue University. p. 176-179.

86. R.Piechna, J., Numerical Study of a Dynamic Behavior of Simple Reed Valve, in Purdue Compressor Technology Conference. 1984, Ray W. Herrick Laboratories, School of Mechanical Engineering, Purdue University. p. 628-634.

87. K.T.Ooi, G.B.Chai, and E.C.Kwek, A Simple Valve Model to Study the Performance of a Small Compressors, in Purdue Compressor Technology Conference. 1992, Ray W. Herrick Laboratories, School of Mechanical Engineering, Purdue University. p. 147-155.

88. Friley, J. and J. Hamilton, Characterization of Reed Type Compressor Valves by the Finite Element Method, in Purdue Compressor Technology Conference. 1976, Ray W. Herrick Laboratories, School of Mechanical Engineering, Purdue University. p. 295-301.

89. Akella, S., et al., Finite Element Analysis of Compressor Valve Dynamics, in Purdue Compressor Technology Conference. 1988, Ray W. Herrick Laboratories, School of Mechanical Engineering, Purdue University. p. 285-290.

90. Fagotti, F., M.G.D. Bortoli, and R. Barnieri, A finite element approach to compressor valve motion simulation, in Purdue Compressor Technology Conference. 1996: Ray W. Herrick Laboratories, School of Mechanical Engineering, Purdue University. p. 359-364.

91. Cyklis, P., CFD simulation of the flow through reciprocating compressor self-acting valves, in Purdue Compressor Technology Conference. 1994, Ray W. Herrick Laboratories, School of Mechanical Engineering, Purdue University. p. 427-432.

92. Matos, F., A. Prata, and C. Deschamps, Numerical simulation of the dynamics of reed type valves, in Purdue Compressor Technology Conference. 2002, Ray W. Herrick Laboratories, School of Mechanical Engineering, Purdue University. p. C15-2.

93. Kim, J., et al., Valve Dynamic Analysis of a Hermetic Reciprocating Compressor, in Purdue Compressor Technology Conference. 2006, Ray W. Herrick Laboratories, School of Mechanical Engineering, Purdue University. p. C107.

94. S.W. Brok, S.T., J.S.V.d. Meer, Modeling of cylinder heat transfer - large effort, little effect?, in Purdue Compressor Technology Conference. 1980, Ray W.

Herrick Laboratories, School of Mechanical Engineering, Purdue University. p. 43-50.

95. Chen, L.T., The effect of heat transfer on the volumetric efficiency for refrigerant compressors. International Communications in Heat and Mass Transfer, 1985. 12(5): p. 531-540.

96. Prasad, B.G.S., Heat transfer in reciprocating compressors - a review, in Purdue Compressor Technology Conference. 1998, Ray W. Herrick Laboratories, School of Mechanical Engineering, Purdue University. p. 857-863.

97. Adair, R., E. Qvale, and J. Pearson, Instantaneous Heat Transfer to the Cylinder Wall in Reciprocating Compressors, in Purdue Compressor Technology Conference. 1972, Ray W. Herrick Laboratories, School of Mechanical Engineering, Purdue University. p. 521-526.

98. Benson, R.S., W. Annand, and P. Baruah, A simulation model including intake and exhaust systems for a single cylinder four-stroke cycle spark ignition engine. International Journal of Mechanical Sciences, 1975. 17(2): p. 97-124.

99. Liu, R. and Z. Zhou, Heat transfer between gas and cylinder wall of refrigerating reciprocating compressor, in Purdue Compressor Technology Conference. 1984, Ray W. Herrick Laboratories, School of Mechanical Engineering, Purdue University. p. 110-115.

100. M.S. Chong, H.C.W., Prediction of heat and mass transfer during compression in reciprocating compressors, in Purdue Compressor Technology Conference. 1976, Ray W. Herrick Laboratories, School of Mechanical Engineering, Purdue University. p. 466-472.

101. Singh, M. and S. Rajvanshi, Heat transfer between rotating eccentric cylinders with different radii. International Journal of Heat and Mass Transfer, 1982. 25(11): p. 1719-1724.

102. Recktenwald, G., J. Ramsey, and S. Patankar, Predictions of heat transfer in compressor cylinders, in Purdue Compressor Technology Conference. 1986, Ray W. Herrick Laboratories, School of Mechanical Engineering, Purdue University. p. 159–174.

103. Keribar, R. and T. Morel, Heat transfer and component temperature prediction in reciprocating compressors, in Purdue Compressor Technology Conference. 1988, Ray W. Herrick Laboratories, School of Mechanical Engineering, Purdue University. p. 454-463.

104. Todescat, M.L., et al., Thermal energy analysis in reciprocating hermetic compressors, in Purdue Compressor Technology Conference. 1992, Ray W. Herrick Laboratories, School of Mechanical Engineering, Purdue University. p. 1419-1428.

105. Fagotti, F., et al., Heat transfer modeling in a reciprocating compressor, in Purdue Compressor Technology Conference. 1994, Ray W. Herrick Laboratories, School of Mechanical Engineering, Purdue University. p. 605-610.

106. Longo, G. and R. Caracciolo, Unsteady state analysis of a hermetic reciprocating compressor: heat transfer inside the cylinder and valve dynamics, in Purdue Compressor Technology Conference. 2002, Ray W. Herrick Laboratories, School of Mechanical Engineering, Purdue University. p. C4-4.

107. Ooi, K.T., Heat transfer study of a hermetic refrigeration compressor. Applied Thermal Engineering, 2003. 23(15): p. 1931-1945.

108. Padhy, S., Heat transfer model of a rotary compressor, in Purdue Compressor Technology Conference. 1992, Ray W. Herrick Laboratories, School of Mechanical Engineering, Purdue University. p. 1405-1418.

109. Padhy, S.K. and S.N. Dwivedi, Heat transfer analysis of a rolling-piston rotary compressor. International Journal of Refrigeration, 1994. 17(6): p. 400-410.

110. Chen, Y., et al., Mathematical modeling of scroll compressors--part II: overall scroll compressor modeling. International Journal of Refrigeration, 2002. 25(6): p. 751- 764.

111. Jang, K. and S. Jeong, Experimental investigation on convective heat transfer mechanism in a scroll compressor. International Journal of Refrigeration, 2006. 29(5): p. 744-753.

112. Ooi, K.T. and J. Zhu, Convective heat transfer in a scroll compressor chamber: a 2-D simulation. International journal of thermal sciences, 2004. 43(7): p. 677-688.

113. Sun, S., et al., Simulation research on scroll refrigeration compressor with external cooling. International Journal of Refrigeration, 2010. 33(5): p. 897-906.

114. Wu H.G., Xing Z.W., and S. P.Ch., Theoretical and experimental study on indicator diagram of twin screw refrigeration compressor. International Journal of Refrigeration, 2004. 27(4): p. 331-338.

115. Ferreira, R.T.d.S. and D.E.B. Lilie, evaluation of the leakage through the clearance between piston and, in Purdue Compressor Technology Conference.

1984, Ray W. Herrick Laboratories, School of Mechanical Engineering, Purdue University. p. 1-6.

116. Yong, H., Leakage calculation through clearances, in Purdue Compressor Technology Conference. 1994, Ray W. Herrick Laboratories, School of Mechanical Engineering, Purdue University. p. 35-40.

117. Pandeya, P. and W. Soedel, Rolling-piston-type rotary compressors with special attention to friction and leakage, in Purdue Compressor Technology Conference. 1978, Ray W. Herrick Laboratories, School of Mechanical Engineering, Purdue University. p. 209–218.

118. Chu, I., et al., Analysis of the rolling-piston type rotary compressor, in Purdue Compressor Technology Conference. 1978, Ray W. Herrick Laboratories, School of Mechanical Engineering, Purdue University. p. 219-225.

119. Reed, W. and J. Hamilton, Internal leakage effects in sliding vane rotary compressors, in Purdue Compressor Technology Conference. 1980, Ray W. Herrick Laboratories, School of Mechanical Engineering, Purdue University. p. 112–117.

120. Rodgers, R., Comprehensive Analysis of Leakage in Rotary Compressors, in Purdue Compressor Technology Conference. 1996, Ray W. Herrick Laboratories, School of Mechanical Engineering, Purdue University. p. 287-293.

121. Yanagisawa, T. and T. Shimizu, Leakage losses with a rolling piston type rotary compressor. I. Radical clearance on the rolling piston. International Journal of Refrigeration, 1985. 8(2): p. 75-84.

122. Yanagisawa, T. and T. Shimizu, Leakage losses with a rolling piston type rotary compressor. II. Leakage losses through clearances on rolling piston faces. International Journal of Refrigeration, 1985. 8(3): p. 152-158.

123. Costa, C., R. Ferreira, and A. Prata, Considerations about the leakage through the minimal clearance in a rolling piston compressor, in Purdue Compressor Technology Conference. 1990, Ray W. Herrick Laboratories, School of Mechanical Engineering, Purdue University. p. 853-863.

124. Xiuling, Y., C. Zhiming, and F. Zhen, Calculating Model and Experimental Investigation of Gas Leakage, in Purdue Compressor Technology Conference. 1992, Ray W. Herrick Laboratories, School of Mechanical Engineering, Purdue University. p. 1249-1255.

125. Yang, H., et al., Study on leakage via the radial clearance in a novel synchronal rotary refrigeration compressor. International Journal of Refrigeration, 2010. 34(1): p. 84-93.

126. Kruse, H. and M. Schroeder, Fundamentals of lubrication in refrigerating systems and heat pumps. International Journal of Refrigeration, 1985. 8(6): p. 347-355.

127. Youbi-Idrissi, M. and J. Bonjour, The effect of oil in refrigeration: Current research issues and critical review of thermodynamic aspects. International Journal of Refrigeration, 2008. 31(2): p. 165-179.

128. Asanuma, M., l. T., and I. H., An Experimental Study of the Shaft Oil Supply Mechanism of a Rotary Compressor, in Purdue Compressor Technology Conference. 1984, Ray W. Herrick Laboratories, School of Mechanical Engineering, Purdue University. p. 383–390.

129. KIM, K.M.O. and H.Y.U.N. CHO, A study on lubricating system of hermetic rotary compressor, in Purdue Compressor Technology Conference. 1988, Ray W. Herrick Laboratories, School of Mechanical Engineering, Purdue University. p. 27-33.

130. Shin, C., J. Park, and Y. Chang, An analytical study of the oil supply system in scroll compressor, in Purdue Compressor Technology Conference. 1998, Ray W. Herrick Laboratories, School of Mechanical Engineering, Purdue University. p. 307–312.

131. Itho, T., et al., Study on the Oil Supply System for Rotary Compressors, in Purdue Compressor Technology Conference. 1992, Ray W. Herrick Laboratories, School of Mechanical Engineering, Purdue University. p. 505-514.

132. Kim, H.J. and T.W. Lancey, Numerical study on the lubrication oil distribution in a refrigeration rotary compressor. International Journal of Refrigeration, 2003. 26(7): p. 800-808.

133. Kim, H.J., Lubrication oil pumping by utilizing vane motion in a horizontal rotary compressor. International Journal of Refrigeration, 2005. 28(4): p. 498-505.

134. Lückmann, A.J., M.V.C. Alves, and J.R. Barbosa Jr, Analysis of oil pumping in a reciprocating compressor. Applied Thermal Engineering, 2009. 29(14-15): p. 3118-3123.

135. Prata, A.T. and J.R. Barbosa, Role of the Thermodynamics, Heat Transfer, and Fluid Mechanics of Lubricant Oil in Hermetic Reciprocating Compressors. Heat Transfer Engineering, 2009. 30(7): p. 533-548.

136. Alves, M.V.C., et al., Fluid Flow in a Screw Pump Oil Supply System for Reciprocating Compressors. International Journal of Refrigeration, 2010. 34(1): p. 74-83.

137. Ooi, K.T., Design Optimization of a Rolling Piston Compressor for Refrigerators, 2005, Applied Thermal Engineering 25 (5-6), 813-829

138. Tan K.M. and Ooi K.T., A Novel Revolving Vane Compressor with a Fixed-vane, 2011, International Journal of Refrigeration, in Press, Corrected Proof

139. Yanagisawa, T. and T. Shimizu, Friction Losses in Rolling Piston type Rotary Compressors. III, 1985, International Journal of Refrigeration 8 (3), 159-165

140. Khonsari, M. M. and E. R. Booser, Applied Tribology: Bearing Design and Lubrication, 2001, John Wiley & Sons Inc.

141. Reason, B. and I. Narang, Rapid Design and Performance Evaluation of Steady-State Journal Bearings - A Technique Amenable to Programmable Hand Calculators, 1982, Tribology Transactions 25 (4), 429-444

142. Hirani, H., K. Athre, et al., Dynamically loaded finite length journal bearings: analytical method of solution, 1999, Journal of Tribology 121, 844-852

143. Hirani, H., T. Rao, et al., Rapid performance evaluation of journal bearings, 1997, Tribology International 30 (11), 825-834

144. A. Harnoy, Bearing Design in Machinery: Engineering Tribology and Lubrication, 2005

145. Müller, H. K. and B. S. Nau, Fluid Sealing Technology: Principles and Applications, 1998

146. Subiantoro, A. and K. T. Ooi, Analytical Study of the Endface Friction of the Revolving Vane Mechanism, 2011, International Journal of Refrigeration 34 (5), 1276-1285

147. M. J. Box, A new method of constraint optimization and comparison with other methods, 1965, The Computer Journal 8, 33-41

Appendix A

Lubrication System with Low Flow Resistance

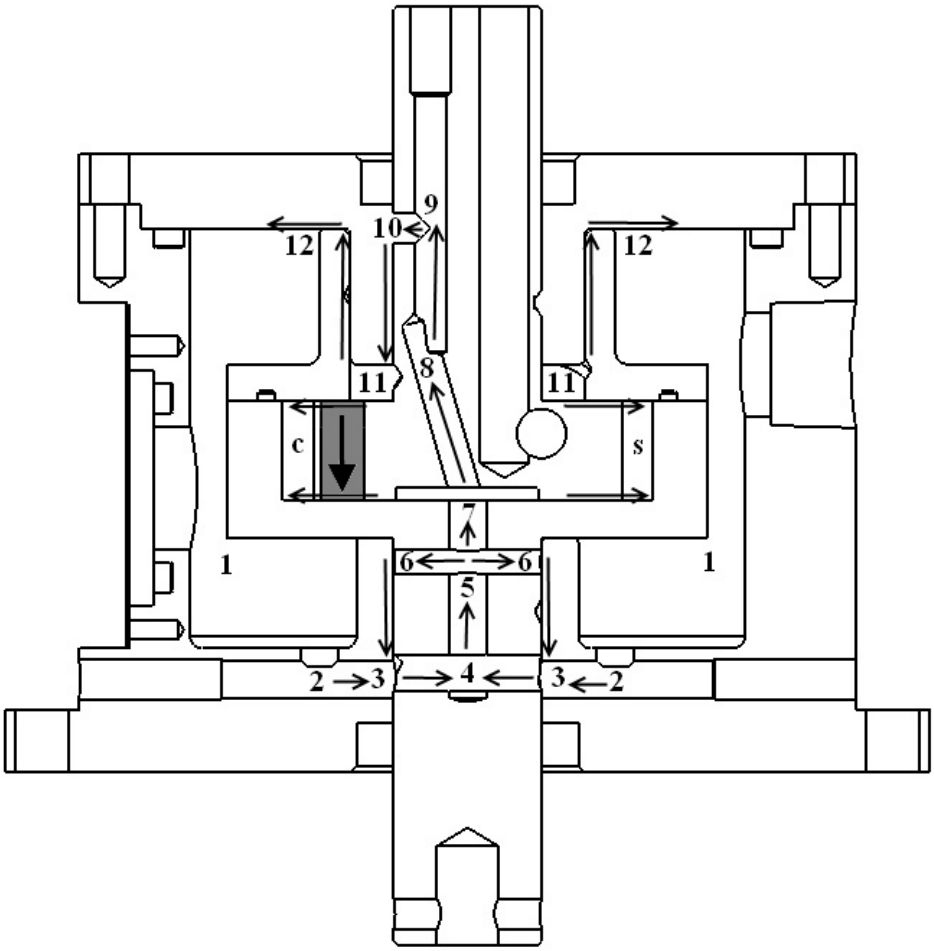

Figure A1 The preliminary design of lubrication system for fixed-vane revolving vane compressor prototype

In the preliminary design of the fixed-vane revolving vane compressor prototype as shown in Figure A1, a balancing through hole shaded in grey is created in the rotor. Therefore, the through hole becomes another flow path and the lubricant is expected to go through. The smallest flow resistance for each flow path and the flow resistance of

the balancing hole in the rotor are presented in Table A1. It is noted that the flow resistance for the balancing hole in the rotor is a constant and it is the smallest among the entire flow resistance network. The results of the oil flow rate are also presented in the same table. The results indicate that the circulation of the oil occurs in the loop of 7-8-9-10-11-7 due to low flow resistance of the rotor balancing hole. This situation is undesirable as the oil will be trapped and the oil temperature will be increased due to frequent rubbing as the compressor operates. Thus, huge amount of heat will be generated and may jeopardize the compressor operation. Furthermore, the other rubbing surfaces may starve from lubricant and leads to metal-to-metal contact.

Table A1 Flow resistance and the corresponding flow rate

Description	Flow resistance (Pa-s m^{-3})	Flow rate (m^3 s^{-1})
Lower radial hole in cylinder shaft (3 to 4)	6.00×10^6	0.800
Upper radial hole in cylinder shaft (5 to 6)	3.03×10^7	0.800
Radial hole in rotor shaft (9 to 10)	7.09×10^6	**58.60**
Upper cylinder bearing clearance (11 to 12)	4.05×10^{12}	0.000
Lower cylinder bearing clearance (6 to 3)	4.05×10^{12}	0.000
Rotor bearing clearance (10 to 11)	4.06×10^{12}	0.017
Spiral groove on cylinder cover	9.79×10^8	-0.025
Spiral groove on cylinder shaft	9.79×10^8	0.000
Spiral groove on rotor shaft	1.20×10^9	**58.60**
Lower end face to compression chamber (7 to c)	1.75×10^{12}	0.817
Lower end face to suction chamber (7 to s)	1.75×10^{12}	0.815
Upper end face to compression chamber (11 to c)	1.75×10^{12}	0.805
Upper end face to suction chamber (11 to s)	1.75×10^{12}	0.803
End of cylinder cover to discharge chamber	7.58×10^{11}	-0.012
Oil sump to cylinder shaft (2 to 3)	1.54×10^7	0.799
Cylinder vertical hole (4 to 5)	1.99×10^6	1.590

Cylinder vertical hole (5 to 7)	1.11×10^{6}	1.600
Slanted hole in rotor (7 to 8)	1.88×10^{7}	**58.60**
Vertical hole in rotor shaft (8 to 9)	2.05×10^{7}	**58.60**
Balancing hole in rotor (11 to 7)	**7.50×10^{5}**	**57.80**

The preliminary lubrication system design study reveals that the balancing hole which is exposed to the oil flow path shall not be drilled through and it reaffirms that the analysis on the lubrication system design is important to ensure sufficient amount of lubricant is delivered to each rubbing surface during compressor operation.

Appendix B

Improvements on Discrepancy between Measured and Predicted Mechanical Power

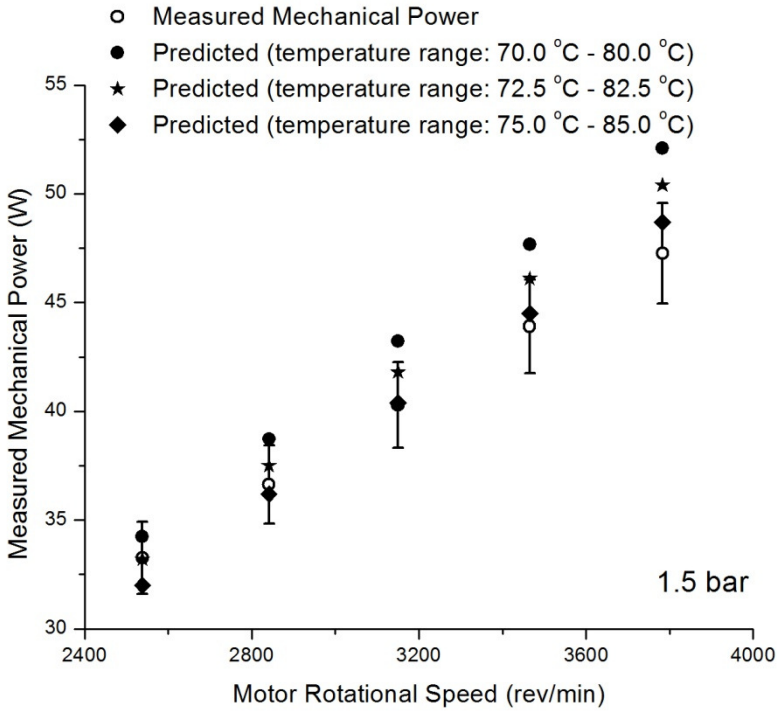

Figure B1 The improvement on the discrepancy between measured and predicted mechanical power

The improvement on the discrepancy between measured and predicted mechanical power is illustrated in the figure above. It is shown that the maximum discrepancy has been reduced from 10.0 % to 4.0 % by adjusting the working temperature range for the lubricant in the bearings, which is deemed as the major possible source of discrepancy.

Appendix C

Variation of Internal Leakages with Compressor Operational Speeds

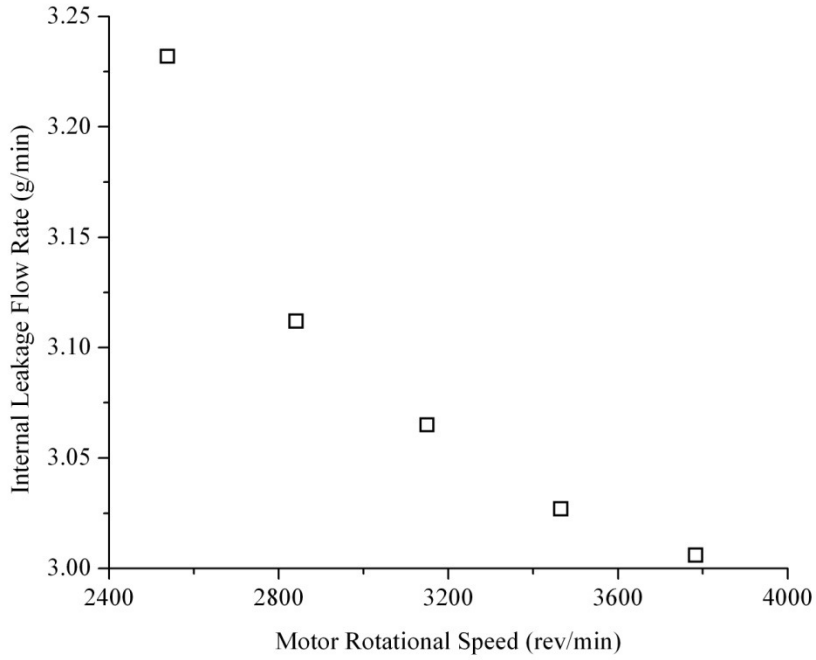

Figure C1 The variation of internal leakages with motor rotational speed

The internal leakage flow rate which accounts for the leakages through the radial clearance at the virtual line contact and the axial clearance at the end faces with pressure ratio of 1.5 and air as the working fluid is illustrated in the figure above. It is shown that the internal leakage decreases by 7 % when the rotational speed increases from 2538 rev/min to 3783 rev/min.

Appendix D

Multi-variable direct search constrained optimization technique

In general, an optimization study can be mathematically represented by:

Optimize $F(x) = f(x_1, x_2, x_3, \dots\dots, x_N)$

Subjected to $L_E(x_i) \leq E(x_i) \leq H_E(x_i)$ $i = 1,2,3, \dots, N$

$L_G(x_j) \leq G(x_j) \leq H_G(x_j)$ $j = 1,2,3, \dots, M$

$L_I(x_k) \leq I(x_k) \leq H_I(x_k)$ $k = 1,2,3, \dots, L$

where E, G and I represent the explicit, geometrical and implicit constraints respectively while L and H represent the lower and the upper limits. I, J and K represent the number of explicit, geometrical and implicit constraints respectively. The optimization method is implemented with the following steps orderly.

i. A feasible starting point that satisfies explicit constraints, geometrical constraints and implicit constraints is picked. Subsequently, 2N-1 additional points are generated based on pseudo random numbers and explicit constraints for each independent free variable by the following equation.

$$x_{i,j} = L_E(x_i) + r_{i,j} \times [H_E(x_i) - L_E(x_i)]$$

where $i = 1,2,3, \ldots, N$ and $j = 1,2,3, \ldots, 2N - 1$.

ii. The additional points and the starting point are called the original complexes. In the above, N is the number of free variable and also the number of explicit constraints. $L_E(x_i)$ and $H_E(x_i)$ represent the lower and the upper limits for the free variables, i.e. the limits of explicit constraints. The pseudo random number is $r_{i,j}$ and it is in between 0 and 1. All the selected points satisfy the explicit constraints for the free variables but may violate the other constraints.

iii. For each random point generation, the point will be checked for its validity under the geometrical constraint and implicit constraint if any. The point will be moved half way towards the centroid of the remaining points if the constraints are violated. The new point is

$$x_{i,j}^{n+1} = \bar{x}_{i,j} + 0.5 \times \left(x_{i,j}^{n} - \bar{x}_{i,j}\right)$$

where n is the iteration number and $\bar{x}_{i,j}$ is the centroid of the remaining points. The centroid of the remaining points is defined by

$$\bar{x}_{i,j} = \frac{1}{2N-1} \sum_{j=1}^{2N-1} \left[x_{i,j} - x_{i,j}(\text{old})\right]$$

This process is repeated until all the constraints are satisfied.

iv. The objective function is evaluated at each point. The point having the worst objective function is reflected by a reflection factor of α (α=1.3 has been used) along the line linking the replaced point and the centroid of the remaining points. The resulting new point is defined as follows.

$$x_{i,j}^{n+1} = \bar{x}_{i,j} + \alpha\left(\bar{x}_{i,j} - x_{i,j}^{n}\right)$$

$x_{i,j}^{n}$ represents the worst point. The reflected point will be checked for its validity against explicit constraint. The point is moved inside the constraint boundary by a factor of δ if the constraint is violated.

v. The objective function is then evaluated. The newly obtained objective function will checked for any improvement. The new point will be moved half towards the centroid of the remaining points if the new point does not yield any improvement in the objective function value.

vi. The above procedures will be repeated until the specified number of consecutive successful iterations is reached or the convergence is met. Convergence is defined as by the following relation.

$$|F_{max} - F_{min}| < \varepsilon\,[1 + |F_{min}|]$$

Appendix E

Panasonic Compressor Specifications Sheet

Panasonic Industrial Company — *Air Conditioning Department*

2R10S3R276A-6A — 220/240 V, 50 Hz R-22

BTU 5,000

2R10S3R276A-6A

Application	Cooling (C) / Heating (H)	
Ref. Charge Limit (C/H)	16.4 oz.	465 g
(C)	19.4 oz.	550 g
Evap. Temp. Range(C/H)	5°F to 53.6°F	-15°C to 12°C
(C)	14°F to 53.6°F	-10°C to 12°C
Specification Number	SC-52170821-B(2)	

Rated Performance @220V/240V[1]

Capacity	5,415/5,455 Btu/hr
Motor Input	510/525 Watts
Current	2.35/2.25 Amperes
E.E.R.	10.62/10.39 Btu/hr/ W

Compressor Data

Pump Type	Rotary	
Displacement	9.5 cc/rev	
Oil	ATMOS M60 or equivalent	
Oil Charge (Precharged)	8.8 fl. oz.	260 cc
Net Weight	19.2 lb	8.7 kg

Motor Data

Motor Type	Permanent Split Capacitor
Locked Rotor Amperes	10/11 A at 220/240 V
Winding Resistance	Main: 5.525Ω, Aux: 5.250Ω
Max. Continuous Current[2]	

Maximum Operating Conditions

Condensing Temp.	149°F	65°C
Return Gas Temp.	95°F	35°C
Discharge Gas Temp.	239°F	115°C
Motor Wire Temp.	266°F	130°C

Electrical Components

Overload Protector	7100543
Texas Instrument part #	MRA 99017
Run Capacitor	20 µF/370 VAC

[1] *Rated @ ASHRAE/T Conditions*

Evaporating Temp.	45°F	7.2°C
Condensing Temp.	130°F	54.4°C
Return Gas Temp.	95°F	35.0°C
Liquid Temp.	115°F	46.1°C
Ambient Temp.	95°F	35.0°C

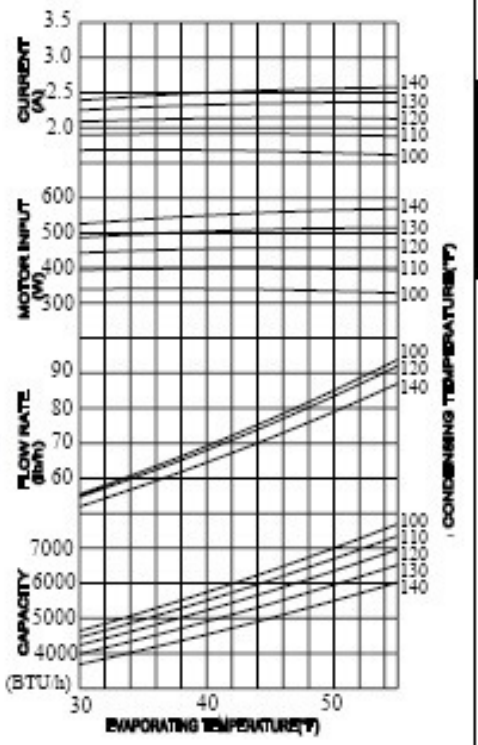

Performance Data @ 220V

Based on:

Return gas Temp.	95°F	35.0°C
Liquid sub-cooling	15°F	8.3°C
Ambient	95°F	35.0°C

EVAP. TEMP.		COND. TEMP. 100°F	110°F	120°F	130°F	140°F
35° F	Btu/hr	5175	4965	4715	4430	4100
	Watts	340	400	460	495	540
	Amperes	1.7	1.9	2.1	2.3	2.5
45° F	Btu/hr	6355	6085	5775	5415	5005
	Watts	340	400	455	510	560
	Amperes	1.7	1.9	2.1	2.4	2.5
55° F	Btu/hr	7695	7355	6970	6525	6025
	Watts	330	395	455	515	570
	Amperes	1.6	1.9	2.1	2.4	2.6

[2] *Contact Panasonic for value.*

2R10S3R276A-6A

220/240 V, 50 Hz R-22

BTU 5,000

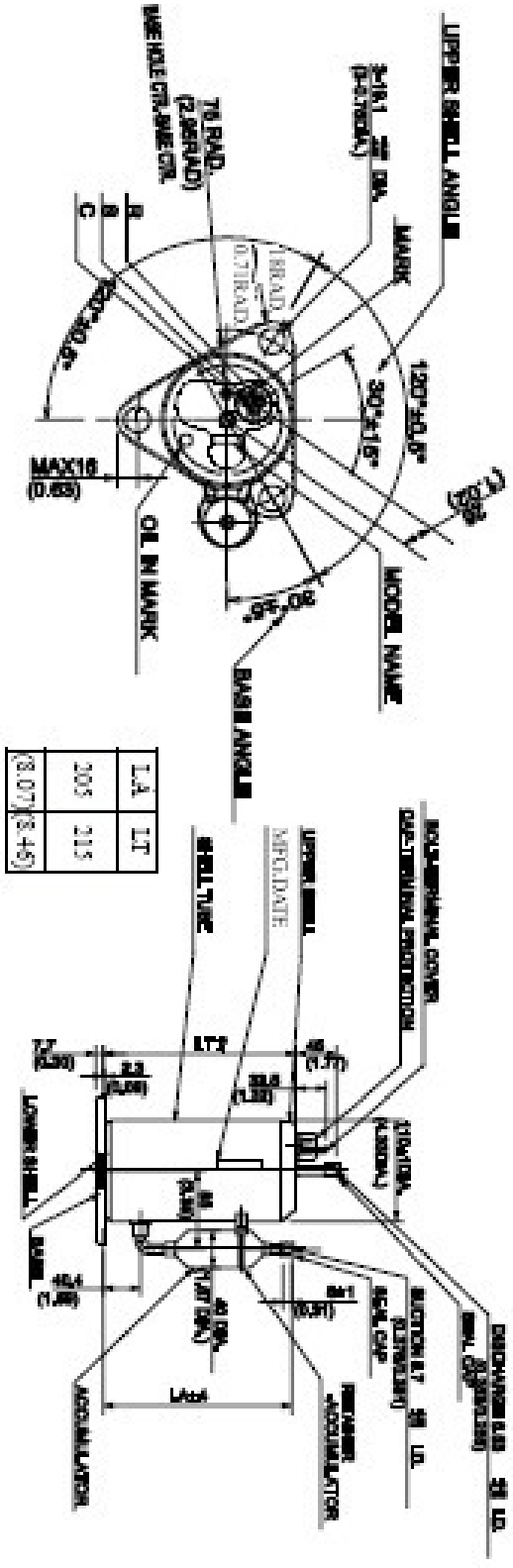

WIRING DIAGRAM

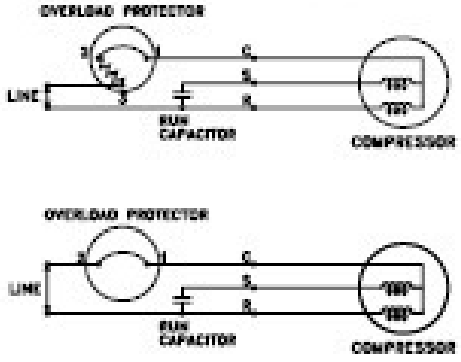

COMPRESSOR ACCESSORIES

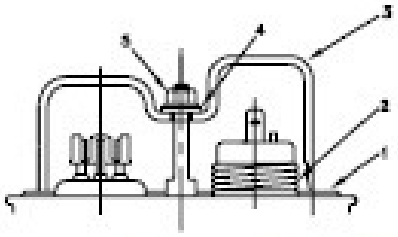

Accesories	Part Number
1 Gasket-Terminal Cover	7070820U
2 Spring-OLP hold down	7041200
3 Terminal Cover	7070222U
4 Gasket-Nut	7070821U
5 Nut-Terminal Cover	7080300
Grommet	7070817

COMPRESSOR MOUNTING